

**EXPERIMENTAL STUDIES ON  
HIGH PERFORMANCE  
ALKALI ACTIVATED SLAG CONCRETE MIXES**

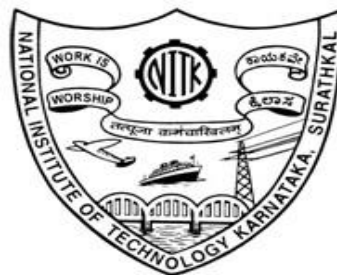
Thesis

submitted in partial fulfillment of the requirements for the degree of

**DOCTOR OF PHILOSOPHY**

by

**MANJUNATH R  
(165033CV16F12)**



**DEPARTMENT OF CIVIL ENGINEERING  
NATIONAL INSTITUTE OF TECHNOLOGY KARNATAKA  
SURATHKAL, MANGALORE-575025**

**JUNE, 2020**

## DECLARATION

I hereby declare that the Research Thesis entitled **EXPERIMENTAL STUDIES ON HIGH PERFORMANCE ALKALI ACTIVATED SLAG CONCRETE MIXES**, which is being submitted to the **National Institute of Technology Karnataka, Surathkal** in partial fulfillment of the requirements for the award of the degree of **Doctor of Philosophy in Civil Engineering**, is a bonafide report of the research work carried out by me. The material contained in this Research Thesis has not been submitted to any University or Institution for the award of any degree.

*Manjunath R*  
*04/06/2020*

.....  
(165033CV16F12, Manjunath R)

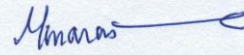
Department of Civil Engineering

Place: NITK, Surathkal

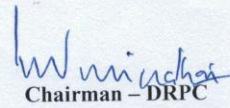
Date: 04/06/2020

## CERTIFICATE

This is to certify that the Research Thesis entitled **EXPERIMENTAL STUDIES ON HIGH PERFORMANCE ALKALI ACTIVATED SLAG CONCRETE MIXES**, submitted by **Mr. MANJUNATH R**, (Register Number: **165033CV16F12**), as the record of the research work carried out by him, is accepted as the Research Thesis submission in partial fulfillment of the requirements for the award of the degree of **Doctor of Philosophy**.



**(Dr. Mattur C. Narasimhan)**  
Professor and Research Guide,  
Department of Civil Engineering,  
NITK, Surathkal



**Chairman - DRPC**  
Department of Civil Engineering  
NITK, Surathkal

Date: *04-06-2020*



**Chairman (DRPC)**  
Department of Civil Engineering  
National Institute of Technology Karnataka, Surathkal  
Mangalore - 575 026, Karnataka, INDIA

***DEDICATED***  
***TO***  
***MY PARENTS,***  
***FAMILY MEMBERS***  
***AND TEACHERS***

## **ACKNOWLEDGEMENTS**

I would like to express my sincere and deepest gratitude to my research supervisor, Dr. Mattur C. Narasimhan, Professor, Department of Civil Engineering, NITK, Surathkal, for his Infinite love, care, motivation and invaluable guidance throughout my research work. I am grateful to him for his keen interest in the preparation of this thesis. It has been my pleasure and honour to work with him.

I wish to thank Prof. Venkat Reddy, Dr. Varghese George, and Dr. K. Swaminathan, the successive Heads of Department of Civil Engineering , NITK, for the kind support and encouragement extended by them. I will always be grateful to all faculty members of the Department of Civil Engg., for their kind support and encouragement, throughout my tenure as a research scholar in the Department.

I wish to place on record my sincere thanks to Dr. K. Udaya Bhat, Professor, Dept. of Metallurgical and Materials Engineering and Dr. B.B.Das, Associate Professor, Dept. of Civil Engineering, the members of my Research Progress Assessment Committee, for their valuable suggestions and the encouragement provided at various stages of this work.

I acknowledge with thanks, the kind support extended by Dr. A.S.Balu, Associate Professor, Department of Civil Engineering, for his kind encouragement and support at various stages of my research work.

I wish to thank Dr. A. Mahesha, Professor and former Head, Dr. U. Pruthviraj, Asst. Professor, members of technical staff of Strength of materials Laboratory, Department of Applied mechanics, for the kind support extended by them, during this research work.

I would like to express my sincere gratitude to Mr. D. Satish Kumar. Asst. General Manager (Research and Development), M/s Jindal Steel Works, Bellary, India for providing the necessary materials required for carrying out my research work.

Further I would also like to thank the Principal and other authorities of M/s BMS College of Engineering, Bangalore, for allowing me to utilise the advanced characterisation equipment such as SEM, EDX and XRD, for my microstructural studies in this research work. I wish to thank Prof. Ramachandra, Department of Mechanical Engineering, and Mr. Rajesh, Operator In-charge, Advanced Characterisation Laboratory, BMSCE for all the kind support provided by them during this research.

I would like to express my sincere gratitude to Dr. Manu Santhanam, Professor and Mr. D. Yuvaraj, Research scholar, Department of Civil Engineering, IIT Madras for the kind support extended by them during this research work.

I am grateful to Mr. Ragavendra, M/s Wisdom Industries, Bangalore for providing the fine quartz powder and quartz sand required for my research work.

Special mention is to be made of the co-operation and help extended to me by all the members of the technical staff at the laboratories of the Civil Engineering Department. My special thanks are due to Mr. Nataraja, Mr. Purushotham, Mr. Githish, Mr. Manohar, Mr. Ramesh Paul, Mr. Ramanath Acharya, Mr. Shashikant, Mr. Vishwanth, Mr. Ranjith, Mr. Ravi, Mr. Yathish and Mr. Dheeraj for their kind help in completing my experimental work. I express my sincere thanks to all the staff members of the office of Head, Civil Engineering Dept.,- Mrs.Vagdevi, Mrs.Vijaylakshmi, Mrs. D.Tara., Mrs.Anivatha, Mrs.Prabhavathi, Mr. Monaappa and Mr. Vishwanth for their kind support at various stages of this work.

I was fortunate to have the encouragement and support of friends like, Mr. K.M.Umesha, Mr. Shivam Kumar, Mr. U.K. Bala Bharathi, Mr. S. Saipuspharaj, all post-graduate students and so also Mr. H.T.Avinash, Research Scholar, throughout my doctoral research work. I am very much thankful to all of them and so also to other friends and fellow research scholars of this institute for their continuous encouragement and suggestions during the course of my research work. The informal support and encouragement of my friends has been indispensable.

I am especially grateful to the blessings and sacrifices incurred by my loving parents Sri. H.C. Ramaiah and Smt. T. Venkatalakshmi, who have provided me the quality education and support and have encouraged in all my endeavours. They have always been a source of inspiration for me. I would also like to thank Mrs. Rashmi, my wife and Ms. Gritha, my loving daughter for the support provided during this work.

Finally, I thank the God Almighty, for making all these events happen smoothly and every one of them who have encouraged, supported and contributed to the successful completion of my doctoral research.

NITK, Surathkal

**(Manjunath R)**

Date: 04-06-2020

## ABSTRACT

In the present study, an attempt has been made to develop high-performance alkali-activated slag concrete (HPAASC) mixes. A total of fifteen self-compacting concrete mixes were developed based on absolute volume method, with Ground Granulated Blast Furnace Slag (GGBFS) as the principal binder with their compressive strength values targeted to be greater than 70 MPa. A Control, reference OPC-based concrete mix was also developed with similar flow ability and compressive strength values. Further the initial setting times of these mixes were also investigated as per relevant IS: 8142-1976. These concrete mixes incorporated slag sand and Electric arc furnace (EAF) slag, as fine and coarse aggregates respectively. In the background of application of Taguchi's DOE method, the flow and strength properties of nine of these mixes were evaluated in an initial calibration phase and the performances of the remaining six mixes were analyzed in the validation phase. After ascertaining the self-compacting nature of the mixes, their mechanical strength properties such as compressive, split tensile and flexural strengths, water absorption and moduli of elasticity were evaluated. Regression equations were developed for the different strength characteristics and predictive capabilities of those regression equations were found to be good. Detailed microstructural studies were carried out on all the fifteen mixes using SEM, EDX and XRD.

In the second phase of the present investigation, five (of the fifteen above) best performing candidate mixes, in terms of their better flow ability and higher mechanical strengths were subjected to various durability tests in order to assess their resistances on exposure to aggressive chemical environments. Tests were conducted in acid and sulphate-rich environments upto to an extended period of 365 days. Further these five mixes were evaluated for their chloride ion penetration by conducting steady and non-steady state tests. The same five mixes were further evaluated for their strength characteristics on exposure to sustained elevated temperatures upto 800°C. Microstructural studies were also carried out on the test specimens of different mixes after them being exposed to aggressive acid and sulphate-rich environments and so also to elevated temperatures using SEM and EDX.

In order to enhance the toughness characteristics of these mixes, appropriate percentages of steel fiber were added and the flow ability and strength characteristics of such fiber-reinforced mixes were evaluated. Such mixes were evaluated for their enhanced toughness characteristics based on methods proposed by Barr and Hasso and ACI.

The high performance self-compacting alkali-activated slag concrete mixes (HPAASC) mixes were further evaluated by testing the flexural behaviour of beams made of such mixes and reinforced with steel-rebar reinforcement, in order to check their applicability in structural concrete elements. A detailed analysis with respect to the sustainability in terms of ecological performance, of all these concrete mixes is also carried out.

A new class of high strength, self-compacting, alkali-activated slag concrete mixes were successfully developed herein, incorporating slag sand and Electric arc furnace slag, both by-products from the iron and steel industry, as fine and coarse aggregates respectively. Addition of small amounts of sodium phosphate, as an additive, has led to a construction-friendly increase in the initial setting times of all the HSAASC mixes tested herein, from an initial-low of 15 minutes to a healthy 60 minutes or so. These mixes developed herein have shown higher mechanical strength properties in terms of compressive, split tensile and flexural strengths and so also greater modulus of elasticity, and lower water absorption characteristics, possibly due to the formation of more amounts of C-A-S-H gels, as reflected from the morphologies obtained during the microstructural analysis. HSAASC mixes developed herein have also shown better durability performances when subjected to acid, sulphates and chloride environments as compared to the control OPCC reference mix. Thus the present class of alkali activated slag concrete mixes are having the required levels of enhanced flow ability, higher mechanical strengths and better durability properties, and hence can be referred to as **HIGH PERFORMANCE ALKALI ACTIVATED SLAG CONCRETE MIXES**. Higher residual strength characteristics were also observed in all the HPAASC mixes developed herein, when subjected to sustained elevated temperatures as compared to the control OPCC mix. Addition of steel fibers to the high performance

alkali activated slag concrete mixes has been shown to marginally increase the compressive strengths. The ultimate flexural strengths of all the candidate mixes, however, were observed to increase substantially. Increase in the percentage of steel fibers has shown to increase the toughness indices of all the candidate mixes tested herein. The flexural performance of all the reinforced HPAASC beams was found to be, in general, similar to that of the reference HSS-OPCC control beam. High performance alkali activated slag concrete mixes developed herein have shown lesser embodied energy as well as lesser emissions of embodied CO<sub>2</sub> as compared to the control OPCC-based mix.

**Keywords:** High performance alkali activated slag concrete mixes; Slag Sand; Electric arc furnace slag; Microstructural studies; Toughness characteristics; Reinforced concrete beams, Waste management.

---

# CONTENTS

<b>No</b>	<b>Title</b>	<b>Page No</b>
	LIST OF FIGURES	vi
	LIST OF TABLES	xi
	NOMENCLATURE	xiii
<b>1</b>	<b>INTRODUCTION</b>	01
1.1	GENERAL	01
1.2	OBJECTIVES OF THE PRESENT RESEARCH	04
1.3	CRITERIA FOR EVALUATING HIGH PERFORMANCE ALKALI ACTIVATED SLAG CONCRETE MIXES	04
1.4	SCOPE OF THE PRESENT WORK	06
1.5	ORGANIZATION OF THE THESIS	08
<b>2</b>	<b>LITERATURE REVIEW</b>	10
2.1	GENERAL	10
2.2	HISTORY OF GEOPOLYMERS AND ALKALI ACTIVATED CEMENTITIOUS SYSTEMS	10
2.3	ACTIVATION MECHANISMS OF ALKALI ACTIVATED SLAG SYSTEMS	11
2.4	REQUIREMENTS FOR ALKALI ACTIVATION OF GGBFS	13
2.5	ALKALI ACTIVATED SLAG MORTAR AND CONCRETE SYSTEMS	14
2.6	EFFECT OF DOSAGE AND MODULUS OF ACTIVATOR SOLUTIONS	15
2.7	WORKABILITY OF ALKALI ACTIVATED COMPOSITES-INFLUENCE OF ADMIXTURES.	17
2.8	MECHANICAL PROPERTIES OF ALKALI ACTIVATED COMPOSITES	18

2.9	ALKALI ACTIVATED COMPOSITES WITH ALTERNATIVE BINDERS.	23
2.10	ALKALI ACTIVATED COMPOSITES WITH DIFFERENT ACTIVATORS	25
2.11	ALKALI ACTIVATED COMPOSITES WITH ALTERNATIVE AGGREGATES.	26
2.12	DURABILITY STUDIES ON ALKALI ACTIVATED COMPOSITES	28
2.13	ELEVATED TEMPERATURE PERFORMANCE OF ALKALI ACTIVATED COMPOSITES	32
2.14	BEHAVIOUR OF ALKALI ACTIVATED COMPOSITES INCORPORATED WITH FIBERS	35
2.15	BEHAVIOUR OF REBAR REINFORCED STRUCTURAL ELEMENTS MADE OF ALKALI ACTIVATED CONCRETE MIXES	37
2.16	SUMMARY OF THE LITERATURE	40
<b>3</b>	<b>MATERIAL CHARACTERIZATION AND MIX PROPORTIONS</b>	<b>43</b>
3.1	INTRODUCTION	43
3.2	PRELIMINARY INVESTIGATIONS ON CONSTITUENT MATERIALS	43
3.2.1	Cement	43
3.2.2	Ground Granulated Blast-Furnace Slag (GGBFS)	43
3.2.3	Fine Quartz powder	43
3.2.4	Fine Aggregates	45
3.2.5	Coarse Aggregates	48
3.2.6	Water	50
3.2.7	Di-basic sodium phosphate	50
3.2.8	Superplasticiser	50
3.2.9	Alkaline Activator	51
3.3	MIX-DESIGNS, PREPARATION OF MIXES AND CASTING OF TEST SPECIMENS	52

	3.3.1	General	52
	3.3.2	Mix Design of AASC mixes – Taguchis DOE approach	53
3.4		CASTING OF TEST SPECIMENS WITH HSAASC MIXES – SPECIMEN DETAILS	59
3.5		CURING OF SPECIMENS	59
3.6		EXPERIMENTAL PROCEDURES	59
	3.6.1	Initial Setting time	59
	3.6.2	Flow ability	60
	3.6.3	Mechanical Properties of Concrete Mixes	60
	3.6.4	Initial Water absorption and Saturated Water absorption	
3.7		MICROSTRUCTURAL STUDIES	60
<b>4</b>		<b>PERFORMANCE OF HIGH STRENGTH SELF-COMPACTING ALKALI ACTIVATED SLAG CONCRETE (HSAASC) MIXES</b>	<b>63</b>
	4.1	GENERAL	63
	4.2	SETTING TIME AND WORKABILITY OF HSAASC MIXES	63
	4.2.1	Initial setting time and workability characteristics of a typical AASC mixes	63
	4.2.2	Compressive strength of typical AASC mixes admixed with different additives	69
	4.2.3	Discussions	71
	4.2.4	Setting time characteristics of HSAASC mixes using penetrometer resistance test.	72
	4.3	FLOW TESTS ON FRESH HSAASC MIXES	74
	4.4	PROPERTIES OF HSAASC MIXES IN HARDENED STATE	79
	4.4.1	Compressive strengths of HSAASC mixes	79
	4.4.2	Modulii of elasticity and Split-tensile strengths of HSAASC mixes	85
	4.4.3	Flexural strengths of HSAASC mixes	88
	4.4.4	Water absorption in HSAASC mixes	89
	4.5	STUDIES ON MICROSTRUCTURES OF HSAASC MIXES	91
	4.6	SUMMARY	98

<b>5</b>	<b>DURABILITY STUDIES ON HSAASC MIXES</b>	100
5.1	GENERAL	100
5.2	RESISTANCE OF HSAASC MIXES AGAINST ACID ATTACK	100
5.2.1	Residual strength and mass loss characteristics of HSAASC mixes subjected to concentrated sulphuric acid solution.	100
5.2.2	Microstructural studies of HSAASC mixes subjected to 5% H <sub>2</sub> SO <sub>4</sub> solution	104
5.3	TESTS FOR RESISTANCE OF HSAASC MIXES AGAINST SULPHATE ATTACK	109
5.3.1	Residual strength and mass loss characteristics of HSAASC mixes subjected to magnesium sulphate solution	109
5.3.2	Microstructural studies of HSAASC mixes subjected to magnesium sulphate solution	112
5.4	CHLORIDE ION PENETRATION RESISTANCE of HSAASC Mixes	118
5.5	SUMMARY	123
<b>6</b>	<b>STRENGTH RETENTION CHARACTERISTICS OF HPAASC MIXES SUBJECTED TO ELEVATED TEMPERATURES</b>	125
6.1	GENERAL	125
6.2	RESIDUAL STRENGTH CHARACTERISTICS OF HPAASC MIXES ON EXPOSURE TO ELEVATED TEMPERATURES	125
6.3	MICROSTRUCTURAL STUDIES OF HPAASC MIXES SUBJECTED TO SUSTAINED ELEVATED TEMPERATURES	131
6.4	SUMMARY	135
<b>7</b>	<b>FLEXURAL TOUGHNESS CHARACTERISTICS OF HIGH PERFORMANCE ALKALI ACTIVATED SLAG CONCRETE MIXES</b>	138
7.1	GENERAL	138
7.2	MATERIALS AND ITS PROPERTIES	138
7.3	EXPERIMENTAL METHODS	139
7.4	FLOW TESTS ON HFSASC MIXES	140

	7.5	COMPRESSIVE STRENGTHS OF HFSASC MIXES	143
	7.6	FLEXURAL STRENGTHS OF HFSASC MIXES	146
	7.7	FLEXURAL TOUGHNESS CHARACTERISTICS OF HFSASC MIXES	148
	7.8	SUMMARY	157
<b>8</b>		<b>FLEXURAL BEHAVIOUR OF REINFORCED HIGH PERFORMANCE ALKALI ACTIVATED SLAG CONCRETE BEAMS</b>	<b>158</b>
	8.1	GENERAL	158
	8.2	EXPERIMENTAL DETAILS	158
		8.2.1 Casting of the Beam Specimens	159
		8.2.2 Setup for testing the reinforced AAS beams	161
	8.3	FLEXURAL BEHAVIOUR OF REINFORCED HPAASC BEAMS	164
	8.3.1	Load at First Crack and Ultimate Loads	164
	8.3.2	Deflection at First Crack and Ultimate Loads	164
	8.3.3	Span Deflection profiles	167
	8.4	MOMENT CURVATURE RELATIONS FOR HPAASC MIXES	169
	8.5	STRAIN VARIATIONS FOR HPAASC MIXES	171
	8.6	CRACK PATTERNS	174
	8.7	SUMMARY	176
<b>9</b>		<b>ECOLOGICAL ANALYSIS OF CONCRETE MIXES</b>	<b>177</b>
	9.1	GENERAL	179
<b>10</b>		<b>CONCLUSIONS</b>	<b>181</b>
		<b>REFERENCES</b>	<b>188</b>
		<b>APPENDIX - I</b>	<b>211</b>
		<b>APPENDIX - II</b>	<b>213</b>
		<b>APPENDIX - III</b>	<b>216</b>
		<b>PUBLICATIONS BASED ON THE PRESENT RESEARCH</b>	<b>223</b>
		<b>RESUME'</b>	<b>225</b>

## LIST OF FIGURES

<b>Fig. No.</b>	<b>Title</b>	<b>Page No.</b>
2.1	Reaction mechanism of alkali-activated slag	13
2.2	Modulus of sodium silicate solution Vs 28-day strength for different types of slags	16
2.3	First full scale structural application of alkali activated slag concrete	40
3.1	Binders used in HSAASC mixes	44
3.2	Natural River Sand	46
3.3	Fine aggregates used in HSAASC mixes	47
3.4	Coarse aggregates used in HSAASC mixes	49
3.5	Instrument used for SEM and EDX analysis	61
3.6	XRD instrument used in the present study	62
4.1	Initial setting times of AASC mix with different additives	65
4.2	Fast setting behaviour of AASC mix with Lime addition	65
4.3	Slump flow of AASC mix with sodium phosphate placing after 20 minutes	68
4.4	Variation of flow ability of different additives with time	68
4.5	Variation of compressive strength values with different additives	71
4.6	Penetration resistance apparatus with tested concrete sample	73
4.7	Initial setting time of various HSAASC mixes	74
4.8	Different Flow tests performed on HSAASC mixes	75
4.9	Compressive Strength values of HSAASC mix – Calibration Phase	80
4.10	Main effects plots - 28-days compressive strength – Calibration Phase	82
4.11	Predictive capability of Regression equations-Compressive strengths - HSAASC Mixes - Validation phase	84
4.12	Modulii of Elasticity of HSAASC Mixes - Calibration Phase	86
4.13	Split tensile strengths of HSAASC Mixes - Calibration Phase	86
4.14	Predictive Capability of Regression Equations – MOE- 28Days - HSAASC Mixes - Validation phase	87

4.15	Predictive Capability of Regression Equations – Split-tensile strengths - 28 Days – HSAASC Mixes - Validation phase	88
4.16	Flexural strengths of HSAASC mixes – Calibration Phase	88
4.17	Predictive Capability of the Regression Equation – 28-Days -Flexural strengths – Validation Phase.	89
4.18	Water absorption values of HSAASC mixes	90
4.19	SEM Images of Mixes, HSAASC-1, HSAASC-2 and HSAASC-3	91
4.20	SEM Images of Mixes, HSAASC-4, HSAASC-5 and HSAASC -6	92
4.21	SEM Images of Mixes, HSAASC-7, HSAASC-8 and HSAASC -9	92
4.22	SEM Images of Mixes, HSAASC -10, HSAASC -11 and HSAASC -12	92
4.23	SEM Images of Mixes, HSAASC-13, HSAASC -14 and HSAASC -15	92
4.24	Typical EDX analyses results of HSAASC Mixes	94
4.25	XRD details of HSAASC-1 – HSAASC-3	96
4.26	XRD details of HSAASC-4 – HSAASC-6	96
4.27	XRD details of HSAASC-7 – HSAASC-9	97
4.28	XRD details of HSAASC-10 – HSAASC-12	97
4.29	XRD details of HSAASC-13 – HSAASC-15	98
5.1	OPCC specimens exposed to the sulphuric acid solution at 90 days and 103 days	101
5.2	HSAASC mixes after being exposed to sulphuric acid attack for 365 days	102
5.3	HSAASC mixes exposed to 5% H <sub>2</sub> SO <sub>4</sub> solution, before and after the tests – (Age - 365 days)	102
5.4	Weight losses in HSAASC mix on exposure to 5% H <sub>2</sub> SO <sub>4</sub> solution	103
5.5	Residual compressive strengths of HSAASC on exposure to conc. 5% H <sub>2</sub> SO <sub>4</sub> solution	103
5.6	SEM Images of Mix HSAASC- 3 - Before and After Immersion in 5% H <sub>2</sub> SO <sub>4</sub> solution	105
5.7	SEM Images of Mix HSAASC-5 - Before and After Immersion in 5% H <sub>2</sub> SO <sub>4</sub> solution	105

5.8	SEM Images of Mix HSAASC-7 - Before and After Immersion in 5% H <sub>2</sub> SO <sub>4</sub> solution	105
5.9	SEM Images of Mix HSAASC-10 - Before and After Immersion in 5% H <sub>2</sub> SO <sub>4</sub> solution	106
5.10	SEM Images of Mix HSAASC-15 - Before and After Immersion in 5% H <sub>2</sub> SO <sub>4</sub> solution	106
5.11	Results of EDX Analyses - Elemental Compositions of HSAASC Mixes after immersion in 5% Conc. H <sub>2</sub> SO <sub>4</sub> solution	107
5.12	Appearance of (a) OPCC and (b) HSAASC specimen exposed to 10 % MgSO <sub>4</sub> after 365 days	110
5.13	Weight changes in different mixes in 10% MgSO <sub>4</sub> solution	110
5.14	Residual compressive strengths of different mixes on exposure to 10 % MgSO <sub>4</sub> solution	111
5.15	Percentage of compressive strengths loss of different mixes in 10 % MgSO <sub>4</sub> solution	112
5.16	SEM Images of Mix HSAASC 3 - Before and After Immersion in 10% MgSO <sub>4</sub> solution	113
5.17	SEM Images of Mix- HSAASC 5 - Before and After Immersion in 10% MgSO <sub>4</sub> solution	114
5.18	SEM Images of Mix HSAASC 7 - Before and After Immersion in 10% MgSO <sub>4</sub> solution	114
5.19	SEM Images of Mix HSAASC 10 - Before and After Immersion in 10% MgSO <sub>4</sub> solution	114
5.20	SEM Images of Mix HSAASC 15 - Before and After Immersion in 10% MgSO <sub>4</sub> solution	115
5.21	Results of EDX Analysis – Elemental Compositions of HSAASC Mixes after Immersion in 10% MgSO <sub>4</sub> solution	116
5.22	Typical HSAASC mix specimens after the bulk diffusion test.	119
5.23	Comparison of the chloride diffusion coefficients of different HSAASC mixes	119
5.24	RCPT Test Set up – Thematic Sketch	120

5.25	Rapid Chloride Permeability test set-up	121
5.26	Comparison of total charge passed in RCPT tests for different HSAASC mixes	122
6.1	Temperature controlled electric furnace used in the present study	126
6.2	Temperature Controlled Oven – Heating Cycle - Time verses Temperature	127
6.3	OPCC specimen spalled during the exposure to 600°C	127
6.4	HPAASC specimens after exposure to different elevated temperatures	128
6.5	Typical HPAASC specimen after being exposed to 800°C – A closer look	128
6.6	Weight loss for HSS-OPCC mix at different temperatures	129
6.7	Percentage weight loss for various HPAASC mixes at different temperatures.	130
6.8	Compressive strength values of various mixes exposed to different temperatures	130
6.9	Residual Compressive Strength co-efficient of various mixes exposed to different elevated temperatures	131
6.10	SEM Images of Mix-HPAASC-3 at different temperatures	132
6.11	SEM Images of Mix-HPAASC-5 at different temperatures	133
6.12	SEM Images of Mix-HPAASC-7 at different temperatures	133
6.13	SEM Images of Mix-HPAASC-10 at different temperatures	134
6.14	SEM Images of Mix-HPAASC-15 at different temperatures	134
6.15	Typical EDX analyses results of all HPAASC Mixes after being exposed to 800° C	136
7.1	Corrugated Steel Fibers used	140
7.2	Compressive Strength values of mixes at age of 3 and 28 days	146
7.3	Failure of the specimen at mid span cross-section	148
7.4	Distribution of steel fibers at mid span cross-section	148
7.5	Load - Deflection behaviour of HFSOPCC for all specimens with different % of steel fibers	150

7.6	Load - Deflection behaviour of HFSASC-1 for all specimens with different % of steel fibers	150
7.7	Load - Deflection behaviour of HFSASC-2 for all specimens with different % of steel fibers	151
7.8	Load - Deflection behaviour of HFSASC-3 for all specimens with different % of steel fibers	151
7.9	Load - Deflection behaviour of HFSASC-4 for all specimens with different % of steel fibers	152
7.10	Load - Deflection behaviour of HFSASC-5 for all specimens with different % of steel fibers	152
7.11	Ultimate Flexural Strength (28-days) of different steel fiber reinforced mixes	153
7.12	Evaluation of Toughness Index - $T_{BH2}$ (Barr and Hasso) and $T_{ACI}$ (ACI)	154
7.13	Toughness indices of HFSASC Mixes – Barr and Hasso Method	158
7.14	Toughness indices of HFSASC Mixes – ACI Method	158
8.1	Reinforcement details provided, and the loading arrangements for testing the RC beam	162
8.2	Formwork and reinforcement cage used for casting the beam specimens	163
8.3	Experimental setup for the testing the beams	164
8.4	LVDTs along with the data acquisition system	165
8.5	Mid span deflections for reinforced HSS-OPCC and HPAASC beams	167
8.6	Deflection profile of beams at first crack loads	170
8.7	Deflection profile of beams at ultimate loads	170
8.8	Moment curvature relations for the test beams	173
8.9(a)	Variations of Strains for mix HSS-OPCC	174
8.9(b)	Variation of Strains for mix HPAASC- 3	174
8.9(c)	Variation of Strains for mix HPAASC-5	175
8.9(d)	Variation of Strains for mix HPAASC-7	175
8.9(e)	Variation of Strains for mix HPAASC-10	176
8.9(f)	Variation of Strains for mix HPAASC-15	176
8.10	Crack Patterns for all the test beams	178

## LIST OF TABLES

<b>Table No.</b>	<b>Title</b>	<b>Page No.</b>
1.1	Targeted criteria for achieving HPAASC mixes	5
2.1	History of Alkali-activated cement systems and alkaline cements	12
2.2	Deterioration mechanism of cement paste at different temperatures	33
3.1	Properties of Ordinary Portland Cement used - 53 Grade	44
3.2	Chemical and Physical properties of GGBFS and Fine Quartz powder	45
3.3	Properties of fine aggregates used in the study	47
3.4	Chemical Composition of fine aggregates used in the study	47
3.5	Results of sieve analysis - Fine aggregates	48
3.6	Physical Properties of Coarse aggregates used in the study	49
3.7	Chemical Composition - EAF slag	49
3.8	Results of sieve analysis - Coarse aggregates (MAS 12.5mm)	50
3.9	Properties of super-plasticizer used - Master Glenium ACE 30 (JP)	51
3.10	Properties of liquid Sodium silicate	51
3.11	Properties of Sodium hydroxide (97% purity)	52
3.12	Input parameters for the Taguchis method	54
3.13	Mix-Parameters for the HSAASC Mixes - Calibration phase	55
3.14	Details of HSAASC mixes – Calibration phase - Quantities in kg/m <sup>3</sup>	56
3.15	Mix design details of HSS - OPCC mix - Quantities in kg/m <sup>3</sup>	57
3.16	Mix-Parameters for the HSAASC Mixes - Validation phase	57
3.17	Details of HSAASC mixes – Quantities in kg/m <sup>3</sup> - Validation phase	58
3.18	Details of Test Specimens used for various tests	59
4.1	Details of trial AAS Concrete mix in kg/m <sup>3</sup>	64
4.2	Details of different additives along with their dosages for kg/m <sup>3</sup>	64
4.3	Compressive strengths of AASC mix with different additives	70
4.4	Flow ability Properties of HSAASC mixes – Calibration Phase	77
4.5	Flow ability Properties of HSAASC mixes – Validation Phase	78

4.6	Response Table for compressive strength at 28 Days -Means of Means - Calibration Phase	81
4.7	Compressive strengths of HSAASC mixes – Validation Phase	83
4.8	Modulii of Elasticity and Split Tensile strength values of HSAASC mixes - Calibration mixes	85
4.9	Atomic percentage of major elements in HSAASC mixes - EDX	95
5.1	Results of EDX Analyses – Atomic percentages of elements in HSAASC mixes after immersion in 5% conc. H <sub>2</sub> SO <sub>4</sub> solution	108
5.2	Results of EDX Analyses - Atomic percentages of elements in HSAASC mixes after immersion in 10% MgSO <sub>4</sub> solution.	117
5.3	Chloride permeability classifications as per ASTM standards	121
5.4	Parameters criteria for assessing HPAASC mixes	124
6.1	Results of EDX Analyses - Atomic percentages of major elements in HPAASC mixes after exposure to 800° C	137
7.1	Properties of Corrugated Steel Fibers	140
7.2	Mix Details for HFSASC mixes.	142
7.3	Flow ability tests of HFSASC mixes	143
7.4	Compressive strengths of HFSASC mixes	145
7.5	Calculation of Toughness indices for HFSOPC-based control concrete mixes	156
7.6	Toughness Indices of HFSASC Mixes	157
8.1	Properties of steel reinforcement bars used	161
8.2	Load at first crack and ultimate load for HSS-OPCC and HPAASC	168
8.3	Mid span deflections at first crack and ultimate load	169
8.4	Ductility values of all the HPAASC beams	171
8.5	Ultimate moment and curvatures for HSS-OPCC and HPAASC beams	172
8.6	Test Results of the crack profiles	177
9.1	Values for EE and ECO <sub>2e</sub> for all the materials used in concrete mixes	180
9.2	Total Embodied energy and Embodied CO <sub>2</sub> emitted for various concrete mixes	181

.....

## NOMENCLATURE

AAFS	Alkali Activated Fly-ash/Slag
AAM	Alkali Activated Materials
AASC	Alkali Activated Slag Concrete
AASFC	Alkali Activated Slag Fly-ash Concrete
AASP	Alkali Activated Slag Paste
ACI	American Concrete Institute
AgNO <sub>3</sub>	Silver Nitrate
ASTM	American Society of Testing and Materials
BOF	Blast Oxygen Furnace
Ca(OH) <sub>2</sub>	Calcium Hydroxide
Ca <sub>3</sub> (PO <sub>4</sub> ) <sub>2</sub>	Tri Calcium Phosphate
CaO	Calcium Oxide
C-A-S-H	Calcium Alumino Silicate Hydrate
C-N-S-H	Calcium Sodium Silicate Hydrate
CF	Carbon Fiber
CS	Copper Slag
C-S-H	Calcium Silicate Hydrate
DOE	Design of Experiments
EAF	Electric Arc Furnace
ECO <sub>2e</sub>	Embodied Carbon-di-oxide
EDX	Energy Dispersive X-ray
EE	Embodied Energy
EFNARC	The European Federation of Specialist Construction Chemicals and Concrete Systems
FNS	Ferro Nickel Slag
GGBFS	Ground Granulated Blast Furnace Slag
GPC	Geopolymer Concrete
H <sub>3</sub> PO <sub>4</sub>	Phosphoric Acid
HFSASC	High Performance, Fiber Reinforced, Self-compacting Alkali-activated Slag Concrete

HFSOPCC	High Performance, Fiber Reinforced, Self-compacting Ordinary Portland Cement Concrete
HM	Hydration Modulus
HMNS	High Magnesium Nickel Slag
HPAASC	High Performance Alkali Activated Slag Concrete Mixes
HP-OPCC	High Performance Ordinary Portland Cement Concrete
HRWR	High Range Water Reducing
HSAASC	High Strength Self-compacting Alkali Activated Slag Concrete Mixes
HSS - OPCC	High Strength Self- Compacting Ordinary Portland Cement Concrete
IS	Indian Standard
IWA	Initial Water Absorption
K <sub>b</sub>	Basicity Co-efficient
KOH	Potassium Hydroxide
LD	Linz-Donawitz
LSS	Liquid Sodium Silicate
LVDT	Linear Variable Differential Transformers
MAS	Maximum Aggregate Size
MK	Metakaolin
M <sub>s</sub>	Activator Modulus
M-S-H	Magnesium Silicate Hydrate
NA	Neutral Axis
Na <sub>2</sub> CO <sub>3</sub>	Sodium Carbonate
Na <sub>2</sub> O	Sodium Oxide
Na <sub>2</sub> SO <sub>4</sub>	Sodium Sulphate
NaCl	Sodium Chloride
NaOH	Sodium Hydroxide
N-A-S-H	Sodium Alumino Silicate Hydrate
NSSM	Non-Steady State Migration
OPC	Ordinary Portland Cement
OPCC	Ordinary Portland Cement Concrete

PCE	Poly-Carboxyl Ether
PVA	Poly Vinyl Alcohol
RCPT	Rapid Chloride Permeability Test
RHA	Rice Hush Ash
SBA	Sugarcane Bagasse Ash
SCC	Self-Compacting Concrete
SEM	Scanning Electron Microscope
SF	Silica Fume
SWA	Saturated Water Absorption
VSI	Visual Stability Index
w/b	water to binder ratio
XRD	X-Ray Powder Diffraction

.....



# CHAPTER 1

## INTRODUCTION

### 1.1 GENERAL

In the modern world, issues associated with global warming and resulting climatic changes are gaining much importance. Global warming is caused by the increased emission of greenhouse gases including Methane and Carbon Dioxide to the atmosphere. The continuous depletion of the protective ozone layer has been an issue of concern, Again there is this issue of continuous depletion of various non-renewable natural resources, most often as the raw materials for many industries.

Concrete is the most extensively used construction material and the demand for the same is continuously increasing, with the requirements of developing the infrastructural facilities. Production of increased quantities of Portland cement, the major constituent in the production of concrete, is leading to large-scale exploitation of the natural reserves of lime-stones, clays and coal. Again there is an expected release of about 0.8-1.0 tonne of carbon dioxide to the atmosphere, for production of every one tonne of cement. Large amounts of natural, crushed aggregates are used as coarse aggregates and river sand, generally extracted from the river beds is used as fine aggregate in production of concrete (almost 70-80% of its bulk). Their increased use is causing lot more stress to the environment. Considering the crucial importance of development of concrete infrastructure for the growth of the country, it has now become inevitable to look for alternate, greener, more durable, less energy-intensive and economical construction materials with lower carbon foot-prints, for use in building the infrastructural facilities.

In view of the above aspects, the search is on for possible alternatives to ordinary Portland cement for use as the primary binder for concrete production. Some of the alternative construction materials have been developed using industrial by-products such as fly ash, ground granulated blast furnace slag (GGBFS), Metakaolin etc. Development of alternate binder systems, using the by-products from various industries, which are generally rich in alumina and silica, in less energy-intensive

processes, with low carbon-footprint, is then a definite, right step in the path of sustainability.

In this context, developments of alkali activated concrete mixes have attracted the attention of concrete researchers in recent years. One of the main drivers for the development of alkali activated concrete based-materials is their environmental credentials. When cured at ambient temperature, no carbon dioxide synthesis is taking place except a small percentage of carbon dioxide emission that can be attributed to the production of the alkali activators. Again, unlike concrete mixes with blended cements and/or blended, site-produced concrete wherein any of the industrial wastes such as fly-ash, ground granulated blast furnace slag (GGBFS), rice-husk ash (RHA) are used as partial replacement/additional ingredient, no Portland cement clinker is used in alkali-activated concrete mixes. Usually materials rich in alumina and/or reactive silica are used as the starting materials in the production of alkali-activated cement systems. These, in general, cannot react directly with water and they require an activator for their activation process. The alkaline environment required for such activation reactions of materials like GGBFS and fly ash is provided by alkaline components such as caustic alkalis, silicate salts and non-silicate salts of weak acids (Bakharev et al. 1999).

These binder systems have the potential of using large volumes of industrial by-products such as Fly-ash and GGBFS, which then leads to an economical and ecofriendly solution methodology for the safe disposal also. Production of about 2.5 cubic meters of high quality geopolymer concrete approximately requires one tonne of high quality low-calcium fly ash and the bulk cost of alkaline activators needed to manufacture this concrete is cheaper than the bulk cost of one ton of production of Ordinary Portland cement. Given the fact that fly ash is considered as a waste material, the low calcium fly ash-based geopolymer concrete is, therefore, cheaper than the Ordinary Portland cement concrete (Hardijito and Rangan 2005). Partial replacement of fly ash with GGBFS in the above mixes may further prove to be more effective by avoiding heat curing (Narasimhan et al. 2011).

GGBFS is used as the major starting material in the production of alkali activated slag concrete (AASC) mixes. GGBFS is obtained as an industrial by-product from steel

industry and is commercially available in the market. No heat-processing of this material is necessary while producing AASC mixes, leading to no emission of carbon dioxide. Only a negligible amount of emission of Carbon dioxide may be associated with the industrial production of the activator solution required for activating the slag.

The current practice of using very large amounts of natural aggregates, both as fine and coarse aggregates, which act as inert filler materials, is highly unsustainable. About 70% volume of concrete is composed of aggregates and availability of good aggregates in any given location is proving to be scarce and costly. Hence the search is on for suitable alternate materials for possible use as aggregates in concrete mixes. Herein the researchers are again trying to check the possibilities of using different types of industrial waste materials such as stone powder (quarry dust), bottom ash, waste glass powder, foundry sand, ore tailings, industrial slags, waste plastics etc., as partial/full replacements of natural aggregates in the concrete mixes.

A large amount of steel is produced in the country as it is a basic material of construction for developing all manufacturing units, transportation vehicles, railway engines and coaches etc. Large percentage of total steel produced in the country is also used as reinforcement bars in RCC Constructions. Production of Iron and steel is always associated with production of large amounts of varieties of slags, economical disposal of which is again a challenge to the Steel Industry. According to National Slag Association, USA, these materials, with some processing, can be advantageously used as aggregates, as partial/full replacement to for replacement to natural aggregates in concrete mixes, leading to sustainability in concrete and steel industry. For example, steel slag or the Linz-Donawitz (LD) slag is produced during the conversion of raw iron into steel using LD process and the byproduct obtained after this process is termed as Blast Oxygen Furnace slag (BOF) slag. Further processed slag sand and Electric arc furnace slag are also made available in both coarser and finer fractions, which can be used as aggregates in concrete systems.

So far, research studies have been carried out on normal-strength alkali activated slag concrete mixes (say in the range of 45 - 55 MPa) using GGBFS as the source

material, and conventional aggregates-natural crushed stone aggregates as coarse aggregates and river sand as fine aggregates. Sometimes other additives/alternatives are also used in such mixes. Research studies on alkali activated slag concrete mixes with steel slag as aggregates (Fine aggregates and coarse aggregates) are still scarce.

## **1.2 OBJECTIVES OF THE PRESENT RESEARCH**

In the present research work, a detailed experimental investigation is carried out for the development of High Performance Alkali activated slag concrete mixes using industrial wastes, both for their binder phase and the aggregate phase. The main objectives of the present research work are identified as follows

- Development of a class of High Strength, Self-Compacting, Alkali Activated Slag Concrete (HSAASC) mixes incorporating steel slag aggregates.
- To ascertain the durability characteristics of the above class of mixes on exposure to aggressive chemical attack. Performance on exposure to acids, sulphates and chlorides to be assessed.
- Evaluation of residual strengths of high-performance alkali-activated slag concrete (HPAASC) mixes when subjected to sustained elevated temperatures. Performance on exposure to up to, say 800<sup>0</sup>C is evaluated.
- Evaluation of toughness characteristics of high-performance alkali-activated slag concrete (HPAASC) mixes on the incorporation of steel fibres.
- Evaluation of performance of structural elements made of, high-performance alkali-activated slag concrete (HPAASC) mixes with rebar reinforcements.

## **1.3 CRITERIA FOR EVALUATING HIGH PERFORMANCE ALKALI ACTIVATED SLAG CONCRETE (HPAASC) MIXES**

HPAASC mixes were developed based on the criteria provided in Table 1.1.

**Table 1.1 Targeted criteria for achieving HPAASC mixes**

TARGETED CRETERIA		LITERATURE HP-OPCC MIXES
<b>1</b>	<b>Compressive Strength</b>	$\geq 70\text{MPa}$
<b>2</b>	<b>Flexural Strength</b>	$\geq 6.0\text{ MPa}$
<b>3</b>	<b>FLOW ABILITY (EFNARC 2002)</b>	
<b>a</b>	Slump Flow Test	$\geq 650\text{ mm}$
<b>b</b>	T <sub>50</sub> cm	$\leq 6\text{sec}$
<b>c</b>	V-Funnel Test	<b>6 – 12 sec</b>
<b>d</b>	L-Box test	$\geq 0.85$
<b>e</b>	J-Ring test	$\leq 12\text{mm}$
<b>f</b>	Visual Stability Index (VSI)	<b>0</b>
<b>4</b>	<b>INITIAL SETTING TIME</b>	$\geq 3\text{ Hours}$
<b>5</b>	<b>DURABILITY</b>	
<b>A</b>	Acid – 5% H <sub>2</sub> SO <sub>4</sub> - 365 DAYS	<b>No Complete Deterioration</b>
<b>B</b>	Sulphate - 10 % MgSO <sub>4</sub> 365 DAYS	
	a. Mass Loss	$\leq 2\%$
	b. Loss in compressive strength	$\leq 25\%$
<b>C</b>	Bulk Diffusion test Chloride Ion Penetration	$\leq 2 \times 10^{-12}\text{ m}^2/\text{sec}$ <b>Very Good</b>
<b>D</b>	Rapid Chloride Permeability test Chloride Ion Penetration	$\leq 1000\text{ Coulombs}$ <b>Very Low</b>

#### **1.4 SCOPE OF THE PRESENT WORK**

The current study aims at the production of greener, sustainable, high performance concrete mixes with the major ingredients (binder and aggregates) used in their production derived from the industrial by-products. Non-use of Portland cement in the current research provides a real value-addition from an environmental view-point. Use of appropriate sized fractions of processed slag, both as fine aggregates and coarse aggregates in these mixes decreases a great load on the natural resources. Again dry curing at ambient temperatures required for these mixes can lead, not only to large savings in the energy, but also to large savings in water specially in arid and in desert environments. As will be brought out in the next chapter, not much research has been carried out, till date, on development and performance evaluation of such cost-effective, greener and sustainable concrete mixes, with successful applications at the industry level.

Taking cognizance of the various aspects involved, an attempt is being made herein to develop high performance alkali activated slag concrete mixes incorporating steel slags as both fine aggregates and coarse aggregates. Higher performance of the mixes in terms of their flow ability parameters in their fresh state (mixes to be self-compacting), mechanical strength parameters in hardened state (compressive strengths more than 70 MPa) and durability on exposure to aggressive chemical environments are being targeted.

For developing the high strength, self-compacting alkali activated slag concrete mixes, initially large numbers of trials were carried out for fixing the range of binder contents, dosage of sodium oxide and water to binder ratio. These concrete mixes were developed using GGBFS as principal binder along with fine amorphous quartz powder, them taken in the proportions 3:1. Combinations of slag sand and quartz sand were used as fine aggregates while 12.5 mm down-sized, electric-arc furnace slag (EAF slag) aggregates were used as the coarse aggregates. In order to reduce the experimental efforts, Taguchi's design of experiments methodology was employed. Further, in order to improve the initial setting times of all the AASC mixes, additional trials were conducted with number of chemical additives as possible retarders.

Based on the results of such trials, the best performing retarder was identified and the same, at its optimum dosage, was incorporated in all the alkali activated slag concrete mixes developed. A total of fifteen mixes were formulated in two phases – The initial nine mixes formed the calibration phase and the results of experiments with remaining six mixes were considered in the validation phase along with a control OPC based reference concrete mix. All these mixes were evaluated for their properties both at fresh-state (flow ability as self-compacting concrete) and hardened-states (mechanical strengths, and water absorption tests) as per standard test procedures. Multi-linear regression equations were developed using the Minitab software for all the various mechanical properties, based on the results for the mixes in the calibration phase. The predictive capabilities of such equations were also verified using the results of tests on the mixes in the validation phase. Further detailed microstructural studies were carried out on all the fifteen mixes by performing the analyses using SEM, EDX and XRD.

In the next phase of the experiments, the best five of the above fifteen mixes, in terms of their better flow ability characteristics as well as higher mechanical strength properties were further evaluated for their durability characteristics. The durability of those five concrete mixes, in terms of their resistances to chloride ion penetration, and degradation on exposure to long-term exposure to concentrated sulphuric acid and magnesium sulphate solutions, is investigated. Also the strength-retention capabilities of these concrete mixes on exposure to sustained elevated temperatures (upto 800<sup>0</sup>C) are studied in detail. Further microstructural studies were carried out by performing SEM and EDX analyses on the test samples of each of the five mixes, after their exposure to acid and sulphate environments, as well as to elevated temperature performance.

In order to improve the ductility behaviour of these high-strength concrete mixes, steel fibers were also added to these mixes and toughness characteristics of fiber-reinforced HPAASC beams were also evaluated. Again, In order to verify the applicability of these concrete mixes in structural elements, flexural performances of reinforced concrete beams cast with these mixes were also studied. Lastly, general assessments of the

ecological analysis of the present class of AASC mixes, as compared to conventional OPC-based reference concrete mix were carried out.

## **1.5 ORGANIZATION OF THE THESIS**

This thesis is presented in ten chapters. A comprehensive list of references follows along with three Appendices.

### **CHAPTER 1**

This chapter gives brief note on alkali activated slag concrete mixes; need and significance, objectives and scope of the present research work.

### **CHAPTER 2**

A comprehensive literature review has been carried out to collect adequate information about alkali activated concrete with different binders, alkaline solution, fine and coarse aggregates and other additives. A review of research works carried out so far on fresh concrete properties, mechanical strength and durability properties and elevated temperature performance of alkali activated concrete is presented. The limited studies on flexural performance of beams made of such mixes and reinforced by tension reinforcement (rebars) are also reviewed.

### **CHAPTER 3**

This chapter provides all the details of various materials used, preliminary investigations on those materials for their characterization, tests carried out, test methodologies adopted, optimization of design parameters of the concrete mixes etc.

### **CHAPTER 4**

This chapter presents the results and discussions on the development of high-strength, self-compacting, alkali activated slag concrete mixes, based on Taguchi's design of experiments, with their flow ability characteristics as well as mechanical properties. The development and validation of the regression equations developed for prediction of mechanical strengths is also discussed. Results of detailed microstructural studies like SEM, EDX and XRD conducted on the concrete mixes developed herein are also discussed.

## CHAPTER 5

This chapter deals with the detailed discussions of results of durability tests conducted on the five best-performing high-strength, self-compacting, alkali activated slag concrete mixes. Further attempts were made to identify the micro-structural changes, in terms of results of SEM and EDX analyses of the various durability test samples of each of these mixes and such results are discussed in this chapter.

## CHAPTER 6

This chapter presents the results and discussions of residual strength characteristics of high performance alkali activated slag concrete mixes when subjected to sustained elevated temperatures. Detailed microstructural studies on all these mixes by performing the analyses using SEM and EDX.

## CHAPTER 7

This chapter presents the results and discussions on flexural toughness characteristics of steel fiber reinforced, high- performance, alkali activated slag concrete mixes.

## CHAPTER 8

This chapter presents the results and discussion thereof, on flexural performance of HPAASC beams reinforced with tension reinforcement in the form of steel bars.

## CHAPTER 9

An assessment of the ecological benefits of HPAASC mixes is made, based on the limited data available, and the results presented in this chapter indicate that the large-volume use of the present class of HPAASC mixes would prove feasible and sustainable, in terms of large-scale infrastructural projects in a developing country like India.

## CHAPTER 10

Observations and conclusions drawn based on the present investigation and, recommendations there-of are presented in this last chapter. Again a few topics with potential scope for further research are also identified.

## **CHAPTER 2**

### **LITERATURE REVIEW**

#### **2.1 GENERAL**

Alkali activated materials (AAM) is their broadest classification, basically consists of a binder system derived from the reaction of an alkali metal ion with a solid precursor (Buchwald et al. 2003, Shi et al. 2006). The obtained alumino silicate based solid reaction product may be a calcium silicate as in alkali-activation of more conventional clinkers or an more aluminosilicate-rich precursor such as a metallurgical slag, natural pozzolan, fly ash or bottom ash. Alkali hydroxides, silicates, carbonates, sulphates, aluminates or oxides are the major sources of alkali generally used – essentially a substance soluble in water which can supply alkali metal cations, raise the pH of the reaction mixture and accelerate the dissolution of the solid precursor (Wagh 2004). Geopolymers are, in many instances, viewed as a subset of AAMs, where the binding phase is almost exclusively aluminosilicate and highly coordinated (Rahier et al. 1997, Davidovits 1991, Duxson et al. 2005). To form such a gel as the primary binding phase, the available calcium contents in the reacting components will have to be low, to enable formation of a pseudo-zeolitic network structure (Provis et al. 2005) rather than the chains characteristic of calcium silicate hydrates. The activator will usually be an alkali metal hydroxide or silicate (Provis 2009). Low-calcium fly ashes and calcined clays are the most prevalent precursors used in geopolymer synthesis (Duxson et al. 2007, Provis and Van Deventer, 2014).

#### **2.2 HISTORY OF GEOPOLYMERS AND ALKALI ACTIVATED CEMENTITIOUS SYSTEMS**

The fact that powdered blast-furnace slag can be stabilized using caustic soda was first demonstrated by Kuhl way back in 1908, with reference to the setting behaviour of mixtures of ground slag powder and caustic potash solution. Purdon (1940) did the first extensive laboratory study on clinker-less cement consisting of slag and caustic soda solution produced by using a base and an alkaline salt. Glukhovsky (1959) was the first to discover the possibility of producing binders using calcium-free,

aluminosilicates (clays) and solutions of an alkaline metal. He called the binders as soil cements and the corresponding concretes as soil silicates. In 1979, Davidovits produced binders using alkalis mixed with a burnt mixture of limestone, kaolinite and dolomite and called them as “geopolymers” due to their polymeric structure. Krivenko (1994) classified the alkali-activated cementitious materials based on the composition of the hydrated products. Accordingly the alkaline aluminosilicate systems were called as geo-cements emphasizing the similarity of their formation process to the geological process of formation of natural zeolites in alkaline earth systems the hydration products are low, basic calcium silicate hydrates (C-S-H). Davidovits (1994) proposed that alkaline liquids can be used with silicon and aluminium-rich source materials, either with a geological origin or from industrial byproducts such as Fly ash, GGBFS and rice husk ash. Portland cement hardens in an alkaline environment and the same happens during the pozzolanic reaction which means that the designation ‘alkaline cement’ is not very accurate; Davidovits even calls Portland cement as alkali activated calcium silicate.

### **2.3 ACTIVATION MECHANISMS OF ALKALI ACTIVATED SLAG SYSTEMS**

The important historic developments of alkali activated binders are summarized by Roy (1999) as shown in Table 2.1. In the activation process of slag (GGBFS), as postulated by (Wang et al 1994), the reaction begins with the attack of alkali on slag particles which break the outer layer and then continues as poly-condensation of reaction products. The initial reaction products are formed due to the processes of dissolution and precipitation. At later stages, however, a solid state mechanism is followed where the reaction occurs on the surface of formed particles dominated by slow diffusion of the ionic species into the unreacted core. In the initial stages of hydration, alkali cations ( $R^+$ ) behave like a mere catalyst in the cation exchange with the  $Ca^{2+}$  ions as per the following reactions, (Krivenko 1994 and Glukhovsky 1994).



**Table 2.1 History of Alkali-activated cement systems and alkaline cements**

<b>Authors</b>	<b>Year</b>	<b>Significance</b>
Feret	1939	Slags used for cement
Purdon	1940	Alkali-slag combination
Glukhovsky	1959	Theoretical basis and development of alkaline cements
Glukhovsky	1965	First called Alkaline cements because natural substances used as components
Davidovits	1979	Geopolymer term – emphasizes greater polymerisation
Malinowski	1979	Ancient aqueduct characterized
Forss	1983	F-Cement (Slag – Alkali -Superplasticiser)
Langton and Roy	1984	Ancient building materials characterized (Roman, Greece, Cyprus)
Davidovits and Sawyer	1985	Patent leading to Pyrament
Wang and Scrivener	1985	Slag and alkali activated slag microstructure
Krivenko	1986	D.Sc. Thesis, $R_2O-RO- R_2O_3-SiO_2-H_2O$
Malolepsy and Petri	1986	Activation of synthetic Melilite slag
Malek et al	1986	Slag cement- low level radioactive forms
Davidovits	1987	Ancient and Modern Concretes compared
Deja and Malolepsy	1989	Resistance to chloride shown
Kaushal et al	1989	Adiabatic cured, nuclear waste forms from alkaline mixtures including Zeolite formation.
Roy and Langton	1989	Ancient Concrete analogs
Majumdur et al	1989	$C_{12}A_7$ – Slag activation
Talling and Brandstetr	1989	Alkali activated slag
Wu et al	1990	Activation of slag cement
Roy et al	1991	Rapid setting alkali activated cements
Roy and Silsbee	1992	Alkali activated cements - Overview
Palomo and Glasser	1992	CBC with metakaolin
Roy and Malek	1993	Slag cement
Glukhovsky	1994	Ancient, modern and future concrete
Krivenko	1994	Alkaline Cement

Source: Roy (1999)

While the alkaline cations act as structure-creators, the anions in the solution play a significant role in activation, especially during the early stages, particularly with regard to paste-setting (Fernandez-Jiménez and Puertas, 2001). The descriptive model showing the reaction mechanism is presented in Fig 2.1.

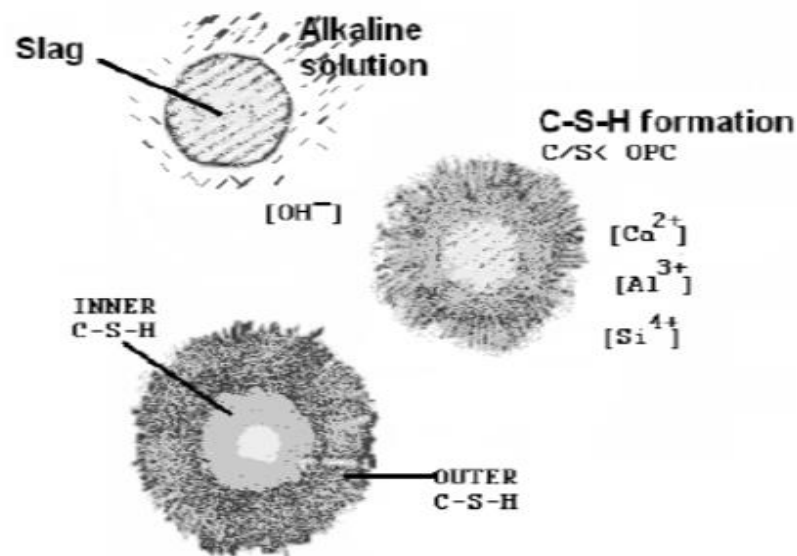


**Fig 2.1 Reaction mechanism of alkali-activated slag**  
**(Fernandez-Jimenez and Puertas 2001).**

The final hydration products in case of activation of slag are similar to the products of OPC hydration i.e. Calcium-Silicate-hydrates (C-S-H), but with low Ca/Si ratio or with substitution of aluminum leading to Calcium aluminosilicate hydrate (C-A-S-H gels). However the rate and intensity of activation of slag differs substantially as compared to that of hydration of OPC. It is reported that the alkalis are not freely available in the pore solution since they are bound to the reaction products thereby negating the potential for alkali-silica reactivity; however this depends on the concentration of alkali used (Fernandez-Jimenez and Puertas 2001).

## 2.4 REQUIREMENTS FOR ALKALI ACTIVATION OF GGBFS

GGBFS is probably the most widely investigated, and the most effective cement replacement material used in concrete manufacturing. It is obtained by finely grinding the granulated blast furnace slag, which in turn is obtained by sudden quenching of molten slag removed from the blast furnace of iron and steel Industry. It mainly consists of oxides of calcium ( $CaO$ ), silica ( $SiO_2$ ), alumina ( $Al_2O_3$ ) and magnesia ( $MgO$ ) along with some other minor oxides in small quantities.

McGannon (1971) quantifies the hydraulic activity of GGBFS in terms of the basicity coefficient ( $K_b$ ) which is the ratio between total content of basic constituents to total content of acidic constituents as given in the equation (2.4)

$$K_b = \frac{CaO + MgO + Fe_2O_3 + K_2O + Na_2O}{SiO_2 + Al_2O_3} \quad (2.4)$$

Wang et al. (1994) and Bakharev et al. (2000) further simplified the equation by excluding the minor components such as  $Fe_2O_3$ ,  $K_2O$ , and  $Na_2O$  (generally less than 1%) in the computation of the basicity coefficient,  $K_b$ .

$$K_b = \frac{CaO + MgO}{SiO_2 + Al_2O_3} \quad (2.5)$$

Based on the basicity coefficient ( $K_b$ ), the GGBFS is classified under three groups - acidic ( $K_b < 0.9$ ), neutral ( $K_b = 0.9$  to  $1.1$ ), and basic ( $K_b > 1.1$ ). Neutral and alkaline based slags are preferred as starting materials for activation in Alkali-activated slag (AAS) binders.

Chang (2003) introduced a parameter termed as hydration modulus (HM) as given in equation (2.6) and suggested that it should be greater than 1.4 in order to ensure good hydration properties.

$$HM = \frac{CaO + MgO + Al_2O_3}{SiO_2} \quad (2.6)$$

## 2.5 ALKALI ACTIVATED SLAG MORTAR AND CONCRETE SYSTEMS

GGBFS has proved to be the most suitable material for alkali activated binders. It is the first industrial by-product to be activated by alkali due to its pozzolanic nature. Most of the application of AAS mixes has taken place in the former Soviet Union, China and

some Scandinavian countries, where the huge impact on the environment in terms of depletion of natural resources such as limestones and other minerals, led to the search for alternative binders. Krivenko (1994) found that alkaline cations play a catalytic role during the early stages of hydration of these slags, involving the interchange of  $\text{Ca}^{2+}$  cations and in the later stages, they themselves combine into the structure to form zeolite-like phases. Taylor (1997) stated that the role of alkalis in alkali activated slag is similar to that in blended GGBFS - OPC cement systems, i.e. to maintain the supply of  $\text{OH}^-$  anions in the system. The hydrated calcium silicate hydrate C-S-H gel with low Ca/Si ratio is the most abundant product formed in the hardened slag-based alkali activated pastes (Bakharev et al 2000).

Brough and Atkinson (2002) found that, while the inner product contains regions of hydrates of AAS mortars having C-S-H gel with higher ratio of Ca/Si (0.9), mixed with higher amounts of magnesium hydrotalcite, the outer product regions have a lower Ca/Si ratio of 0.7 and lower contents of magnesium hydrotalcite. Pan et al. (2003) developed a composite cementitious material with alkali-slag-red mud and solid water glass with modulus 1.2. They concluded that the hardened paste mainly consisted of calcium silicate hydrate (C-S-H) gel, very fine in size, and extremely irregular in shape. According to (Bellmann and Stark 2009), since blast furnace slag contains less lime, calcium hydroxide is not formed during the hydration of the slag particles; instead ettringite and calcium silicate hydrate (C-S-H) with low calcium/silicate ratio are formed.

## **2.6 EFFECT OF DOSAGE AND MODULUS OF ACTIVATOR SOLUTIONS**

Activator modulus ( $M_s$ ) is defined as the mass ratio of  $\text{SiO}_2$  to  $\text{Na}_2\text{O}$  or ( $\text{K}_2\text{O}$ ) in an alkaline activator. The dosage or total mass of  $\text{Na}_2\text{O}$  in the alkaline activator solution includes the sum of mass of  $\text{Na}_2\text{O}$  present in sodium silicate solution and that present in the sodium hydroxide. Glukhovskiy et al. (1980) classified the alkaline activators into six groups according to their chemical composition namely hydroxides, caustic alkalis, Non-silicate strong and weak acid salts, Aluminates, and Alumino-silicates. The majority of the researchers have found that activation with sodium silicate blended with

sodium hydroxide leads to higher strength. Wang et al. (1994) reported that the nature of the activator influences the mechanical strength of alkali activated slag mortars and that use of sodium silicate powder leads to lower performance as compared to that obtained when taken in a liquid form. Further activator modulus plays a major role in the strength development according to the type of slag as shown in Fig 2.2.

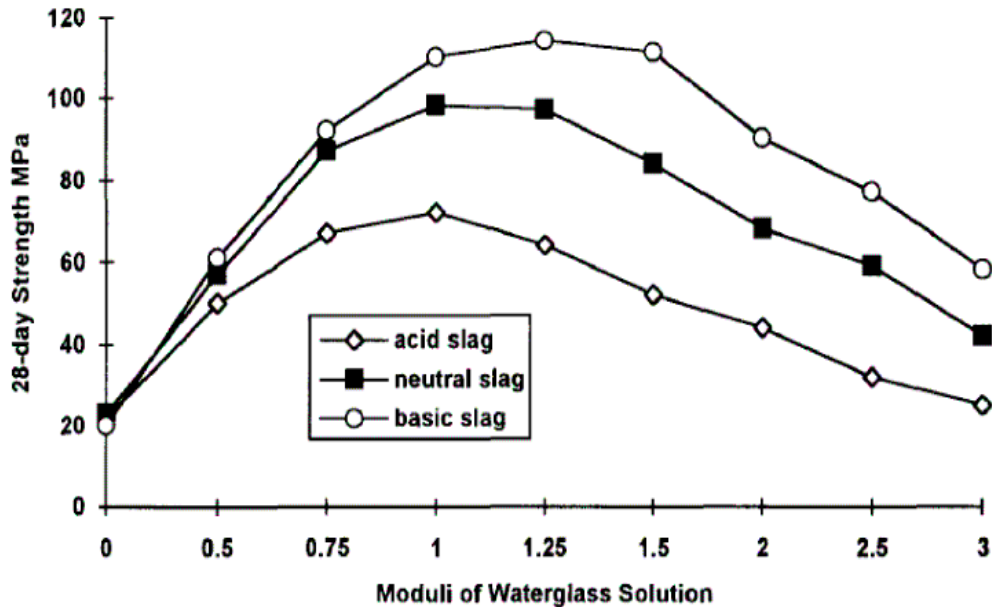


**Fig 2.2 Modulus of sodium silicate solution Vs 28-day strength for different types of slags (Wang et al. 1994).**

The fineness of slag, concentration and nature of activators, and curing temperatures play a major role on the mechanical properties of the alkali activated blast furnace slag mortars as reported by Fernandez-Jimenez et al. (1999). They also noticed that optimum  $\text{Na}_2\text{O}$  concentration in the alkaline activators varied between 3% to 5% by mass of slag. Bakharev et al. (1999) found liquid sodium silicate (LSS) to be a better activator as compared to sodium hydroxide and sodium carbonate activators in terms of the strengths developed in geo-polymer concretes. Bakharev et al. (2000) investigated the effect of admixtures and the type of activator used on the workability of AAS Concrete mixes. They observed that concretes developed using liquid sodium silicate as activator solution exhibited enhanced workability and provided better mechanical properties and also showed reduced shrinkage as compared to normal OPC-based concrete.

Puertas et al. (2000) investigated the strength behaviour of activated fly ash-based cements blended with blast furnace slag with different proportions, using sodium hydroxide solution. They concluded that increase in the slag content and molarity of NaOH solution resulted in an increase in the compressive strength. Again slag cements activated with sodium silicate solution with modulus varying in the range of 0.6 to 1.5, and with appropriate dosage of Na<sub>2</sub>O will provide higher compressive strengths as compared to Portland cement-based concretes (Krizan and Zivanovic 2002).

The chemical composition in the reaction system plays a major role in determining the physical and mechanical properties along with fire resistance characteristics of granulated blast furnace slag-based geopolymer systems (Cheng and Chiu 2003). Hardijito and Rangan (2005) observed that, at a constant ratio of water glass to sodium hydroxide maintained at 2.5, increase in molarity of sodium hydroxide solution increased the strength of geopolymer concrete mixes.

## **2.7 WORKABILITY OF ALKALI ACTIVATED COMPOSITES - INFLUENCE OF ADMIXTURES.**

Collins and Sanjayan (1999) observed that the partial replacement of slag with ultra-fine fly ash significantly improved the workability and setting action of AASC mixes at early stages. Addition of lignosulphonate admixture showed increase in workability of the AASC mixes with liquid sodium silicate or for combined (NaOH+Na<sub>2</sub>CO<sub>3</sub>) activators. Addition of naphthalene formaldehyde superplasticiser, showed increase in workability in the initial stages, but quick setting occurred at the later stages (Bakharev et al. 2000). Palacios et al. (2009) observed that the dosages of the super-plasticizers required to attain similar reduction in the yield stress was about ten times lower than for ordinary Portland cement as compared with sodium hydroxide activated slag pastes.

Cahit et al. (2013) observed that the higher percentage of sodium present in the NaOH and sodium silicate activators led to the development of higher workability and strengths of slag pastes; however setting time were rapidly decreased.

Jang et al. (2014) investigated the fresh and hardened properties of alkali-activated fly-ash/slag pastes with polycarboxylate-based and naphthalene-based super plasticizers. The polycarboxylate-based superplasticiser showed a retarding effect on alkali-activated fly ash/slag pastes and improved the workability more significantly than naphthalene-based superplasticiser. The rheological behaviour in AAS pastes activated with NaOH alone or combined with  $\text{Na}_2\text{CO}_3$  were similar to the rheology observed in OPC pastes, and fit the Bingham model. Conversely, the AAS pastes activated with water glass fit the Herschel–Bulkley model and their rheology proved to depend on both the activator modulus and the dosage of sodium oxide (Puertas et al. 2014). The study conducted by Ellis et al. (2016) showed that initial setting times and compressive strengths of the materials are highly dependent on the composition of the starting materials, alkaline solution and its admixtures.

## **2.8 MECHANICAL PROPERTIES OF ALKALI ACTIVATED COMPOSITES**

Criado et al. (2007) studied in detail, the alkali activation of fly ash pastes with four different alkaline solutions having different soluble silica contents.  $\text{Na}_2\text{O}$  dosages upto 8% by weight of binder, were used to activate soluble silica contents, with sodium alumino-silicate hydrate (NASH) gel as the primary product. Based on the microstructural studies, they concluded that the amount of gel formed has a decisive effect on the mechanical strength developing in the material. Cengiz et al. (2009) showed that an increase in sodium concentration of the activators in general, results in an increase in all of compressive, flexural and tensile strengths of AAS mortars and also suggested that there is an optimum ratio to obtain highest compressive and tensile strengths. Rattanasak and Chindaprasirt (2009) studied the leaching of  $\text{SiO}_2$  and  $\text{Al}_2\text{O}_3$  by mixing fly-ash with NaOH solution for different time intervals. They found that solubility of fly-ash based geopolymer mortars depended on concentration of NaOH and duration of mixing. They developed geopolymer mortar with a strength upto 70 MPa with a mixture made with a 10M NaOH solution and ratio of sodium silicate to sodium hydroxide maintained at one.

Mishra et.al (2008) conducted a series of experiments on fly- ash based alkali activated concrete mixes by varying the concentration of NaOH and heat-curing time. Performance of mixes produced with different NaOH concentrations (8M, 12M, and 16M) and periods of heat-curing at 60°C (24hrs, 48hrs and 72hours) were observed. Compressive strengths up to 46 MPa were obtained with curing at 60°C.

Ravikumar et al. (2010) showed that, while the concentration of activator solution has a major influence on the compressive strength of the activated concretes made with fly-ash, it is the activator to binder ratio influences the compressive strength of activated GGBFS concretes the most.

In the studies by Guo et al. (2010), high compressive strengths upto 64 MPa were obtained with fly-ash based alkali activated concrete, using the combination of sodium hydroxide and sodium silicate as activator solutions, using initial heat-curing at 75°C for 8 hours followed by curing at 23°C for 28 days. Manjunath et al. (2011) developed geopolymer mortars with better strengths at ambient curing; the strengths increase with the increase in the GGBFS content; but it was found that addition of small quantity of silica fume had no significant effect on the strength development characteristics. Lee and Lee (2013) investigated the setting and mechanical strength properties of alkali-activated fly ash/slag concrete mixes produced at room temperature. Based on their test results, they concluded that, with increases in the amounts of slag and NaOH solution, there was a decrease in the setting time of the concrete mixes.

Keun et al. (2012) concluded that the calcium hydroxide based AAS concrete mixes showed an enhanced workability, delayed slump loss and so also increasing compressive strengths with w/b ratio as that observed in OPC concretes.

Didamony et al. (2012) showed the influence of using sea water on the properties of activated slag pastes mixed with sodium hydroxide and sodium silicate liquid (6 by wt. % of slag). Their results have revealed that the bulk density and compressive strength were increased by increasing sodium silicate content in the presence of NaOH.

Chi and Huang (2013) used alkali-activated fly ash/slag (AAFS) mortars with various ratios of fly-ash to slag. They used constant Sodium oxide (Na<sub>2</sub>O) concentrations of 4%

and 6% (by total weight of cementitious material), and modulus of one. The total liquid/binder ratio was kept at a constant of 0.5. Except drying shrinkage, better engineering properties such as compressive and flexural strengths and lower water absorption were obtained in AAFS mortars as compared with OPC based mortars.

Jin et al. (2014) studied the strength and the drying shrinkage characteristics of reactive MgO-modified AAS (MAAS) pastes, measured up to 90 days. They concluded that MgO, with high reactivity, accelerated the early hydration of AAS, while MgO with medium reactivity had little effect on the characteristics.

Experimental results of Yang et al. (2015) show that the addition of nano-TiO<sub>2</sub> enhances the mechanical strength, and decreases the shrinkage of alkali-activated slag pastes (AASP). Results of microstructural studies therein also demonstrated that the addition of nano-TiO<sub>2</sub> into the AASP results in more hydration products and denser structure, leading to a large reduction of the total porosity of AASP, possibly due to enhanced hydration of AASP. Bernal (2015) investigated the effects of increased activator dose on the properties of alkali-activated slag/metakaolin based concrete blends in fresh and hardened states. While there were no significant losses in the compressive strengths due to higher activator dose, decreased permeability characteristics were recorded.

Ground granulated blast furnace slags from different manufacturing locations were selected and were activated using Calcium oxide powder by Yeonung et al. (2016). They studied the influence of the slag characteristics on strength development and the reaction products. Despite the seemingly similar characteristics of the slags, each slag developed significantly different strengths varying from 25 to 52 MPa at 28-days. The main reaction products obtained were C-S-H and calcium hydroxide. Ettringite was also found in case of raw slag with calcium sulphates. Zuhau et al. (2017) investigated possible use of fly-ash and a local high-magnesium nickel slag (HMNS) as source materials to manufacture geopolymer cement pastes under the room temperature conditions. Their results show that, by using optimal quantities of alkali activator and HMNS, the compressive strengths upto 60 MPa can be achieved in the resulting geopolymer cements which are comparable to hardened Portland cements.

Puertas et al. (2018) studied the behaviour of the fresh and hardened properties of alkali-activated slag concrete along with OPC based reference concrete. The results concluded that the slump and rheological behaviour vary between OPC-based and AAS concrete mixes. In OPC-based mixes and NaOH-activated AAS concretes, longer mixing times showed an adverse effect on rheology, with a slight improvement in the hardened properties. On activation with water glass, however, longer mixing times improved both the rheological behaviour as well as the mechanical strength properties of AAS concrete mixes. Chaitanya and Gunneswara (2018<sup>a</sup>) presented a methodology for designing mix proportions of alkali-activated slag concrete (AASC) for a targeted compressive strength, using particle packing theory. It was observed that the sodium hydroxide concentration and alkaline solution to binder ratio are the most important influential parameters affecting the workability and compressive strengths of AAS concrete mixes.

Hilal et al. (2018) have investigated on the performance and microstructure of AASC mixes subjected to different 28-day curing regimes namely, air curing, intermittent water curing (7 days in water followed by 21 days in air), and continuous water curing. Three concrete mixes were prepared with fixed contents of slag, desert dune sand, and aggregates and were activated by alkaline solutions consisting of sodium silicate and sodium hydroxide. The ratio of alkaline activator solution (AAS) to slag was varied between 0.45 and 0.55. It was observed that the alkaline solution: Slag ratio of 0.50 showed the optimal performance. Intermittent water curing was found to be the most effective curing regime, resulting in a reduction in porosity and sorptivity, and also led to increases in bulk electrical resistivity, modulus of elasticity, and compressive strengths of the mixes.

In a detailed experimental investigation, Ning et al. (2018) developed alkali-activated slag/fly-ash concretes of three representative strength grades - 40, 60, and 80 MPa. While they maintained a low water/binder ratio, and low sodium oxide/binder ratio, they used sodium carbonate as an admixture. Higher slumps upto 200mm were achieved in the mixes, and so also quite satisfactory initial setting times (1-3 hrs) were recorded. While Calcium alumino-silicate hydrate (C-A-S-H) gel was recognized as the

main reaction product in these mixes, sodium aluminosilicate hydrate gel (N-A-S-H) was detected only in air cured counterparts.

The results of Ali et al. (2019) showed that the increases in sodium hydroxide molarity and the ratio of sodium hydroxide to sodium silicate, enhanced all the mechanical properties of the AASC mixes; However, an increase in alkaline solution-to-slag ratio beyond 0.5 or in the curing temperature greater than 90° C had an adverse effect on the strength performance of alkali-activated slag concrete. A curing period of 2 days at 30°C, 60°C and 90°C showed the best results in terms of the mechanical properties of AASC.

Possible utilization of sea-water and sea-sand in production of large volumes of alkali activated slag concrete mixes was contemplated in building artificial islands by Shutong et al. (2019). The study mainly aimed at evaluating the mechanical properties of four different types of AASC mixes – Mixes using freshwater and river sand (FRASC) (control), mixes using freshwater and sea sand (FSASC), mixes using seawater and river sand (SRASC) and mixes using seawater and sea sand (SSASC). While all the four ASSC mixes showed similar strength performances, the AASC prepared with seawater or sea sand showed better resistance to chloride ion permeability, even though their drying shrinkage values were slightly higher. Analyses of results of microstructural studies carried out using SEM (scanning electron microscope) and XRD (X-ray diffraction), also showed slight variations on the morphology and hydration products in the ASSC mixes using both seawater and sea sand, as compared to other mixes.

Zhenzhen et al. (2019) explored the influence of alkaline activator (NaOH or NaOH/Na<sub>2</sub>CO<sub>3</sub> solutions) on the performance of alkali-activated slag (AAS) mortars using pottery sand as fine aggregate. The setting time, fluidity, compressive strength, and drying shrinkage were measured for all the AAS mortars. Their results showed that both the Na<sub>2</sub>CO<sub>3</sub>-to-NaOH ratio and Na<sub>2</sub>O content had significant effects on the fresh and hardened properties of AAS mortars. Higher Na<sub>2</sub>CO<sub>3</sub>-to-NaOH ratio and lower Na<sub>2</sub>O content resulted in AAS mortars having longer initial and final setting times. Further higher Na<sub>2</sub>CO<sub>3</sub>-to-NaOH ratios led to higher later-age compressive strengths of

AAS mortars; the AAS mortars having a Na<sub>2</sub>O dosage of 6% showed the best performance.

## **2.9 ALKALI ACTIVATED COMPOSITES WITH ALTERNATIVE BINDERS.**

The effect of admixing silica fume (SF) as a partial binder in an otherwise GGBFS based alkali-activated cement paste was studied by Alaa and Mervat (2013). The replacement of slag with silica Fume in the range of 0-15%, in increments of 5% (by weight) was considered (i.e. 100% slag only to 85% slag+15% SF), Sodium silicate solution was used as an activator. It was observed that admixing with silica fume was beneficial in terms of higher strength development, 5% being the optimum percentage of SF replacement.

Aylin and Kemalettin (2013) investigated the strength of alkali activated blast furnace slag mortars (AAS) with small percentages of very finely ground pumice powder added to them. Alkaline activator with the combination of sodium silicate and sodium hydroxide with a modulus of 0.75 was used in the mixes. They recorded compressive strengths in the range of 29-50MPa at different ages (i.e. 7, 28 and 90 days). Small increases in the strengths above were recorded on addition of 10% of fine pumice powder. Moruf et al. (2014) studied the effect of blending ultrafine, palm-oil fuel ash with GGBFS for the development of high strength alkali-activated concrete. They concluded that higher compressive strengths in alkali- activated concretes with combined GGBFS-ultrafine palm oil fuel ash (AAGU) binders can be achieved only when finely divided, ground blast furnace slag (GBFS) is employed.

Wen and Tsung (2014) used de-sulphurized slag powder (DSP), a waste from Iron and Steel Industry, and ground granulated blast furnace slag (GGBFS) as raw materials for producing mortars with no-Portland-cement based binders. They concluded that the molten iron desulphurization slag is a harmless industrial waste that can serve as an efficient alkali activator. Its high alkali (CaO) contents provide sufficient conditions for triggering the hydration process of GGBFS, attaining the highest strength development for specimens (about 17MPa) with GGBFS/DSP ratios of 8:2 and 7:3. Pereira et al.

(2015) used sugarcane bagasse ash (SBA) along with blast furnace slag (BFS) as source materials for preparing alkali- activated mortars. 8 Molar solutions of either NaOH or KOH along with sodium silicate solution prepared such that the activating solutions had modular ratio ( $\text{SiO}_2/\text{Na}_2\text{O}$ ) of 0.5 were used. Reasonably high compressive strengths, in the range of 16 MPa to 51 MPa, were recorded.

Gao et al. (2015) have attempted a detailed study on the performance on alkali activated, ternary systems. The binders used were GGBFS, fly-ash and limestone. They concluded that good workability can be achieved in alkali activated slag–fly-ash–limestone blends by using higher amounts of fly-ash and limestone. It has been recorded that, while for a constant limestone powder replacement, a higher compressive strength was observed in samples with a higher slag content, for a constant slag content, the compressive strength increases with increasing limestone powder content.

Borges et al. (2016) studied the effect of silicate content on the performance of blended metakaolin/blast furnace slag alkali-activated mortars. A reference alkali activated metakaolin (only) based mortar was compared with mortars with 60% MK: 40% BFS, however containing different moduli  $\text{SiO}_2/\text{Na}_2\text{O}$  in the activator. Based on the results obtained, they concluded that the inclusion of (BFS) in MK activated mortars showed a reduction in the amount of alkaline activator required for maintaining the same workability, with significant improvements in the mechanical strength properties.

The blending of alkali activated slag concrete with Ferro nickel slag (FNS) as a partial binder was investigated by Ruilin et al. (2018). It was observed that, a partial substitution at dosages below 40% of FNS did not lead to any significant influence on the initial and final setting times; however blending FNS above 60% prolongs the setting times but also causes a substantial reduction of mechanical strengths. Abdollahnejad et al. (2019) researched on the possible utilisation of fired- and unfired-ceramic wastes as a partial binder component in alkali activated slag concrete mixes. The results showed that replacing ground granulated blast-furnace slag with either type of ceramic wastes reduced the compressive strength; mainly due to the reduction in the calcium content.

## **2.10 ALKALI ACTIVATED COMPOSITES WITH DIFFERENT ACTIVATORS**

Cengiz et al. (2009) investigated the feasibility of using an alkali-activated ground Turkish slag to produce a mortar without Portland cement (PC). Three different activators were used such as liquid sodium silicate (LSS), sodium hydroxide (SH) and sodium carbonate (SC) at different sodium concentrations. Based on the results of the tests conducted, they found that LSS- and SH-activated slag pastes took more time to set under ambient curing as compared to a Portland cement paste. LSS-, SH- and SC-activated slag mortars developed maximum compressive strengths of 81(highest), 29 (lowest), and 36 MPa, respectively and maximum flexural tensile strengths of 6.8 (highest), 3.8 (lowest), and 5.3 MPa, respectively, by 28-days.

Haha et al. (2011) studied the hydration of two GGBFS containing a high and low  $\text{Al}_2\text{O}_3$  contents (12% and 7% by weight), activated with sodium hydroxide and hydrous sodium metasilicate. They concluded that in all systems, C-S-H incorporating aluminum and, a hydrotalcite-like phase with Mg/Al ratio equal to 2, were the main hydration products. The C-S-H gels present in NaOH activated pastes were more crystalline and contained less water; a calcium silicate hydrate (C-S-H) and a sodium rich, calcium sodium silicate hydrate (C-N-S-H) with a similar Ca content were observed at longer hydration times. Keun et al. (2012) strengthened the practical application of the  $\text{Ca}(\text{OH})_2$ -based alkali-activated, slag (GGBFS) system. 7.5%  $\text{Ca}(\text{OH})_2$  was used for the main activator and either 1%  $\text{Na}_2\text{SiO}_3$  or 2%  $\text{Na}_2\text{CO}_3$  was added as an auxiliary activator. Test results showed higher calcium silicate hydrate (C-S-H) gels for water curing than for air-dried curing and while using  $\text{Ca}(\text{OH})_2$  alone as the activator.

Chi (2012) investigated the AASC specimens both with and without, phosphoric acid ( $\text{H}_3\text{PO}_4$ ) cured in air, under the saturated limewater and in a curing room at relative humidity of 80% RH and temperature of 60°C, respectively. The performance of AASC mixes were found to be comparable with those of reference concretes produced using ordinary Portland cement concrete (OPCC).

Puertas and Torres (2014) explored the feasibility of using urban and industrial glass waste as a potential alkaline activator for blast furnace slag (AAS). AAS pastes were

prepared with three activators namely the water glass, a NaOH/Na<sub>2</sub>CO<sub>3</sub> mix and the solutions resulting from dissolving glass waste in NaOH/Na<sub>2</sub>CO<sub>3</sub>. They concluded that the strength and microstructural development in the pastes activated with glass waste were similar and comparable to the parameters observed in AAS pastes prepared with conventional activators.

Wan et al. (2014) studied the use of anhydrous sodium sulphate (Na<sub>2</sub>SO<sub>4</sub>) as an alkaline activator in a system in which Portland cement of about 10% - 20% and ground granulated blast-furnace slag of about 90% - 10% were mixed and added to light-burnt dolomite (LBD). The effect of hydration and strength of the cement were also analyzed. The strength of the resulting mixes improved after the 3<sup>rd</sup>, 7<sup>th</sup> and 28<sup>th</sup> - days and confirmed that the pore structure of the paste became dense after 28-days of aging.

## **2.11 ALKALI ACTIVATED COMPOSITES WITH ALTERNATIVE AGGREGATES.**

Puertas et al. (2009) investigated the alkali–silica reaction in water glass activated slag (water glass-AAS) and ordinary Portland cement (OPC) mortars using three types of (siliceous and calcareous) aggregates. The tests were conducted as per the method recommended in ASTM C1260-94. Based on the results obtained, they concluded that, water glass-AAS mortars are stronger and more resistant to alkali-aggregate reactions than OPC based mortars.

Semiha and Cuneyt (2014) showed the possible utilization of ground waste-PET bottle aggregate in alkali-activated, slag and slag/metakaolin blended mortars. In PET-aggregate mixtures, slag aggregate were replaced with waste PET aggregate, in amounts of 20 - 100% by volume. Sodium hydroxide (NaOH) pellets and liquid sodium silicate were used as activators. It was found that the compressive strengths of alkali-activated slag mortars decreases with increase in amount of waste PET aggregate; but however they suggested potential for the use of waste PET as aggregates in the production of alkali-activated slag mortars.

Mithun and Narasimhan (2016) proposed copper slag (CS) as an alternative to river sand for use as fine aggregate in alkali-activated slag concrete (AASC) mixes. They verified the comparable performances of such mixes with CS aggregate as compared to a control OPC-based concrete mix, in terms of their workability, strength and durability parameters. Parthiban and Saravana (2016) studied the influence of using recycled concrete aggregates (RCA) derived from the demolished concrete waste on the mechanical properties of fly-ash based geopolymer concrete (GPC) under ambient curing conditions. Based on the test results, they concluded that workability of mixes containing increased amounts of RCA could be quite improved, using higher of dosages of an appropriate super-plasticizer. AAC mixes with replacement of RCA even upto 50% exhibited improved compressive strength and water absorption characteristics.

Alaa et al. (2016) investigated the possibility of using granulated blast-furnace slag (GBFS) as a partial or full replacement for natural silica sand in alkali-activated slag (AAS) mortars. The ratio of binder to fine aggregate was 1:2. The strength-behaviour of the mortar mixtures on after exposure to elevated temperatures in the range 200°C - 800°C (at intervals of 200°C) for two hours was also investigated. The results indicated that the compressive strengths of the mortar specimens increased with increasing percentages of GBFS sand content and showed better performance after exposure to elevated temperatures as compared to controlled OPC- based concrete mix.

Palankar et al. (2017) investigated the mechanical strength and fatigue performance of alkali activated Slag Fly-ash based concrete mixes (AASFC) incorporating steel slag as coarse aggregates. AASFC mixes were prepared with steel slag coarse aggregates replacing the conventional granite-chip coarse aggregates at different replacement levels (0 - 100% by volume, in increments of 25%). The incorporation of steel slag aggregates resulted, in general, decreases in the mechanical strength parameters of AASFC mixes. The fatigue lives of AASFC mixes containing steel slag were again found to be lower than AASFC with natural coarse aggregates.

## 2.12 DURABILITY STUDIES ON ALKALI ACTIVATED COMPOSITES

Durability-related issues of any new class of concretes are of always of research concern as their acceptance in the field of concrete construction depends on their assured performance in aggressive environments. Densities of paste, permeability, and relative availability of pores - their sizes and interconnectivity, in the entire concrete microstructure have a predominant effect on the concrete durability aspects (Ranani 2012).

Chloride permeability and hence its relative corrosion of the steel rebars is a major cause of deterioration of reinforced concrete infrastructure (Koch et al 2002). The increase in the slag content in the AASC mixes improved the structural density showing a decreased RCPT values (Rodríguez et al. 2008). The corrosion resistance of AASC mixes had been shown to be very similar to OPC based concretes when immersed in 3.5% NaCl solution (Chaparro et al. 2012). Ravikumar and Neithalath (2013) studied the chloride transport resistance of alkali silicate-powder activated slag concretes. Two different values of each of Na<sub>2</sub>O to source material ratios (n) and two SiO<sub>2</sub> to Na<sub>2</sub>O ratios of the activator (Ms) were considered to produce concretes proportioned using two slag contents (300 kg/m<sup>3</sup> and 400 kg/m<sup>3</sup>). Rapid chloride permeability (RCP) and non-steady state migration (NSSM) tests were used to evaluate the chloride transport behaviour. In the tests, alkali silicate powder activated concretes demonstrated comparable or better chloride transport resistance than OPC-based concretes. The chloride migration coefficients determined for AASC mixes, using NSSM tests, showed smaller values when compared to OPC-based concrete mixes (Ismail et al. 2013).

It can be appreciated that chloride ion penetrability in a concrete mix mainly depends on the concrete microstructure (Ravikumar and Neithalath, 2013); but the RCPT values of AASC mixes are affected by the activator modulus and its alkalinity. Higher activator modulus leads to a better resistance to chloride penetration in that lower amounts of charge passed are recorded (Otaibi 2008, Law et al. 2012). It has been shown that the corrosion resistance also depends on the type of activator used in the AASC mixes (i.e KOH or NaOH). AASC mixes activated using Calcium hydroxide

showed a better resistance against chloride permeability. Calcium hydroxide available in the matrix reacts with chloride ions leading to the formation of calcium hypochlorite, which reduces the free chlorides available in the pore solution (Park et al. 2015).

There are investigations that are mainly focusing on the chloride permeability of AASC. While the test results therein have indicated a good resistance of these mixes against chloride ion penetration (Bernal et al. 2011, 2012); There are however, a few difficulties in ascertaining the chloride permeability of AAC using the RCPT test. This is because of the fact that the pore solution chemistry of AAC may greatly affect the results of RCPT values more than the pore structure (Shi 1996). Several other researchers also sound the same concern on using the RCPT test for measuring the chloride permeability of AAC mixes (Stanish et al. 1997, Adam 2009, Chi 2012). However a recent review suggested that chloride permeability of AAC is comparable with the OPC based materials (Provis 2018). Silica-fume admixed AASC showed a decreased electrical conductivity and hence improved resistance against chloride penetration (Rostami and Behfarnia 2017).

Thomas et al. (2018) reported the results of a detailed experimental study of chloride permeability of alkali-activated fly-ash-based concrete, alkali-activated slag (GGBFS) concrete, and also Portland cement-based concrete mixes. Contrary to previous studies, the RCPT provided a good estimate of chloride permeability in both alkali-activated slag and alkali-activated fly-ash-based concrete mixes. RCPT results showed excellent correlation with diffusion coefficients determined from salt ponding tests. Resistivity measurements, however, exhibited a poor correlation with diffusion coefficients and overestimated the resistance to chloride ion penetration. Again AC and DC resistivity measurements showed significant disagreement between them for alkali-activated concrete mixes.

Alkali activated binder showed mass losses of about 6% and 7%, when immersed in concentrated hydrochloric acid and sulphuric acid solutions, respectively, for a period of 30 days. However for the same acids with similar concentrations, OPC-based mixes recorded higher mass-losses of about 78%-98% (Davidovits et al 1990).

Shi and Stegemen (2000) investigated the corrosion of different hardened cementing materials such as Portland cement (PC), alkali activated blast furnace slag cement (ASC), lime fly ash (LFA) blend and high alumina cement (HAC), with gypsum and lime in nitric acid (pH=3) and acetic acid (pH= 5). They observed that PC paste corroded faster than ASC and LFA pastes and HAC paste quickly dissolved in the acid solution.

Bakharev et al. (2003) studied the durability of alkali activated slag (AAS) concrete containing a neutral slag with basicity coefficient as 0.93. Liquid sodium silicate and sodium hydroxide were mixed providing a modulus Ms of 0.75 and 4% sodium oxide in the alkaline mixture that was added to slag. Strength losses upto 47% and 33% were obtained for OPC and AAS concretes respectively, on exposure to acetic acid solution (pH= 4) for an extended period of one year. The poorer performance of OPC-based concrete is attributed to the presence of higher calcium contents present in OPC based concrete, which form soluble compounds on reacting with acetic acid; on the other hand, the AASC mixes, having lower Ca/Si ratio, are more stable in acidic environments.

In another investigation by Gourley and Johnson (2005), higher mass losses upto about 25% were observed with OPC based concrete designed for a service life of 50 years after 80 immersions cycles in concentrated H<sub>2</sub>SO<sub>4</sub> solution (pH=1). However specimens of AAC mix required 1400 immersions cycles to produce the same amounts of mass losses which accounted for a calculated service life of about 900 years. Similarly better acid-resistance was reported by Sathia et al. (2008) for fly-ash based geopolymer concrete mixes prepared with increased fly-ash contents with sodium silicate and sodium hydroxide used as activators, as compared to normal OPC based concrete. Again, in the studies by Pacheco et al. (2010), alkali-activated concrete mixes showed a mass loss of about average 2.6% only after being immersed in sulphuric, hydrochloric and nitric acids solutions for a period of 28 days. However OPC based concrete showed a mass loss value of more than twice as compared to AAC mixes.

Chaitanya and Gunneswara (2018<sup>b</sup>) investigated the durability performance of AASC mixes prepared using GGBFS as the sole binder material. Durability tests like

sorptivity tests and acid attack with three different acids namely HCL, H<sub>2</sub>SO<sub>4</sub> and HNO<sub>3</sub> having a concentration of 5%, up to age of 56 days were carried out in order to evaluate the performance of AASC subjected to aggressive environments. Sorptivity of AASC mixes was found to be more significantly affected by the activator concentration. Results from acid attack test and XRD indicated higher durability of AAS-based concrete mixes.

Hammad et al. (2018) evaluated the performance of low calcium fly-ash based geopolymer (FA-GPm) and alkali-activated slag based mortars (AASm) subjected to an aggressive sewer environment. Specimens were extracted from field exposure, after 6 and 12 months. It was concluded that the overall matrix deterioration was much higher in FA-GPm, as a result crystallization of thenardite (Na<sub>2</sub>SO<sub>4</sub>) mineral, as compared to AASm after 12 months of exposure to the aggressive environment.

The destruction of calcium silicate hydrate is the major deterioration mechanism in case of sulphate-attack on AASC specimens, gypsum being one of the major reaction products (Bakharev et al. 2002). Studies by Heikal et al. (2014) suggest a better durability performance of the specimens of sodium silicate activated slag cements (strength loss of just about 23%) as compared to OPC-based concrete (strength loss upto 37%) mixes, when immersed in 5% magnesium sulphate solution for 180 days.

Palankar et al. (2016) studied the durability performance of alkali activated concrete mixes containing steel slag aggregate as partial-to-full replacement (0%, 50% and 100% by volume) to natural quartz-based coarse aggregates. The test results confirmed that, while alkali activated concrete mixes with natural aggregates exhibited better resistance to sulphuric acid and magnesium sulphate environments as compared to OPC-based concretes, such resistances decreased with increased replacement of natural aggregates with steel slag aggregates, possibly due to incomplete weathering of steel slag aggregates leading to expansive reactions at later ages.

### **2.13 ELEVATED TEMPERATURE PERFORMANCE OF ALKALI ACTIVATED COMPOSITES**

The uncontrolled fire incidents, especially those occurring in the underground constructions may result in severe damage to the human life along with enormous loss of unmovable assets. Further severe damage is also caused to the structures themselves due to such fire accidents (Petzold et al, 1971, Jumppanen 1986, Khoury 1992). Concrete and steel are the two major components of any civil engineering structure. During fire accidents, severe damages in the form of spalling, degradation of mechanical strength etc., can take place in the concrete components, although it is an incombustible material. The impulsive release of huge amounts of heat and aggressive fire gases are mainly responsible for these damages in concrete. The phenomenon of concrete spalling and reduction of concrete strengths generally occur after being exposed to temperatures beyond 300<sup>0</sup> C (Phan 1996, Sakkas et al. 2013).

The resistance to degradation of OPC concrete when exposed to elevated temperatures are dependent on the type of constituent materials. The extent of deterioration also depends on the mineralogy and porosity of aggregates used (Hosny and Abu 1994).

In OPC based concrete (OPCC) mixes, cement paste is the least stable constituent at elevated temperatures. Both chemical and physical properties of the OPCC display deteriorations, on being exposed to elevated temperatures beyond 400<sup>0</sup>C or so, which are due to loss of interlayer and chemically bound water and hence the decomposition of calcium hydroxide (CH) and calcium silicate hydrate (C-S-H). Such decompositions are responsible for causing an increase in volume that takes place during process of cooling, due to rehydration of calcium oxide, leading to severe cracking, as suggested by investigators like Sullivan and Sharshar (1992), Bazant and Kalpan (1996) and Handoo et al. (2002).

In addition to the above, during heating over a temperature range of 480<sup>0</sup>C and 510<sup>0</sup> C, explosive spalling of concrete occurs leading to large reduction in the load carrying capacity of concrete structures (Georgali and Tsakiridis 2005). The following effects, as detailed in Table 2.2 occur, in that order, when cement paste is exposed to elevated temperatures (Özge et al. 2008). Several studies have been carried out by many

researchers reporting the improved mechanical properties of concrete exposed to elevated temperatures with partial replacement of OPC with fly-ash, GGBFS and other replacement materials (Chan et al. 1999, Poon et al. 2001, Xiao et al. 2006, Seleem 2011). For the blended concrete mixes with 80% OPC blended with GGBFS, and with a low water/binder ratio of 0.23, the compressive strengths were very much improved and so also there was substantial reduction in the cracking characteristics of those mixes at elevated temperatures (Wang 2008).

**Table 2.2 Deterioration mechanism of cement paste at different temperatures**  
(Özge et al. 2008)

Capillary and gel water evaporate	100–150 <sup>0</sup> C
Shrinkage and cracking accompanied by a tensile strength reduction	150–250 <sup>0</sup> C
Evaporation of chemically bound water from aluminous and ferrous constituents with the beginning of compressive strength reduction	250–300 <sup>0</sup> C
CH dehydrates to calcium oxide with an accompanying 44% volume reduction along with strength reduction	400 <sup>0</sup> C
Decomposition of C-S-H with significant strength reduction	600 <sup>0</sup> C

However there is very limited literature available on the elevated temperature performance of alkali activated fly-ash/slag concrete mixes. It is reported that residual strength characteristics of AAS exposed up to 1000<sup>0</sup>C were similar to OPC regardless of the activator type used and that decalcification of C-S-H led to strength decreases as in OPC-based concrete (Cheng and Chui 2003, Mejía de Gutierrez et al. 2004).

Studies carried out by researchers like Zuda et al. (2006), Guerrieri and Sanjayan (2009), Guerrieri et al. (2009 and 2010), Sakkas (2013) have reported better stability of AAC mixes (fly ash/slag based) at elevated temperatures (upto 1200<sup>0</sup>C) and hence a greater potential for their use in high temperature applications, as compared to OPCC-

based mixes. This may be due to the presence of a highly condensed binder gel, the low contents of chemically bonded water in the alkali-activated gel products and the absence of CH as a reaction product in AAS systems. Again, it was observed that, with the increase in sodium dosage, initial reference strengths increased; but the residual strengths, after exposure to higher temperatures exponentially decreased.

Natali et al. (2013) investigated the high temperature behaviour of ambient cured alkali-activated concrete mixes using combinations of ladle slag and metakaolin or ladle slag and fly ash. The ladle slag/ fly-ash based AAMs exhibited superior strength gains and better thermal stability than the ladle slag/ metakaolin based AAMs, when exposed to temperatures upto 1000°C which may be due to the lower thermal stability of C–A–S–H phases formed in the latter group of samples.

Park et al. (2016) studied the physico-chemical properties of binder gel in alkali-activated fly ash/slag exposed to high temperatures. Test results showed that the strength increased until exposure to a temperature of 400°C and thereafter started to decrease. The strength increases below 400°C were attributed to the additional binder gel which gets formed on exposure to such temperatures, decreasing the porosity. The dehydration of C-A-S-H and the formation of N-A-S-H simultaneously occurred at temperature of 400°C, inducing the transformation of pore structure from micro-porous to meso-porous state.

Danial et al. (2018) studied the influence of alkali activator concentration and curing conditions (ambient, water, and hydrothermal curing) on the heat resistance properties of AAS mortars. The results revealed that the hydrothermal curing has a positive effect on the compressive strength of AAS mortars, after exposure to high temperatures, as compared to ambient and water curing conditions, regardless of the dosage of alkali activator. In terms of flexural strength, the hydrothermal cured AAS mortars experienced strength gain after exposure to high temperatures and the increase is higher at a certain level of alkali activation.

Behfarnia and Shahbaz (2018) investigated the tensile strength properties of Alkali activated slag concrete specimens after exposure to elevated temperatures upto 800°C., in a fossil fuel gas furnace. The specimens had been initially water-cured for varying

periods of 7, 28 and 90 days. The results concluded that the residual tensile strengths of the AAS concrete mixes, after exposure to elevated temperatures, were noticeably higher than that of normal control OPC-based concrete mix.

#### **2.14 BEHAVIOUR OF ALKALI ACTIVATED COMPOSITES INCORPORATED WITH FIBERS.**

Bernal et al. (2010) investigated the early-age mechanical and permeability properties of alkali-activated slag concrete (AASC) mixes reinforced with steel fibers. They observed slight reductions in compressive strengths on incorporating the fibers. However, split-tensile and flexural strengths improved significantly with increasing fiber volume.

It was observed by Natali et al. (2011) that by incorporating 1% of fibers (by weight of binder content) embedded in the geopolymer matrix it was possible to increase the flexural strength in the range of 30-70%, depending on the type of fiber used, as compared to that with unreinforced matrix. They also observed that geo-polymers exhibited the best energy absorption capacity on addition of PVC or carbon fibers; On addition of these fibers, the post-crack behaviour was significantly improved, resulting in an enhanced ductility of the material.

Alaa (2013) adopted different fibers in AAS system to modify some of the properties of the system and concluded that alkali-activated slag/Steel fibers with the ratio of 80/20, show a slight increase in the workability with usage of admixture and a decreased shrinkage. He also observed an increase in compressive and flexural strengths as well as toughness of the AAS system. However polypropylene fibers have not provided significantly increased compressive strength but slight increase in tensile strength. Carbon fibers and Basalt fibers also failed to improve the compressive strength.

The effects of length and volume fraction of steel fibers on the mechanical properties and drying shrinkage behaviour of steel fiber reinforced alkali-activated slag/silica fume (AASS) mortars was investigated by Serdar and Bulent (2013). Steel fibers with

two different lengths of 6 mm and 13 mm, and four different volume fractions of 0.5%, 1.0%, 1.5% and 2.0% by total volume of concrete mixes were used. Portland cement (PC) based mortar having 1.5% of 13 mm long a steel fiber was used as the reference mix. Test results showed that the mechanical strength performance of AASS mortars was significantly better than PC-based control mortar. They also observed dramatically improved mechanical strength performance of AASS mortars with the increment of fiber length from 6 mm to 13 mm. Drying shrinkage of AASS mortars was observed to decrease with the increase in fiber dosage.

Se et al. (2015) explored, in detail, the rheological and mechanical properties of fiber-reinforced alkali-activated slag based, clinker less composites. Single fiber pull-out test and matrix fracture tests were conducted to characterize the micro-mechanical behaviour of the composites. They concluded that low plastic viscosity, low yield stress, and high ductility can be attained for an alkali-activated slag-based binder with water to binder ratio 0.40 along with incorporation of PVA fibers of 1.3 % (by volume of composites).

A detailed investigation on the effects of the concentration of alkaline activator ( $\text{Na}_2\text{O}$  and silica modulus) and the fiber aspect ratio (using different length of fibers with the same diameter) on the mechanical strength properties of alkali activated slag (AAS) pastes, reinforced with carbon fibers (CF), was conducted by Vilaplana et al. (2016). They observed that while addition of CF increased the compressive strength only upto 20%, the bending strength got increased up to five times (500%). Choi et al. (2016) made a detailed study of meso-level composite properties of an ultra-high ductile polyethylene-fiber-reinforced alkali-activated slag-based composite. Four mixtures were formulated with 1.75 of polyethylene fibers (by volume of slag) with varying water-to-binder ratio. Enhanced tensile strain capacity (of up to 7.50%) and tensile strength (upto 13.06 MPa) were observed in these polyethylene-fiber-reinforced alkali-activated slag-based composites. Again the average tensile strength to compressive strength ratio of the composites in this series of tests was a high 19.8%, which is nearly double that of normal concrete mixes

## **2.15 BEHAVIOUR OF REBAR REINFORCED STRUCTURAL ELEMENTS MADE OF ALKALI ACTIVATED CONCRETE MIXES**

Over the years, very limited studies have been carried out on the flexural characteristics of structural beams, with steel rebar reinforcement, made up of alkali activated concrete mixes. Sumajouw and Rangan (2006) conducted extensive studies on reinforced beams and columns made of fly-ash based geopolymer concrete (GPC) mixes. The behaviour and failure modes of reinforced GPC columns and beams were similar to those observed in the case of conventional reinforced beams made with PC-based concrete mixes.

Detailed test results of Chang (2009) showed that Geo-polymer concrete (GPC) beams can achieve sufficient strength for structural designs, but both compressive strength and flexural tensile strength are affected by drying, any differential drying shrinkage leading to micro cracking at the drying surfaces. Further the shear characteristics of the reinforced GPC beams were also similar to those of reinforced OPCC beams.

Narasimhan et al. (2011) studied the flexural strength properties of reinforced fly-ash and GGFBS based geopolymer concrete beams. According to them, load deflection curves of GPC-RC beams are very much similar to normal RC beams. They recorded appreciable first load and ultimate loads for the beams; the ratio of ultimate load to first crack load were in the range of 1.7 - 2.7.

Dattatreya et al. (2011) conducted tests on a set of under-reinforced geopolymer concrete beams, which were observed to behave quite similarly in terms of first load crack, width of crack, load deflection behaviour, flexural stiffness, and ultimate load as compared to reinforced OPCC beams, under flexural loading. A slightly more brittle failure was observed during crushing of reinforced GPC when compared to conventional reinforced OPCC beams. Similar observations were made by Yost et al. (2013), Kumaravel and Thirugnanasambandam (2013) also during their experimental investigations on fly-ash based geopolymer concrete beams. Similar results on flexural and shear performance for slag-based alkali-activated concrete beams, as with OPC-based RC-beams were observed also by Lee et al. (2017).

Pradeep et al. (2012) and Sanjay et al. (2012) carried out investigations into the flexural behaviour of heat-cured fly ash and GGBS based geopolymer concrete (90% FA + 10% GGBS, by volume), with normal aggregates as well as recycled aggregates. Sodium hydroxide (NaOH, 12-16M) solution along with Sodium silicate solution, taken in the ratio (1:2.5), was used as the activator solution. From their test results, they concluded that with increase in tensile reinforcement, the first crack load and the stiffness of the beam will also increase. The service load deflections were well within the limits prescribed under IS: 456-2000. They experimental ultimate moment carrying capacity was within +1.5% to +1.7% of the theoretical ultimate moment capacity computed for the beam.

Thus, it is suggested to use the current provisions in the design codes for OPC-based reinforced concrete elements for a conservative design of reinforced geopolymer concrete members as well (Sarker 2015).

Kathirvel and Kaliyaperumal (2016) also researched on the possible use of recycled concrete aggregates in fly-ash based geo-polymer concrete mixes. They observed that, increase in the recycled concrete aggregate content in the representative AASC mixes showed a marked increase in the load carrying capacity upto 22.5%, upto aggregate replacement level of 75%. Further increase in the RCA content showed a detrimental effect. Again, the geopolymer concrete beams with higher RCA contents also showed an improved deflection as well as ductility characteristics. The failure of beams, designed as under-reinforced beams, was mainly due to the flexural failure and no sign of shear cracks were observed.

Un et al. (2016) experimented on long-term behaviour of concrete beams constructed of geopolymer concrete (GPC) mixes. Self-weight and sustained load of 1 kPa was applied on top of the beams at the age of 14 days to simulate construction conditions. Predictions of beam deflections were performed by using alternative methods like, Rate of creep method (RCM), Effective Modulus method (EMM) and Age-adjusted Effective Modulus (AEMM). Experimentally determined properties of the GPC mixes like, elastic modulus and modulus of rupture were used in the predictions of long-term

deflections. It was concluded that the AEMM can be used for satisfactory prediction of long-term deflections for GPC beams with minor parameter modifications.

In order to facilitate, fast-track constructions, it is imperative that the advancements in pre-cast technology should be fully exploited in the context of any new concrete material. Large-scale adoptability of alkali-activated concretes in pre-cast industry is then to be verified and ascertained (Jeyasehar et al. 2013). Possible use of geo-polymer concretes/alkali-activated slag concretes as fast-repair materials, if demonstrated, would prove quite useful, since undertaking small repairs is inevitable for maintaining any infrastructure facility, functional (Wanchai 2014).

In a scenario, where new exploits in the domains of nano-science and nano-technology are affecting all types of human activities, effect of incorporating nano-silica in geo-polymer concrete mixes for use in flexural members was investigated (Adak et al. 2017). The results showed a comparatively higher flexural performance for reinforced concrete beams made with GPC mixes cured at ambient temperature, as compared to GPC mixes with nano-silica incorporated and cured at ambient temperature, as compared to GPC beams which were heat cured or were of OPCC beams, both without nano-silica. Similar load-deflection characteristics, moment-curvature relationship along with cracking behaviour were observed for all the reinforced GPC beams as compared to reinforced OPCC beams.

The first full-scale structural application using alkali activated slag concrete in terms of a full-fledged multi-storied building, Chongqing Jianke, the CRICS office building has been constructed in China. Designed by the Chongqing Architectural Design Institute, this building is located in the Yuzhong District, Chongqing, China. The building was constructed by Chongqing Construction Engineering Group Corporation (CCEGC) (Fig 2.3). The total built-up area of the said building is 413033 Sq.m, of which 4500 m<sup>2</sup>, three floors (12 m in height) have been built using alkali-activated slag concrete (AASC) and 550 m<sup>3</sup> of AAS concrete was used. It consists of various structural components such as slabs, beams and columns – all are made of AASC (Yang et al 2018).



**Fig 2.3 First full scale structural application of alkali activated slag concrete**

**Ref: (Yang et al 2018).**

## **2.16 SUMMARY OF THE LITERATURE**

Based on the detailed literature review it can be observed that the mechanical and durability properties of mortar/concrete mixes with alkali activated binders, are affected by several factors and acceptable performance characteristics can be achieved in them as compared to Ordinary Portland Cement Concrete Mixes. Alkali Activated Slag Concrete (AASC) mixes are now distinctly differentiated with the geopolymer concrete (GPC) mixes based on the hydration products obtained. While presence of principally Calcium-silicate-hydrates (C-S-H), along with Calcium alumino-silicate hydrates (C-A-S-H), and Sodium-alumino-silicate-hydrates (N-A-S-H) gels, and/or Calcium-Sodium-silicate-hydrates (C-N-S-H) in the hardened state of AAC mixes. Further C-A-S-H gels are the predominant reaction product formed in case of AASC systems. Geopolymer concretes should show the signatures of 3-D net-works of silicates, silicate-siloxo and silicate - disiloxo's having their ratio of Si: Al being 1, 2 and 3 respectively.

Further these AASC mixes can be prepared with different, alternative binders along with different alternative activator solutions.

The major factors affecting the strength of AASC are type and chemical composition of slag, percentage of sodium oxide, water content, water to slag ratio and curing conditions. Sodium hydroxide and sodium silicate solutions, individually or in combination, present themselves as very effective alkaline activators, both in terms of their performance as well as cost. However w/b ratio and activator dosages are to be properly controlled so as to obtain significantly improved strengths in AASC mixes. Increase in the modulus,  $M_s$  of the activator solution decreases the workability.

Many researchers have suggested use of molarity of sodium hydroxide solution and the activator modulus ( $M_s$ ) is defined as the mass ratio of  $\text{SiO}_2$  to  $\text{Na}_2\text{O}$  in an alkaline activator for describing the chemistry of the activator solution in their studies on fly ash-based geopolymers fly ash/slag based AAC and only GGBFS based AASC mixes. In general, increase in molarity causes an increase in the strength and an optimum modulus of 2.5 is recommended in the mixes for better strength and durability properties. While not many chemical admixtures are commercially available, as of now, Ligno-sulphate based, Naphthalene based and PCE based HRWR admixtures can lead to more acceptable performances of the AAS concrete mixes. It is also possible to consider a host of alternative materials such as coarser GGBS, recycled aggregates (construction demolition wastes), steel slag, copper slag, waste bottle aggregates and waste plastics, as fine/coarse aggregates in production of AASC mixes, at appropriate, optimum replacement levels. The role of ratios of Aggregate to binder, and fine to coarse aggregates, also play a very important role on the strength parameters of AASC mixes.

Standard codal provisions for mix design of AAS Concrete mixes are not yet formulated and hence mix proportions are being arrived at, as of now, on a trial and error basis, to meet the specified requirements. Alkali-activated slag concrete mixes, with satisfactory properties both in their fresh and hardened states can be produced even with curing under ambient (room temperature) conditions. Further fibre reinforced, alkali activated

slag concrete mixes can be produced with optimum quantity approximately selected fibres for better performance.

Alkali activate slag concrete mixes using conventional aggregates exhibit relatively better performance, when subjected to a variety of chemically aggressive environments, when compared with OPC based concrete mixes. Alkali activated slag concrete mixes also provide a comparatively better performance, when subjected to elevated temperatures, compared to normal ordinary Portland cement concrete mixes.

Alkali Activated slag concrete also provides better performance in freezing and thawing conditions. Results of limited studies on structural elements (steel rebars reinforced) made of AASC mixes haven exhibited comparable, and at times, better performance under loads, as compared to OPC-based structural concrete elements. The Energy consumption and cost in developing normal strength AASC mixes are comparatively low when compared to the normal ordinary Portland concrete mixes. However, there is very limited research available on development of high performance alkali activated slag concrete mixes produced using the industrial wastes. Hence the present research aims at evaluating the performances of these mixes in terms of their flow ability, strength, durability, exposure to elevated temperature, on addition of steel fibers along with the flexural performances of these mixes with rebars. The present study also aims at evaluation of these mixes by carrying out detailed microstructural characterization.

.....

## **CHAPTER 3**

### **MATERIALS CHARACTERIZATION AND MIX PROPORTIONS**

#### **3.1 INTRODUCTION**

This chapter describes the details of all the experimental work conducted in the present investigation. Preliminary test results on constituent materials, design of high strength self-compacting alkali activated slag concrete mixes, methodology adopted, preparation of test specimens and results of preliminary investigations, methods of tests conducted on high strength self-compacting alkali activated slag concrete mixes, both in fresh and hardened states, are discussed.

#### **3.2 PRELIMINARY INVESTIGATIONS ON CONSTITUENT MATERIALS**

##### **3.2.1 Cement**

Cement is the most important constituent of a concrete mix. In the present study, Ordinary Portland Cement (OPC) of 53 grade conform to specification laid out in IS 12269:2013 and was used in the preparation of all test specimens of a reference concrete mix, used for comparison purposes. The properties of the cement used are given in Table 3.1.

##### **3.2.2 Ground Granulated Blast-Furnace Slag (GGBFS)**

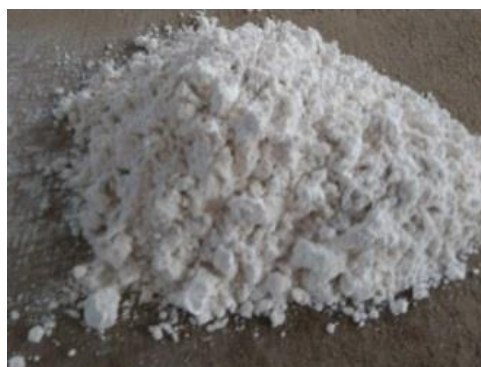
For the various tests conducted in the present investigation, GGBFS was procured from M/s Jindal Steel Industries, Bellary, India as shown in Fig 3.1a. The properties of the GGBFS used are given in Table 3.2 and they satisfy the requirements as specified in IS 12089 – 1987.

##### **3.2.3 Fine Quartz powder**

In the various development of alkali activated slag concrete mixes tested in the present investigation, fine quartz powder was used as an additional binder as shown in Fig 3.1b. This material was procured from M/s Wisdom Industries, Bangalore, India. The properties of the fine quartz powder used are given in Table 3.2.



a. GGBFS



b. Fine quartz powder

**Fig 3.1(a-b) Binders used in HSAASC mixes**

**Table 3.1 Properties of Ordinary Portland Cement used - 53 Grade**

Sl.No	Test	Results obtained	Limits as per IS 12269 - 2013
1	Specific Gravity	3.12	-
2	Standard Consistency, %	30	-
3	Fineness of cement ( $m^2/kg$ ) (Blaine's air permeability)	330	$\geq 225$
4	Setting time		
	Initial (minutes)	67	$\geq 30$
	Final (minutes)	378	$\leq 600$
5	Compressive Strength (MPa)		
	3-Days	29.5	$\geq 27$
	7-Days	39.8	$\geq 37$
	28-Days	57.4	$\geq 53$

**Table 3.2 Chemical and Physical properties of GGBFS and Fine Quartz powder**

<b>Oxide Content</b>	<b>GGBFS (% by weight)</b>	<b>Fine Quartz Powder (% by weight)</b>
CaO	33.8	0.03
Al <sub>2</sub> O <sub>3</sub>	16.6	0.05
Fe <sub>2</sub> O <sub>3</sub>	1.25	0.03
SiO <sub>2</sub>	32.5	99.8
MgO	9.7	-
Na <sub>2</sub> O	0.15	-
K <sub>2</sub> O	0.06	-
SO <sub>3</sub>	0.89	-
Insoluble Residue	4.02	-
Loss of Ignition	0.35	-
Glass Content %	91	-
Blaine fineness m <sup>2</sup> /kg	370	450
Specific gravity	2.91	2.65
Basicity (k <sub>b</sub> )	0.88 (Acidic Slag)	-
Hydration Modulus (HM)	1.86 (>1.4)	-

\*As given by the manufacturer

### 3.2.4 Fine Aggregates

#### 3.2.4.1 River Sand

In the present investigation, natural river sand as shown in Fig 3.2 was used as fine aggregate for the preparation of OPC-based concrete mix. The specific gravity,

fineness modulus (FM) and water absorption of river sand used were 2.65, 2.59 and 1.52% respectively. Results of sieve analysis carried out on river sand confirm to the grading requirements of Zone-II specified for fine aggregates as per IS: 383:1970 as shown in Table 3.5.



**Fig 3.2. Natural River Sand**

#### *3.2.4.2 Slag Sand*

Processed Slag sand shown in Fig 3.3a was used as fine aggregates procured from M/s Jindal Steel Industries, Bellary, India for the production of all the HSAASC mixes in the present investigation. Table 3.3 and 3.4 respectively show the physical characteristics and chemical composition of slag sand. As per the results of sieve analyses carried out for slag sand, shown in Table 3.5, it conforms to the grading requirements of Zone-II specified for fine aggregate as per IS: 383:1970.

#### *3.2.4.3 Quartz Sand*

In the present study quartz sand as shown in Fig 3.3b procured from M/s Wisdom Industries, Bangalore, India was used as a partial fraction of fine aggregates in order to provide better pore filling effect in the various HSAASC mixes developed herein. Table 3.3 shows the physical characteristics of quartz sand. The combination of processed slag sand and quartz sand, on mixing in the ratio 3:1, also conforms to the grading requirements of Zone-II specified for fine aggregates as per IS: 383-1970 as shown in Table 3.5.



a. Slag Sand

b. Quartz Sand

**Fig 3.3 (a-b) Fine aggregates used in HSAASC mixes**

**Table 3.3 Properties of fine aggregates used in the study**

Sl. No	Test	Fine Aggregate	
		Slag Sand	Quartz Sand
1	Specific Gravity	2.65	2.65
2	Fineness Modulus	2.75	2.41

**Table 3.4 Chemical Composition of fine aggregates used in the study**

Oxide Content	Slag Sand (% by weight)	Quartz Sand (% by weight)
CaO	36.1	0.03
Al <sub>2</sub> O <sub>3</sub>	17.7	0.05
Fe <sub>2</sub> O <sub>3</sub>	0.3	0.03
SiO <sub>2</sub>	31.2	99.8
MgO	4.8	-
Minor Minerals	1.13	-
Insoluble Residue	8.5	-
LOI	0.20	-

**Table 3.5 Results of sieve analysis - Fine aggregates**

Sieve Size	Cumulative Percentage Passing			
	River Sand	Slag Sand	Quartz Sand	Slag Sand : Quartz Sand (3:1)
10 mm	100	100	100	100
4.75 mm	99.0	100	100	100
2.36 mm	96.3	99.6	99.8	99
1.18 mm	75.8	85.5	91.5	85.1
600 $\mu$	53.4	36.2	49.8	38.5
300 $\mu$	14.2	17	2.7	15.7
150 $\mu$	2.9	4.6	0.9	4.3
Grading as per IS 383-1970	Zone II	Zone II	Zone II	Zone II

### 3.2.5 Coarse Aggregates

#### 3.2.5.1 Crushed granite chips (Jelly)

Crushed granite chips of 12.5mm downsize as shown in Fig 3.4a was used as the coarse aggregate in the OPC based control concrete mix. They were tested as per relevant Indian standard codes. The specific gravity, fineness modulus and water absorption of the coarse aggregate were 2.67, 6.87 and 0.6% respectively. The results of sieve analysis satisfy the requirements of aggregates as IS: 383-1970 as shown in Table 3.6.

#### 3.2.5.2 Electric arc furnace slag (EAF slag)

In the present investigation processed Electric arc furnace slag as shown in Fig 3.4b of size 12.5mm downsize was used as coarse aggregate procured from M/s Jindal Steel Industries, Bellary, India, in all the HSAASC mixes. Table 3.6 and 3.7 respectively shows the physical characteristics and chemical compositions of coarse aggregates. As per the results of sieve analyses shown in Table 3.8, the EAF-slag aggregates also conform to the specifications of IS: 383-1970 shown in Table 3.8. All aggregates were used in saturated surface dry condition.



a. Jelly



b. EAF Slag

**Fig 3.4 (a-b) Coarse aggregates used in HSAASC mixes**

**Table 3.6 Physical Properties of Coarse aggregates used in the study**

Sl. No	Test	Coarse Aggregate (MAS 12.5mm)	
		Jelly	EAF Slag
1	Specific Gravity	2.65	3.0
2	Fineness Modulus	6.8	6.9

**Table 3.7 Chemical Composition - EAF slag**

Oxide Content	EAF slag (% by weight)
CaO	34.70
Al <sub>2</sub> O <sub>3</sub>	4.19
Fe <sub>2</sub> O <sub>3</sub>	24.20
SiO <sub>2</sub>	19.12
MgO	6.20
Minor Minerals	1.63
Insoluble Residue	9.7
LOI	0.26

**Table 3.8 Results of sieve analysis - Coarse aggregates (MAS 12.5mm)**

IS Sieve Designation (mm)	Cumulative % Passing	
	Jelly	EAF slag
20	100	100
16	100	100
12.5	96.5	97.6
10	57.3	59
4.75	1.6	1.96
Both types of Coarse aggregates satisfy the requirements of aggregates as per IS:383-1970		

### 3.2.6 Water

In the present investigation tap water available in the institute laboratory was used for preparation of alkaline activator solutions, for mixing of the AAS and OPC-based concrete mixes and for curing of OPC- based reference concrete specimens.

### 3.2.7 Di-basic Sodium Phosphate

Commercially available Di-basic sodium phosphate procured from M/s Loba Chemie Pvt. Ltd, Mangalore, India, with 98% purity was used as chemical additive in the present investigation.

### 3.2.8 Superplasticiser

Commercial available, poly-carboxyl ether (PCE) based high-range water-reducing (HRWR) admixture procured from M/s BASF Pvt. Ltd; Mangalore, India was used as a super-plasticizer in the present investigation. Properties of the super-plasticizer used are given in Table 3.9.

**Table 3.9 Properties of super-plasticizer used - Master Glenium ACE 30 (JP)**

Specific Gravity	1.09
Chloride Content	Nil
Solid content	34%
Recommended dosage	12ml/kg of binder
Operating Temperature	10 to 40°C
Color	Light dark brown liquid

### 3.2.9 Alkaline Activator

The alkaline activator solutions used in this study were mixtures of sodium silicate solution and sodium hydroxide flakes of 97% purity. Both the liquid sodium silicate and sodium hydroxide flakes were procured from a local supplier. Properties of sodium silicate were determined as per IS 14212 – 1995. Properties of both these ingredients are shown in Table 3.10 and 3.11 respectively.

**Table 3.10 Properties of liquid Sodium silicate**

Constituent	% by weight
Na <sub>2</sub> O	14.7
SiO <sub>2</sub>	32.8
Solids	47.5
Water content	52.5
Modulus (Ms) (SiO <sub>2</sub> /Na <sub>2</sub> O)	2.23
Specific gravity	1.57

The alkaline solutions were prepared by dissolving specified quantities of sodium hydroxide flakes in the small quantity of total calculated water along with the sodium silicate solution, so as to obtain a desired modulus (Ms). The remaining water was then

added to bring the total water/binder ratio to any desired value of (0.40 - 0.44). In order to reduce the heat liberated during mixing and also to prevent the quick-setting of slag, the alkaline solutions prepared were allowed to cool and mature for 24 hours, prior to use in the preparation of any of the AASC mixes.

**Table 3.11 Properties of Sodium hydroxide (97% purity)**

Molecular formula	NaOH
Molar mass	40 g/mol
Appearance	White solid
Specific Gravity	2.1
Solubility in water Reference temperature (25 <sup>0</sup> C)	114 g/100 ml

### 3.3 MIX-DESIGNS, PREPARATION OF MIXES AND CASTING OF TEST SPECIMENS

#### 3.3.1 General

The AASC mixes developed herein were initially targeted to achieve the property of self-compacting as per the relevant EFNARC guidelines, along with the higher compressive strength values varying in the range 70-90MPa. In order to develop these mixes series of trials were conducted and then the range of binder contents, dosage of sodium oxide and w/b ratio was fixed. In general AASC mixes are often encountered with issues relate to rapid initial setting action and hence an attempt was being made for enhancing the initial setting time of all the AASC mixes. Several trials were performed using various chemical additives with appropriate dosages and the additive with optimum dosage showing enhanced initial setting time and better mechanical property was selected for the further mixes. In order to reduce the experimental efforts Taguchi design of experiments was adopted. Initial nine mixes were designed based on the Taguchis L-9 orthogonal array as the calibration phase and based on the results obtained in the calibration phase, multi linear regression equations were developed. In order to

validate these developed regression equations, another set of six mixes were randomly selected and experiments were conducted and verified with developed regression equations.

### **3.3.2 Mix Design of AASC mixes – Taguchi’s DOE approach**

A set of fifteen mixes were developed with GGBFS as the prime binder, with the total binder content in the range of 700 - 800 kg/m<sup>3</sup> (in increments of 50 kg/m<sup>3</sup>), of fresh concrete. As a possible measure to further improve the microstructure within the binder phase of the concrete mixes, fine quartz powder (15% w.r.t to total binder content) was also used in these mixes. The alkaline solutions – mixtures of sodium hydroxide and sodium silicate, were having Na<sub>2</sub>O percentages varied between 5 to 7%, but with a constant activator modulus of 1.0 maintained in all of them. The net w/b ratios of all the AASC mixes were varied within a narrow range of 0.40 – 0.44. Further the OPC reference concrete mix was developed with a total binder content of 600 kg/m<sup>3</sup> (85% - OPC and 15% - Fine quartz powder w.r.t to total binder content). A constant w/b ratio of 0.40 was maintained for the control OPC reference concrete mix.

Taguchi’s DOE methodology (Montgomery 2004) was used to reduce the experimental efforts. Initially, in the calibration-phase, only nine mixes based on Taguchis L-9 orthogonal array were considered, with each of the three input parameters – the binder content, the w/b ratio and the Na<sub>2</sub>O dosages, considered as the most influencing parameters, taken at three levels, as detailed in Table 3.12 (Chitawadagi et al. 2010, Malkapur et al. 2017). Thus the input parameters had the values as given in Table 3.13, in the initial calibration mixes. Again, ranges (limits) of binder contents and w/b were selected, based on experience of large number of initial trials, so as to ensure that each of these mixes attains the required level of flowability specified for self-compacting mix as per EFNARC (2002) guidelines. The dosages of sodium oxide in the alkaline solution greater than 8% caused the leaching of alkalis, decreasing the performance of any alkali-activated slag concrete mix and hence the dosage was restricted to a maximum of 7%.

In order to enhance the initial setting times of the AAS concrete mixes, commercial available di-basic Sodium phosphate was used as a retarder (at 1% of total binder

content, by weight). Again, in order to ensure enhanced flow ability characteristics in all the mixes so as to be self-compacting, a commercial available, PCE-based high-range water reducing (HRWR) admixture - Glenium ACE 30 (JP) supplied by M/s BASF, Pvt. Ltd., Mangalore, India was used in smaller percentages.

**Table 3.12 Input parameters for the Taguchis method**

<b>Factors</b>	<b>Level 1</b>	<b>Level 2</b>	<b>Level 3</b>
Binder Content (kg/m <sup>3</sup> )	700	750	800
w/b ratio	0.40	0.42	0.44
Na <sub>2</sub> O (%)	5	6	7

In the absence of any national code or general guidelines for the design of high strength, self-compacting AASC mixes, absolute volume method was used for proportioning of all the trial mixes developed herein. The ratio of fine aggregates (FA) to coarse aggregates (CA) was maintained a constant at 60:40 (by volume) in all the mixes. The calculations of the proportion of ingredients for OPC-based reference concrete mix and a representative HSAASC mix are given in (Appendix-I) and (Appendix-II). Details of the quantities of all the individual ingredients in the initial nine mixes (HSAASC-1 to HSAASC-9), and the reference HSS-OPCC mix computed based on absolute volume method, are given in Tables 3.14 and 3.15.

In order to ensure better mixing of all the materials, a ribbon-type mixer with a horizontal shaft was used. After thorough mixing, concrete mixes were discharged from the mixer and were subjected to different flow ability tests to ascertain that the mixes do qualify as self-compacting mixes as per the EFNARC (2002) guidelines. Flow and strength properties of the first nine mixes were used for performance evaluation purposes in an initial, calibration phase. The final setting times of the test specimens cast were in the range of 5 - 6 hours in the case of all the alkali-activated slag concrete mixes.

**Table 3.13 Mix-Parameters for the HSAASC Mixes - Calibration phase**

<b>Mix Designation</b>	<b>Binder Content (kg/m<sup>3</sup>)</b>	<b>w/b ratio</b>	<b>Na<sub>2</sub>O (%)</b>
HSAASC -1	700	0.40	5
HSAASC -2	700	0.42	6
HSAASC -3	700	0.44	7
HSAASC -4	750	0.40	6
HSAASC -5	750	0.42	7
HSAASC -6	750	0.44	5
HSAASC -7	800	0.40	7
HSAASC -8	800	0.42	5
HSAASC -9	800	0.44	6

The strength test results of HSAASC mixes were statistical then analysed to derive the strength-prediction equations, the predictive capabilities of which were then assessed and ascertained with results of actual experiments on the next six new mixes in the validation phase. Details of Mix- parameter of these six mixes in the validation phase, with randomly selected input parameters and the details of individual quantities in each of these mixes are tabulated in Table 3.16 and 3.17.

**Table 3.14 Details of HSAASC mixes – Calibration phase - Quantities in kg/m<sup>3</sup>**

MIX ID	Binder		Fine Aggregates		Coarse Ag- gregate	Alkaline Solution			Additive
	GGBFS	Fine quartz powder	Slag Sand	Quartz sand	EAF slag	Sodium silicate solution	NaOH Flakes	Water	Sodium phosphate
<b>HSAASC-1</b>	595	105	547	181	490	107	25	224	7.0
<b>HSAASC-2</b>			538	179	485	128	30	226	7.0
<b>HSAASC-3</b>			511	171	460	149	35	229	7.0
<b>HSAASC-4</b>	637.5	112.5	506	169	456	137	32	227	7.5
<b>HSAASC-5</b>			476	159	429	161	37	230	7.5
<b>HSAASC-6</b>			492	164	444	114	27	270	7.5
<b>HSAASC-7</b>	680	120	443	148	400	171	40	230	8.0
<b>HSAASC-8</b>			461	154	416	122	28	272	8.0
<b>HSAASC-9</b>			429	144	387	146	34	275	8.0

**\*HRWR admixture is added at 0.4% (by weight of total binder) in all HSAASC mixes**

**Table 3.15 Mix design details of HSS - OPCC mix - Quantities in kg/m<sup>3</sup>**

Binder content		Fine aggregates		Coarse aggregates Jelly MAS - 12.5mm	Water	w/b
Cement	Fine quartz Powder	River Sand	Quartz Sand			
540	60	670	225	603	240	0.40

\*HRWR admixture is added at 0.4% (by weight of total binder) in HSS-OPCC mix.

**Table 3.16 Mix-Parameters for the HSAASC Mixes - Validation phase**

Mix Designation	Binder Content (kg/m <sup>3</sup> )	w/b ratio	Na <sub>2</sub> O (%)
HSAASC -10	700	0.42	7
HSAASC -11	750	0.44	6
HSAASC -12	800	0.40	5
HSAASC -13	700	0.44	6
HSAASC -14	750	0.40	5
HSAASC -15	800	0.42	7

**Table 3.17 Details of HSAASC mixes – Quantities in kg/m<sup>3</sup> - Validation phase**

MIX ID	Binder		Fine Aggregates		Coarse Aggregate	Alkaline Solution			Additive
	GGBFS	Fine quartz powder	Slag Sand	Quartz sand	EAF slag	Sodium silicate solution	NaOH flakes	Water	Sodium phosphate
<b>HSAASC-10</b>	595	105	503	168	489	149	35	216	7
<b>HSAASC-11</b>	637.5	112.5	442	147	430	137	32	258	7.5
<b>HSAASC-12</b>	680	120	437	146	425	122	28	256	8
<b>HSAASC-13</b>	595	105	491	164	479	128.	30	241	7
<b>HSAASC-14</b>	637.5	112.5	484	161	471	114	27	240	7.5
<b>HSAASC-15</b>	680	120	404	135	393	171	40	247	8

**\*HRWR admixture is added at 0.4% (by weight of total binder) in all HSAASC mixes**

### 3.4 CASTING OF TEST SPECIMENS WITH HSAASC MIXES –

#### - SPECIMEN DETAILS

In order to evaluate the strength characteristics of all the different mixes, standard test specimens were cast and were tested at different ages viz. 3, 7, 28 days. In each case, the averages of results with three test specimens were considered. The details of the specimens used for the various tests are given in Table 3.18.

**Table 3.18 Details of Test Specimens used for various tests**

SI No.	Types of test	Specimen Geometry	Specimen Dimensions (mm)	Relevant Standards
1	Cube compressive strength	Cubes	100x100x100	IS 516-1959
2	Split tensile strength	Cylinders (dia)x(height)	100x200	IS 5816-1999
3	Modulus of rupture	Beams	100x100x500	IS 516-1959
4	Modulus of elasticity	Cylinders (dia)x(height)	150x300	IS 516-1959
5	Initial and Final Water absorption	Cubes	100x100x100	ASTM C642-06

### 3.5 CURING OF SPECIMENS

The test specimens of HSAASC mixes were cured in the ambient laboratory conditions, having temperature  $30\pm 3^{\circ}\text{C}$ , with relative humidity  $85\pm 10\%$ . Test specimens of OPCC-mix concrete were cured in water a curing water tank for specified number of days (3, 7 and 28) until they were tested.

### 3.6 EXPERIMENTAL PROCEDURES

#### 3.6.1 Initial Setting time

In order to increase the initial setting time of all the AASC mixes, different chemical additives like Lime, Sucrose, Phosphoric acid, Citric acid, Tartaric acid, Borax and Sodium phosphate were taken in appropriate dosages and effects of their addition on workability and stiffening behaviour of a candidate AASC mixes were evaluated. Further the effect of using cold water and cold alkaline solution, while mixing, on the workability and setting behaviour of AASC mixes were also studied. To check the accuracy of the visually observed initial setting times of the candidate mixes, all the AASC mixes were also evaluated for their initial and final setting times as per the procedure laid out in IS 8142:1976.

### **3.6.2 Flow ability**

Slump flow, V- funnel, L- box, J-ring and Visual stability index tests were carried out for ascertaining the different flow ability properties generally prescribed for SCC mixes as per the EFNARC guidelines.

### **3.6.3 Mechanical Properties of Concrete Mixes**

For each mix, specimens were tested in triplicates using calibrated testing machines. Compression tests on cubes, flexural strength tests on prisms and modulus of elasticity tests on concrete cylinders made of all the fifteen trial mixes were conducted as per the guidelines in IS 516-1959, while split-tensile strength tests on cylindrical specimens were performed as per provisions of IS 5816:1999. Tests were conducted at different ages.

### **3.6.4 Initial Water absorption and Saturated Water absorption**

Initial Water absorption and Saturated Water absorption tests were conducted conforming to the standard procedure laid out in ASTM C642-06.

## **3.7 MICROSTRUCTURAL STUDIES**

After testing for 28-days compressive strength, fractured samples extracted from the central core of the fractured concrete cube specimens from all the fifteen HSAASC mixes were collected and further analyzed for microstructural studies. Such fractured specimens about 5-10 mm of size from each of the mix were initially oven dried and

were then subjected for analysis using a Scanning Electron Microscope (SEM) along with Energy dispersive X-ray (EDX). Since in the case of AASC mixes, much of the alkali activation reactions would have been completed at the early ages and also all the microstructural studies were performed at the age of 28-days, it was felt that immersion of these samples either in acetone or isopropyl solution, for about 24 hours, to arrest any further hydration reactions was not required and hence was not adopted.

The SEM and EDX analyses were carried out on a TESCAN Vega 3LMU instrument (Czech Republic - Make) as shown in Fig 3.5 with a maximum magnification of up to 10 lakhs and resolution of 3nm. With this facility, the micrograms can be taken with voltages varying between 5 – 30 kV, with a working distance of 1- 40 mm. All the micrograms were taken only in the secondary electron mode of imaging.

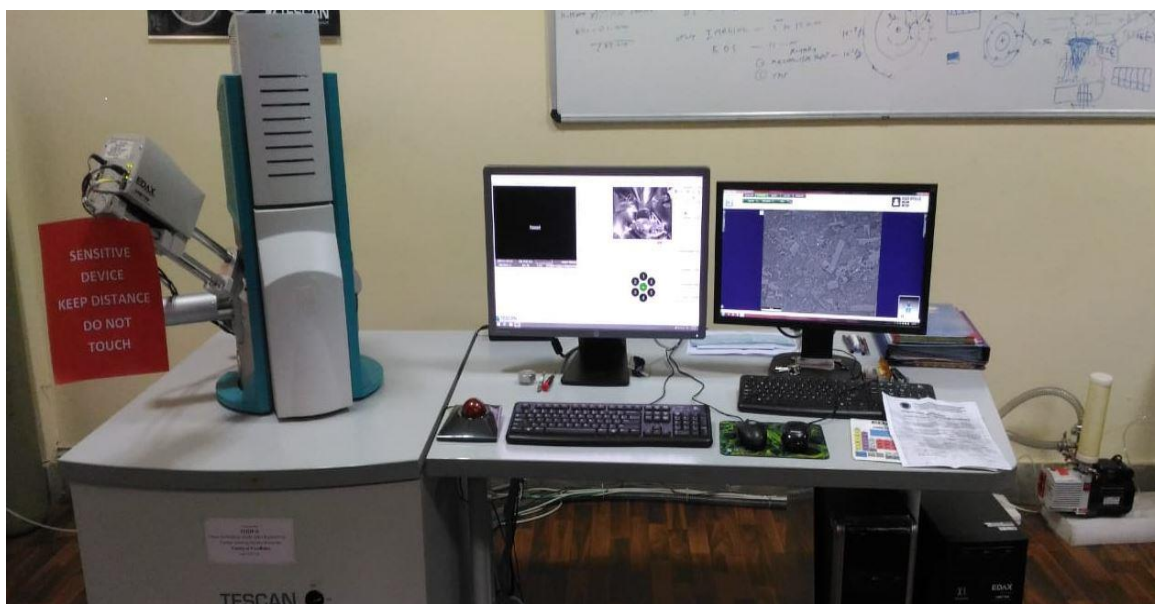


**Fig 3.5 Instrument used for SEM and EDX analysis**

The XRD instrument used in the present study is of M/s PANalytical - (Netherlands) make as shown in Fig 3.6. Diffraction analyses were made between  $2\theta$  angles varying from 1 to 80 degrees, using copper K radiations. A working voltage of 45kV and a current of 30mA were maintained constant during the experimental process. Initially the fractured specimens were finely crushed and passed through 90-micron sieve. The obtained powdered samples were then oven dried and then were subjected to XRD analyses.



**Fig 3.6 XRD instrument used in the present study**

.....

## **CHAPTER 4**

### **PERFORMANCE OF HIGH STRENGTH SELF-COMPACTING ALKALI ACTIVATED SLAG CONCRETE (HSAASC) MIXES**

#### **4.1 GENERAL**

The present chapter discusses the flow ability characteristics and the mechanical properties of the various HSAASC mixes, as in discussed in Chapter 3, in comparison with those of the reference HSS-OPCC mix. The formulation of all the mixes developed therein was based on Taguchi's L-9 orthogonal array. In order to enhance the initial setting times of the various AASC mixes, several chemical additives were used at appropriate proportions and their flow and setting characteristics were evaluated. Flow and strength properties of a set of nine mixes were used for performance evaluation purposes in an initial, calibration phase. Strength prediction equations were derived based on such results, the predictive capability of which were then assessed and ascertained with actual results of experiments on the next six new mixes, in the validation phase. Microstructure studies were conducted on samples from the fractured pieces of test specimens from different mixes, using advanced SEM, EDX and XRD analyses and the results of all such tests and analyses are discussed in this chapter.

#### **4.2. SETTING TIME AND WORKABILITY OF HSAASC MIXES**

##### **4.2.1 Initial setting time and workability characteristics of a typical AASC mixes**

Tests for the initial setting time were carried out on trial self-compacting AASC mix having their quantities available in Table 4.1, with different additives as shown in Table 4.2. The initial setting time of AASC mix with different additives is shown in Fig 4.1. The lime was added to the AASC mix with a percentage of 8% with respect to the binder content. Initially at the stage of mixing, the AASC mix in the mixer showed a trend of faster setting action and finally a sudden final setting of AASC mix was observed within about five minutes of discharging the concrete from the mixer. Figure 4.2 shows the setting behaviour of AASC mix with lime.

**Table 4.1 Details of trial AAS Concrete mix in kg/m<sup>3</sup>**

<b>MIX</b>	<b>GGBFS</b>	<b>Sodium Silicate solution</b>	<b>NaOH Flakes</b>	<b>Water</b>	<b>w/b</b>	<b>River Sand</b>	<b>Jelly</b>	<b>HRWA</b>	<b>Wet Weight</b>
AASC	800	171	40	231	0.40	573	382	2.4	2200

**Table 4.2 Details of different additives along with their dosages for kg/m<sup>3</sup>**

<b>Designation</b>	<b>A 0</b>	<b>A1</b>	<b>A2</b>	<b>A3</b>	<b>A4</b>	<b>A5</b>	<b>A6</b>	<b>A7</b>	<b>A8</b>	<b>A9</b>
<b>Additives</b>	-	Lime	Sucrose	Phosphoric acid	Citric acid	Tartaric Acid	Borax	Sodium phosphate	-	-
<b>Dosage - % Binder (by weight)</b>	-	8	2	0.85	2	0.85	0.40	2	Cold Water	Cold alkaline solution

This behaviour is due to the much faster reaction of the lime with the alkaline solution which causes an early initial setting time. However normal AASC mix with no additives showed an initial setting time of about 15 minutes as compared to the AASC mix with addition of lime.

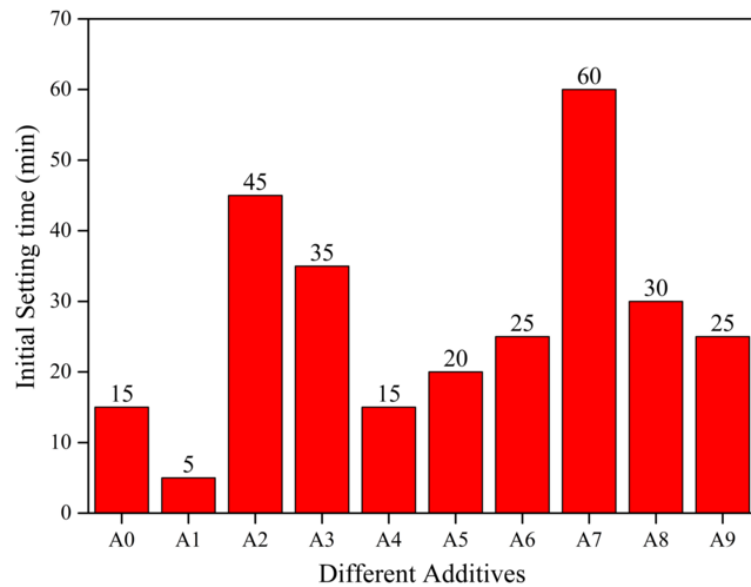


**Fig 4.1 Initial setting times of AASC mix with different additives**



**Fig 4.2 Fast setting behaviour of AASC mix with Lime addition**

Sucrose was added to the AASC mix; with an idea of deaccelerating the rate of formation of C-S-H gels, as has been reported in the case of OPC based concrete systems. But use of even sucrose as an additive to an AASC mix has not led to any meaningful extension of the setting time of AASC mixes, either but just showed an enhanced performance as compared to lime. The addition of sucrose has led to a marginal increase in the initial setting time to about 20 min, as compared to the normal AASC mix (with no additives) and this behaviour is due to the reversal process of initiating the setting time in case of an AASC mix.

Introduction of acids like Phosphoric acid, Citric acid and Tartaric acid into the AASC mixes also did show any appreciable increase in the initial setting, except for small increase in case of phosphoric acid upto about 35 minutes. However addition of citric acid and Tartaric acids led to decreased initial setting times of about 15-20 minutes and with an initial flow of about 500-600 mm. The slump-flow of the mix was repeatedly checked at regular intervals. Better flow-ability properties were observed in the case of phosphoric acid with a flow value of greater than 600 mm, which again was retained for more than 15 minutes; however, after 15 minutes, a sudden decrease in the flow to about 550mm – 450 mm was observed. In further 20 – 25 minutes, the concrete mix was observed to be stiffening and losing its workability and hence the test specimens were immediately cast with the stiff AASC mix. Thus the addition of all the acid additives led to slight increases in initial setting times as compared to the normal AASC mix without additives. One major issue observed during the addition of these acid additives to the AASC mixes, however, is the release of a pungent smell, which caused difficulty during their mixing.

When Borax was added to the AASC mix at an initial low dosage of 0.4% (by weight of total binder), there were no problems faced during the initial mixing of the concrete in the mixer. During the slump flow test, flow greater than 600 mm was observed in the initial 15 – 20 minutes for the AASC mix admixed with Borax; again this mix retained a good slump-flow, marginally lower by about 50mm, for about 30 minutes. Further, the slump flow started decreasing faster with loss in flow of almost 100 mm observed by 45 minutes; however the concrete at this stage was still quite workable, with possible necessity of a vibrator for compaction.

The addition of Borax, might probably have delayed an early formation of C-S-H gels. To check the possibility of extending the initial setting time further, on addition of Borax, trials were performed with addition of different percentages of Borax (such as 0.2, 0.6 and 0.8% , by weight, of the binder) to the reference AASC mix. Trends similar to above were observed with addition of 0.2% of Borax, with the maximum slump-flow recorded at 30 minutes; Increase in the percentage of Borax added beyond 0.4%, however showed a reversed trend, with earlier initial setting, leading to large decreases in the flow behaviour of AASC mix, even before 30 minutes. Thus it can be said that an optimum percentage of Borax at, say, 0.4% can be used to provide a better flow and setting performance of the AASC mixes as compared to normal AASC mix without additives. It is important to recognise that these characteristics of an AASC mix may be quite sensitive to even small variations in the dosages of the additives used.

Addition of sodium phosphate with an initial dosage percentage of 2.0% of binder (by weight) showed a greater increase in the initial setting time, with a slump flow of almost 700mm as shown in Fig 4.3 was retained even after 15-20 minutes after placing. Herein an increase in the initial setting time was observed upto 40-50 minutes with a decreased slump-flow measuring upto about 500mm even at the end of one hour since mixing, as shown in Fig 4.4. Thus the AASC mix added with sodium phosphate continued to have a satisfactory flow available with it upto a good one hour after mixing. Further, the concrete mix started to show signs of faster setting and hence was poured into the test moulds. Due to such enhanced performance with sodium phosphate, as an additive, further trials were also made with alternate percentages of Sodium phosphate at 1.0%, 1.5% and 2.5% as well. Decrease in the percentage of sodium phosphate upto to 1%, showed similar increase in the initial setting time as compared with 2%. However increase in sodium phosphate to 2.5% showed a reversed action in that the initial setting time got reduced to about 25 minutes. This increase in the initial setting time might have been caused due to the dissolution of calcium present in the slag which reacts with phosphate leading to the formation of tri calcium phosphate ( $\text{Ca}_3(\text{PO}_4)_2$ ) which possibly delays the activation of the slag grains initially (Chang et al. 2005, Gong and Yang 2000).



Fig 4.3 Slump flow of AASC mix with sodium phosphate placing after 20 minutes

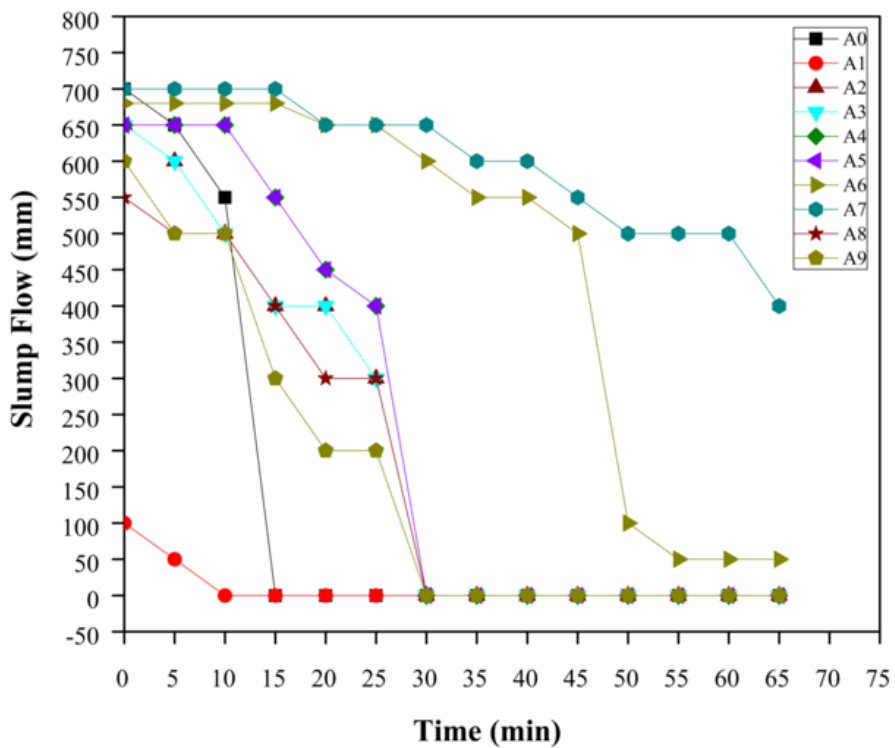


Fig 4.4 Variation of flow ability of different additives with time

It has been reported in literature, that lower ambient temperature retards the onset of setting of AASC mixes. Hence it was felt that use of cold water during mixing may facilitate retarding the initial stiffening and extend the initial setting time of these mixes. Hence cold water (water kept in a deep freezer at about 15° C for 24 hours) was used during the mixing of the AASC mix (instead of normal tap water). Similarly use of the alkaline solution, kept in the deep freezer at 15° C for 24 hours, for mixing, was also tried as a possible means of delaying the initial setting. However no much advantage was gained in increasing the setting time of the candidate AASC mix even in these two cases.

#### **4.2.2 Compressive strength of typical AASC mixes admixed with different additives**

The compressive strength tests were performed on standard cube specimens of all the AASC mix containing different additives as per IS 516:1959 at 3, 7 and 28 days. It was observed that 28-day strengths obtained for the various mixes were in the range of 40 – 90 MPa as shown in Table 4.3. Again the variation of such compressive strength test results, for AASC mixes with different additives are shown in Fig 4.5.

In the case of AASC mixes admixed with Lime and Sucrose, however, the initial 3-days strength values in the range of 45MPa – 50MPa were observed to increase marginally to a range of 52 - 59 MPa by 28-days. However a decrease in strength was observed compared to normal AASC mix without additives. In case of lime admixed AASC mixes, decrease in strength may be probably due to its flash setting action, causing an improper compaction, leading to the increased porosity of the concrete specimens, causing the decrease in the compressive strength values. Further addition of sucrose, slightly decreases the alkali activation process at the early stages forming a covering layer over the slag grains leading to the decrease in the formation of the C-S-H gels. It can be observed that, while with addition of acidic additives such as Phosphoric, Citric and Tartaric acid, the AASC mix showed satisfactory early-strengths (at 3-days), the reported strengths show a decreasing trend with age during the period of 3 to 28 days as compared to normal AASC mix without additives varying in the range of 65 MPa – 80 MPa. This may possibly be due to dissolution of the initially formed of

C-A-S-H gels in the presence of any of Citric, Tartaric and Phosphorous acid. It may also be possible due to the weakening of covalent bonds in the C-S-H gels formed that the strength values decrease with age.

It is indeed interesting to observe the higher early 3-day strength of the order of 75 MPa with Borax used as an additive, wherein advantage of delayed initial setting time also had been realized. Again herein no additional strength-gains have been recorded with further increase in age upto 28-days.

The best performance in terms of a reasonably delayed initial setting coupled with enhanced strength characteristics at all ages in an AASC mix, however, appears to come with admixing of Sodium phosphate as an additive, as can be seen from test results in Fig 4.5 and Table 4.3.

While no appreciable increase in initial setting time had been recorded by use of either cold water (at 15<sup>0</sup> C) or cold alkaline solution, it however appears that they also can be applied in a bid to increase the early 3-day strength with no strength degradation with age later.

**Table 4.3 Compressive strengths of AASC mix with different additives**

Mix designation	Additive Used	Cube Compressive Strength (MPa)		
		3-days	7-days	28-days
A0	NIL	65	70	80
A1	Lime	45	50	52
A2	Sucrose	50	55	59
A3	Phosphoric acid	50	45	40
A4	Citric acid	50	45	40
A5	Tartaric acid	60	50	45
A6	Borax	75	75	77
A7	Sodium Phosphate	85	87	90
A8	Cold water	75	80	84
A9	Cold alkaline soln.	79	82	84

The highest compressive strengths in the range of 85 – 90 MPa have been recorded at 3 - 28 days of age with AASC mix admixed with 1% of Sodium phosphate, which are quite encouraging. The alkali metal ions of sodium, supplemented additionally by sodium phosphate, however may further enhance the activation process at the later stages.

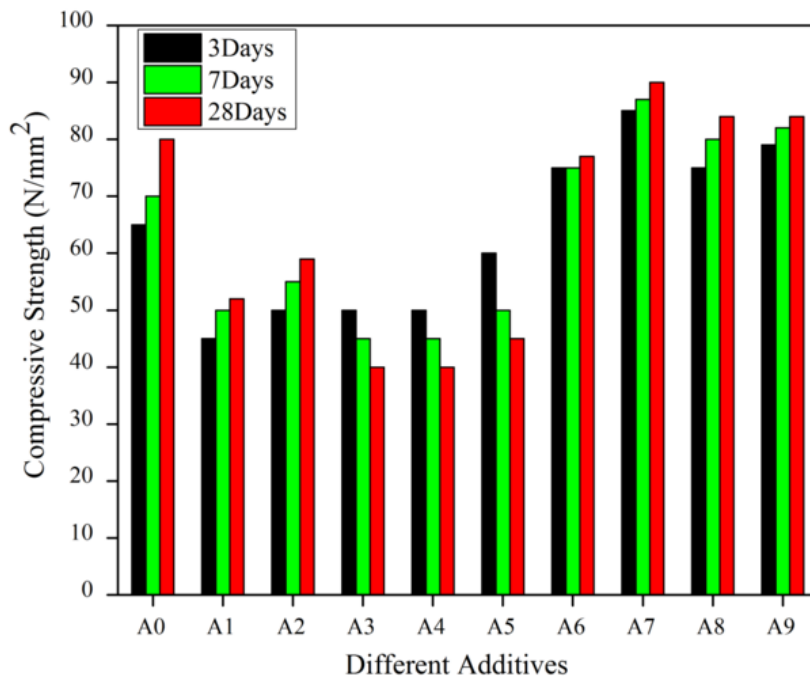


**Fig 4.5 Variation of compressive strength values with different additives**

#### 4.2.3 Discussions

1. The initial setting time of AASC mix can be increased by addition of several additives such as Borax, Phosphoric acid and Sodium phosphate compared to normal AASC mix without additives. However Sodium phosphate (at 1% dosage) and Borax (at 0.4% dosage) showed higher increases in the initial setting time and workability. Further increase or decrease in dosages of these additives, as referred to above dosages, may also cause a reversed effect on the AASC mixes.

2. Acceptable range of compressive strengths were obtained for Borax, Cold water, Cold alkaline solution and Sodium phosphate which are in the range of 75 – 90 MPa. The AASC mix with dosage of sodium phosphate at 1% of total binder (by weight)

showed the highest compressive strength of 90 MPa and a maximum initial setting time of 60 min, amongst all the additives, as compared to normal AASC mix without additives. This may be due to the synergic effect of phosphate ions causing a retarding effect to the activation process and hence lower rate of formation of C-A-S-H gels in the initial hours; while the metal (Sodium) alkali ions contribute to the activation of all the slag grains leading to higher later-age strengths.

#### **4.2.4 Setting time characteristics of HSAASC mixes using penetrometer resistance test.**

In order to verify the initial setting time characteristics performed by visual observation using different additives for a typical AASC mix, all the fifteen HSAASC mixes with sodium phosphate as additive (1% w.r.t to total binder content) were again checked for their initial setting time using the standard procedure laid out in IS:8142-1976.

The entire test is carried on a cube of size 150mmx150mmx150mm. The prepared HSAASC mixes is sieved through 4.75 mm sieve so that enough mortar is available to fill the test specimen to a depth of at least 140 mm. Then the mortar is mixed thoroughly and placed in the cube specimen in layers. Further each layer of mortar is compacted using the tamping rod. The final height of mortar after tamping should not be less than 13 mm from the height of the cube specimen. This space is provided for the collection and removal of any bleeding water.

Before testing, any bleeding water present on the surface of the mortar is removed by means of a pipette. Then the needle is attached with the penetration resistance apparatus as shown in Fig 4.6 and needle is placed in contact with the mortar surface. Then a vertical downward force is gradually and uniformly applied, until the needle penetrates to a depth of 25 mm, as indicated by scribe mark provided in the apparatus. Further the force required for producing a penetration of 25mm and the time of inserting the penetrometer i.e. time when alkaline solution is mixed with binder is noted down. Similar procedure is repeated for the remaining needles of 645, 323, 161, 65, 32 and 16 mm<sup>2</sup> as shown in Fig 4.6. A minimum of six penetrations is performed and continued until the penetration resistance of at least 26.97 MPa is reached. Then graph is plotted

between time (min) along with penetration resistance (MPa) and connected by using smooth curve. Penetration resistance corresponding to 3.43 MPa and 26.97 MPa gives initial setting and final setting time of all the HSAASC mixes tested herein.

The initial setting time of all the fifteen HSAASC mixes tested herein were in the range of 50-60min as shown in Fig 4.7 which is in par with the results obtained through trials carried out by mean of visual observations.



**Fig 4.6 Penetration resistance apparatus with tested concrete sample**

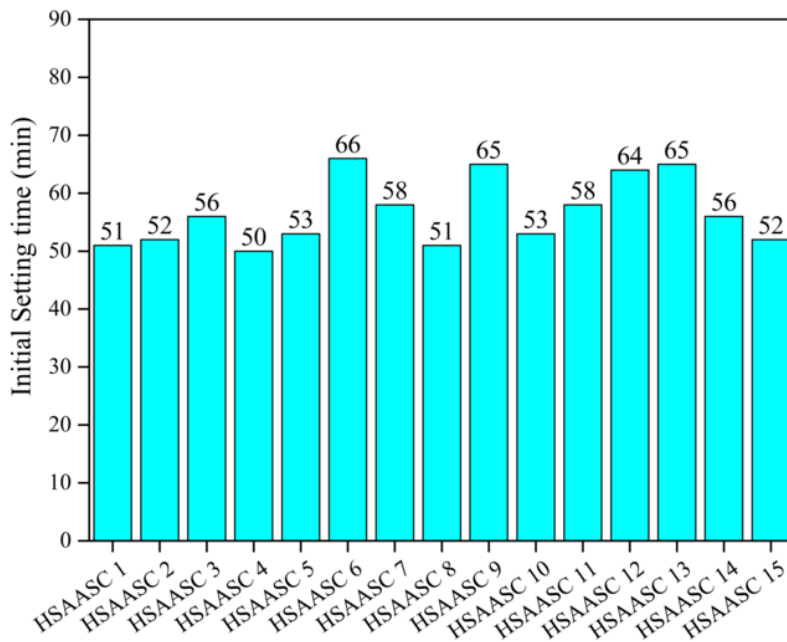


**Fig 4.7 Initial setting time of various HSAASC mixes**

### 4.3 FLOW TESTS ON FRESH HSAASC MIXES

Slump flow, V- funnel, L- box, J-ring and Visual stability index tests were carried out for ascertaining the different flow ability properties generally prescribed for SCC mixes, on all the fifteen HSAASC mixes – nine of the calibration phase and six of the validation phase, immediately after mixing. The slump flow tests were carried out using the Abram’s cone, to evaluate the flowing ability of all the different HSAASC mixes as shown in Fig 4.8a. The times  $T_{50}$  taken for the concrete mixes to reach a spread of 500 mm were also evaluated.

From Table 4.4, it can be clearly observed that the first three mixes in the calibration phase (HSAASC-1 to HSAASC-3), with a minimum binder content of  $700 \text{ kg/m}^3$ , showed slump flows in the range 785 -800 mm and  $T_{50}$  values of about 4.0 – 4.5 seconds, satisfying the relevant EFNARC guidelines wherein a slump flow ranging from 650 – 800 mm and  $T_{50}$  of less than 5 seconds are specified. With increased binder contents of 750 and  $800 \text{ kg/m}^3$  (mixes HSAASC-4 to HSAASC-9), however, decreased

slump flows, all ranging between 700mm – 755mm respectively and increased  $T_{50}$  values at 4.5 - 5.0 seconds were recorded. Similar behaviour can be observed in the six HSAASC mixes of the validation phase, again all of them recording slump flow values in the range of 710mm - 780mm and  $T_{50}$  values of about 4.5 – 4.9 seconds them also satisfying the relevant EFNARC guidelines. The decrease in the flow with increased binder contents is mainly attributed to the large increases in the surface area of solids resulting on addition of higher amounts of finer quartz powder material, which hence use larger amounts of water present just for wetting the smaller sized particles.



**a – Slump Flow Test**



**b – V-Funnel Test**



**c - L -Box Test**



**d - J-Ring Test**

**Fig 4.8 (a-d) Different Flow tests performed on HSAASC mixes**

V-Funnel tests (Fig. 4.8b) were carried out on all the HSAASC mixes – both of the calibration and validation phases. The times taken for emptying the V-Funnel were in the range of 8.5 – 10.4 seconds for the binder contents varying between 700 – 800 kg/m<sup>3</sup> as observed in Table 4.4 and Table 4.5 all satisfying the EFNARC guidelines (values to range between 6-12 sec). Based on results of the V- funnel tests of the various mixes, it can be concluded again that all the HSAASC mixes could easily fill and/or pass through small constrictions in the form-works and so also areas between highly congested rebars, leading to better structural conditions. It is the availability of relatively higher volumes of pastes and smaller size of the coarse aggregates used that have favoured higher flowing ability of these mixes.

L-Box tests were conducted on the various HSAASC mixes for testing their passing ability (Fig. 4.8c). It can be seen that all the fifteen candidate mixes tested herein have excellent abilities to pass through narrow passages between the reinforcing bars, the blocking ratios  $H_2/H_1$  being in the range 0.88 - 0.95 satisfying the relevant EFNARC guidelines, as observed in Table 4.4 and Table 4.5. The mixes with a relatively lower binder content of 700 kg/m<sup>3</sup>, and hence slightly higher content of coarser materials, exhibited the minimum passing ability ( $H_2/H_1 = 0.88$ ). But it can be clearly seen that, an increase in the binder content, which in turn increases the volume of pastes, along with the finer material, leads to an increase in the passing ability of any of the mixes.

The times  $T_{200}$  and  $T_{400}$ , taken by the concrete-front to flow through distances of 200mm and 400mm in the horizontal channel, from the plane of rebars, was also measured for all the concrete mixes with their values ranging between 4 to 10.9 seconds as shown in Table 4.4 and Table 4.5. These results suggest that all the HSAASC mixes developed were quite suitable for application in structural elements with congested reinforcements.

J-Ring tests (Fig. 4.8d) were also performed on all the fifteen HSAASC mixes and the results of those tests are also shown in Table 4.4 and Table 4.5. It is observed that differences between the measured levels of concrete inside and outside of the J-ring were ranging between 7.8– 9.7 mm, satisfying the EFNARC guidelines (values to be  $\leq 10$  mm) for all the mixes.

**Table 4.4 Flow ability Properties of HSAASC mixes – Calibration Phase**

Tests for	Filling Ability			Passing Ability						Segregation Resistance
	Slump Flow Test		V-Funnel Test	L-Box Test			J-Ring Test			Visual Stability Index (VSI)
	Spread mm	T <sub>50</sub> sec	T <sub>vf</sub> sec	<sup>\$</sup> T <sub>200</sub> sec	<sup>\$</sup> T <sub>400</sub> sec	H <sub>2</sub> /H <sub>1</sub>	Spread mm	T <sub>50</sub> sec	Difference in Height mm	
<b>HSS - OPCC</b>	675	5.0	10.1	6.0	10.1	0.86	660	7.9	11	0
<b>HSAASC-1</b>	800	4.0	8.5	4.0	6.9	0.93	795	4.8	7.8	0
<b>HSAASC-2</b>	780	4.2	9.2	4.5	6.4	0.90	773	5.0	8.0	0
<b>HSAASC-3</b>	785	4.5	9.8	5.0	7.6	0.90	782	4.9	7.8	0
<b>HSAASC-4</b>	755	4.6	9.8	7.8	9.6	0.93	750	5.6	8.7	0
<b>HSAASC-5</b>	740	4.5	10.0	7.0	10.1	0.95	736	5.8	9.0	0
<b>HSAASC-6</b>	730	5.0	10.0	7.4	10.0	0.90	720	5.0	9.4	0
<b>HSAASC-7</b>	725	5.0	10.1	7.9	10.2	0.91	718	5.5	9.0	0
<b>HSAASC-8</b>	700	4.9	10.4	8.1	10.3	0.90	693	5.7	9.1	0
<b>HSAASC-9</b>	720	4.8	10.0	8.0	10.2	0.88	714	5.8	9.7	0

**Table 4.5 Flow ability Properties of HSAASC mixes – Validation Phase**

Tests for	Filling Ability		Passing Ability							Segregation Resistance
	Slump Flow Test		V-Funnel Test	L –Box Test			J-Ring Test			Visual Stability Index (VSI)
Mix ID	Spread mm	T <sub>50</sub> sec	T <sub>vf</sub> sec	<sup>\$</sup> T <sub>200</sub> sec	<sup>\$</sup> T <sub>400</sub> sec	H <sub>2</sub> /H <sub>1</sub>	Spread mm	T <sub>50</sub> sec	Difference in Height mm	
<b>HSAASC-10</b>	735	4.7	10.2	6.1	10.4	0.89	728	5.6	8.7	0
<b>HSAASC-11</b>	710	4.9	10.0	6.8	10.6	0.90	700	5.8	9.2	0
<b>HSAASC-12</b>	750	4.5	9.1	8.4	10.8	0.89	740	5.0	9.0	0
<b>HSAASC-13</b>	730	4.6	9.5	8.0	10.9	0.88	725	5.0	9.2	0
<b>HSAASC-14</b>	725	4.5	9.0	7.2	10.0	0.90	720	5.0	9.4	0
<b>HSAASC-15</b>	780	4.5	8.5	7.6	10.7	0.92	771	4.8	8.5	0

Again it was also observed in these tests that there were no significant decreases in the slump-flow values measured with the J-ring, differences ranging between 5 – 10mm with respect to the initial slump flows as shown in Table 4.4 and Table 4.5.

Visual Stability index (VSI) tests were also simultaneously conducted on all the test mixes with different binder contents and with their varying dosages of Na<sub>2</sub>O and w/b ratio, as per ASTM C 1611– 2014. With the type of spreads depicted in Fig 4.8a and Fig. 4.8d obtained for all the fifteen mixes, it could be inferred that all the candidate mixes tried herein were quite stable with no signs of segregation or bleeding. Hence all these mixes were assigned a VSI value of zero. This behaviour can be attributed to the higher contents of total fine powdery materials incorporated in the HSAASC mixes leading to higher paste-volumes, with appreciable decreases in the yield stresses induced in the concrete, causing the concrete to flow like a fluid. Materials of slag sand and EAF slag used as aggregates in all the HSAASC mixes herein showed remarkable compatibility with the binder materials. The liquid sodium silicate component of the alkaline solution provided a viscous nature to the mix which inhibits the segregation and bleeding. The choice and size (12.5mm down) of the aggregates, taken at relatively lower volumes, play a lead role in causing the higher flows, without segregation or bleeding.

#### **4.4 PROPERTIES OF HSAASC MIXES IN HARDENED STATE**

##### **4.4.1 Compressive strengths of HSAASC mixes**

All HSAASC mixes tested herein have shown higher compressive strength values on testing as per IS 516:1959. It can be observed that compressive strengths in the range of 84 MPa – 94 MPa have been obtained, higher than reference OPC-based concrete mix being 79MPa as shown in Fig 4.9, for binder-contents in the range of 700 - 800kg/m<sup>3</sup>. The physical and structural characteristics of the binders formed in the mixes are responsible for causing the higher early strength in AASC mixes. The dissolution and precipitation processes are the major mechanisms in the kinetics of AASC at higher alkalinity as compared to the diffusion-controlled process that happens during the hydration of OPC (Wang and Scrivener 1995). As generally observed in any alkali-activated slag concrete system, higher strengths have been obtained at as early an age

as three days. Similar behaviour has been observed in case of all the HSAASC mixes tested herein, due to the early activation of slag occurring in the presence of alkaline solution leading to the early formation of semi-crystalline C-A-S-H gels.

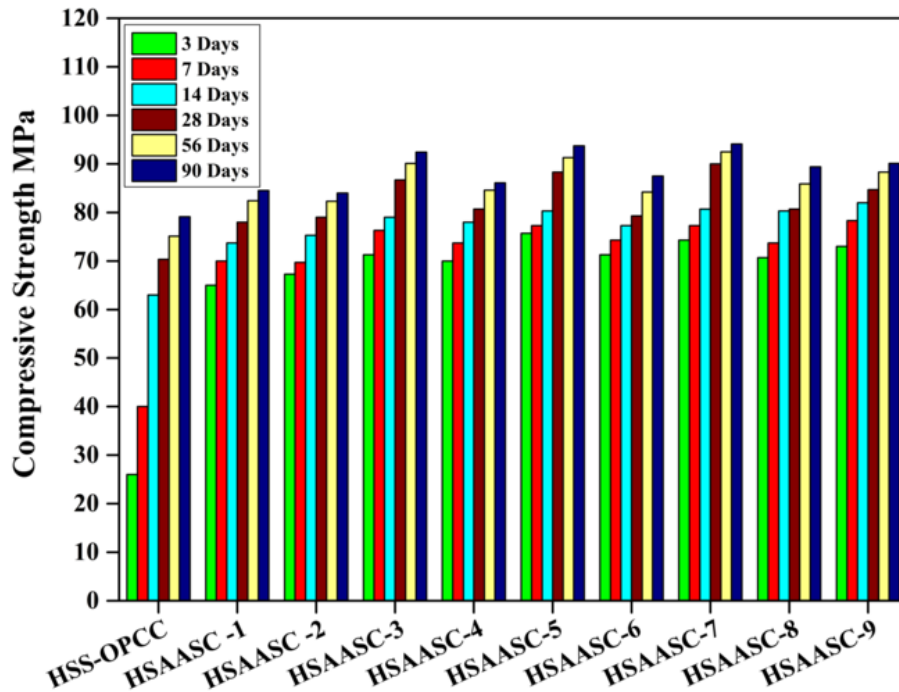


**Fig 4.9 Compressive Strength values of HSAASC mix – Calibration Phase**

Also the unreacted CaO generally present in GGBFS may react with the reactive SiO<sub>2</sub> present in the fine amorphous quartz leading to the formation of additional C-A-S-H gels (Fernandez-Jimenez and Puertas 2003, Wang and Scrivener 2003) all accounting for higher early-age strengths. The crystalline quartz sand, added as a partial fraction of fine aggregate appears to have provided for effective pore filling effect inside the AASC system leading to the decreased porosities and denser microstructures. The highest 90-days compressive strength of about 94 MPa was achieved in the mix HSAASC -7 with a total higher binder content of 800 kg/m<sup>3</sup>. The quantity of alkaline solution in this HSAASC-7 mix is about 45% higher as compared to all the other mixes, and the amounts of fine amorphous quartz (binder) as well as the quartz sand (filler) are also higher as clearly observed from Table 3.14. The faster rate of activation of GGBFS

has caused an increased strength in this mix as compared to other mixes which is due to the higher amounts of OH<sup>-</sup> ions available, in the increased amounts of the alkaline solution, has caused an increased strength in this mix, as compared to other mixes.

Based on Taguchis DOE analysis, the results for only 3, 7, 14, and 28-compressive strengths obtained for the nine HSAASC mixes in the calibration phase were statistically analysed using the commercially available MINITAB Ver. 17 software. The corresponding response tables and main-effects plots are drawn for compressive strengths at each of the above representative ages. Such calculated responses of compressive strengths at 28-days age are shown for the mixes tested in the calibration phase in Table 4.6 and the corresponding main-effect plots are given in Fig. 4.10.

Based on the results of mean of means given, it can be inferred that, out of the three mix-parameters considered, the strength of AASC mixes is primarily affected by the % Na<sub>2</sub>O (Rank 1), while the Binder content (Rank 2) and water-binder ratio (Rank 3) of mixes have relatively lower influence, in that order.

**Table 4.6 Response Table for compressive strength at 28 Days -Means of Means  
- Calibration Phase**

<b>Level</b>	<b>Binder Content (A)</b>	<b>w/b (B)</b>	<b>Na<sub>2</sub>O % (C)</b>
<b>1</b>	81.22	82.89	79.33
<b>2</b>	82.78	82.67	81.45
<b>3</b>	85.11	83.56	88.33
<b>Delta</b>	3.89	0.89	9.00
<b>Rank</b>	<b>2</b>	<b>3</b>	<b>1</b>

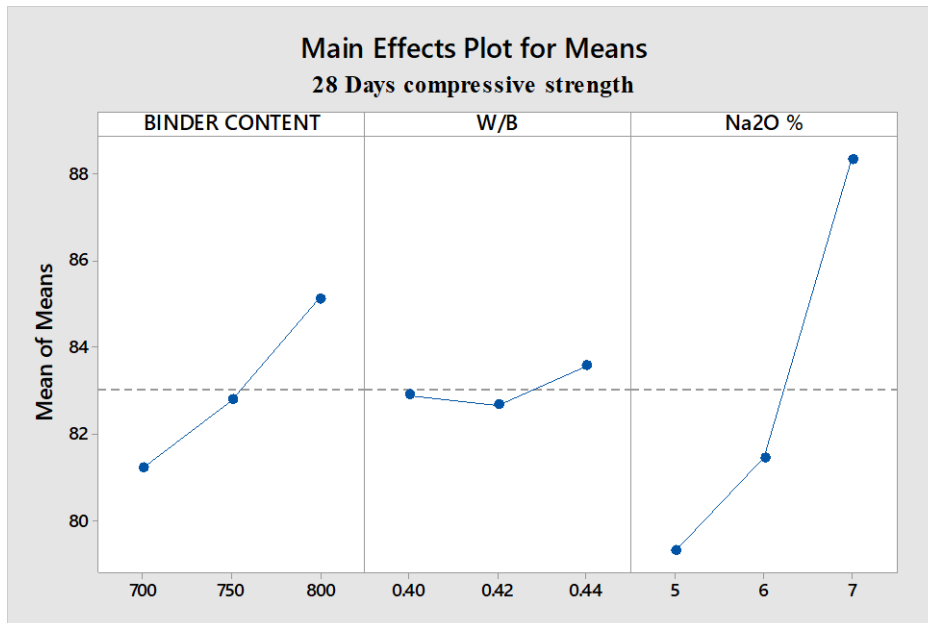


**Fig 4.10 Main effects plots - 28-days compressive strength – Calibration Phase**

From Fig. 4.10, it can be clearly observed that while with an increase in percentage of Na<sub>2</sub>O or in the binder content used, higher increases in the 28-day compressive strength are observed for the HSAASC mixes, only a marginal increase in 28-day compressive strengths are recorded with increase in the w/b ratio. Again, the statistical analysis of the strength results, led to the following regression equation for possible prediction of 28-day strength of the HSAASC mixes.

**Compressive Strength @ 28-days (MPa) = 19.9 + 0.0389 A + 16.7 B + 4.500 C ... (Eqn. 4.1)**

Where A, B and C respectively stand for Binder Content (kg/m<sup>3</sup>), water-binder ratio and percentage of Na<sub>2</sub>O in the mixes.

Similar trends, as obtained with strength at 28-days of age, were also observed in the main-effect plots and mean-of-means responses of the compressive strengths recorded for the HSAASC concrete mixes (Calibration phase) at an early 3-days and at so also intermediate 7-days and 14 days of ages, as well. The following regression equations derived, indicate that the strengths of HSAASC mixes at these earlier ages are most influenced by the binder content, followed by the Na<sub>2</sub>O dosage and w/b ratio in that order. The corresponding predictive equations of HSAASC mixes are obtained as,

**Compressive strength @ 3-days (MPa) =**

$$- 1.4 + 0.0478 A + 52.7 B + 2.388 C \dots \text{(Eqn. 4.2)}$$

**Compressive strength @ 7-days (MPa) =**

$$0.2 + 0.0444 A + 66.6 B + 2.165 C \dots \text{(Eqn. 4.3)}$$

**Compressive strength @ 14-days (MPa) =**

$$11.38 + 0.050 A + 49.9 B + 1.445 C \dots \text{(Eqn. 4.4)}$$

Now that the strength-prediction equations have been derived, the efficiency of these equations to accurately predict the strengths of any other HSAASC mix, with different values for the three mix-parameters, needs to be verified. Towards this end, compressive strength tests were conducted, at each of the four specified ages, on test specimens from each of the six mixes in the validation phase. Such results obtained experimentally are tabulated in Table 4.7, along with the strength values predicted for the same mixes from the regression equations above.

**Table 4.7 Compressive strengths of HSAASC mixes – Validation Phase**

MIX ID	Cube Compressive Strength (MPa)							
	3-Days		7-Days		14-Days		28-Days	
	Exp.	Pre.	Exp	Pre	Exp	Pre	Exp	Pre
HSAASC- 10	71.0	71.0	74.0	74.4	77.3	77.5	85.0	85.6
HSAASC- 11	71.7	72.0	75.0	75.8	79.0	79.5	83.3	83.4
HSAASC -12	69.7	70.0	72.3	73.2	77.0	78.6	80.7	80.2
HSAASC- 13	70.3	70.0	73.0	73.6	76.3	77.0	81.0	81.5
HSAASC-14	67.3	67.5	69.7	71.0	75.3	76.0	79.3	78.3
HSAASC-15	75.3	76.0	77.7	79.0	81.7	82.5	86.0	89.5

**Exp:** Experimental Compressive Strength

**Pre:** Predicted Compressive Strength

The same results are presented graphically in Fig. 4.11, where, it can be verified that the R-Sq. values in the graphs are varying between 0.97 - 0.99, indicating the very good predictive capability of each of these equations. Hence it can be said that the equations of this type can be derived and hence used to predict the compressive strengths of this class of mixes.

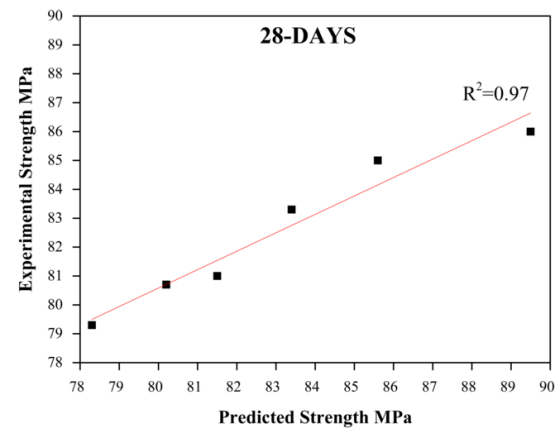
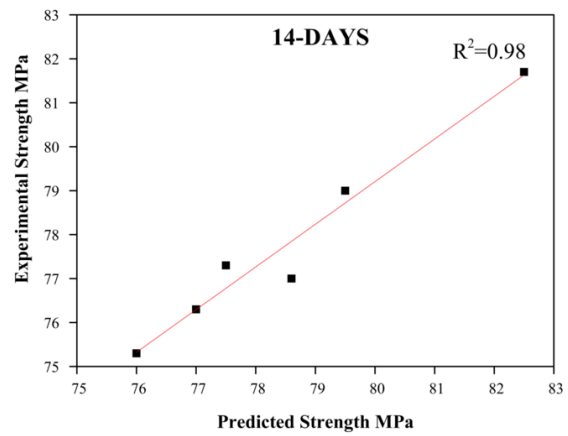
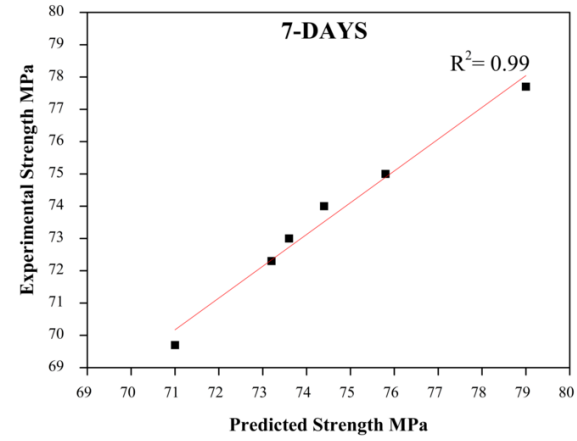
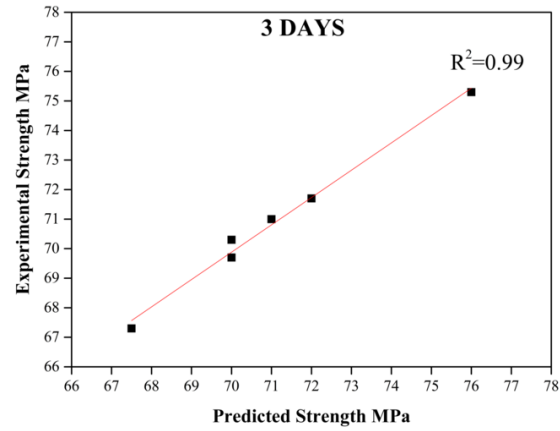


**Fig 4.11 Predictive capability of Regression equations - Compressive strengths - HSAASC Mixes - Validation phase**

#### 4.4.2 Moduli of elasticity and Split- tensile strengths of HSAASC mixes

Tests were also carried out to determine the modulus of elasticity (MOE) and split tensile strengths of the HSAASC mixes, as per IS 516:1959 and IS 5816:1999 respectively, using standard cylindrical specimens at the age of 28 days, for all the nine mixes in the calibration phase. The MOE and split- tensile strength values so determined experimentally were in the range of 30.1 – 36.2 GPa and 5.1 – 6.0 MPa, comparable with OPCC-based reference mix as can be seen in Table 4.8 and Fig. 4.12 and Fig 4.13. Relatively higher MOE and split tensile strength values have been observed for all the HSAASC mixes tested here in, due to the better activation of slag grains along with fine quartz powder, in the presence of OH<sup>-</sup> ions supplied by the activator.

**Table 4.8 Moduli of Elasticity and Split Tensile strength values of HSAASC mixes - Calibration mixes**

<b>MIX ID</b>	<b>Moduli of Elasticity (GPa)</b>	<b>Split Tensile strength (MPa)</b>
HSS - OPCC	30.0	5.1
HSAASC -1	30.4	5.4
HSAASC-2	30.7	5.5
HSAASC-3	33.4	5.9
HSAASC-4	31.2	5.0
HSAASC-5	33.7	5.7
HSAASC-6	31.4	5.3
HSAASC-7	36.2	6.0
HSAASC-8	30.1	5.5
HSAASC-9	32.1	5.1

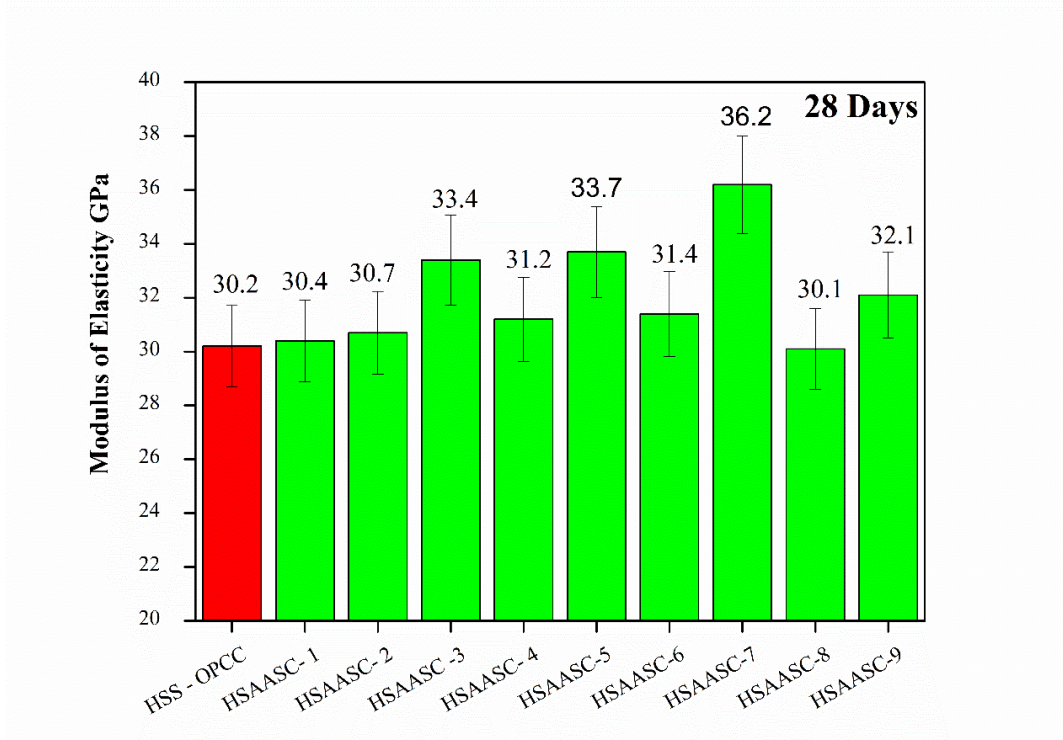


**Fig 4.12 Moduli of Elasticity of HSAASC Mixes - Calibration Phase**

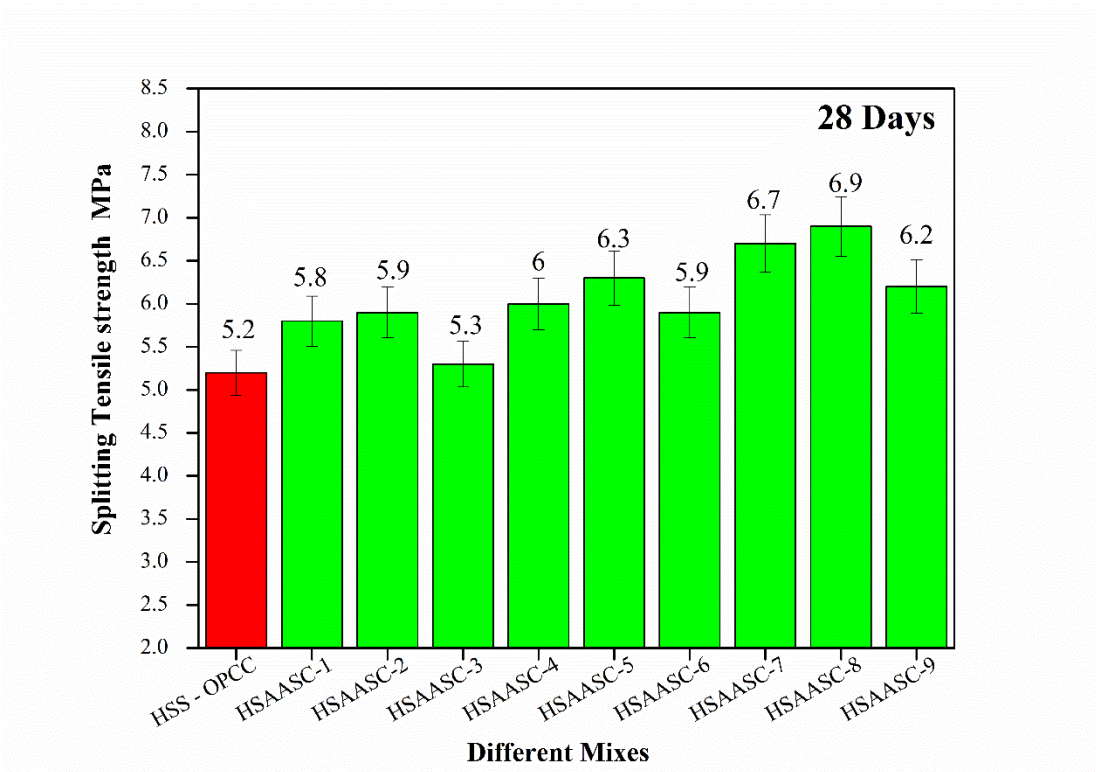


**Fig 4.13 Split tensile strengths of HSAASC Mixes - Calibration Phase**

The response table and mean-of-means showed that modulus of elasticity and split-tensile strengths of all the HSAASC mixes also, as in case of 28-day compressive strengths, are primarily affected by the % Na<sub>2</sub>O (Rank 1), followed by Binder content (Rank 2) and the water-binder ratio (Rank 3) in that order. Regression equations were again derived for possible prediction of the MOE and split-tensile strengths of any new HSAASC mix as,

$$\text{MOE at 28 Days (GPa)} = 13.9 + 0.01313 A - 7.2 B + 1.9 C \dots \text{(Eqn. 4.5)}$$

$$\text{Split tensile strength at 28 Days (MPa)} = 3.94 + 0.00067 A - 0.83 B + 0.233 C \dots \text{(Eqn. 4.6)}$$

In order to check the efficiency of the above equations, MOE and splitting tensile strength tests were conducted, at 28-days of age, on test specimens from each of the mixes, in the verification phase. The experimentally obtained MOE and Split tensile strength values are compared with the predicted values obtained from the regression equations. Fig 4.14 and Fig 4.15 clearly depicts the good predictive capability of each of the equations (4.5) and (4.6), with R-Sq. values in the graphs being quite high at 0.98 and 0.99 respectively.

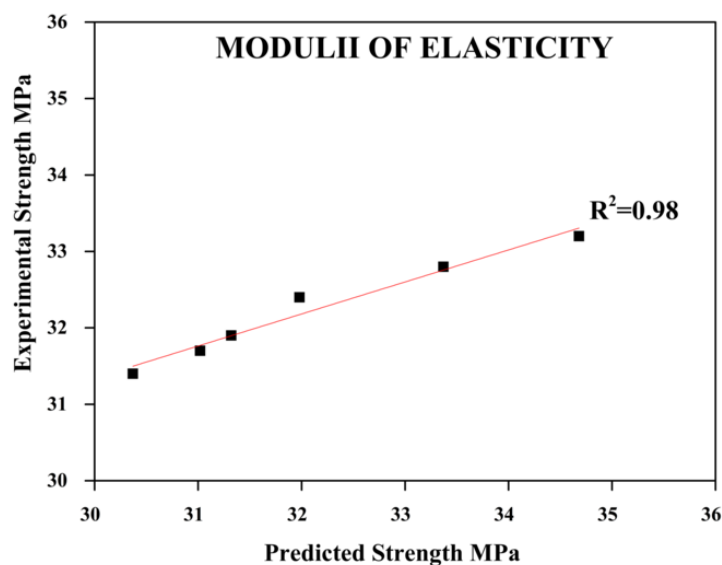


**Fig 4.14 Predictive Capability of Regression Equations – MOE - 28 Days – HSAASC Mixes - Validation phase**

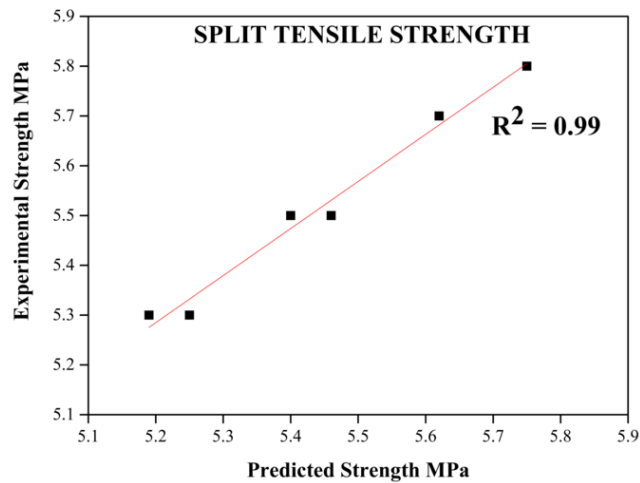


**Fig 4.15 Predictive Capability of Regression Equations – Split-tensile strengths - 28 Days – HSAASC Mixes - Validation phase.**

#### 4.4.3 Flexural strengths of HSAASC mixes

Tests were carried out to determine the flexural strengths or moduli of rupture of all the HSAASC mixes, as per IS 516-1959. Flexural strengths values recorded for the nine HSAASC mixes tested here in the calibration phase, ranging between 6.5 – 7.5 MPa, were found to be marginally higher than control OPC based reference concrete mix, as shown in Fig 4.16.

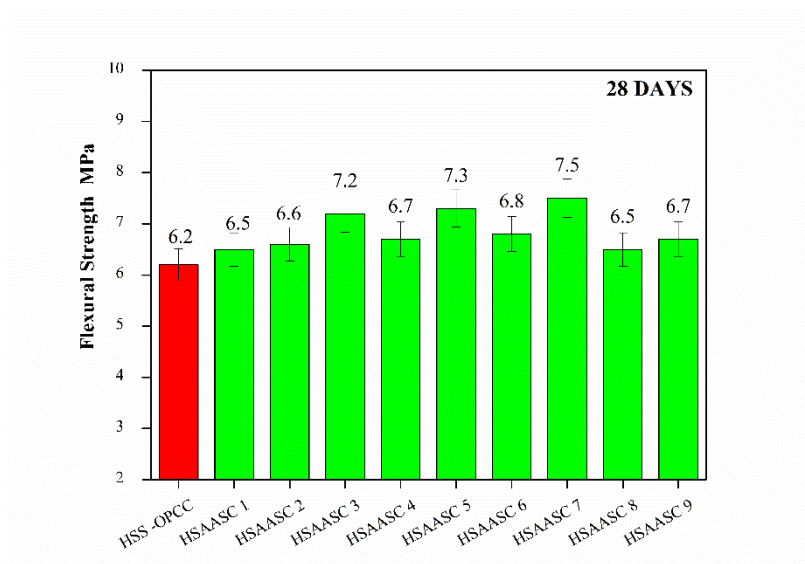


**Fig 4.16 Flexural strengths of HSAASC mixes – Calibration Phase**

Again increased flexural strengths were observed with an increase in % sodium oxide in the alkaline solution as well as binder content. The following regression equation was derived for possible prediction of the 28-day flexural strength of any new HSAASC mix, by following the same steps as used earlier.

$$\text{Flexural strength @ 28-Days (MPa)} = 3.60 + 0.00117 A + 0.50 B + 0.3633 C \dots$$

(Eqn.4.7)

A high R-Sq. value of 0.98 in the graph in Fig 4.17 again endorses the good predictive capability of the above regression equation.

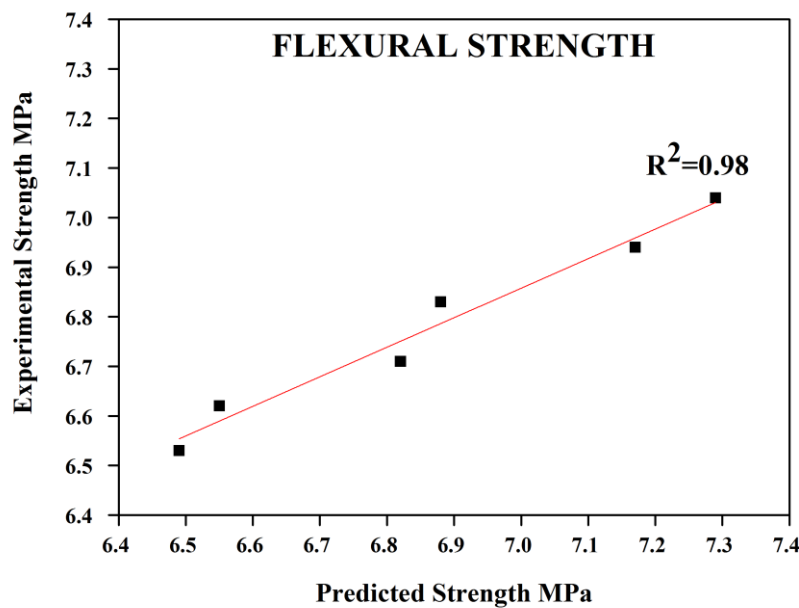


**Fig 4.17 Predictive Capability of the Regression Equation – 28-Days -Flexural strengths – Validation Phase.**

#### 4.4.4 Water absorption test on HSAASC mixes

All the fifteen candidate HSAASC mixes were also subjected to water absorption tests to determine the initial water absorption (IWA) and saturated water absorption (SWA), as per (ASTM C 642-06), in order to get a general idea of the volume of the pores present inside their microstructure. From Fig 4.18, both IWA and SWA values were in the range of 2.4% - 3.5% for all the fifteen candidate HSAASC mixes tested herein, and are marginally lower than normal AAS concrete mixes as well as control OPC based

reference concrete mix. All the mixes do qualify to be classified under the category of good concrete (Ganesan et al. 2015, Bernal et al. 2011).

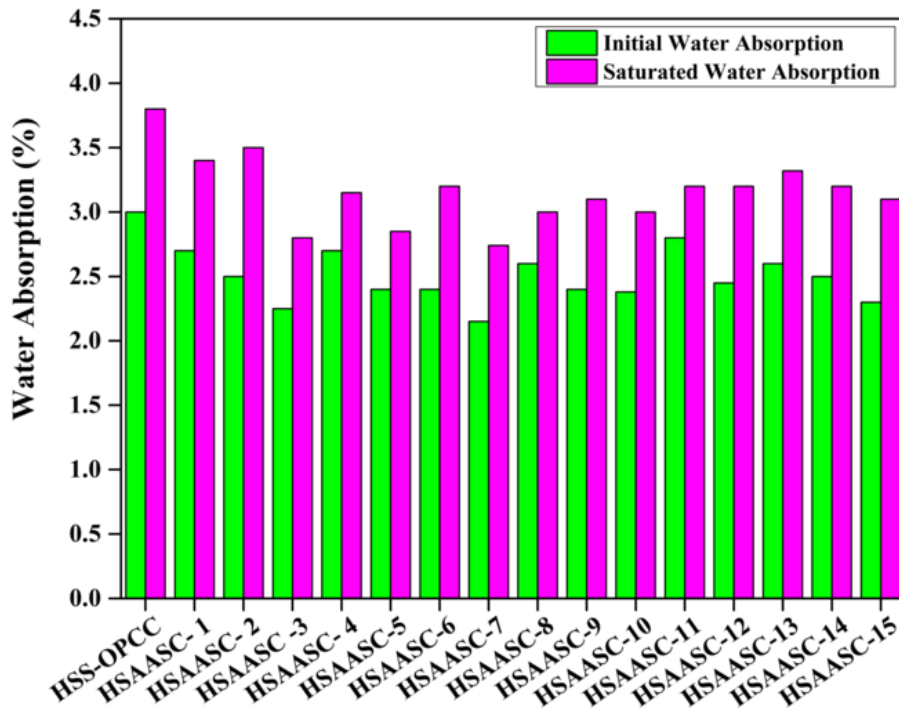


Fig 4.18 Water absorption values of HSAASC mixes

While a detailed study of microstructures developed in the various mixes is presented in the later paragraphs, it can be argued that it may be due to the fact that a good portion of the higher slag-contents has reacted with the activator solution, forming good microstructure quite early that leads to much higher early strengths in all the HSAASC mixes. While, with lower binder contents, there are possibilities of lesser pore-filling by C-A-S-H gel, with increased binder contents and continued activation by the alkaline solution, more amounts of slag grains gets activated. Thus the production of additional C-A-S-H gels along with the pore-filling or/and pore-refinement effects brought about by finer materials like fine amorphous quartz and quartz sand, might have led to much denser microstructures causing a further reduction in porosity of these AASC mixes.

#### 4.5 STUDIES ON MICROSTRUCTURES OF HSAASC MIXES

Detailed analysis of morphological features revealed in secondary electron images taken from a scanning electron microscope on the fractured samples extracted from the central core of the fractured concrete cube specimens on all the fifteen HSAASC mixes, with the size of specimen being 5-10mm. Further the elemental composition details thereof were obtained through EDX analyses by means of area scan of the entire fractured sample. The identification of prominent mineralogical phases that have developed in the hardened concrete was performed using the XRD analysis. Crushed powdered samples passing through 75 micron sieve were used for performing the XRD analysis - which can help in better understanding of the process of alkali activation and strength-gain characteristics of AAS-based products. All the samples were oven-dried before subjecting to SEM, EDAX and XRD analysis. Appropriate samples (obtained from test specimens of 28-days of age) of all the fifteen HSAASC mixes (HSAASC-1 to HSAASC-15) each with varied binder content, the percentage of sodium oxide and w/b ratio, were tested for analyzing their microstructures.

Typical SEM images of all these mixes are shown in Fig 4.19 to 4.23. It can be appreciated that the secondary electron-based mode of images indicate the mixes to be in different stages of activation process of GGBFS – a few showing gradually developing C-A-S-H products in stratified layers with lesser number of un-hydrated slag particles, a few where denser microstructures but with micro-cracks/voids can be observed, and finally, a large number of micrograms with fully developed, continuous, dense microstructures are also being observed.

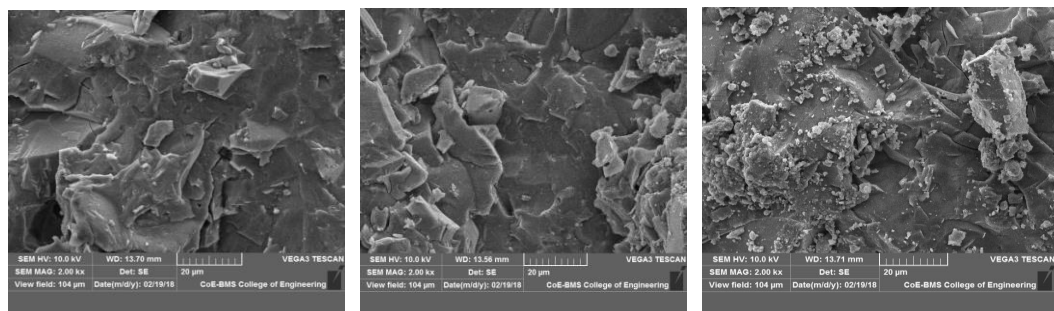


**Fig 4.19 SEM Images of Mixes, HSAASC-1, HSAASC -2 and HSAASC-3**

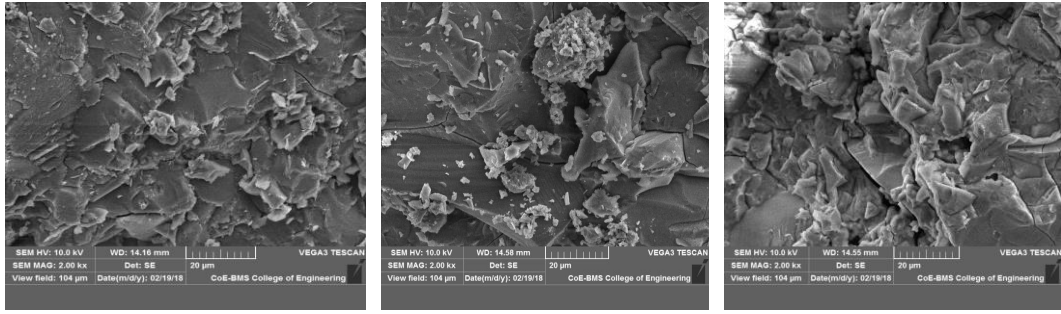


**Fig 4.20 SEM Images of Mixes, HSAASC-4, HSAASC-5 and HSAASC -6**

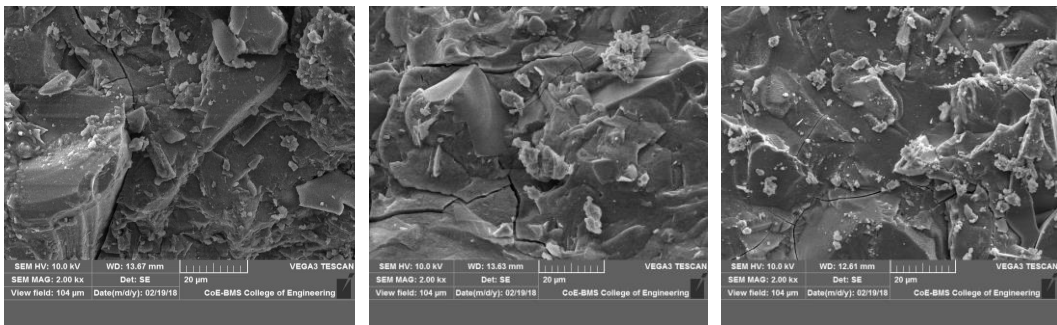


**Fig 4.21 SEM Images of Mixes, HSAASC -7, HSAASC -8 and HSAASC-9**

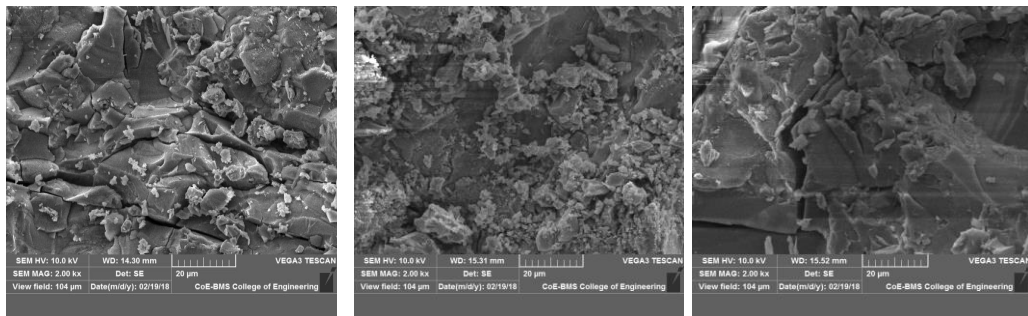


**Fig 4.22 SEM Images of Mixes, HSAASC -10, HSAASC -11 and HSAASC -12**

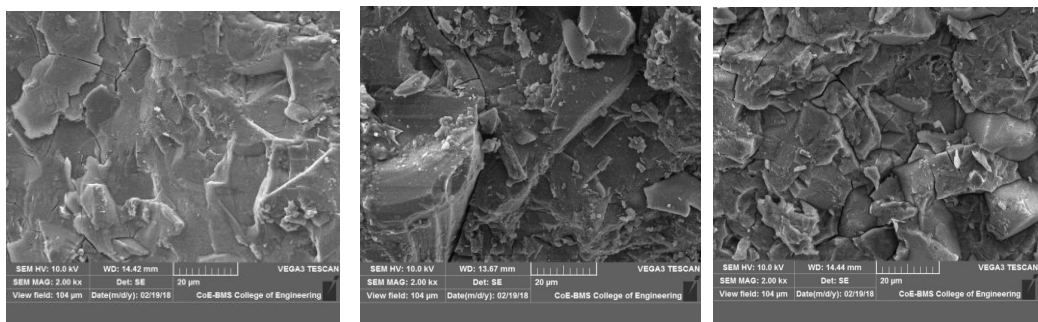
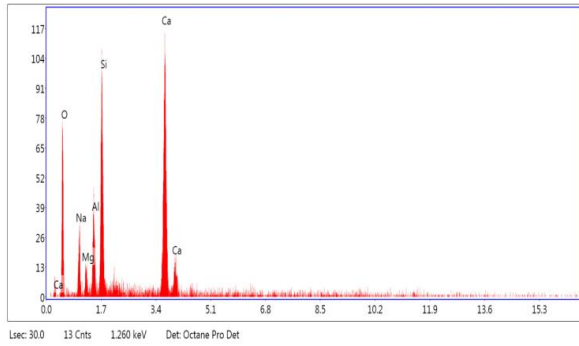


**Fig 4.23 SEM Images of Mixes, HSAASC -13, HSAASC -14 and HSAASC -15**

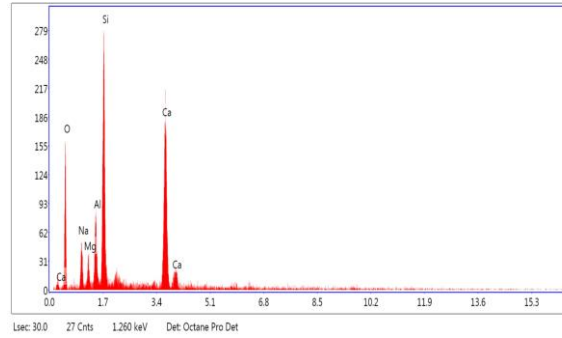
The final dense microstructures developed in almost all of the mixes are due to the complete activation of bulk of the GGBFS along with the fine quartz powder available in them, in the presence of OH<sup>-</sup> ions present in the alkaline solution. In some HSAASC mixes, products of alkali activation forming in the form of dense clusters are also observed in the SEM images. It is the fully developed denser micro-structures, preferably without accompanying micro-cracks/voids in them, which are responsible for the higher strengths of these mixes (Puertas et al. 2011). Quartz sand (added as a fine aggregate fraction) and any part of the fine quartz powder left unreacted in the mixes could also provide the pore-filling effect leading to higher strengths and lower water absorption values as well.

Detailed EDX analyses were also attempted while studying the microstructures of the various HSAASC mixes, with the scanning electron microscope. Typical EDX-plots obtained for five of the mixes are shown in Fig. 4.24. In each of these plots, peaks that correspond to various elements like O<sub>2</sub>, Ca, Si, Na and Al are seen suggesting the presence of these elements in the constitution of those mixes. The details of average atomic percentages, measured over a small sampling area in the microgram of the corresponding mixes, as obtained from the analyzer, are given in Table 4.9.

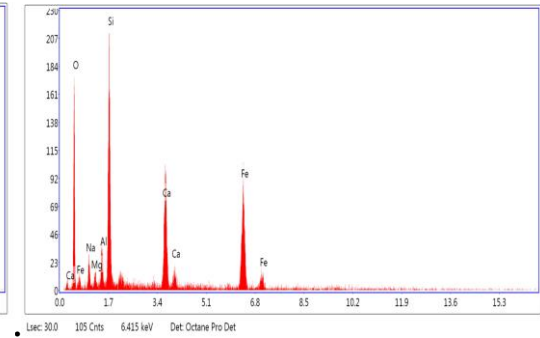
Figs 4.25– 4.29 are the XRD plots for all the HSAASC mixes tested herein. In these plots, different reaction products like Quartz, C-A-S-H gels, Hydrotalcite and calcite etc., are identified by matching the values of  $2\Theta$  for those products as measured in several studies available in the literature (Provis and Bernal 2014, Behfarnia and Rostami 2017, Lecomte et al. 2006, Ibrahim et al. 2018, Sun et al. 2018, Khan et al. 2018). Significant formation of C-A-S-H gels has been clearly identified along with other reaction products. These C-A-S-H gels, mostly in semi-crystalline phase, are largely responsible for the enhanced mechanical properties of all the HSAASC mixes tested herein.



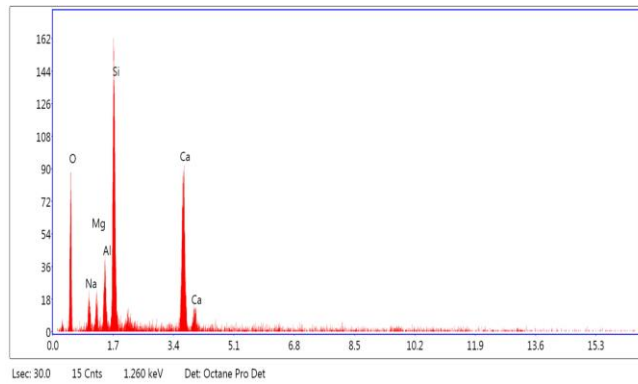
HSAASC -2



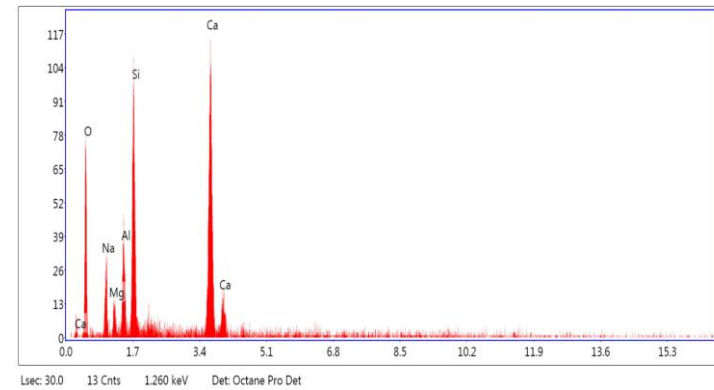
HSAASC -4



HSAASC -9



HSAASC -12



HSAASC -15

**Fig 4.24 Typical EDX analyses results of HSAASC Mixes**

**Table 4.9 Atomic percentages of major elements in HSAASC mixes - EDX Analyses**

<b>MIX ID</b>	<b>ATOMIC PERCENTAGES OF ELEMENTS</b>					
	<b>O</b>	<b>Na</b>	<b>Mg</b>	<b>Al</b>	<b>Si</b>	<b>Ca</b>
<b>HSAASC-1</b>	64.59	5.77	1.80	3.88	11.48	10.2
<b>HSAASC-2</b>	65.35	7.87	1.68	4.31	9.9	8.5
<b>HSAASC-3</b>	66.35	6.62	1.64	3.95	13.12	8.33
<b>HSAASC-4</b>	63.67	6.52	1.89	4.28	13.38	10.27
<b>HSAASC-5</b>	63.51	5.58	1.86	4.28	13.07	11.70
<b>HSAASC-6</b>	65.72	4.90	2.04	4.53	12.17	10.64
<b>HSAASC-7</b>	66.34	5.82	1.99	4.0	12.24	9.61
<b>HSAASC-8</b>	66.83	6.42	2.24	4.05	11.44	9.02
<b>HSAASC-9</b>	61.34	6.35	1.69	2.88	13.34	6.17
<b>HSAASC-10</b>	66.18	6.68	1.62	4.06	12.12	9.35
<b>HSAASC-11</b>	64.85	5.33	1.69	4.11	11.95	10.1
<b>HSAASC-12</b>	65.50	4.68	2.05	3.60	14.84	9.33
<b>HSAASC-13</b>	64.21	5.53	2.08	4.39	13.13	10.67
<b>HSAASC-14</b>	63.18	6.42	1.58	4.21	12.79	11.82
<b>HSAASC-15</b>	65.35	7.87	1.68	4.31	10.3	9.9

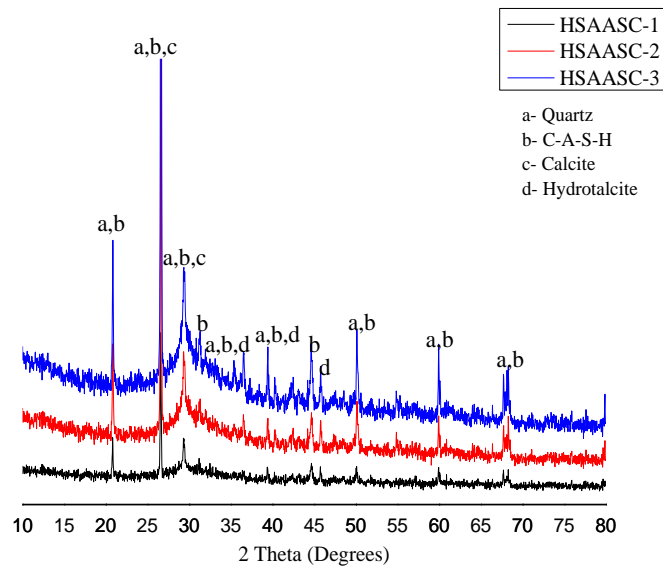


**Fig 4.25 XRD details of HSAASC-1 – HSAASC-3**

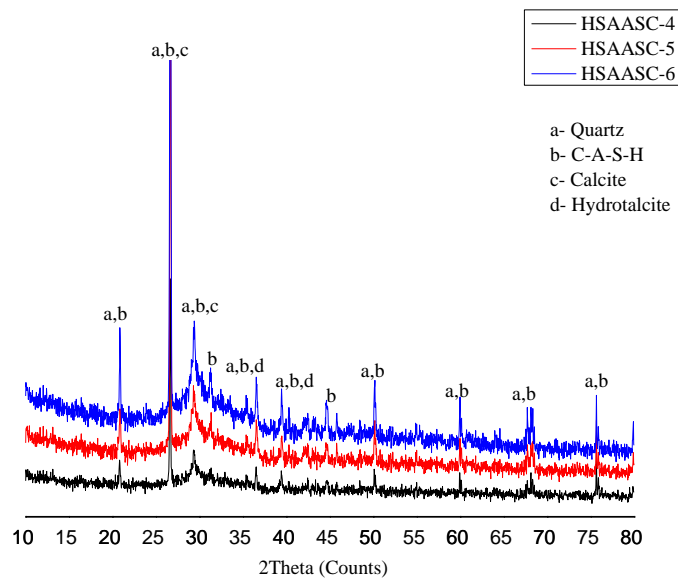


**Fig 4.26 XRD details of HSAASC-4 – HSAASC-6**

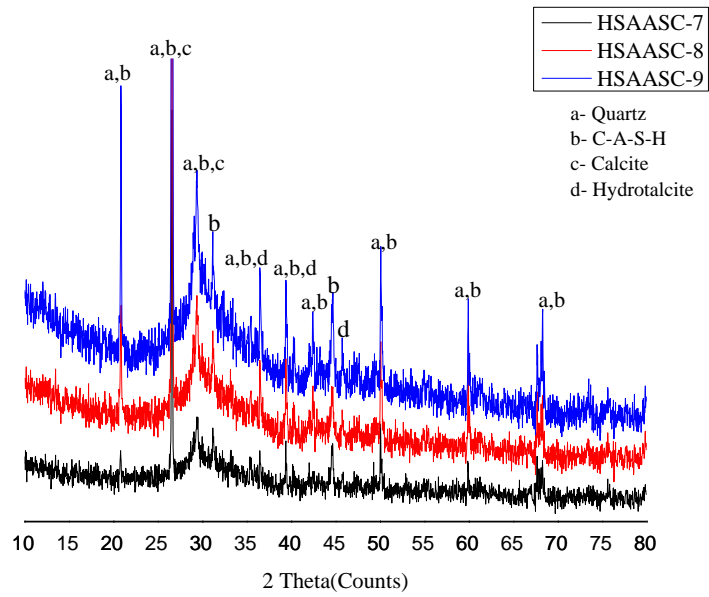


**Fig 4.27 XRD details of HSAASC-7 – HSAASC-9**

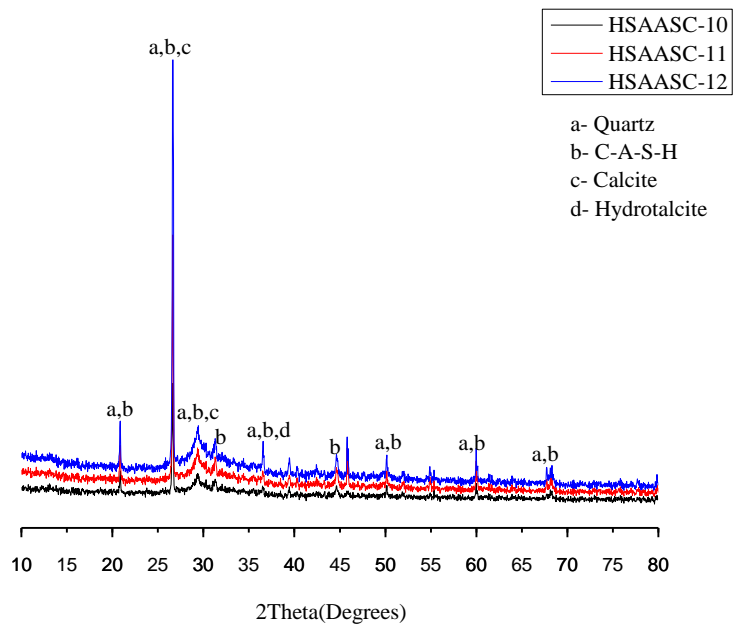


**Fig 4.28 XRD details of HSAASC-10 – HSAASC-12**

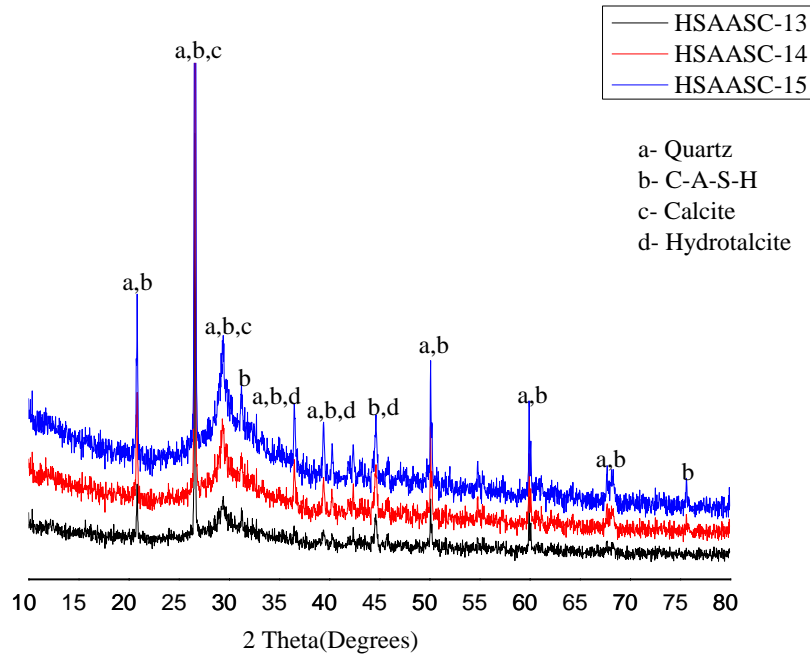


**Fig 4.29 XRD details of HSAASC-13 – HSAASC-15**

#### 4.6 SUMMARY

In the present chapter a new class of high strength, self-compacting, alkali-activated slag concrete (HSAASC) mixes was successfully developed herein, incorporating slag sand and EAF slag, both by-products from the iron and steel industry, as fine and coarse aggregates respectively. While finely ground, blast furnace slag was used as the principal aluminosilicate source material in these mixes, effect of partial replacement of GGBFS with fine amorphous quartz powder in terms of possible pore-filling and pore-refinement in them has been explored. Such partial replacement of GGBFS, taken at relatively higher contents, causes a slight decrease in the flowability characteristics. This may be due to the increased yield stresses in the mixes due to the increase in the total amount of finer particles. Addition of small amounts of sodium phosphate, as an additive, has led to a construction-friendly increase in the initial setting times of all the HSAASC mixes tested herein from an initial-low of 15 minutes to a healthy 60 minutes or so. The regression equations developed herein for the various strength parameters, based on a statistical analysis under Taguchi's Design of experiments (DOE) approach,

have exhibited very good predictive capabilities. It is clearly evident, from the SEM images, that it is possible to design and develop HSAASC mixes, with very dense micro-structures, with much less micro-cracks and pores, leading to better engineering properties. Further five best performing mixes, in terms of both flow characteristics as well as mechanical properties, out of the fifteen HSAASC mixes tested herein were selected for evaluating the durability characteristics under different types of simulated aggressive environments. The results of such tests are discussed in the next chapter.

.....

## **CHAPTER 5**

### **DURABILITY STUDIES ON HSAASC MIXES**

#### **5.1 GENERAL**

The present chapter discusses the durability performances of five best performing mixes, out of the fifteen HSAASC mixes tested earlier, in terms of both their flowability characteristics and mechanical strength properties. Mixes with Mix-Ids, HSAASC-3, HSAASC-5, HSAASC-7, HSAASC-10 and HSAASC-15 were chosen for evaluating their durability characteristics. Performance of these five representative mixes on long-term exposure to acid, sulphate and chloride-rich environments mixes are discussed here. Such performances are also compared with the reference OPC-based concrete mix.

#### **5.2 RESISTANCE OF HSAASC MIXES AGAINST ACID ATTACK**

Concrete mixes are susceptible to chemical attack in a variety of exposure conditions unless some precautions are taken. The aggressive environments may include natural environments such as in acid rains or man-made such as exposure to chemical effluents from industries, waste waters from drainage systems etc., which affect the long-term performance of concrete elements due to the evolution of highly concentrated toxic acids. Concrete undergoes degradation under the influence of such aggressive environments due to chemical processes involving exchange of ions, thus causing changes in the microstructure of the binding matrix leading to reduction in the mechanical strength.

##### **5.2.1 Residual strength and mass loss characteristics of HSAASC mixes subjected to concentrated sulphuric acid solution.**

100 mm-cube test specimens of the five candidate HSAASC mixes, after their initial 28-days of ambient room-temperature curing, were exposed to 5% concentrated sulphuric acid solution for different periods namely, 56, 90, 180, 270 and 365 days (12- months) along with those of the OPC-based reference concrete mix. The pH of the acid solution was regularly monitored and maintained within a small range of 0.3 – 0.5

(Rajamane et al. 2012<sup>a</sup>). Acid solution was replaced fully, once every 15 days. In the case of the OPC-based reference concrete specimens, there was full degradation of the cover mortar layer, completely exposing the coarse aggregates by 90-days of exposure as shown in Fig 5.1 (a). Further it can be also observed that, a complete loss of the integrity of the specimens had taken place by the age of 103 days as shown in Fig 5.1 (b). Test specimens of HSAASC mixes, however, maintained their integrity with distress observed only on the outer surfaces, as shown in Fig 5.2.

Only a few cracks had been developed, even by the end of 365 days of exposure to 5% sulphuric acid solution; again only the outer surfaces were more affected and mortar was removed off in the form of layers as shown in Fig 5.3, due to extensive possible formation of gypsum which is basically expansive in nature (Allahverdi and Škvára 2000).

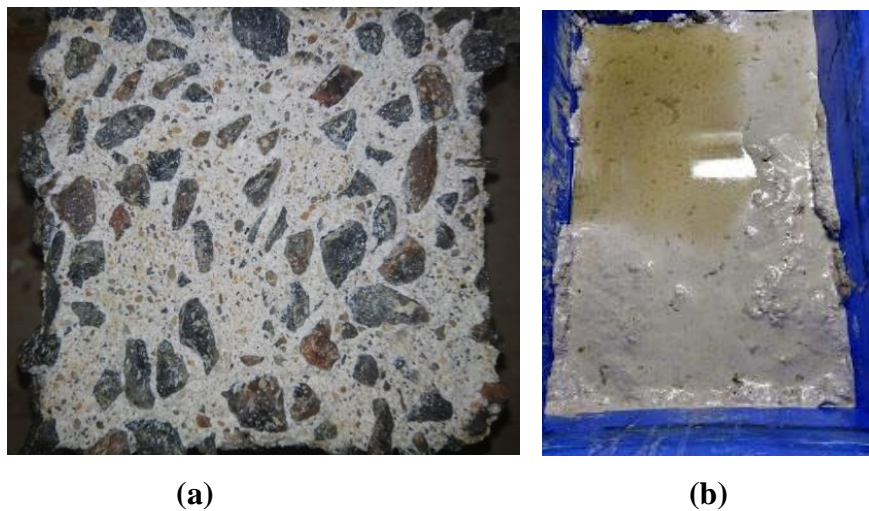


**Fig 5.1 OPC specimens exposed to the sulphuric acid solution at 90 days and 103 days**

While, compared to similar specimens tested at 28-days of curing, OPC-based reference concrete mix samples had about 75% loss of weight at 56-days, 95% loss by 90-days and complete dissolution -100% loss at the age of 103-days of exposure (to sulphuric acid) respectively; the weight losses in all the HSAASC mixes were less than 10% even after 365-days of exposure as shown in Fig 5.4 (Davidovits et al. 1990, Pacheco et al. 2010). The variations of residual compressive strengths of both the OPC and HSAASC mixes, with period of exposure to sulphuric acid solution are shown in Fig

5.5. It can be observed that, the corresponding losses in compressive strengths, after 365-days for HSAASC were much lower, in the range of 36.4 - 39.1%, as compared to that of the control OPC-based reference concrete mix (almost 90% loss in cube compressive strength at the age of 90 days only). While the losses in compressive strengths under acid-attack may be attributed due to the decalcification of C-A-S-H gels present in AASC matrices, higher resistances to mass-loss and strength-losses of HSAASC mixes may be attributed to their denser microstructures with better pore filling by products of alkali activation, leading to lower penetration of the acid solution inside the HSAASC specimens. This leads to lesser opportunities for causing any further reactions.



**Fig 5.2 HSAASC mixes after being exposed to sulphuric acid attack for 365 days**



**Fig 5.3 HSAASC mixes exposed to 5% H<sub>2</sub>SO<sub>4</sub> solution, before and after the tests – (Age - 365 days)**

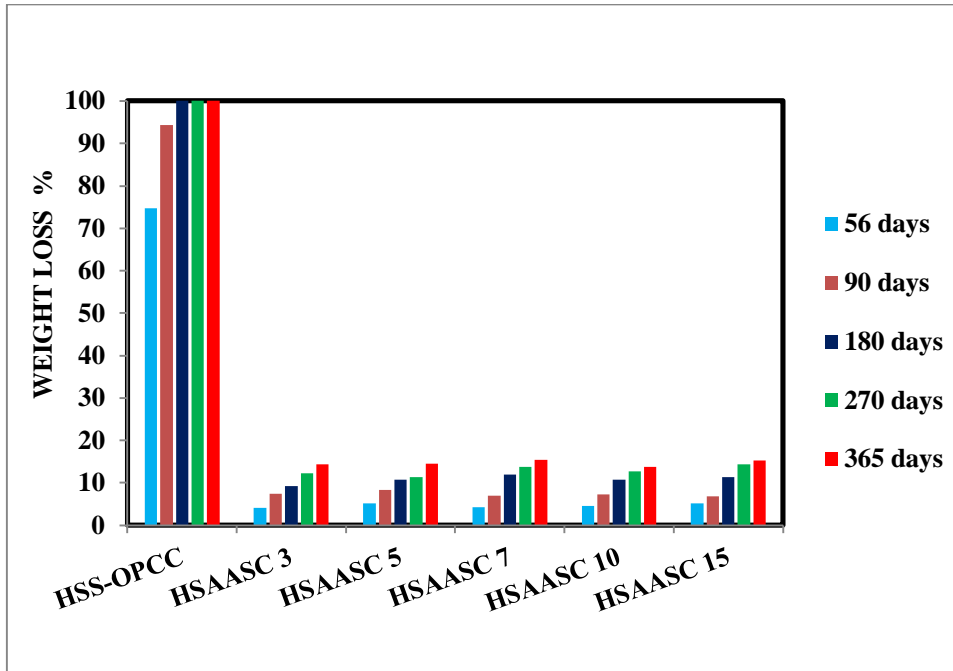


Fig 5.4 Weight losses in HSAASC mix on exposure to 5% H<sub>2</sub>SO<sub>4</sub> solution

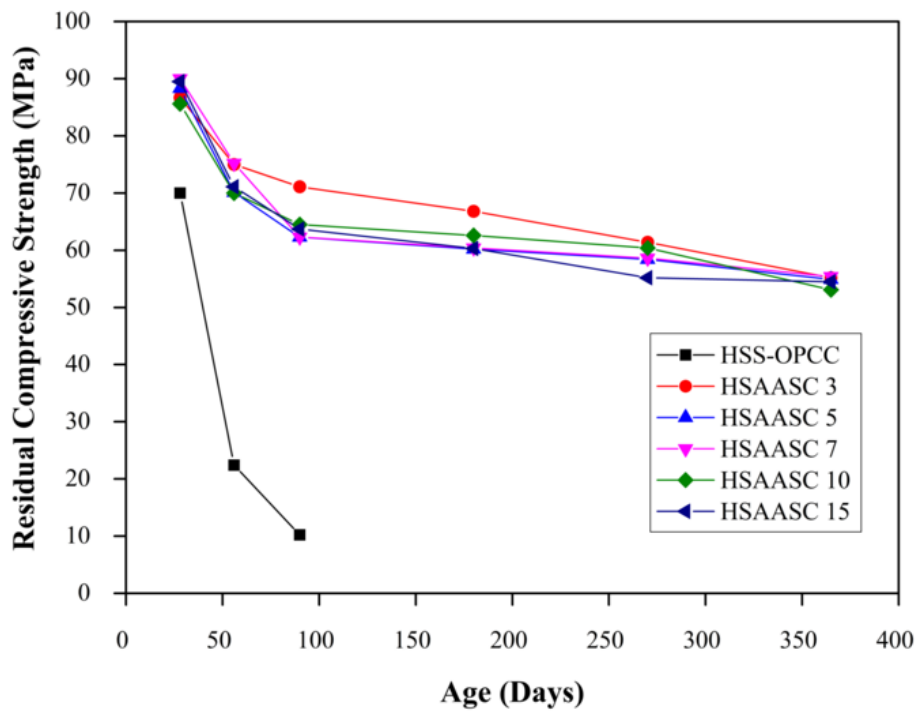


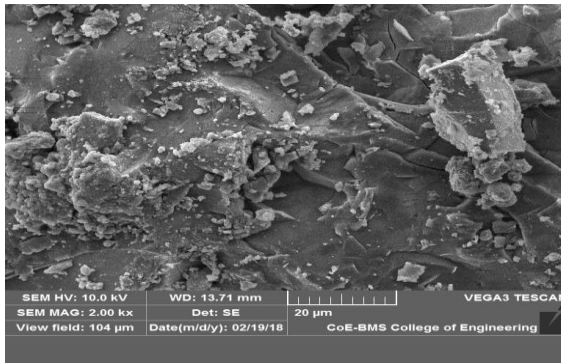
Fig 5.5 Residual compressive strengths of HSAASC on exposure to conc. 5% H<sub>2</sub>SO<sub>4</sub> solution

Again, no deterioration of the EAF-slag coarse aggregates in these mixes has been observed and they have proved to be stable on long-term exposure to acidic environments.

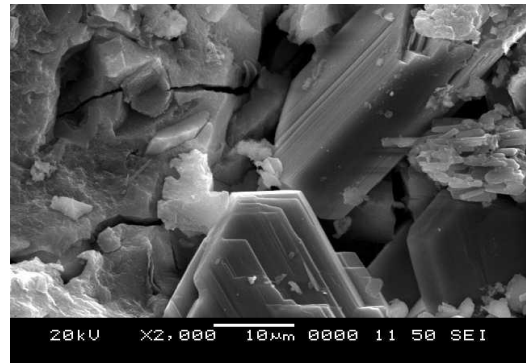
### **5.2.2 Microstructural studies of HSAASC mixes subjected to 5% H<sub>2</sub>SO<sub>4</sub> solution**

Detailed analysis were carried out on the secondary electron images taken from the SEM on the fractured samples, having a size of 5-10 mm, extracted from the central core of the fractured concrete cube specimens of all the five HSAASC mixes, after being immersed in 5% concentrated sulphuric acid solution for a period of 365 days. Further the elemental composition of all these acid-subjected specimens were obtained through detailed EDX analyses.

The secondary electron images captured from SEM for all the mixes are shown in Fig 5.6 - 5.10. Different types of morphologies developed due to continuous chemical attack of the acid can be appreciated in these micrographs. In general, the continuous, dense semi-crystalline phases of C-A-S-H or C-S-H gels of the mixes (before exposure to acids) appear to disintegrate and develop needle like structures (possibly gypsum), clusters of flat plate-like agglomerates, particulates, voids and micro-cracks, during the prolonged exposure to the acid solution. This clearly suggests decalcification of the C-A-S-H /C-S-H gels, which is also clearly reflected from the changes in the morphologies observed in the SEM images for all the five candidate HSAASC mixes tested herein. It can be said that it is such changed nature of the microstructures of the mixes, with more void phase and macro-cracks, which is mainly responsible for the decreased compressive strengths of all the five HSAASC mixes, after exposure to acid-attack (Sturma et al. 2018). The EDX plots obtained for all the five HSAASC mixes are shown in Fig 5.11. The presence of peaks corresponding to various elements like O<sub>2</sub>, Ca, C, Si, S, Fe, Na, K and Al are seen in most of the EDX plots. The detailed average atomic percentages of the mixes measured over the entire sampling area of the respective mixes as obtained from the EDX analyses are given in Table 5.1.

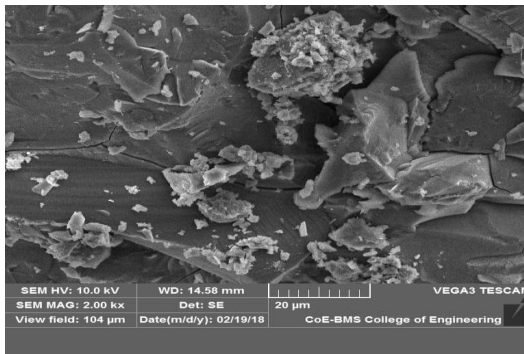


**Before Immersion**

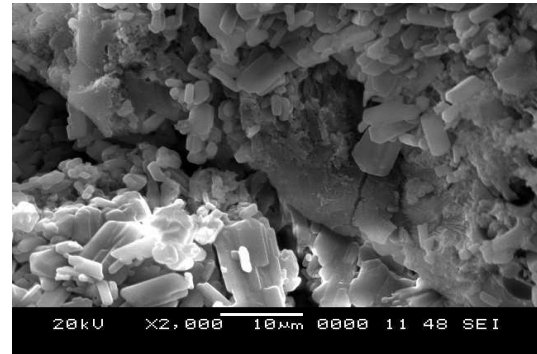


**After Immersion for 365 days**

**Fig 5.6 SEM Images of Mix HSAASC- 3 - Before and After Immersion in 5% H<sub>2</sub>SO<sub>4</sub> solution**

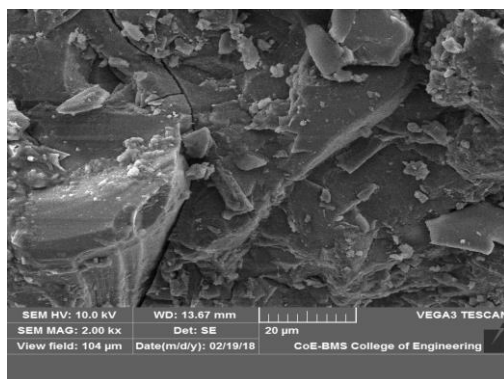


**Before Immersion**

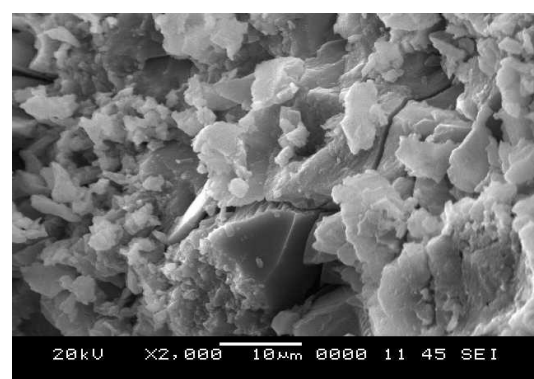


**After Immersion for 365 days**

**Fig 5.7 SEM Images of Mix HSAASC-5 - Before and After Immersion in 5% H<sub>2</sub>SO<sub>4</sub> solution**

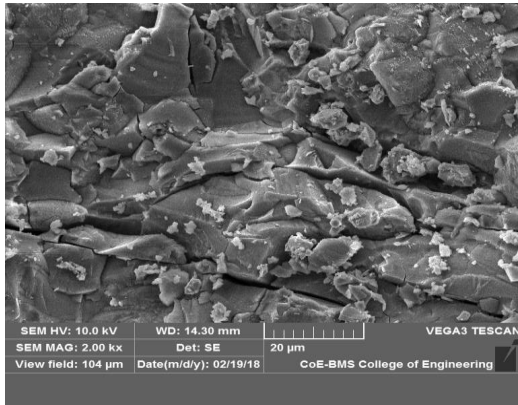


**Before Immersion**

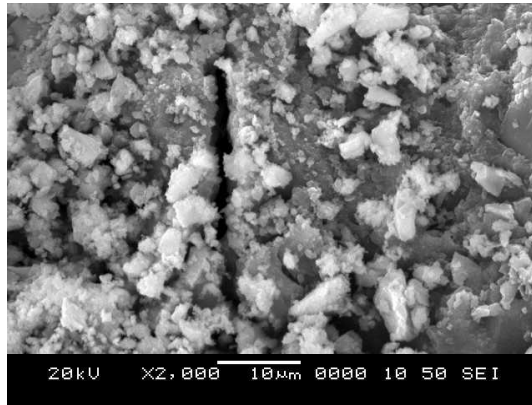


**After Immersion for 365 days**

**Fig 5.8 SEM Images of Mix HSAASC-7 - Before and After Immersion in 5% H<sub>2</sub>SO<sub>4</sub> solution**

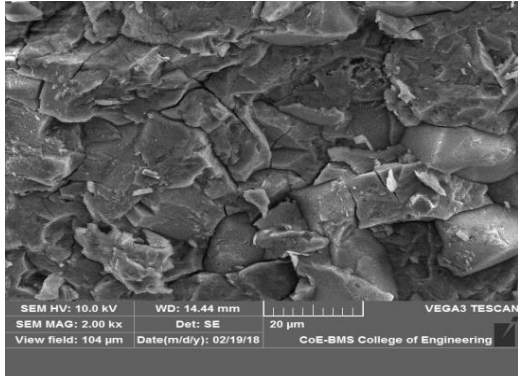


**Before Immersion**

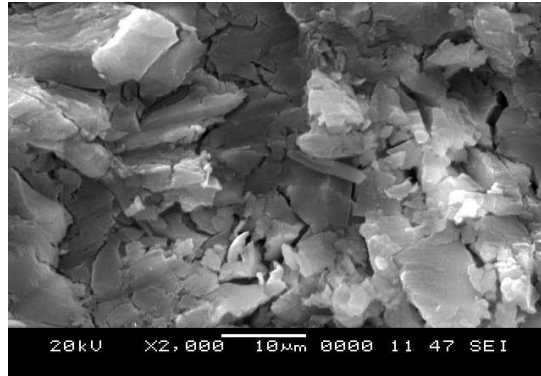


**After Immersion for 365 days**

**Fig 5.9 SEM Images of Mix HSAASC-10 - Before and After Immersion in 5% H<sub>2</sub>SO<sub>4</sub> solution**

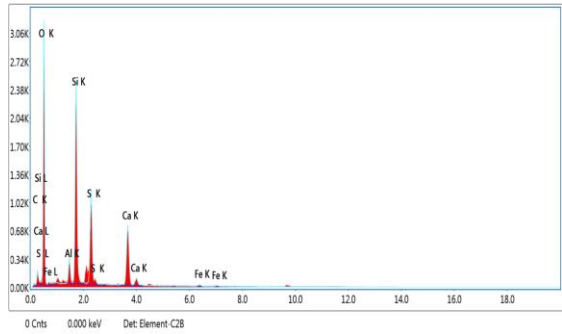


**Before Immersion**

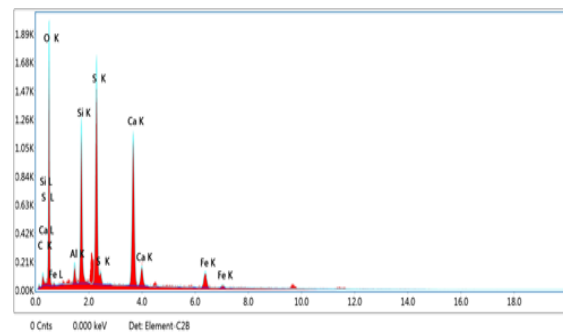


**After Immersion for 365 days**

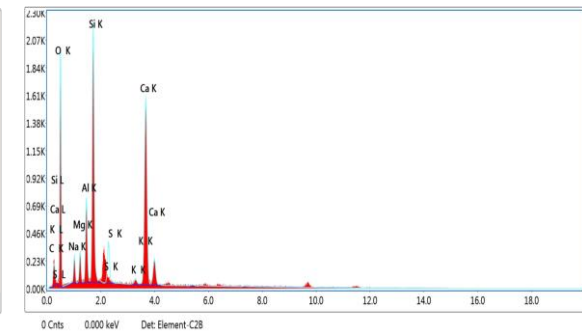
**Fig 5.10 SEM Images of Mix HSAASC-15 - Before and After Immersion in 5% H<sub>2</sub>SO<sub>4</sub> solution**



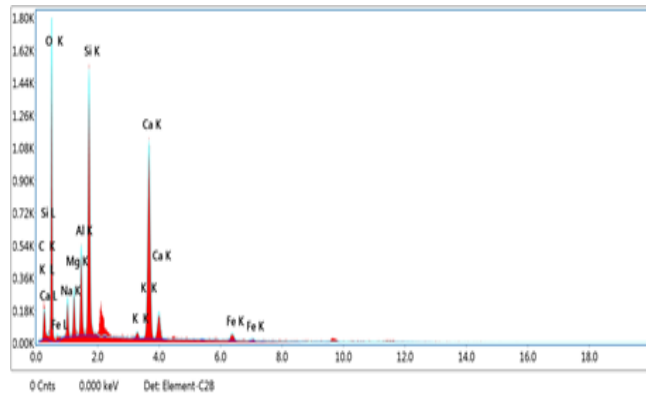
HSAASC-3



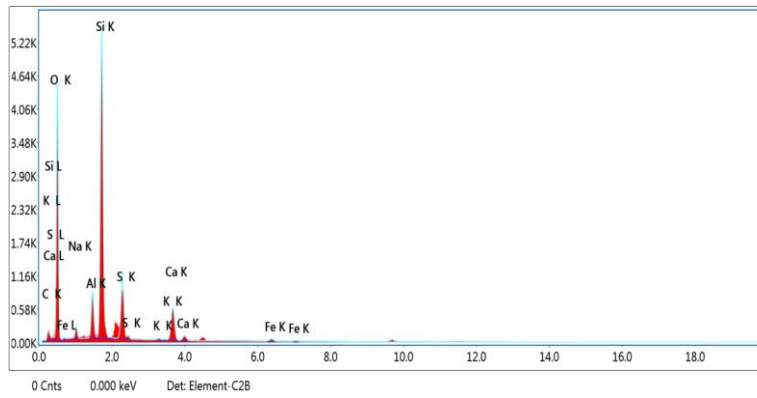
HSAASC-5



HSAASC-7



HSAASC-10



HSAASC-15

**Fig 5.11 Results of EDX Analyses - Elemental Compositions of HSAASC Mixes after immersion in 5% Conc. H<sub>2</sub>SO<sub>4</sub> solution**

**Table 5.1 Results of EDX Analyses - Atomic percentages of elements in HSAASC mixes after immersion in 5% conc. H<sub>2</sub>SO<sub>4</sub> solution**

<b>MIX ID</b>	<b>Atomic Percentages of Elements EDX Analysis - After acid attack</b>						
	<b>O</b>	<b>S</b>	<b>Fe</b>	<b>C</b>	<b>Ca</b>	<b>Al</b>	<b>Si</b>
<b>HSAASC-3</b>	68.19	6.36	0.22	7.26	5.39	1.59	10.99
<b>HSAASC-5</b>	64.98	10.3	1.81	4.15	6.28	2.04	10.44
<b>HSAASC-7</b>	60.01	6.89	0.70	8.50	7.50	3.5	12.90
<b>HSAASC-10</b>	60.42	7.4	2.11	9.26	6.90	2.71	11.30
<b>HSAASC-15</b>	61.83	5.9	0.87	7.46	8.70	3.0	12.35

### **5.3 TESTS FOR RESISTANCE OF HSAASC MIXES AGAINST SULPHATE ATTACK**

The strength of the concrete gets degraded, as a result of chemical reactions occurring when concrete is exposed continuously to a sulphate solution of adequately high concentration. Such deterioration of concrete under sulphate attack is widespread in arid provinces where sulphate minerals are present in the soil and groundwater. Weakening of concrete due to sulphate attack is normally attributed to hydration products of Portland cement reacting with sulphates to form expansive reaction products like ettringite and gypsum, leading to high internal stresses and succeeding in disruption of the concrete (Shi et al. 2006).

#### **5.3.1 Residual strength and mass loss characteristics of HSAASC mixes subjected to magnesium sulphate solution.**

Generally, sulphate resistance of OPC-based concrete mixes is evaluated in terms of the deterioration of standard-sized concrete specimens on exposure to a concentrated sulphate solution for extended periods of time. Compression tests are generally carried out on 100 or 150 mm test cubes, after immersion in any of sodium, magnesium or calcium sulphate solutions and deterioration is measured in terms of loss in strength upto different ages.

In the present work, concrete test specimens of all the five selected HSAASC mixes, after 28-days of initial curing, were immersed in 10% Magnesium sulphate ( $\text{MgSO}_4$ ) solution, for periods extending upto twelve months. While the concentration of magnesium sulphate solution was regularly changed, maintaining a constant, relatively higher concentration of 10% (Rajamane et al. 2012<sup>b</sup>). The sulphate solutions in the containers were replaced every two weeks for the first two months, and then replaced every month upto 12 months. The mass changes and residual compressive strengths were measured after 28 days, at regular intervals namely 56, 90, 120, 185, 270 and 365 days respectively.

Both the OPC and AAS based concrete mixes maintained their integrity with very minor distress on the surface when examined visually as shown in Fig 5.12, even by the end of one year.

Initially, at the early ages, say upto 56-days, the test specimens showed a slight increase in their weights (upto a max of 1.7% for HSAASC-5 mix), which however started decreasing slowly with further exposure. The HSAASC specimens showed only minor losses in their weights, varying in the range of 2.1 to 2.9 %, upto the end of one year of exposure to sulphate solution (Fig 5.13). The corresponding weight-loss for OPC-based reference concrete mix was also comparable at 2%. The corresponding losses in compressive strengths of all the HSAASC mixes were in the range of 15.5% - 20.5%, which were slightly higher than the strength-loss for the reference OPC-based concrete mix (about 15.3%).

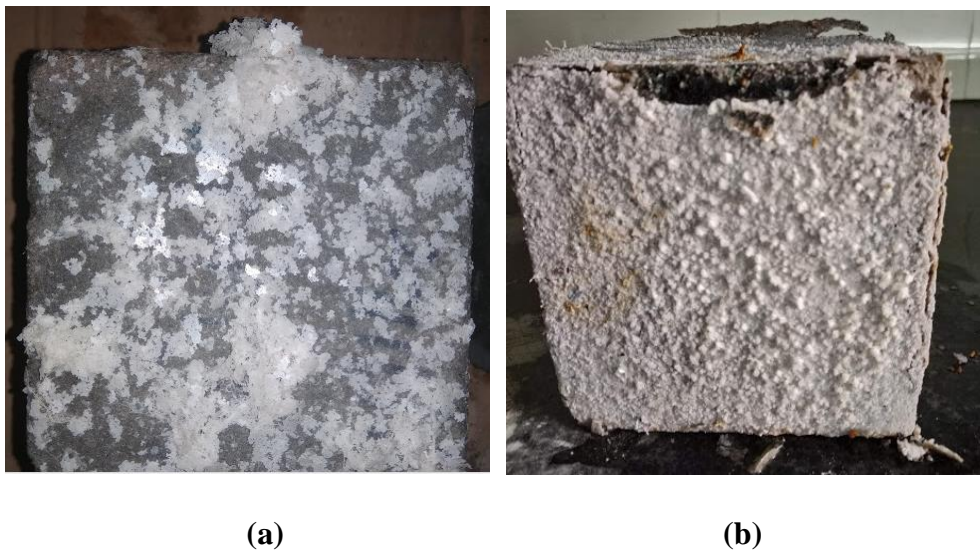


**Fig 5.12 Appearance of (a) OPCC and (b) HSAASC specimen exposed to 10 %  $MgSO_4$  after 365 days**

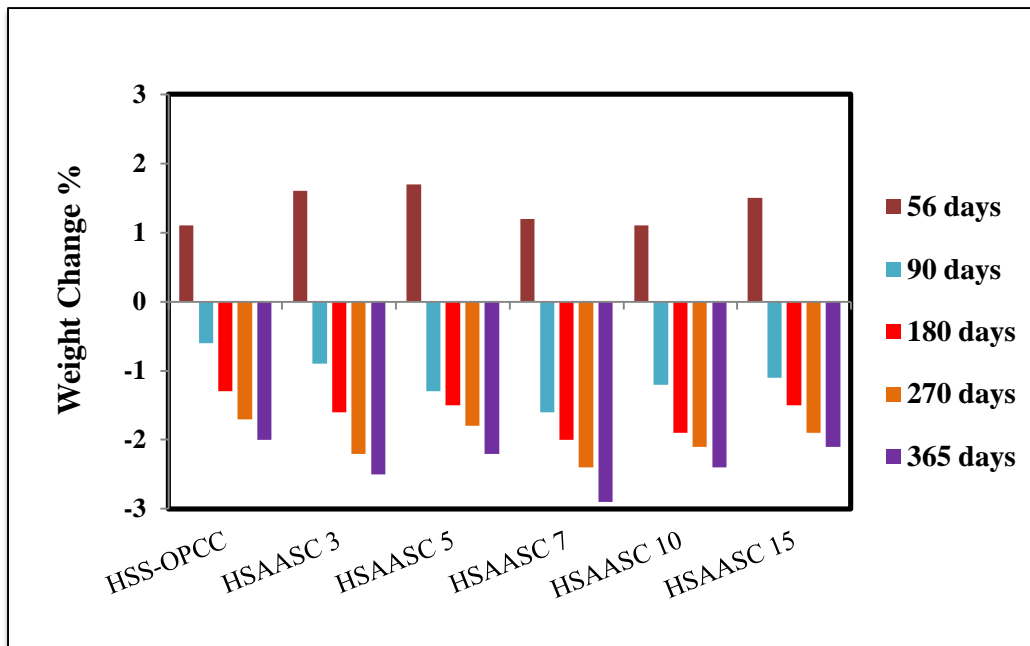


**Fig 5.13 Weight changes in different mixes in 10% MgSO<sub>4</sub> solution**

Fig 5.14 and Fig 5.15 show the residual compressive strength values and percentage losses in strengths of all the mixes tested herein. Calcium hydroxide is one of the major hydrated product that is usually formed in case of OPC based concrete mixes, which is completely absent in the alkali activated products that are formed in any of the AASC mixes (Bakharev et al. 2002), which instead consist of C-A-S-H gels and hydrotalcite. This prevents the formation of brucite, Mg(OH)<sub>2</sub>, which otherwise acts as protective film in case of OPCC mixes. The marginally lower strength- performances of any of the AASC mixes herein when subjected to magnesium sulphate environment is due to the absence of brucite layer, leading to direct attack of magnesium ions on the C-A-S-H gel structure resulting in the formation of M-S-H and gypsum. Both M-S-H and gypsum are expansive in nature and the additional volumes of these products cannot get accommodated within the limited pore spaces present in AASC mixes thus leading to cracking of concrete specimens and hence loss in strengths (Mithun and Narasimhan 2016).

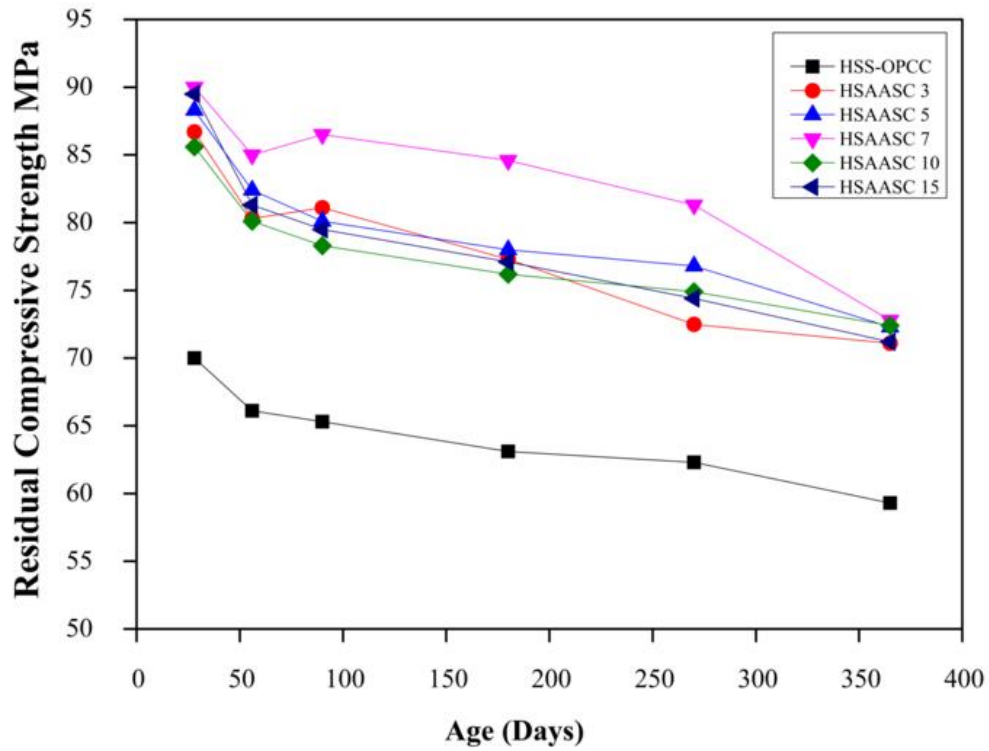


**Fig 5.14 Residual compressive strengths of different mixes on exposure to 10 % MgSO<sub>4</sub> solution**

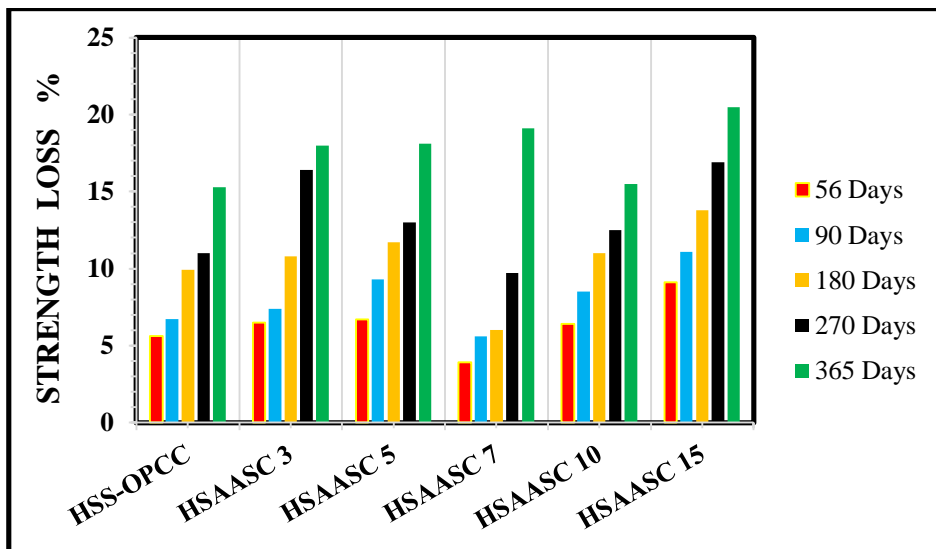


**Fig 5.15 Percentage of compressive strengths loss of different mixes in 10 % MgSO<sub>4</sub> solution**

The deterioration of the hydrated products may also be reflected by the weight-losses at the later ages. However it has been observed that the aggregates have not shown any deterioration and have proved to be stable in magnesium sulphate solution. Further, a few earlier studies have reported a lower performance of hydrated cement paste when subjected to  $MgSO_4$  environments (Hughes 1985, Mangat and Khatib 1992, Al-Amoudi et al. 1995). However the decrease in strength characteristics of all the HSAASC mixes in sulphate environment are mainly governed by the cations which accompany the sulphate anions (Mithun and Narasimhan 2016).

### **5.3.2 Microstructural studies of HSAASC mixes subjected to magnesium sulphate solution**

Detailed analysis were carried out on the secondary electron images taken from the scanning electron microscope using the fractured samples extracted from the central core of the fractured concrete cube specimens of all the five HSAASC mixes, having a size of 5–10 mm after being immersed in 10% magnesium sulphate solution for an extended period of 365 days. Further the changed elemental compositions of all these sulphate-immersed specimens were obtained through detailed EDX analyses. Again the SEM-based micrographs in Fig 5.16 - 5.20 suggest gradual deterioration of continuous denser, initial microstructure of each of the HSAASC mixes, on continuous exposure to a sulphate-rich environment (upto one year). One can appreciate possible development of phases/products with a wide variety of morphologies-including plate-like structures (M-S-H) which is basically expansive in nature, particulate morphologies-sometimes rounded, else angular; fibrous (needle) structures (gypsum), elongated crystals etc., all associated with larger void spaces and possible micro-cracks, on long-term exposure to  $MgSO_4$  solution.

It can clearly be inferred from these images that large amount of degradation of the C-A-S-H gels and other such binding products in AASC mixes has taken place during the period of exposure. Possible formation of expansive reaction products like gypsum and M-S-H, leading to development of macro-cracks might as well be responsible for decrease in the compressive strengths of all the five HSAASC mixes. The EDX plots

obtained for all the five HSAASC mixes subjected to  $MgSO_4$  solution for an extended period of one year are shown in Fig 5.21. The presence of peaks corresponding to elements like  $O_2$ , Ca, C, Si, S, Mg, Na, and Al are seen in all the EDX plots. The detailed average atomic percentages of the various elements, measured over the entire sampling area of the respective mixes, as obtained from the EDX analyses are given in Table 5.2.

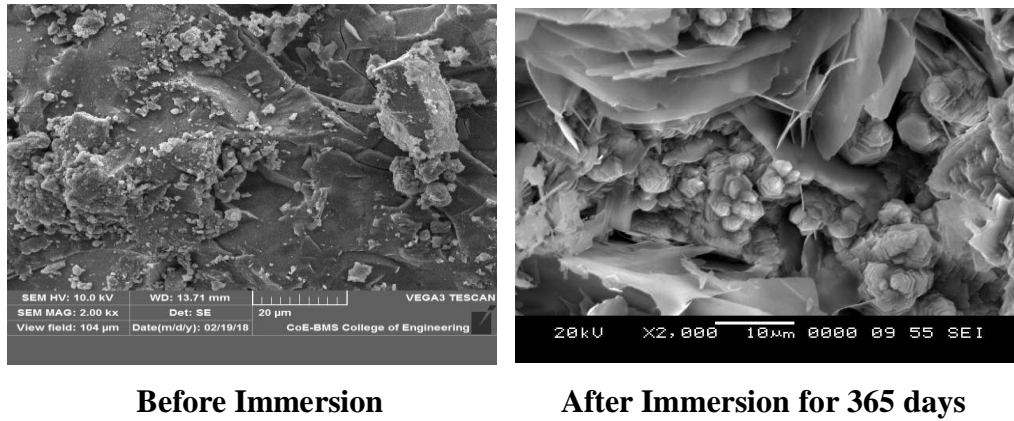


**Fig 5.16 SEM Images of Mix HSAASC-3 - Before and After Immersion in 10%  $MgSO_4$  solution**

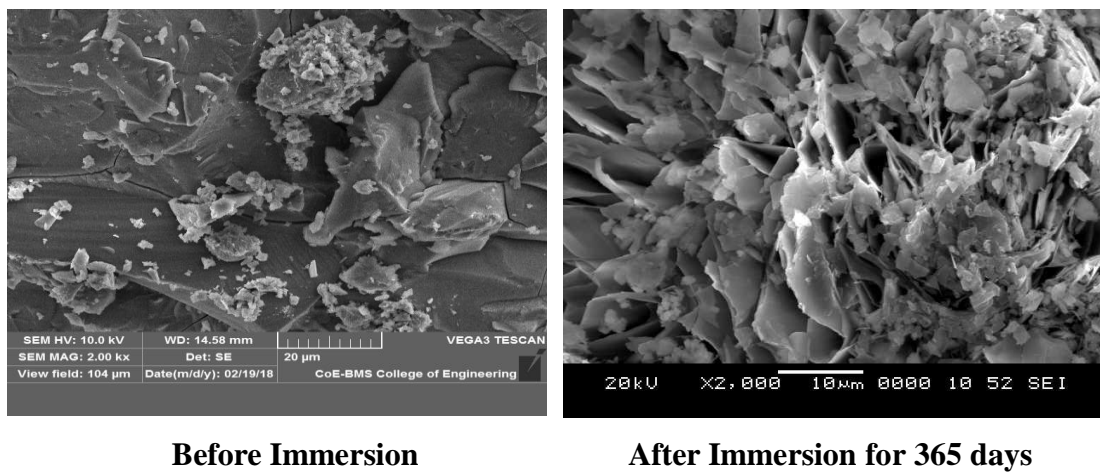
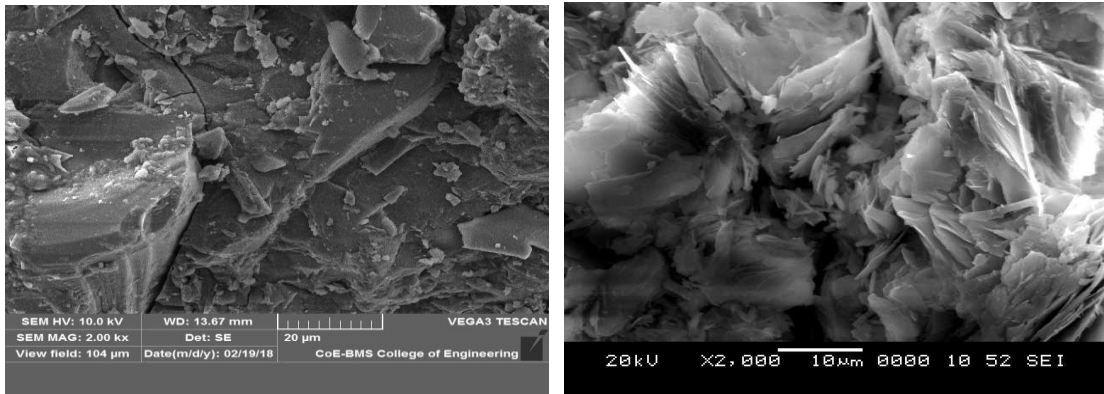


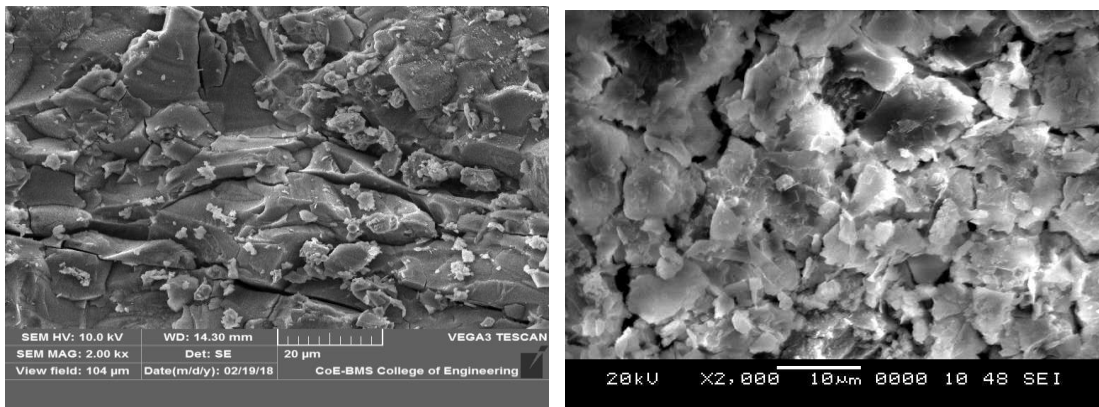
**Fig 5.17 SEM Images of Mix- HSAASC -5 - Before and After Immersion in 10%  $MgSO_4$  solution**



**Before Immersion**

**After Immersion for 365 days**

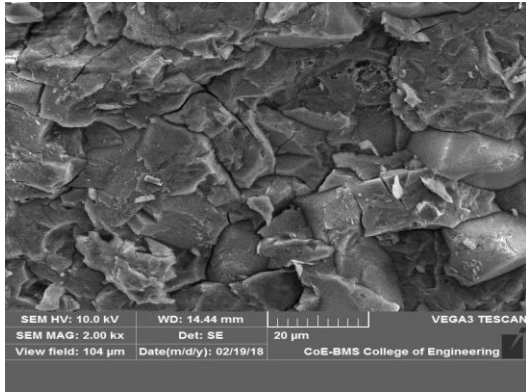
**Fig 5.18 SEM Images of Mix HSAASC-7 - Before and After Immersion in 10% MgSO<sub>4</sub> solution**



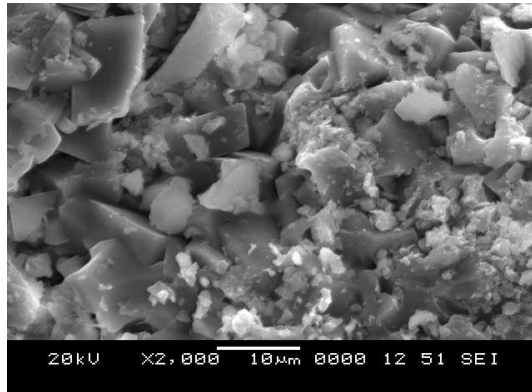
**Before Immersion**

**After Immersion for 365 days**

**Fig 5.19 SEM Images of Mix HSAASC-10 - Before and After Immersion in 10% MgSO<sub>4</sub> solution**

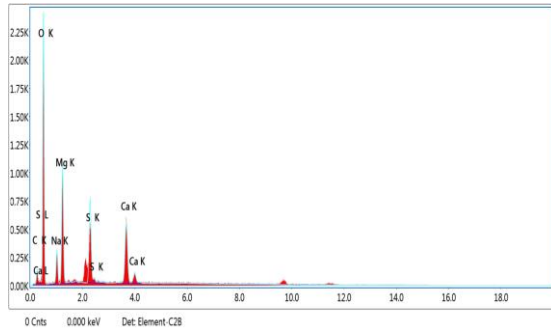


**Before Immersion**

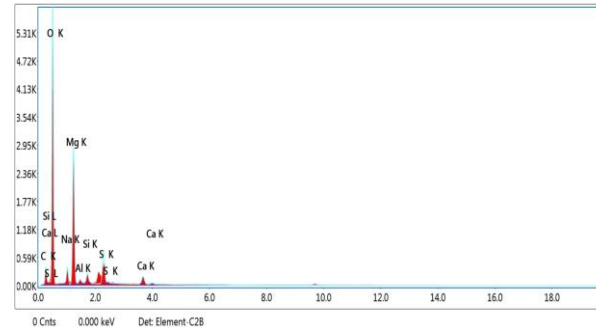


**After Immersion for 365 days**

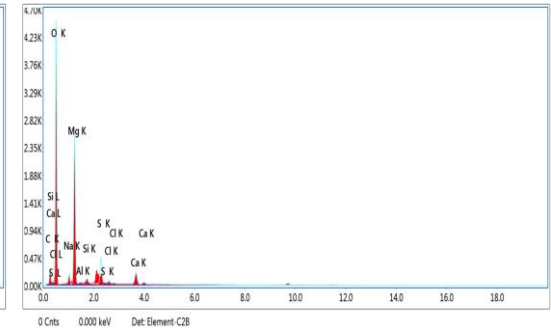
**Fig 5.20 SEM Images of Mix HSAASC-15 - Before and After Immersion  
in 10% MgSO<sub>4</sub> solution**



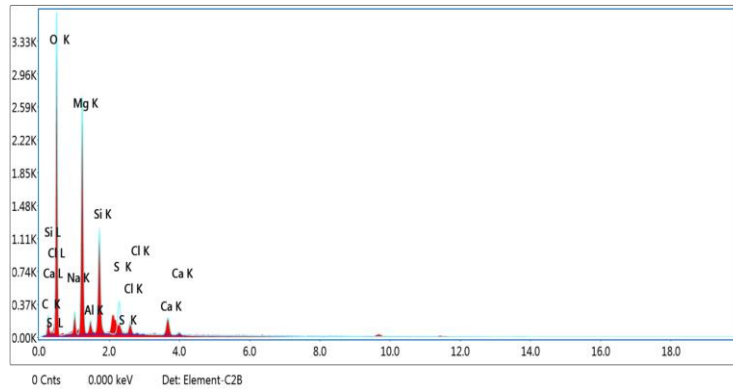
HSAASC-3



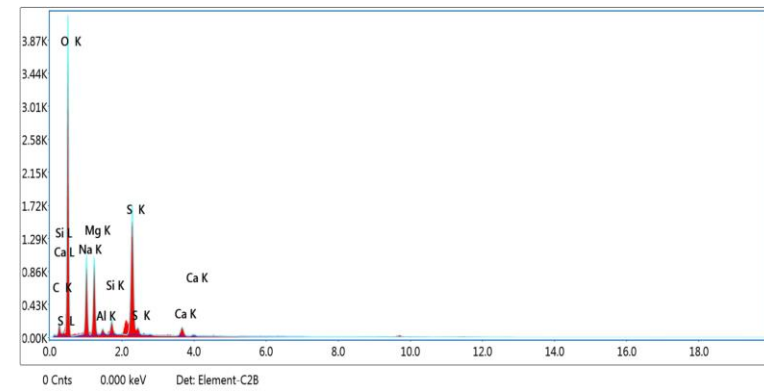
HSAASC-5



HSAASC-7



HSAASC-10



HSAASC-15

**Fig 5.21 Results of EDX Analyses - Elemental Compositions of HSAASC Mixes after Immersion in 10% MgSO<sub>4</sub> solution**

**Table 5.2 Results of EDX Analyses - Atomic percentages of elements in HSAASC mixes after immersion in 10% MgSO<sub>4</sub> solution.**

MIX ID	Atomic Percentage of Elements - EDX Analyses – After Sulphate Attack							
	O <sub>2</sub>	Na	Mg	S	C	Ca	Si	Al
<b>HSAASC-3</b>	60.0	2.40	11.1	4.3	7.43	3.44	10.1	1.10
<b>HSAASC-5</b>	50.2	1.80	15.9	1.4	13.0	4.96	11.2	1.50
<b>HSAASC-7</b>	51.5	1.8	17.0	2.3	6.3	6.35	12.7	1.69
<b>HSAASC-10</b>	50.3	2.46	16.9	1.9	5.7	6.42	13.8	2.48
<b>HSAASC-15</b>	52.2	1.8	16.6	3.7	4.93	7.0	11.5	1.87

#### 5.4 CHLORIDE ION PENETRATION RESISTANCE OF HSAASC MIXES

The chloride ion penetration resistances were measured by carrying out bulk-diffusion test as well as RCPT test, on all the concrete mixes. The chloride ion penetrations were evaluated in terms of non-steady state diffusion coefficients by carrying out bulk-diffusion tests on the test specimens as per ASTM C-1556-04. In this method, movement of chloride ions in saturated pore systems within the concrete mixes were evaluated in terms of apparent chloride diffusion coefficients. This test requires cylindrical specimens having a size of 100mm dia with a height of 200mm. The test specimens were immersed in 3.5% sodium chloride (NaCl) solution for a period of 35-days, after being subjected to initial ambient laboratory curing for a period of 28 days. These specimens were then split longitudinally by loading in a CTM. The freshly split surfaces were then sprayed with 0.1 M Silver nitrate ( $\text{AgNO}_3$ ) solution. The depth of chloride ion-penetration is measured as the depth up to which the colour of concrete changes to white due to formation of  $\text{AgCl}_2$  precipitate (Fig. 5.22). From the depths of chloride penetration so measured, the diffusion coefficients can be calculated by the equation –

$$X_D = 4(Dt)^{0.5} \quad \text{(Eqn.No 5.1)}$$

where  $X_D$  = depth of chloride penetration in metres,

$D$  = diffusion coefficient ( $\text{m}^2/\text{sec}$ )

and  $t$  = duration of exposure = 35 days

Average values of the three specimens were taken for evaluating the diffusion co-efficients. The bulk diffusion coefficient values for all the mixes tested herein are in the range of  $0.19 \times 10^{-12}$  to  $0.34 \times 10^{-12}$   $\text{m}^2/\text{sec}$  as shown in Fig.5.23 (Ganesan et al. 2015).

It can be observed that all the HSAASC mixes are showing diffusion coefficient values much lower than the value of  $1 \times 10^{-12}$   $\text{m}^2/\text{sec}$  specified, to be classified as low permeable concretes (Basheer 2001). The values are also much lower as compared to the diffusion coefficient for the reference OPC based concrete mix ( $2.5 \times 10^{-12}$   $\text{m}^2/\text{sec}$ ).



**Fig 5.22 Typical HSAASC mix specimens after the bulk diffusion test.**

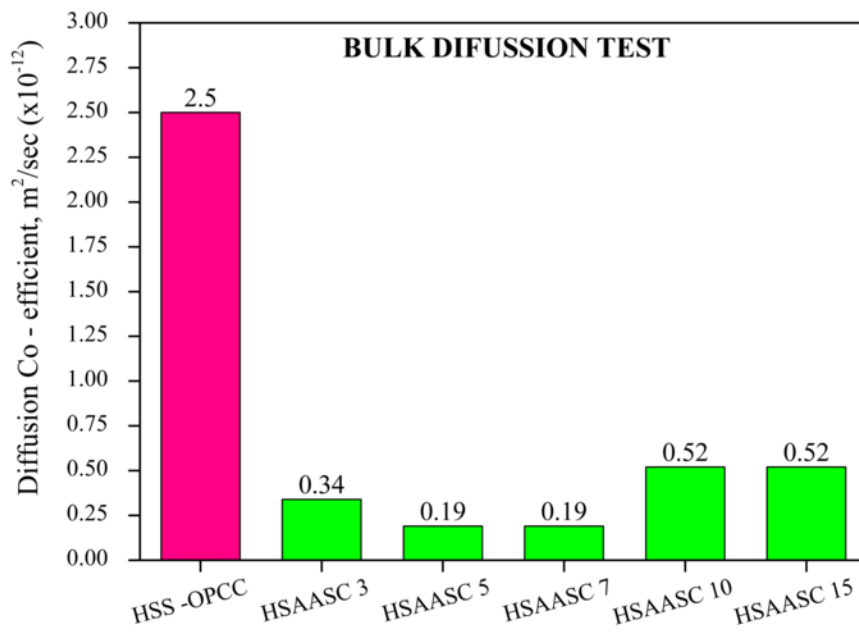


**Fig 5.23 Comparison of the chloride diffusion coefficients of different HSAASC mixes**

Such low diffusion coefficients of the mixes may be attributed to the dense matrices with lower total porosity, increased tortuosity and lower water absorption properties of the HSAASC mixes tested herein. These lower chloride diffusion coefficients also suggest a better protection for the steel rebars, placed in structural elements made of these HSAASC mixes, against possible corrosion.

Rapid chloride permeability test (RCPT) was used to evaluate the electrical conductivity of concrete. The procedure consists of monitoring the total amount of charge passed through 50mm thick slices of concrete cylinders of 100mm diameter, over a period of 6 hours, when a standard potential difference of 60V DC is maintained across the specimen as shown in Fig 5.24 and 5.25. The specimens are initially vacuum saturated for 18-hours prior to the test. To prevent the evaporation of water from the specimens during the test, the curved surfaces are wrapped with adhesive tape. On one side, the test specimen is exposed to 3% NaCl solution (catholyte) and on the other side to 0.3N NaOH solution (anolyte). The total charge passed through the specimens in coulombs may be considered as an index to chloride penetrability of concrete. Typical values of RCPT test values (Coulombs) suggested by ASTM C-1202 for classifying the mixes, based on their chloride-ion permeability are given in Table 5.3.

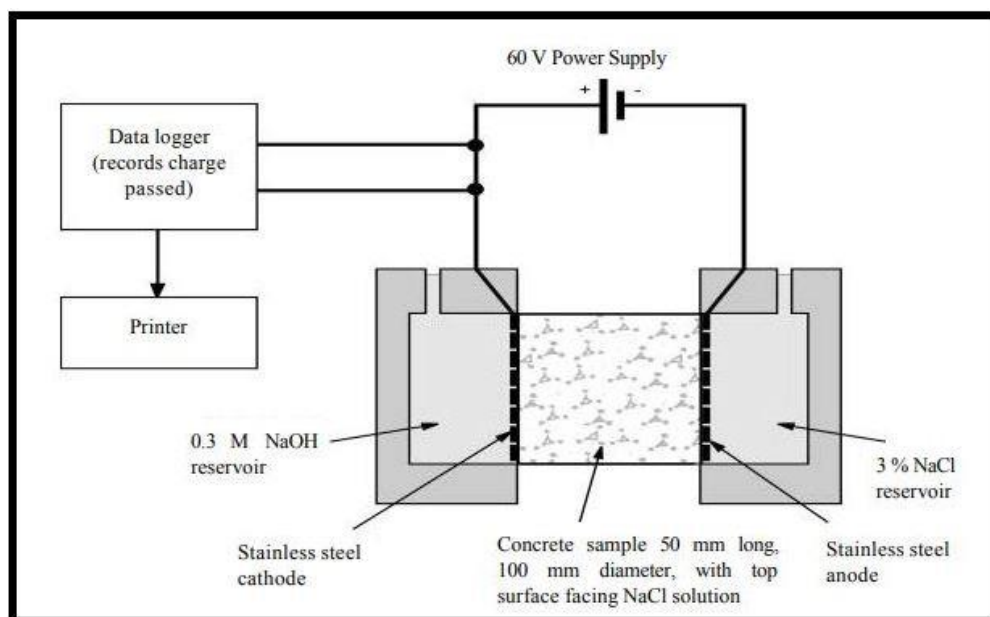


**Fig 5.24 RCPT Test Set up – Thematic Sketch (Stanish et al. 1997)**

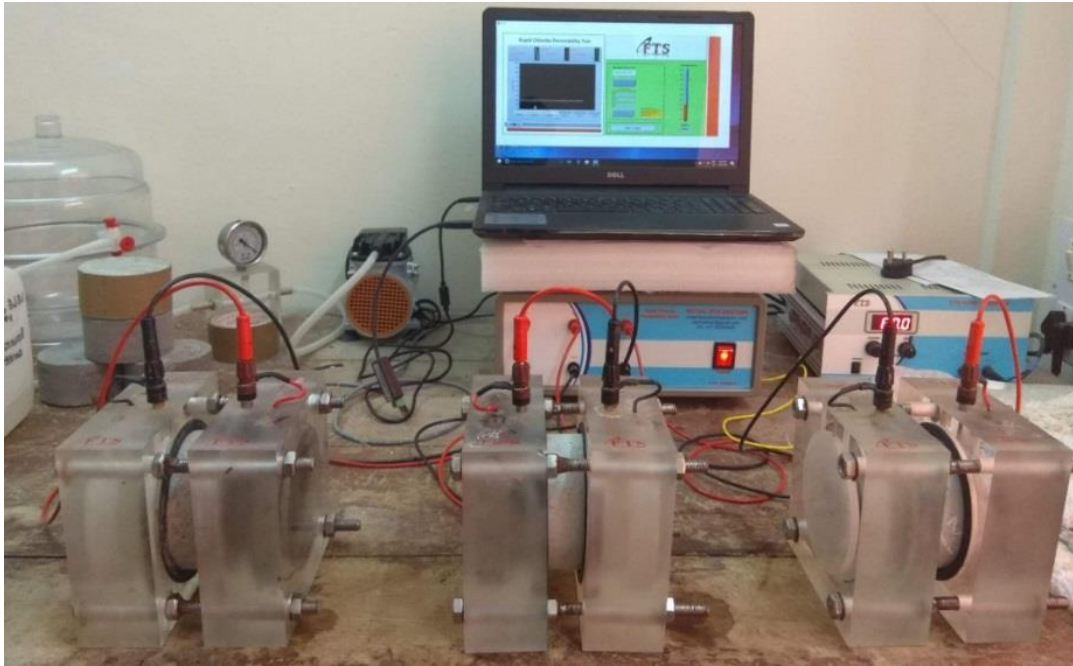


**Fig 5.25 Rapid Chloride Permeability test set-up**

**Table 5.3 Chloride permeability classifications as per ASTM standards**

<b>Chloride permeability</b>	<b>RCPT (Charge passed in coulombs)</b>
<b>High</b>	> 4000
<b>Moderate</b>	2000 – 4000
<b>Low</b>	1000 - 2000
<b>Very Low</b>	100 - 1000
<b>Negligible</b>	< 100

In case of RCPT tests, all the five HSAASC mixes tested have recorded chloride ion penetrations, measured as total charge passed, in the lower range of 618 - 835 coulombs as shown in Fig 5.26. Such values also enable the HSAASC mixes to be classified under very low category as per ASTM C-1202. However, these values are higher than that of the OPC-based reference concrete mix (RCPT value-582 Coulombs), suggesting marginally lower chloride-ion penetration resistance of the HSAASC mixes, as compared to the reference OPC-based concrete mix, which appears contradictory to the

results obtained above in the bulk-diffusion tests. The lower total penetration resistance (higher values of charge passed) in RCPT tests in case of AASC mixes, as compared to reference OPC-based concrete mixes, may be attributed to the fact that, under the influence of the impressed current, it is not just the negatively charged chloride ions supplied externally; but all the other ions present in the pore solutions of AAS concrete which permeate through the concrete causing higher values of total charges passed. This then leads to questions on the very suitability of the RCPT test for ascertaining the chloride penetration resistance of concrete mixes like AASC which may contain several charged alkali metal ions like Ca, Na, Si etc. (Stanish et al. 1997, Adam 2009, Chi 2012). However, it has been suggested that the RCPT may still be used for comparative evaluation of the chloride-ion penetration resistance of alkali-activated concretes (Thomas et al. 2018).

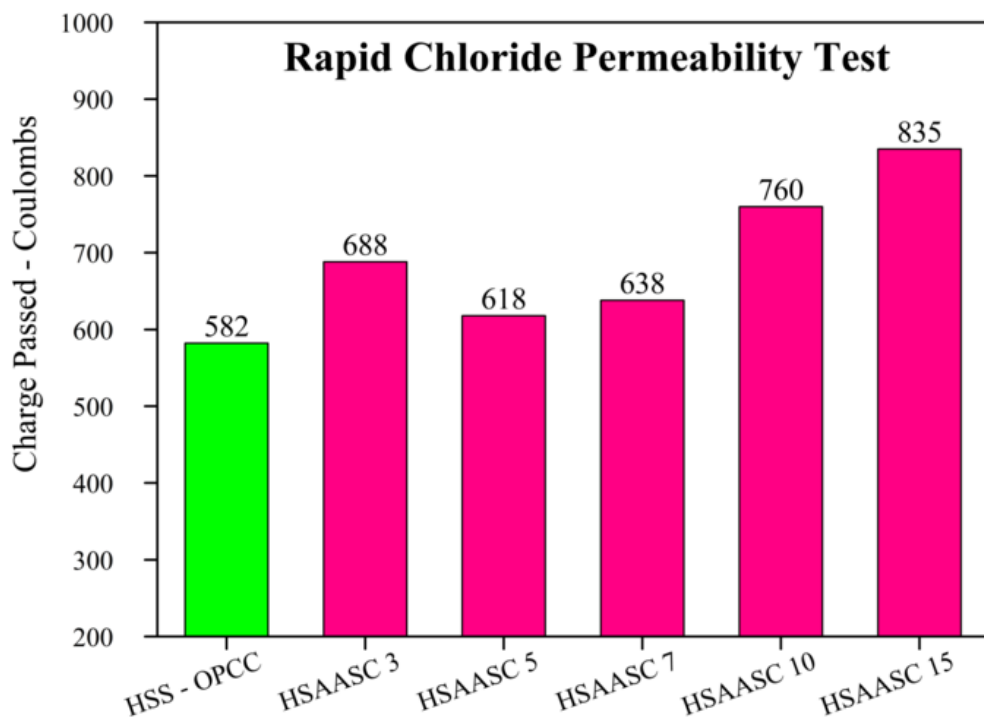


**Fig 5.26 Comparison of total charge passed in RCPT tests for different HSAASC mixes**

## 5.5 SUMMARY

In the present chapter, the relative performances of a set of high-strength, alkali-activated slag concrete mixes are compared to those of a high-strength, self-compacting ordinary Portland cement concrete (HSS-OPCC) mix in terms of their durability characteristics on exposure to acid, sulphate and chloride environments. The results show that possibly because of both pore-filling and pore-refinement effects, brought in with increased total binder contents, (GGBFS + fine quartz powder), the HSAASC mixes could exhibit a reduced chloride permeability compared to HSS-OPCC-based reference mix, as indicated by the results of bulk diffusion tests. Strength-retention characteristics of all the HSAASC mixes on exposure to magnesium sulphate showed comparable rate of strength deterioration as HSS-OPCC mix, as measured at the end of one year. The deterioration of HSS-OPCC samples, both in terms of mass and strength losses, on subjecting to sulphuric acid attack was much higher than all the HSAASC mixes tested herein. While the HSS-OPCC samples showed a complete deterioration by the age of 103 days, when subjected to acidic environments, test specimens of the five HSAASC mixes had retained their structural integrity and 50-60% of their original strengths, even after one year of such exposure.

In the previous chapter, the present class of alkali activated slag concrete mixes, all of which were produced using large quantities of industrial by-products (which otherwise present safe-disposal problems), had been shown to have the required levels of enhanced flow ability (to be categorized under self-compacting mixes), and higher mechanical strengths. Herein this chapter, they are also found to be possessing comparable, if not too much better, durability characteristics, as compared to OPC-based reference concrete mixes, in terms of their resistances against acid-, sulphate- and chloride environments as shown in Table 5.4. Hence it may be appropriate to refer to them as **High-Performance Alkali Activated Slag Concrete (HPAASC) Mixes**. Because of their favorable performance characteristics, it is justified to assume that they can effectively contribute, as a sustainable concrete construction technology, in building large-scale infrastructural facilities.

**Table 5.4 Parameters criteria for assessing HPAASC mixes**

	<b>EVALUATION CRETERIA</b>	<b>Target</b>	<b>High Performance OPCC (Literature)</b>	<b>High Performance AASC Developed</b>	<b>REMARKS</b>
1	<b>HIGH COMPRESSIVE STRENGTH</b>	$\geq 70\text{MPa}$	✓	✓	Achieved
2	<b>HIGH FLEXURAL STRENGTH</b>	$\geq 6.0\text{ MPa}$	✓	✓	
3	<b>HIGHER FLOW ABILITY – (Self-Compacting) EFNARC 2005</b>				
	a. Slump Flow test	$\geq 650\text{ mm}$	✓	✓	Achieved
	b. $T_{50}$ cm	$\leq 6\text{sec}$	✓	✓	Achieved
	c. V-Funnel test	6 – 12 sec	✓	✓	Achieved
	d. L –Box test	$\geq 0.85$	✓	✓	Achieved
	e. J-Ring test	$\leq 12\text{mm}$	✓	✓	Achieved
	f. Visual Stability Index	0	✓	✓	Achieved
3	<b>INITIAL SETTING TIME</b>	$\geq 3\text{hours}$	✓	x	Initial setting time - To be improved - AASC
4	<b>DURABILITY</b>				
	<b>(i) ACID -<math>\text{H}_2\text{SO}_4</math> @ 1 Year</b>				
	a. Mass Loss	$\leq 10\%$	x	✓	Complete Deterioration HP-OPCC
	b. Strength Loss	$\leq 40\%$	x	✓	Complete Deterioration HP-OPCC
	<b>SULPHATE-<math>\text{MgSO}_4</math>@1Year</b>				
	a. Mass Loss	$\leq 3\%$	x	✓	Achieved
	b. Strength Loss	$\leq 20\%$	x	✓	Achieved
	<b>BULK DIFFUSION TEST</b>	$\leq 1 \times 10^{-12}\text{ m}^2/\text{sec}$	x	✓	Low Permeable Concrete (Basheer 2001)
	<b>RCPT</b>	$\leq 1000\text{ Coulombs}$	✓	✓	Very Low – ASTM C 1202

## **CHAPTER 6**

### **STRENGTH RETENTION CHARACTERISTICS OF HPAASC MIXES SUBJECTED TO ELEVATED TEMPERATURES**

#### **6.1 GENERAL**

Performance of constructional materials and concrete members against fire and elevated temperature has always been a major issue of concern amongst the designers of concrete structures, and worldwide as a phenomenon seriously threatening people's lives and safety. When exposed to high temperatures, concrete undergoes major physical and chemical changes, ultimately leading to its deterioration and destruction (Khaliq and Khan 2015).

As discussed in earlier chapter, the present class of alkali activated slag concrete mixes, all of which are produced using large quantities of industrial by-products (which otherwise present safe disposal problems) and are having the required levels of enhanced flow ability, higher mechanical strengths and better durability properties, can be referred to as High-Performance Alkali Activated Slag Concrete Mixes.

The elevated-temperature resistance tests were done on 100 mm cubes; concrete specimens from each mix were placed in a temperature controlled furnace and heated from room temperature (30<sup>0</sup>C) to elevated temperatures in the range 200 - 800<sup>0</sup>C. The specimens were held, soaked at the particular high temperature for 90 minutes and then were allowed to cool down in the furnace, until the temperature in the furnace attains to normal room temperature. The concrete specimens were then tested for changes in their masses (mass-loss) and residual compressive strengths.

#### **6.2 RESIDUAL STRENGTH CHARACTERISTICS OF HPAASC MIXES ON EXPOSURE TO ELEVATED TEMPERATURES**

The specimens were placed in a temperature-controlled electric furnace as shown in Fig 6.1 and the target temperature was set. The increase in the temperature, within the furnace was noted for every 10 minutes, until it reached the set target temperature. Figure 6.2 shows the time verses temperature plots for differently set target temperatures of 200<sup>0</sup>C, 400<sup>0</sup>C, 600<sup>0</sup>C and 800<sup>0</sup>C.



**Fig 6.1 Temperature controlled electric furnace used in the present study**

It can be observed that the rate of increase of temperature is almost constant at around 5-6<sup>o</sup> Centigrade per minute in each of the cases; the specimens were then kept soaked, within the furnace at the target temperature, for a period of 90 minutes. Subsequently, the oven was switched off and the test specimens were allowed to cool down in the furnace, until the temperature in the furnace attains to normal room temperature and were tested for their residual compressive strengths. Again for comparison purposes, similar tests were conducted on test specimens of the HSS-OPC based reference concrete mix, heated to temperatures in the range 100<sup>o</sup>C - 500<sup>o</sup> C, at intervals of 100<sup>o</sup> C, the changes in the maximum temperature of exposure and the interval having been affected, taking into cognizance, severe spalling of the specimens of these high strength OPC-based concrete mixes, within 600<sup>o</sup> C.

The test specimens of OPC based reference SCC mix, on heating to a temperature up to 200<sup>o</sup>C, did not show any noticeable change in their color. Further when temperature was increased from 300<sup>o</sup>C to 500<sup>o</sup>C, the colour changed from normal grey to light pink colour, with their structural integrity being maintained up to 500<sup>o</sup>C. However severe spalling of OPC-based reference concrete specimens started occurring by the time the temperature within the furnace was nearing 600<sup>o</sup>C, as shown in Fig 6.3.

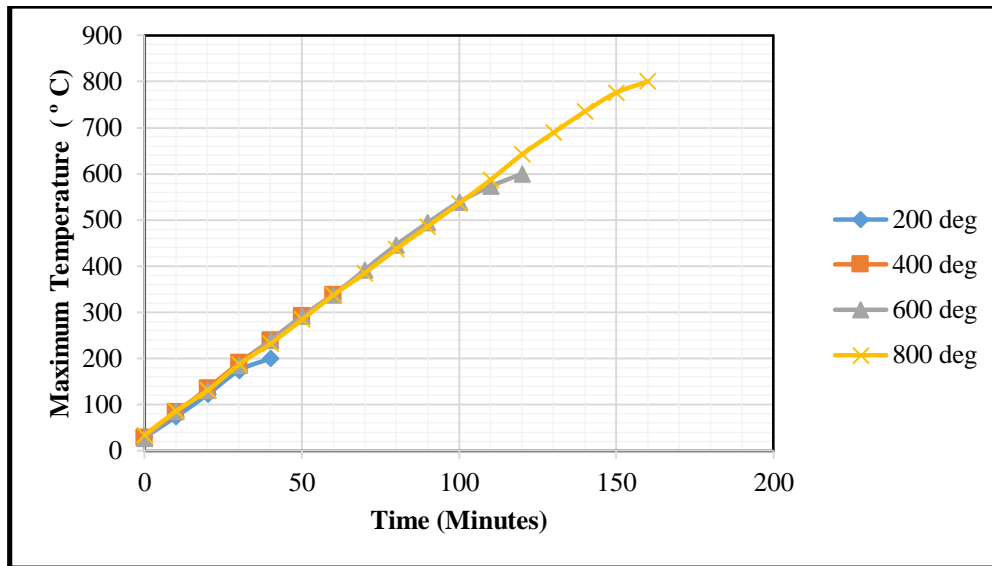


**Fig 6.2 Temperature Controlled Oven – Heating Cycle - Time verses Temperature**



**Fig 6.3 OPCC specimen spalled during the exposure to 600°C**

HPAASC mixes, however maintained their structural integrity and the colour of the specimens remained almost the same, even upto 600°C. When the temperature was increased to 800°C, the colour of the specimens slightly changed to whitish grey with visible minor cracks as shown in Fig 6.4 and 6.5. Results of weight-losses in OPC-based reference concrete mix (upto 500<sup>0</sup> C only) and the five candidate HPAASC mixes (upto 800<sup>0</sup>C), on exposure to the elevated temperatures, are shown in Fig 6.6 and 6.7. It can be observed that weight losses increased, with the increase in temperature of exposure, for both HPAASC mixes and HSS-OPC-based concrete mix.

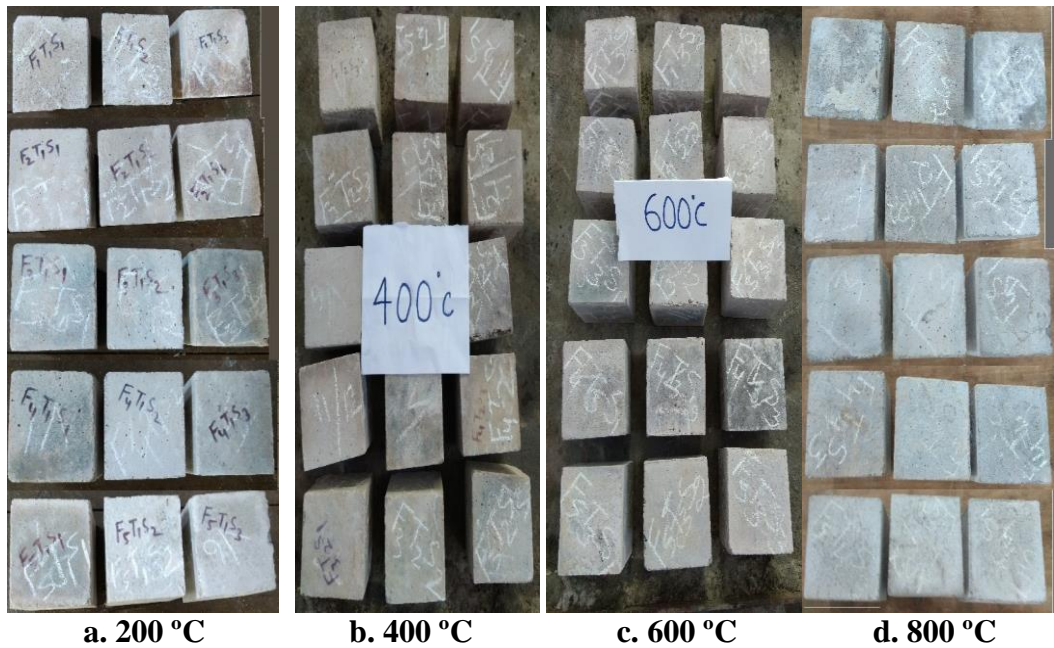


**Fig 6.4 HPAASC specimens after exposure to different elevated temperatures**



**Fig 6.5 Typical HPAASC specimen after being exposed to 800°C – A closer look**

It can be seen that the OPC based reference concrete mix, showed a lower weight- loss of about 7%, only, at 500<sup>0</sup>C , as compared to 10-13% recorded by specimens of HPAASC mixes, when exposed up to a temperature of 400°C. In the case of HPAASC mixes, the maximum losses in weights occurred in the temperature range of 200°C to 400°C, after which the rate of such losses in weights decreased significantly, with final losses being in the range of 14 - 15%, on exposure up to 800°C, as shown in Fig 6.8. The residual strength co-efficients of all the mixes plotted are shown in Fig 6.9.

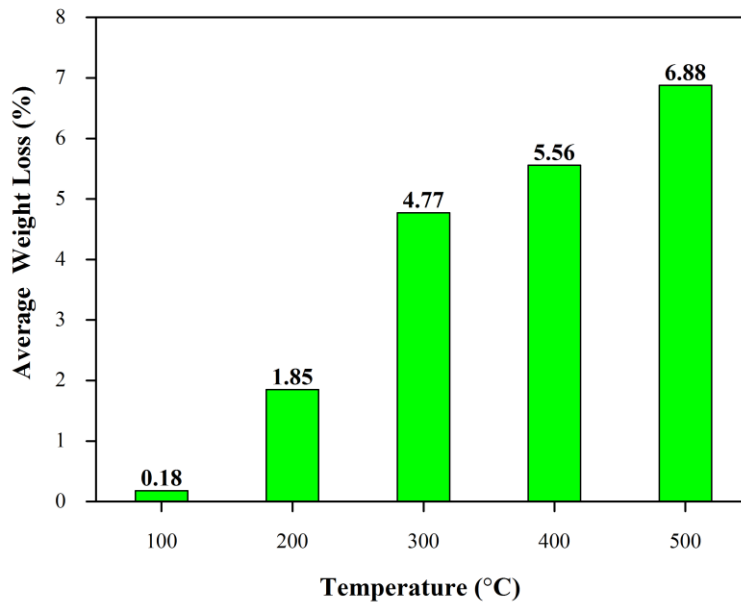


**Fig 6.6 Weight loss for HSS-OPCC mix at different temperatures**

Such weight losses, on heating to temperatures in the range of 100-200°C, are due to evaporation of higher amounts of water in the macro-pores which get evaporated easily, leading to increased losses in weight; subsequently however, it is the water in the capillary pores which gets evaporated, with difficulty, even on application of heat, accounting for reduced rates of weight-losses. As indicated earlier, severe spalling and total structural distress had been observed in the OPC-based reference concrete mix, by the time the temperature of exposure had reached 600°C. Test specimens of all the five HPAASC mixes almost retained their original compressive strengths up to 200°C. Any further increase in temperature caused a decrease in their strength, right up to a temperature of 800°C.

While strength retentions in the range of 40-50% of their initial strengths were observed at 600°C, a sharp reduction in the strengths (strength retentions in the range of 21-26% of their initial strengths) were observed for all the HPAASC mixes, on exposure to a higher temperature of 800°C.

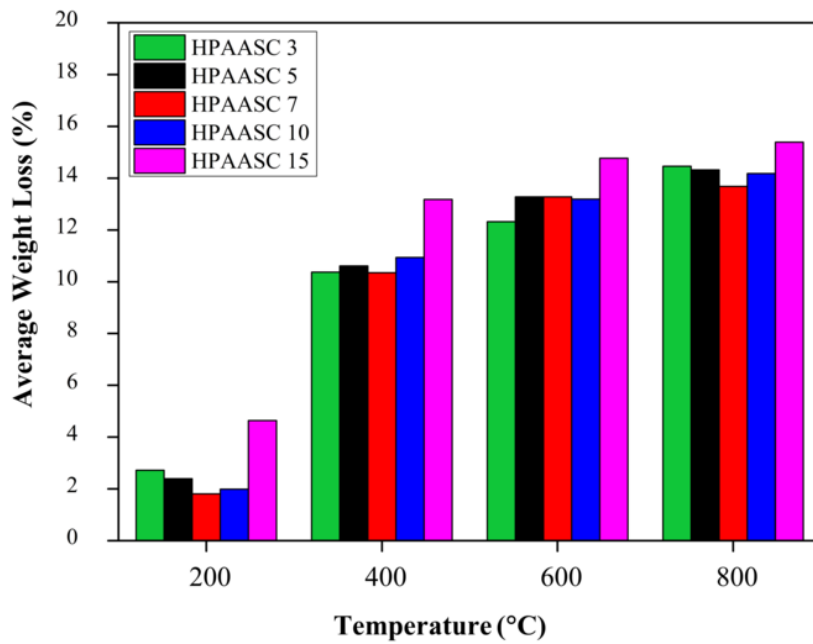


**Fig 6.7 Percentage weight loss for various HPAASC mixes at different temperatures.**

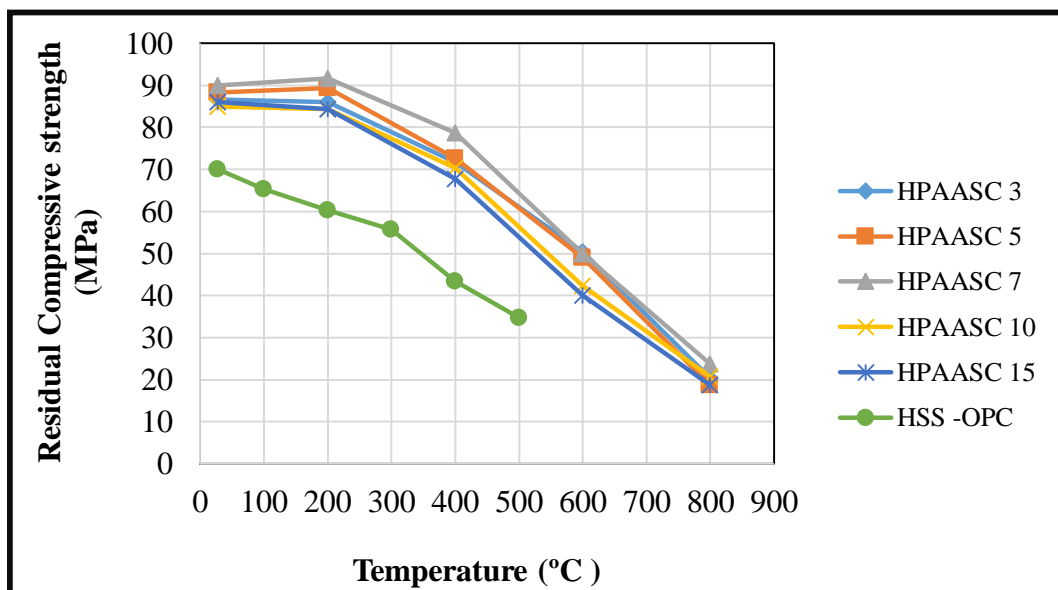


**Fig 6.8 Compressive strength values of various mixes exposed to different temperatures**

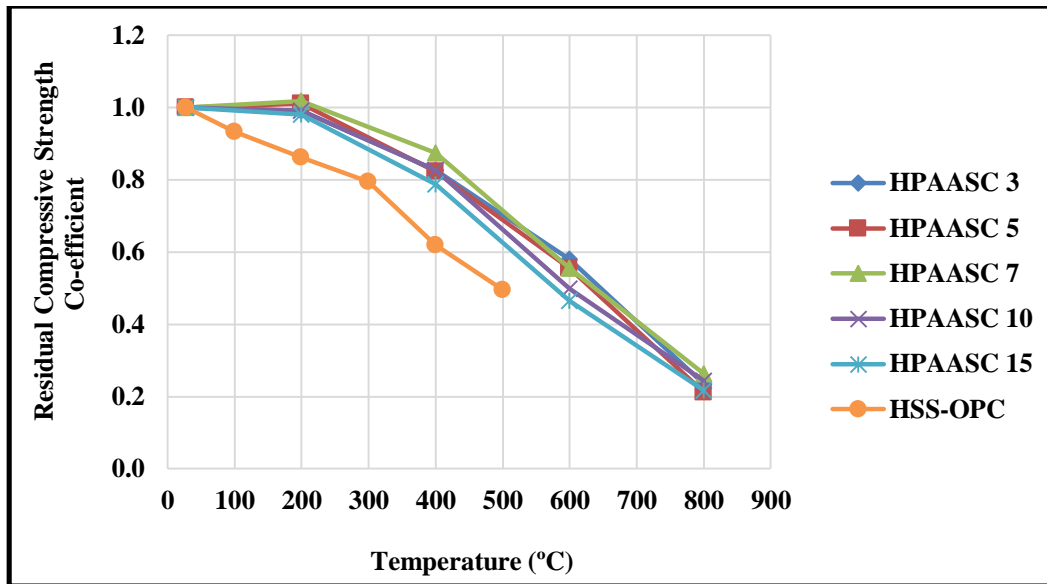


**Fig 6.9 Residual Compressive Strength co-efficient of various mixes exposed to different elevated temperatures**

Such strength reductions are possibly due to the continuous decomposition of the C-A-S-H/C-S-H gels and loss of chemically bound water; Formation of cracks on the surface of concrete due to the differences in the rates of thermal expansion of aggregates and paste (Poon et al. 2001, Xu et al. 2001, Li et al. 2004), may further facilitate early failure of those specimens at lower strength-levels.

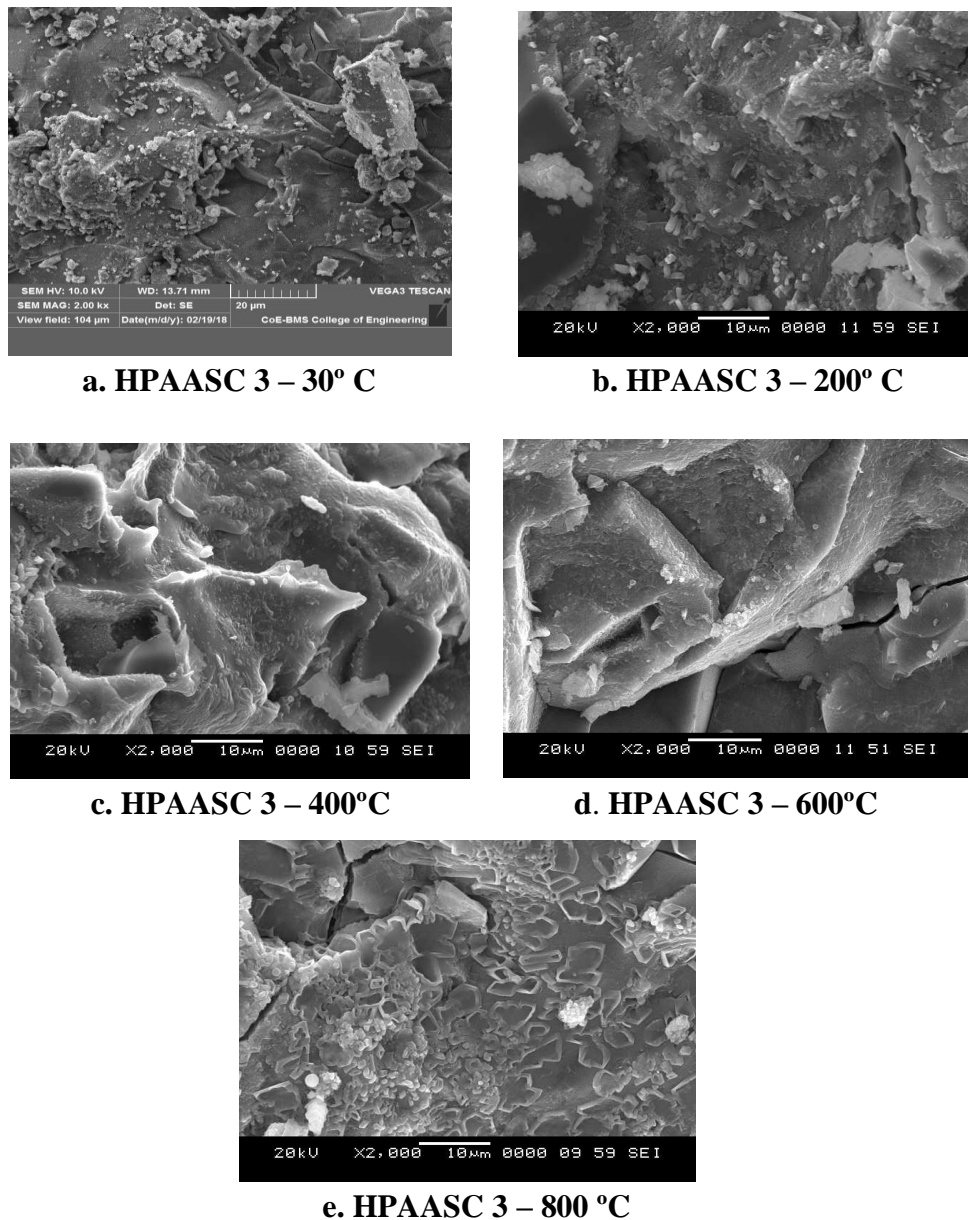
From all the above results it can be inferred that, all the five HPAASC mixes have exhibited better high-temperature performance (with respect to retention of compressive strength) than the HSS-OPCC mix; the best strength performance has been, however, obtained with HPAASC 7 mix.

### **6.3 MICROSTRUCTURAL STUDIES OF HPAASC MIXES SUBJECTED TO SUSTAINED ELEVATED TEMPERATURES**

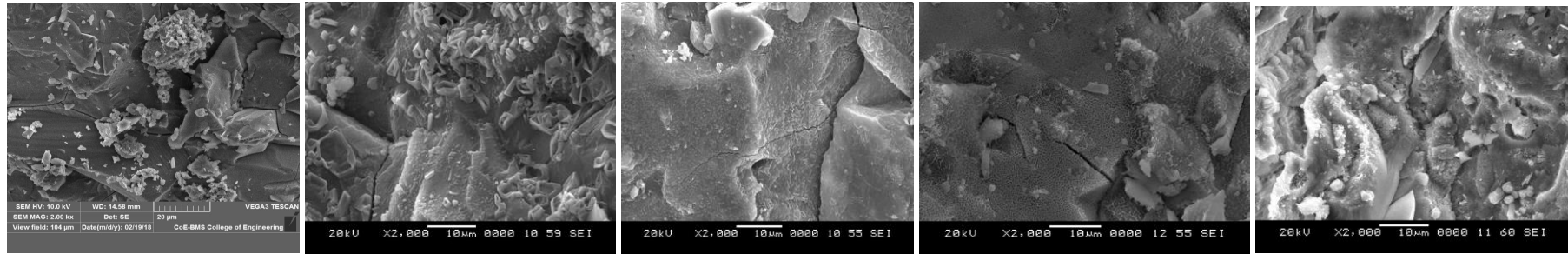
In order to find out the changes in the microstructural details of all the HPAASC mixes, on exposure to increasing levels of sustained temperatures, namely 200°C, 400°C, 600°C and 800°C, scanning electron microscope analyses were carried out on very small samples of size 5-10mm, extracted from the central core of the fractured concrete cube specimens on all the five HPAASC mixes at their respective temperatures.

Fig 6.10 – 6.14 show the SEM-derived micrographs of all the five HPAASC mixes, both before and after having been exposed to elevated temperatures. Further the elemental composition of all the five HSAASC mixes, at each of the temperature above were obtained through detailed EDX analyses.

It can be clearly observed that the specimens of all the five HPAASC mixes at ambient room temperature (30<sup>0</sup> C) were showing denser morphologies as shown in the micrographs in Fig 6.10 – 6.14.

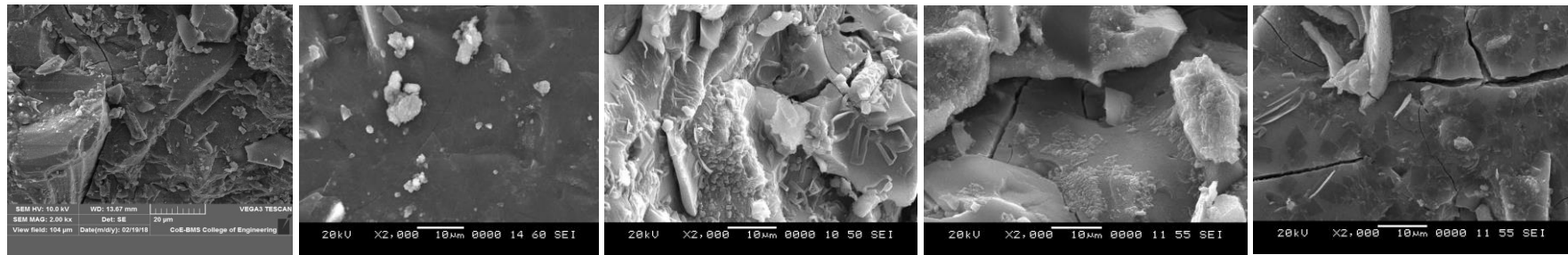


**Fig 6.10 (a-e) SEM Images of Mix- HPAASC- 3 at different temperatures**



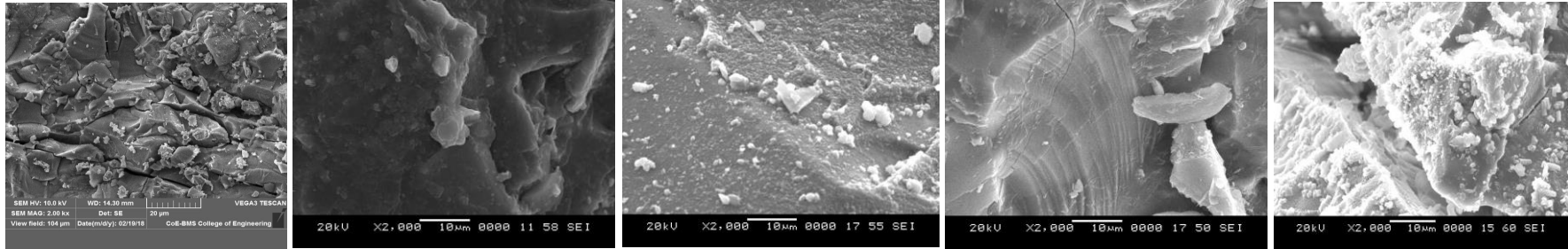
**a. HPAASC 5 - 30°C      b. HPAASC 5 – 200°C      c. HPAASC 5 – 400°C      d. HPAASC 5 – 600°C      e. HPAASC 5 – 800°C**

**Fig 6.11 (a-e). SEM Images of Mix- HPAASC- 5 at different temperatures**



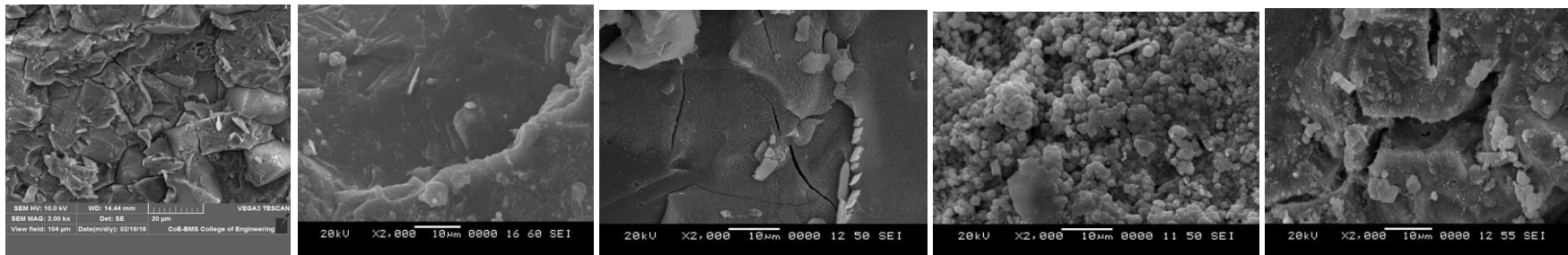
**a. HPAASC 7- 30°C      b. HPAASC 7- 200°C      c. HPAASC 7- 400°C      d. HPAASC 7- 600°C      e. HPAASC 7- 800°C**

**Fig 6.12 (a-e). SEM Images of Mix- HPAASC- 7 at different temperatures**



**a. HPAASC 10 - 30°C    b. HPAASC 10 – 200°C    c. HPAASC 10 – 400°C    d. HPAASC 10 – 600 °C    e. HPAASC 10 – 800°C**

**Fig 6.13 (a-e). SEM Images of Mix- HPAASC- 10 at different temperatures**



**a. HPAASC 15- 30°C    b. HPAASC 15 – 200°C    c. HPAASC 15 – 400°C    d. HPAASC 15 – 600°C    e. HPAASC 15 – 800°C**

**Fig 6.14 (a-e). SEM Images of Mix- HPAASC- 15 at different temperatures**

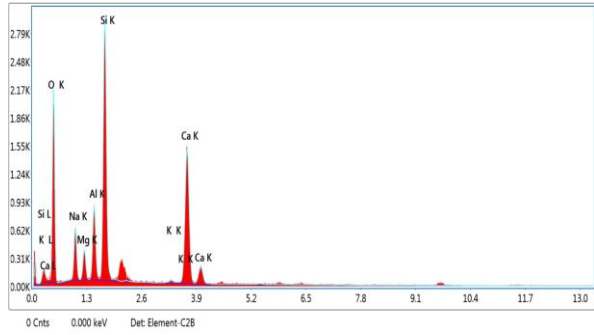
The initial increase in the temperature up to 200°C has caused development of a few cracks in some of the mixes, while in others; slight changes in the morphological features are observed. However further increase in the temperature between 400°C - 800°C has significantly caused the initiation and widening of minor cracks with major cracks becoming more predominantly visible when exposed to 800°C.

It can clearly be inferred from the images in Fig 6.10 - 6.14, that increasing degradation of the C-A-S-H – like gels also takes place with heating the test specimens to higher levels of sustained temperatures. Such continuous degradation in the binder-phase along with the development of large numbers of micro- and macro-cracks, are responsible for causing the mass loss, along with continuously decreasing compressive strengths (with increasing temperature of exposure) for all the five HPAASC mixes tested herein (Rovnanik et al. 2013, Behfarnia and Shahbaz 2018, Turker et al. 2016).

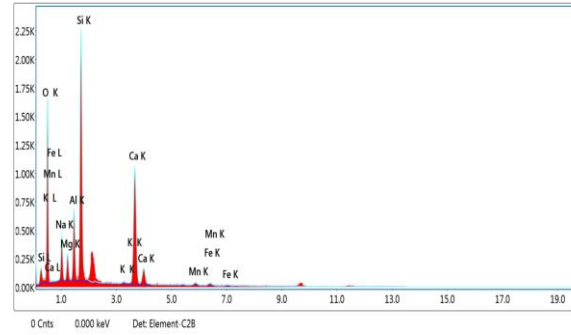
Detailed analyses of EDX plots were also carried out, as shown in Fig 6.15, based on the entire sampling areas of the SEM micrographs of the respective HPAASC mixes, taken after they were exposed to different levels of elevated temperatures. Typical results of elemental compositions obtained thereof on exposure to a representative 800°C of temperature, represented as average atomic percentages of different elements, are shown in Table 6.1.

#### **6.4 SUMMARY**

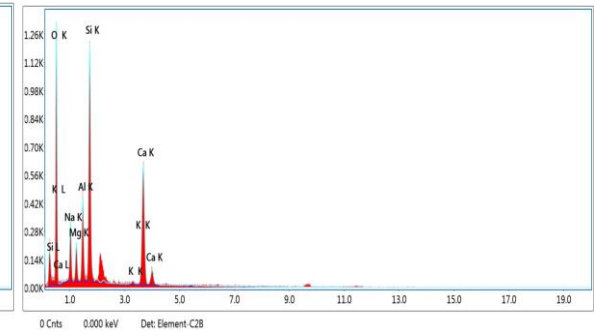
In the present chapter, HPAASC specimens were prepared and exposed to sustained elevated temperature in the range of 200 - 800°C in an electric furnace for a sustained duration of 90 minutes. Results indicated that all the HPAASC mixes maintained their structural stability even after exposure to 800°C, without showing any signs of spalling as observed in case of HSS-OPCC, while reaching to a temperature at 600°C. Further the residual compressive strength results of all the HPAASC mixes were in the range of 21-26% when exposed to a temperature of 800°C. However the HSS-OPCC showed a residual strength of about 50% when subjected to temperature of about 500°C.



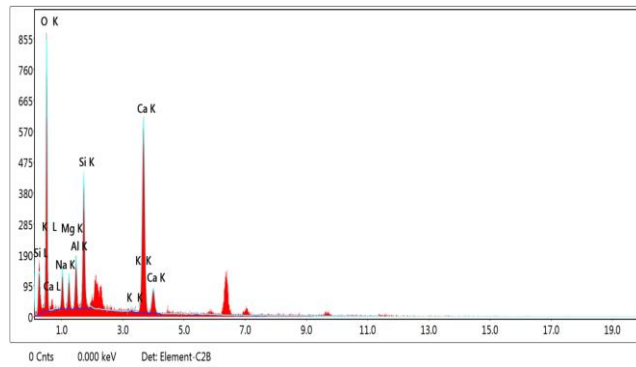
HPAASC 3



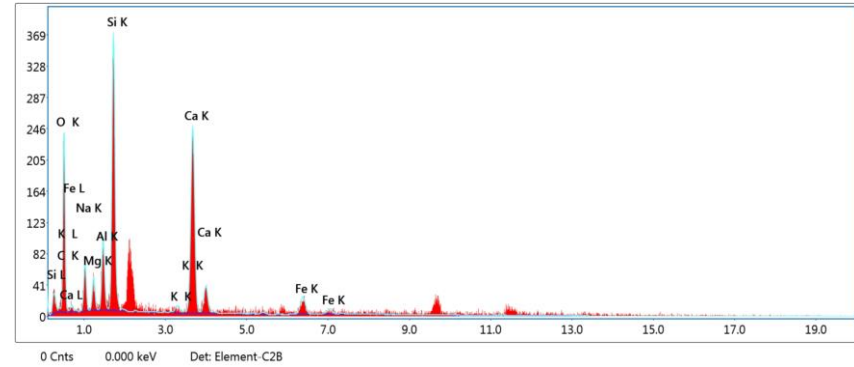
HPAASC 5



HPAASC 7



HPAASC 10



HPAASC 15

**Fig 6.15 Typical EDX analyses results of all HPAASC Mixes after being exposed to 800° C**

**Table 6.1 Results of EDX Analyses - Atomic percentages of major elements in HPAASC mixes after exposure to 800° C**

<b>MIX ID</b>	<b>Atomic Percentage of Elements - EDX Analyses – After Exposure to High Temperature</b>							
	<b>O</b>	<b>Na</b>	<b>Mg</b>	<b>S</b>	<b>C</b>	<b>Ca</b>	<b>Si</b>	<b>Al</b>
<b>HPAASC-3</b>	60.0	2.40	11.1	4.3	7.43	3.44	10.1	1.10
<b>HPAASC-5</b>	50.2	1.80	15.9	1.4	13.0	4.96	11.2	1.50
<b>HPAASC-7</b>	51.5	1.8	17.0	2.3	6.3	6.35	12.7	1.69
<b>HPAASC-10</b>	50.3	2.46	16.9	1.9	5.7	6.42	13.8	2.48
<b>HPAASC-15</b>	52.2	1.8	16.6	3.7	4.93	7.0	11.5	1.87

**CHAPTER 7**  
**FLEXURAL TOUGHNESS CHARACTERISTICS OF**  
**HIGH PERFORMANCE**  
**ALKALI ACTIVATED SLAG CONCRETE MIXES**

**7.1 GENERAL**

The present chapter discusses the evaluation of flow ability and flexural toughness characteristics of High Performance Alkali activated slag concrete (HPAASC) mixes on incorporation of steel fibers. In spite of the fact that there have been smaller improvements in the split-tensile and flexural strengths as well as modulus of elasticity, in the present class of HPAASC mixes, they continue to be brittle in nature; so structural elements undergo failures, without associated larger deflections and hence warning. In order to improve their deflection and cracking behaviour during failure under loads, addition of increasing amounts of corrugated steel fibers within a range of 0.4 - 0.8% with respect to total volume of concrete, in all the HPAASC mixes is contemplated. Results showed acceptable flow ability characteristics for self-compacting concrete as per EFNARC guidelines for mixes with fibers. The HPAASC mixes, on such incorporation of steel fibers, showed improved ultimate flexural performances as compared to mixes without fibers. Further the toughness indices calculated based on methods suggested by Barr and Hasso (1985) and ACI (1988) showed comparable toughness behaviour of the HPAASC mixes, as compared to control HSS-OPCC mix admixed with steel fibers.

**7.2 MATERIALS AND ITS PROPERTIES**

Corrugated steel fibers as shown in Fig 7.1 procured from M/s Fiber Zone, Ahmedabad, India were used in fiber reinforced high performance alkali activated slag concrete mixes tested in the present investigation. Their physical properties are shown in Table 7.1.



**Fig 7.1 Corrugated Steel Fibers used**

**Table 7.1 Properties of Corrugated Steel Fibers**

<b>Fiber type</b>	<b>Corrugated Steel Fibers</b>
<b>Length of steel fibers (l) (mm)</b>	25
<b>Diameter of steel fibers (d) (mm)</b>	0.5
<b>Aspect ratio (l/d)</b>	50
<b>Density kg/m<sup>3</sup></b>	7850
<b>Ultimate Tensile strength (N/mm<sup>2</sup>)</b>	1280

### **7.3 EXPERIMENTAL METHODS**

In the present phase of experiments, the same five mixes that were considered for detailed durability studies (Chapter 5) and study of performance under elevated temperatures (Chapter 6), based on their higher performances in terms of their flow ability properties and strengths (Chapter 4), were again taken as candidate mixes for a detailed study on evaluation of the effect of incorporation of increasing dosages of steel fibers in them. They are mixes HPAASC-3, HPAASC-5, HPAASC-7, HPAASC-10 and HPAASC-15. Increasing dosages of corrugated steel fibers were considered for incorporation, as additional ingredient, in each of the five candidate mixes. A drastic

decrease in the flow ability characteristics was observed on incorporation of fibers at dosages greater than 0.8% and hence fiber-incorporation was restricted to a maximum of 0.8%. Hence representative dosages of 0.4, 0.6 and 0.8% of fiber were considered. Every 0.2% addition works out to be about 15.7 kgs of fibers to be added for cubic meter of wet concrete. These High Performance, Fiber Reinforced, Self-compacting Alkali-activated Slag Concrete mixes - HFSASC mixes are redesignated, for convenience, as detailed in Table 7.2. The effects of such incorporation of steel fibers (at different volume fractions) on the flow ability, compressive strengths and flexural toughness characteristics of these mixes were studied and the results of such studies are presented in this chapter.

#### **7.4 FLOW TESTS ON HFSASC MIXES**

The flow tests such as Slump flow, V- funnel, L- box, J ring and Visual stability Index, were performed on HFSASC mixes immediately after mixing. The slump flow tests were carried out using the Abram's cone, to evaluate the filling ability of the different HFSASC concrete mixes. The times ( $T_{50}$ ) taken for the concrete to reach a spread of 500 mm were also evaluated. It is observed from the results in Table 7.3, HFSASC (1 - 5) mixes with different percentage of steel fibers showed slump flows in the range of 650mm – 685mm and  $T_{50}$  values less than 6 seconds. Thus they satisfy the EFNARC guidelines wherein a slump flow ranging from 650 – 800 mm and  $T_{50}$  of less than 6 seconds are specified. With the increase in the percentage of steel fibers along with their respective increases in binder content showed a decrease in the flow characteristics. This behaviour may be attributed to the large increases in the surface area of solids resulting in addition of higher amounts of finer quartz powder which hence the uses a larger amounts of alkaline solutions present just for wetting the smaller-sized particles. The steel fibers added also caused an increase in the stiffness of the HPAASC mixes causing a decrease in the flow values. The V – Funnel tests were carried out on all the HFSASC (1 - 5) mixes. It is observed from Table 7.3, that the times taken for emptying the V-Funnel were less than 12 sec still satisfying the EFNARC guidelines (values to range between 6 –12 sec). Increase in the percentage of steel fibers along with their respective increments in the binder, did not show any appreciable decreases in the times

taken for emptying the V-Funnel. This clearly indicates the better filling abilities of all the HFSASC mixes developed herein.

The HFSASC mixes (1- 5) were tested for their passing ability by conducting the L-Box tests. It was observed that all the HFSASC candidate mixes tested herein, with the three dosages level of steel fibers, have acceptable abilities to pass through the reinforced bars, the blocking ratios  $H_2/H_1$  being in the range 0.85 to 0.94, satisfying the relevant EFNARC guidelines as shown in Table 7.3. The times  $T_{200}$  and  $T_{400}$ , taken by the flow to move through distances of 200mm and 400mm in the horizontal channel, from the plane of rebars in the L-box, were also found to be satisfactory with their maximum values being 10.1 and 12.4 seconds as shown in Table 7.3.

**Table 7.2 Mix Details for HFSASC mixes.**

Reference Mix	% of Fibers added	Designation for HFSASC Mixes
HSS-OPCC	0.4	HFSOPCC – 0.4
	0.6	HFSOPCC – 0.6
	0.8	HFSOPCC – 0.8
HPAASC - 3	0.4	HFSASC 1 – 0.4
	0.6	HFSASC 1 – 0.6
	0.8	HFSASC 1 – 0.8
HPAASC - 5	0.4	HFSASC 2 – 0.4
	0.6	HFSASC 2 – 0.6
	0.8	HFSASC 2 – 0.8
HPAASC - 7	0.4	HFSASC 3 – 0.4
	0.6	HFSASC 3 – 0.6
	0.8	HFSASC 3 – 0.8
HPAASC - 10	0.4	HFSASC 4 – 0.4
	0.6	HFSASC 4 – 0.6
	0.8	HFSASC 4 – 0.8
HPAASC - 15	0.4	HFSASC 5 – 0.4
	0.6	HFSASC 5 – 0.6
	0.8	HFSASC 5 – 0.8

Table 7.3 Flow ability tests of HFSASC mixes

Tests For	Filling Ability			Passing Ability						Segregation Resistance
MIX ID	Slump Flow Test		V-Funnel Test	L –Box Test			J-Ring Test			Visual Stability Index (VSI)
	Spread mm	T <sub>50</sub> sec	T <sub>vf</sub> sec	<sup>s</sup> T <sub>200</sub> sec	<sup>s</sup> T <sub>400</sub> sec	H <sub>2</sub> /H <sub>1</sub>	Spread mm	T <sub>50</sub> sec	Difference in Height mm	
HFSOPCC - 0.4	664	6.0	10.1	7.3	10.1	0.90	652	10.9	14.0	0
HFSOPCC - 0.6	660	5.7	10.8	7.9	11.5	0.86	645	11.5	15.8	0
HFSOPCC - 0.8	650	6.0	11.7	8.2	12.1	0.83	630	13.1	18.8	0
HFSASC 1 - 0.4	685	5.1	9.4	7.5	10.6	0.94	676	8.6	10.0	0
HFSASC 1 - 0.6	674	4.8	10.5	7.0	11.1	0.87	670	9.1	10.9	0
HFSASC 1 - 0.8	660	5.0	11.2	8.2	11.9	0.85	650	11.1	11.5	0
HFSASC 2 - 0.4	665	5.3	11.0	7.0	10	0.92	661	8.0	11.0	0
HFSASC 2 - 0.6	665	5.5	11.0	8.0	11.1	0.87	660	9.9	11.4	0
HFSASC 2 - 0.8	660	5.6	12.0	9.2	12.0	0.85	650	12.3	12.0	0
HFSASC 3 - 0.4	665	6.0	11.5	7.9	11.2	0.92	657	9.1	11.3	0
HFSASC 3 - 0.6	657	5.9	11.0	8.5	11.0	0.86	649	10.9	11.3	0
HFSASC 3 - 0.8	660	6.0	12.0	9.0	12.3	0.85	650	12.9	13.5	0
HFSASC 4 - 0.4	680	6.0	10.1	7.6	10.4	0.88	686	10.2	12.0	0
HFSASC 4 - 0.6	670	5.9	11.3	7.5	12.1	0.85	660	12.0	12.5	0
HFSASC 4 - 0.8	656	6.0	11.6	9.0	12.4	0.85	640	12.1	13.0	0
HFSASC 5 - 0.4	689	5.5	11.0	8.3	12.0	0.90	670	10.8	12.3	0
HFSASC 5 - 0.6	670	6.0	12.0	9.0	11.5	0.86	654	12.0	12.8	0
HFSASC 5 - 0.8	650	6.5	12.5	10.1	12.8	0.88	635	12.5	13.8	0

Based on results of both the V-funnel tests and L-box tests, it can be concluded that the HFSASC mixes can easily pass through and fill even the areas with larger congestion of rebars, leading to better structural conditions. Increases in the percentage of fibers increases the stiffness of the mixes, causing a decrease in the flowing and filling abilities of the mixes, as compared to normal HPAASC mixes; however availability of relatively higher volumes of pastes and smaller size of the aggregates still ensure sufficient flow characteristics in these mixes to satisfy the relevant EFNARC guidelines.

J-Ring tests were also performed on all the HFSASC mixes and the results are tabulated in Table 7.3. It can be observed that differences in the heights of concrete between the inside and outside of the ring are in a satisfactory range 10mm – 13.8mm (should be less than 12 mm) in all the mixes.

Visual stability index tests were simultaneously conducted on all the HFSASC mixes as per ASTM C1611– 2014. All the HFSASC mixes clearly showed the good stability, with no signs of segregation or bleeding. Hence a VSI value of zero could be assigned to all the mixes.

Thus it can be said that, higher contents of finer powdery materials (both the binder materials – GGBFS and fine quartz powder), partial substitution of slag sand with quartz sand, choice of smaller-sized (12.5 mm down) EAF-Slag coarse aggregates and appropriate chemistry of alkaline solution ( $\text{Na}_2\text{O}\%$  considered) - all have synergically contributed to the favorable flow-characteristics of the HFSASC mixes.

## **7.5 COMPRESSIVE STRENGTHS OF HFSASC MIXES**

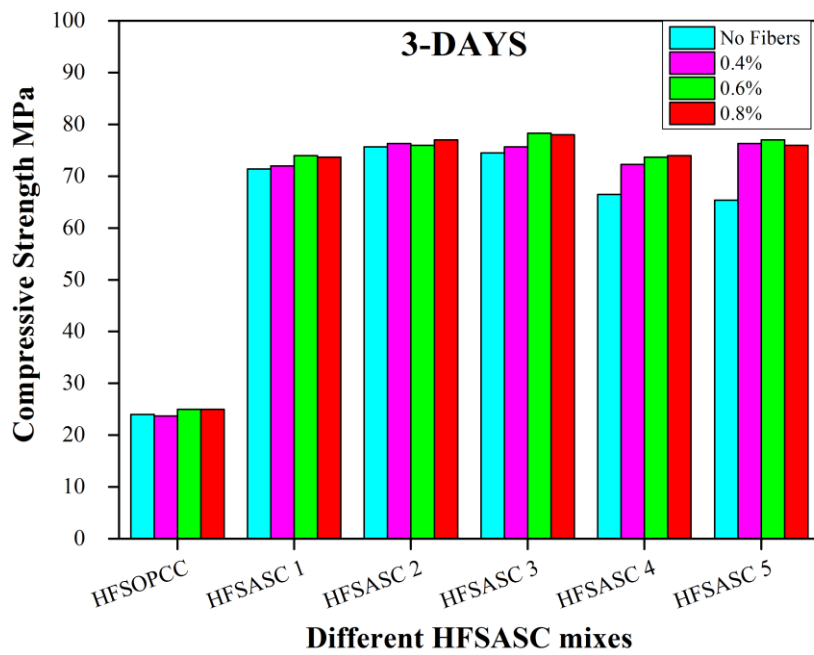
All HFSASC mixes were tested for their compressive strengths at 3- and 28-days of age, as per IS 516:1959 and the results are tabulated in Table 7.4. It can be observed that higher compressive strengths in the range of 83MPa - 98 MPa have been obtained as shown in Fig 7.2. Marginal increases in compressive strengths (10 -15%) have been recorded with increased percentage of fibers, as compared to normal HPAASC mixes. This behaviour may be attributed to the better stitching of the main crack plane, with

increase contents of the steel fibers within the AAS matrixes leading to enhanced strength performances.

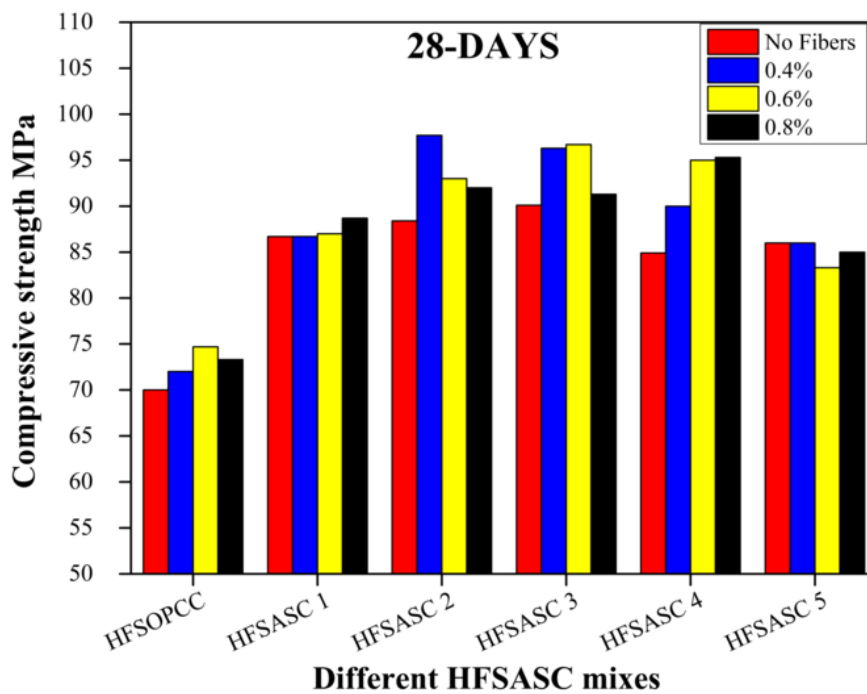
It can also be observed that the 3-day compressive strengths of all the Fiber reinforced ASC mixes are quite comparable, (within a smaller 72.0 - 78.3 MPa range), such early strengths are again a good higher percentage (almost 80%) of their respective 28-day strengths. The 3-day strengths of OPC-based reference concrete mixes are, for record, about 33% of their 28-day strengths.

**Table 7.4 Compressive strengths of HFSASC mixes**

Reference Mix	Designation for HFSASC Mixes	Compressive Strength MPa	
		3 days	28 days
HSS-OPCC	HFSOPCC – 0.4	23.7	72.0
	HFSOPCC – 0.6	25.0	74.7
	HFSOPCC – 0.8	25.0	73.3
HPAASC - 3	HFSASC 1 – 0.4	72.0	86.7
	HFSASC 1 – 0.6	74.0	87.0
	HFSASC 1 – 0.8	73.7	88.7
HPAASC - 5	HFSASC 2 – 0.4	76.3	97.7
	HFSASC 2 – 0.6	76.0	93.0
	HFSASC 2 – 0.8	77.0	92.0
HPAASC - 7	HFSASC 3 – 0.4	75.7	96.3
	HFSASC 3 – 0.6	78.3	96.7
	HFSASC 3 – 0.8	78.0	91.3
HPAASC - 10	HFSASC 4 – 0.4	72.3	90.0
	HFSASC 4 – 0.6	73.7	95.0
	HFSASC 4 – 0.8	74.0	95.3
HPAASC - 15	HFSASC 5 – 0.4	76.3	86.0
	HFSASC 5 – 0.6	77.0	83.3
	HFSASC 5 – 0.8	76.0	85.0



(a)



(b)

**Fig. 7.2 Compressive Strength values of mixes at age of 3 and 28 days**

## 7.6 FLEXURAL STRENGTHS OF HFSASC MIXES

The flexural strength characteristics of the present set of HFSASC mixes were evaluated in terms of the Load-deflection behaviour of beam specimens under flexure. The beam specimens (100mm x 100mm x500mm in size) were subjected to third point bending tests, on a span of 400 mm, in a 400 kN-capacity universal testing machine (UTM). All the specimens were initially preloaded to approximately 1kN, which was well below the cracking loads for the specimens, to eliminate initial seating problems. The rate of straining was maintained very low till the first crack. Deflections measurements were made at regular increments of loads, initially, using dial gauges, at both the support points (moving upwards) and mid-span (moving downwards) downward movements at the mid-span. Accordingly total mid-span deflections were computed.

After the onset of first crack, usually nearer the mid-span section, additional observations were made with the dial-gauges at decreasing loads so as to be able to plot the post-crack behaviour of the prisms as well. Such post-crack behaviour of the beams could be very erratic, as it depends on whether the propagating crack had encountered a new fiber or not, as the beam attempts to sustain the load. The procedure was continued till the load-deflection behaviour in the post-crack region is also captured for sufficiently larger total deflections. Figure 7.3 and 7.4 shows the typical failure pattern of a test specimen and almost uniform distribution of fibers across the mid-span section of a test beam, respectively. Tests were conducted on five specimens of each candidate mix. The load-deformation curves for all the candidate HFSASC mixes tested here in are shown in Figs 7.5 – 7.10. From these figures it clearly seen that there is almost a linear behaviour in the load-deflection curves, until their peak load (First-Crack load) in all the mixes, and any possible increases beyond the first crack depend on the availability of higher volume fraction of steel fibers in the HFSASC matrices.

It had been observed that the flexural strengths of the present class of HPAASC mixes, when not reinforced with steel fibers, were smaller percentages of their compressive strengths.



(a)



(b)

**Fig 7.3 Failure of the specimen at mid span cross-section**



(a)



(b)

**Fig.7.4 Distribution of steel fibers at mid span cross-section**

Now it can be seen the ultimate flexural strengths of such mixes can be greatly improved by incorporating steel fibers in them and made higher than those of the control OPCC mixes as shown in Fig 7.11.

The increments in the ultimate flexural strengths, for the maximum percentage of steel fibers, are in the range of 20.8% - 44.0% for the various HFSASC mixes, as compared to normal HPAASC mixes without fibers, due to the better bonding of the steel fibers with the AASC matrix. It is also observed that the drop in the load at first-crack is never totally regained in the post-crack region in any of the beams. This type of post-crack softening behaviour is seen in almost all of the specimens, possible due to slightly lower volume fraction of steel fibers. Further there are only very few number of the fibers available to stitch the crack and arrest/resist its further propagation across the

mid-span cross-section of all the beams tested herein. Since all the mixes developed were targeted for retaining the property of self-compacting even after the addition of steel fibers, as per the relevant EFNARC guidelines.

It can be appreciated that the shape of load- deflection curve is mostly dependent upon the fiber content and so also the fiber distribution across the mid-span cross-section of the test specimen. The effective crack-arresting effect provided by the fibers leads to requirement of more energy for the progress of the fracture processes (Bernal et al. 2010). The requirement of a fiber found in the path of the crack to get either pulled out, or undergo yielding and hence fail before the crack can extend/propagate increases the deflections sustained by the beams. Thus increase in the amount of steel fibers significantly increases the area under the load-deflection curves, suggesting better ductile performances of these mixes as compared to reference OPCC mixes (Figs. 7.5 – 7.10).

## **7.7 FLEXURAL TOUGHNESS CHARACTERISTICS OF HFSASC MIXES**

Toughness is measure of the capacity of a material to absorb energy. This is the most important property of any steel fiber reinforced concrete mix, acquired by it due to the post-cracking ductility imparted to it by the fibers. There are number of recommendations with respect to method of calculation of the toughness indices of concrete mixes, proposed by different researchers/agencies, those due to Barr and Hasso, ACI, and ASTM C 1018 to name a few. All these methods have been shown to have their own advantages and disadvantages.

In the present investigation, the toughness indices as recommended by Barr and Hasso (1985) and ACI (1988) have been used to evaluate the toughness characteristics of the HFSASC mixes. The pertinent calculations involved in such evaluations are indicated in Fig 7.12.

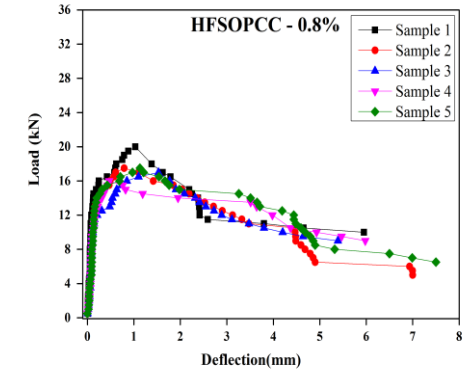
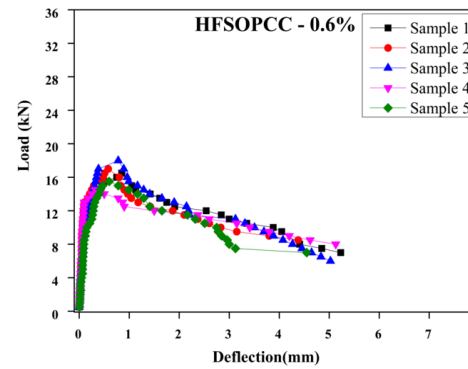
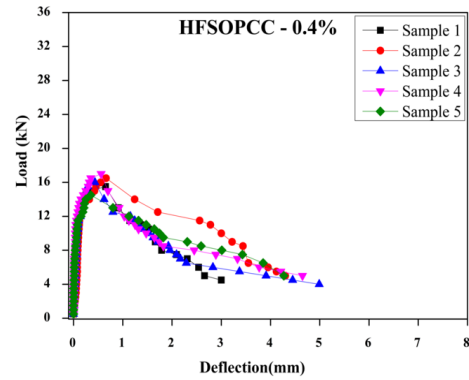


**Fig 7.5 Load - Deflection behaviour of HFSOPCC for all specimens with different % of steel fibers**

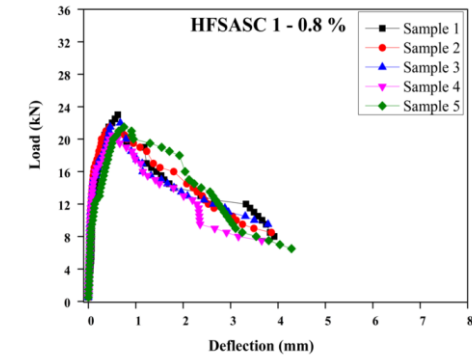
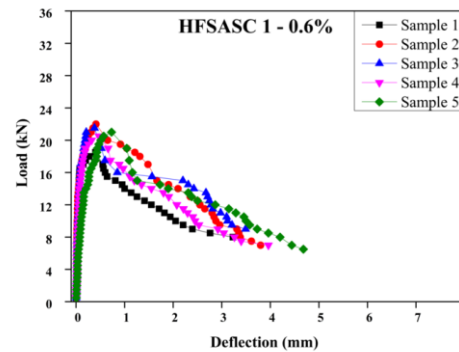
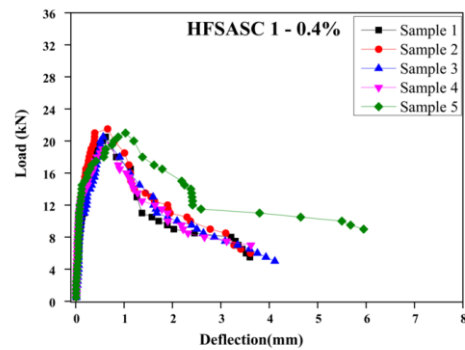


**Fig 7.6 Load - Deflection behaviour of HFSASC-1 for all specimens with different % of steel fibers**

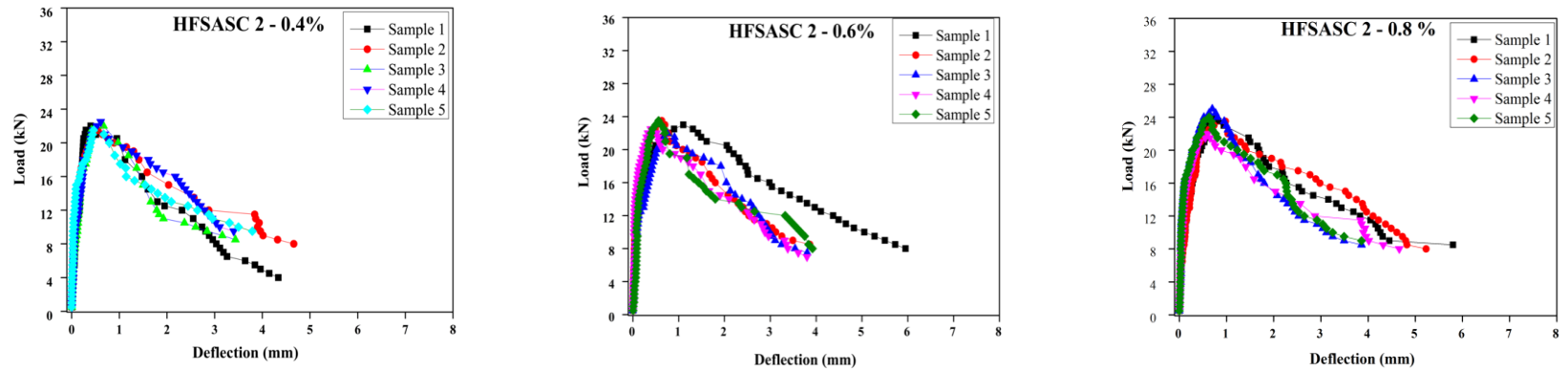


**Fig 7.7 Load - Deflection behaviour of HFSASC-2 for all specimens with different % of steel fibers**

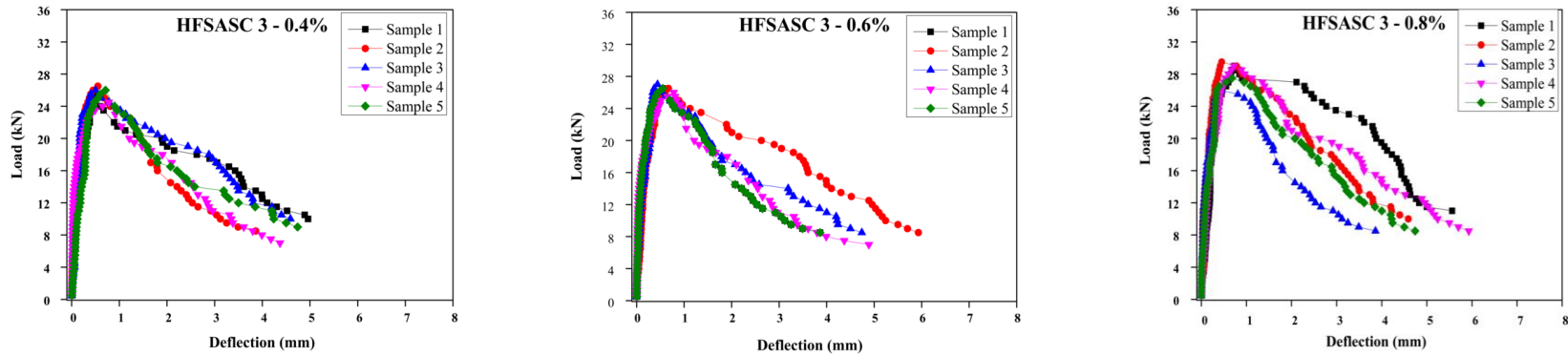


**Fig 7.8 Load- Deflection behaviour of HFSASC-3 for all specimens with different % of steel fibers**

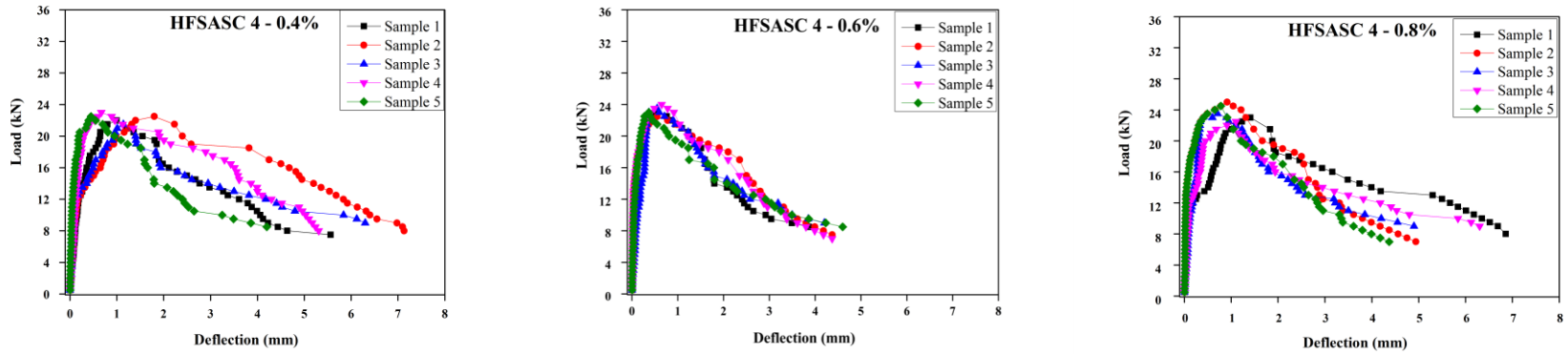


**Fig 7.9 Load- Deflection behaviour of HFSASC-4 for all specimens with different % of steel fibers**

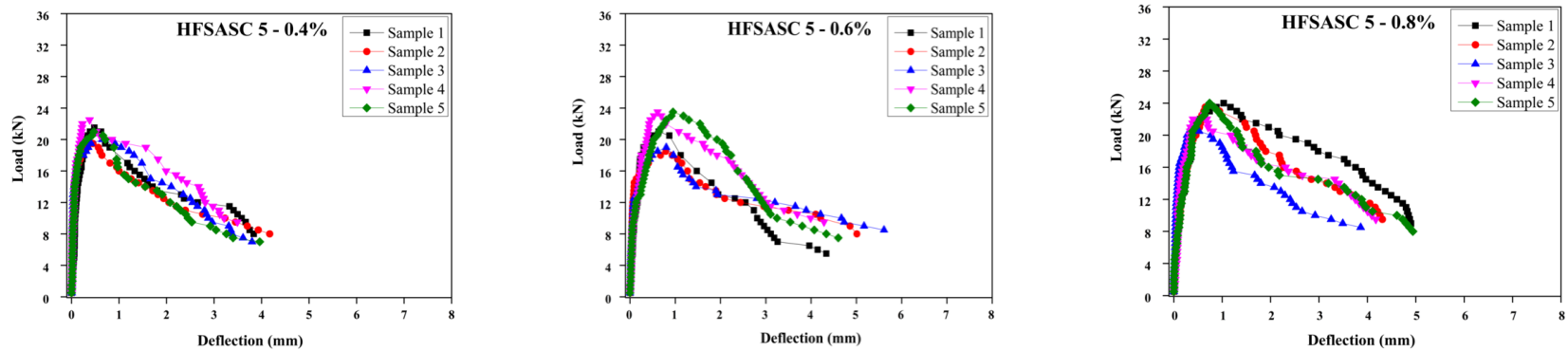


**Fig 7.10 Load- Deflection behaviour of HFSASC-5 for all specimens with different % of steel fibers**

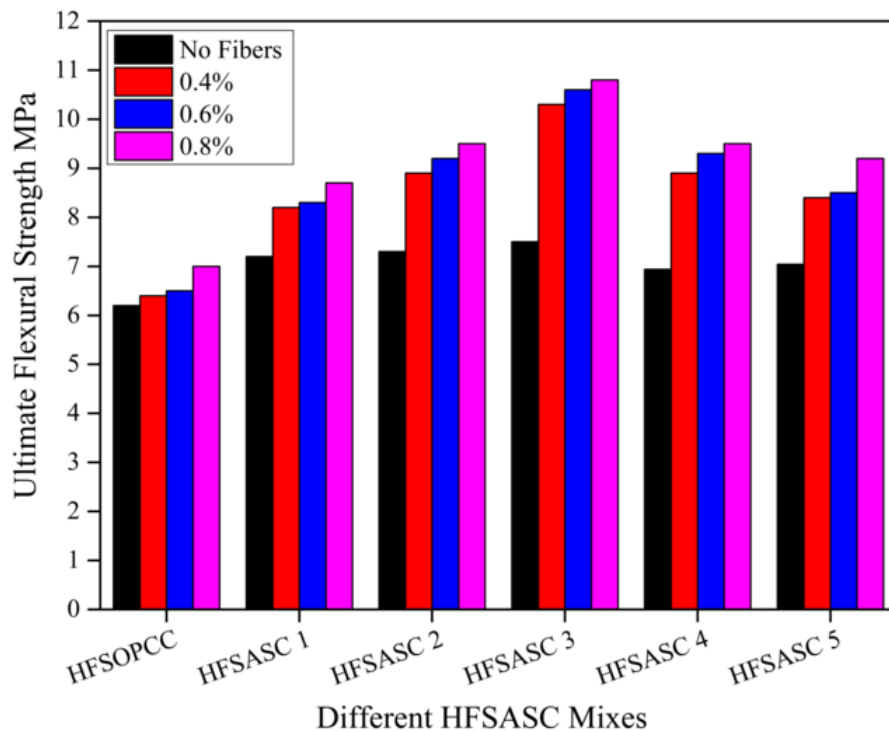


**Fig 7.11 Ultimate Flexural Strength (28-days) of different steel fiber reinforced mixes**

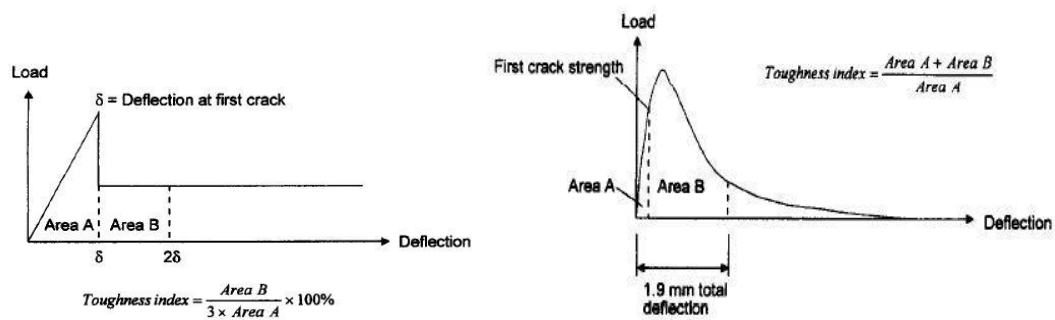


**Fig. 7.12 Evaluation of Toughness Index - $T_{BH2}$  (Barr and Hasso) and  $T_{ACI}$  (ACI) (Taylor et al. 1997)**

Thus, the accurate measurement of the area under load-deflection curves, obtained during testing of beam-specimens, is a very important factor that affects the accuracy of calculation of various toughness indices for that concrete mix. In the present

investigation, trapezoidal method is used for the measurement of areas under the load-deflection plots obtained in the flexure tests.

In Table 7.5, details calculations made for evaluation toughness indices, with increasing steel fiber content, for OPC-based reference concrete mixes, using both the method – one due to Barr and HASSO ( $T_{BH2}$ ) and the other recommended by ACI ( $T_{ACI}$ ). It can be clearly observed that increase in steel fibers, leads to corresponding increases in both the toughness indices for these fiber-reinforced self-compacting OPC-based concrete mixes.

Similar procedure was followed for determining the relevant areas under the load-deflection curves and computing the toughness indices for all the individual beam specimens of the five candidate HFSASC mixes, with increasing fiber contents. The average values of the two chosen toughness indices of all the five candidate HFSASC mixes are tabulated in Table 7.6. Variations of toughness indices calculated based on either of the methods (Barr and Hasso Method and ACI method) are shown in Fig 7.13 and 7.14 (average values plotted)

It is also clearly observed that there are substantial increases in the areas under the load-deflection curves with the increase in the percentage of steel fibers, leading to higher toughness indices, by either of the method, for all the HFSASC mixes also. In fact, the toughness indices for each of the HFSASC mixes are higher than those of fiber-reinforced OPC-based reference concrete mixes, with similar steel fiber contents. This can be attributed to the better bonding and hence improved crack-stitching by the steel fibers within the alkali activated slag matrix showing a better post-cracking behaviour of all the steel fiber reinforced mixes.

Again, amongst the five candidate mixes, the mix HFSASC-3 has exhibited the best energy-absorption capabilities in that they have recorded the maximum toughness indices at each of the fiber content. The  $T_{BH2}$  and  $T_{ACI}$  indices for HFSASC-3 are respectively 1.35 and 1.6 times of the values of the corresponding control OPC-based concrete mixes. Thus it can be said that the toughness performance of HFSASC mixes, with steel fibers incorporated them, are quite satisfactory from a practical application point of view.

**Table 7.5 Calculation of Toughness indices for HFSOPC-based control concrete mixes**

<b>MIX</b>	<b>SPECI - MEN</b>	<b>A<sub>c</sub><sup>δ</sup> (kN-mm)</b>	<b>A<sub>2c</sub><sup>δ</sup> (kN-mm)</b>	<b>T<sub>BH2</sub></b>	<b>A<sub>1.9 mm</sub> (kN-mm)</b>	<b>T<sub>ACI</sub></b>
HFSOPCC - 0.4	1	9.45	19.14	34.2	41.10	4.35
	2	8.6	20.11	44.6	46.48	5.4
	3	9.85	21.25	38.5	32.30	3.28
	4	9.39	20.9	40.85	45.0	4.8
	5	11.7	23.8	34.5	37.5	3.21
	<b>Avg.</b>			<b>38.5</b>		<b>4.2</b>
HFSOPCC - 0.6	1	11.6	22.85	32.3	34.0	2.93
	2	6.77	15.0	55.0	28.6	4.22
	3	4.5	12.3	58	31.0	6.90
	4	3.76	10.17	57	30.50	8.11
	5	9.64	17.35	27	30.07	3.12
	<b>Avg.</b>			<b>46.0</b>		<b>5.0</b>
HFSOPCC - 0.8	1	4.0	9.325	44.4	24.9	6.22
	2	8.59	20.63	46.7	34.40	4.0
	3	3.25	8.82	57.0	22.97	7.0
	4	4.65	12.19	54	28.6	6.15
	5	4.15	8.8	37.5	27.0	6.5
	<b>Avg.</b>			<b>48.0</b>		<b>6.0</b>

**Table 7.6 Toughness Indices of HFSASC Mixes**

Mix Designation	Toughness Index	
	T <sub>BH2</sub>	T <sub>ACI</sub>
HFSOPCC – 0.4	39	4.2
HFSOPCC – 0.6	46	5.0
HFSOPCC – 0.8	48	6.0
HFSASC 1 - 0.4	46	6.7
HFSASC 1 - 0.6	52	7.2
HFSASC 1 - 0.8	59	8.2
HFSASC 2 - 0.4	47	6.8
HFSASC 2 - 0.6	57	7.4
HFSASC 2 - 0.8	68	8.4
<b>HFSASC 3 – 0.4</b>	<b>50</b>	<b>7.6</b>
<b>HFSASC 3 – 0.6</b>	<b>59</b>	<b>7.7</b>
<b>HFSASC 3 – 0.8</b>	<b>71</b>	<b>9.1</b>
HFSASC 4 – 0.4	46	7.0
HFSASC 4 – 0.6	55	7.3
HFSASC 4 – 0.8	61	8.0
HFSASC 5 – 0.4	43	6.6
HFSASC 5 – 0.6	50	7.0
HFSASC 5 – 0.8	56	7.5

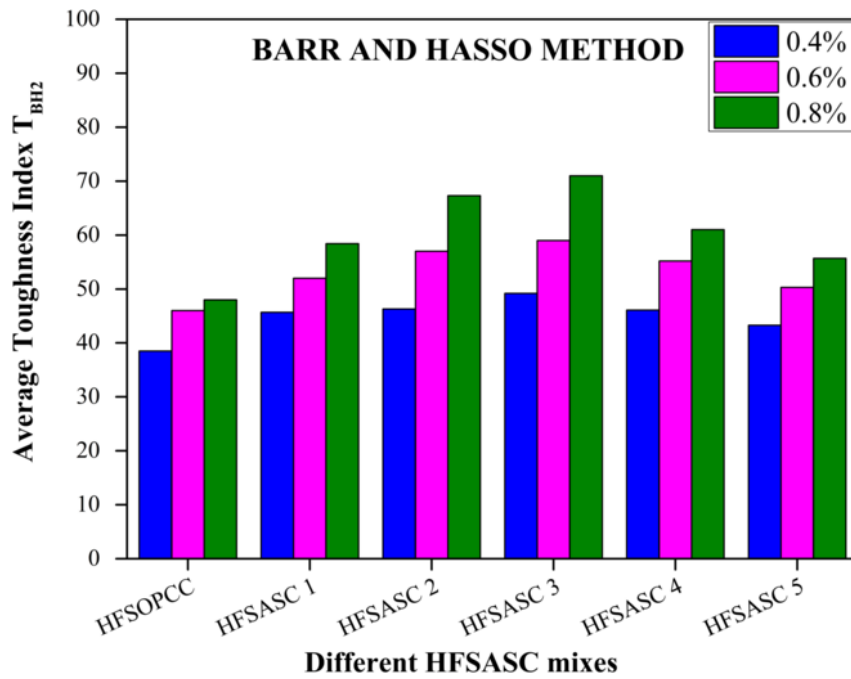


Fig 7.13 Toughness indices of HFSASC Mixes – Barr and Hasso Method

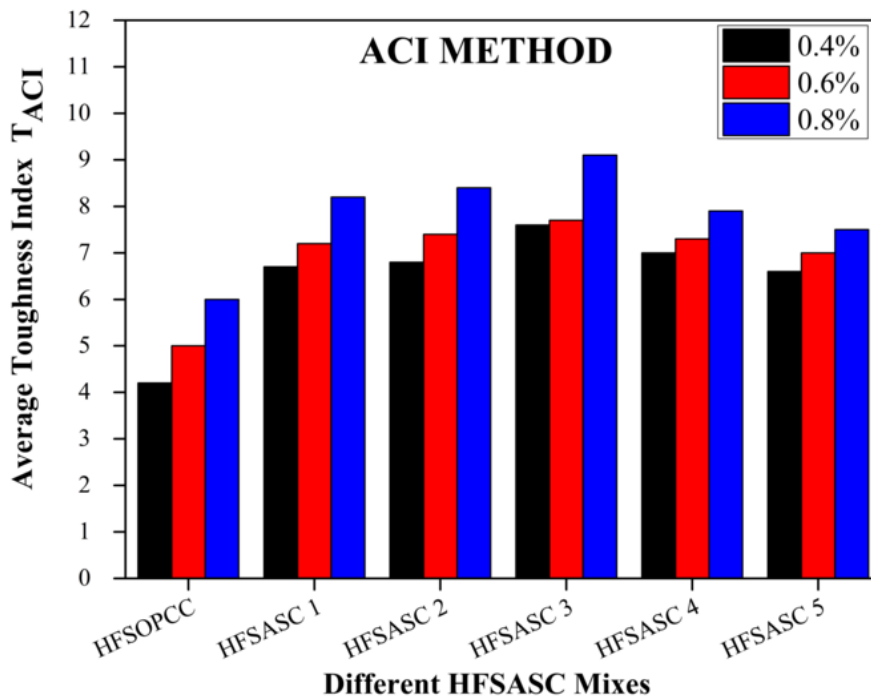


Fig 7.14 Toughness indices of HFSASC Mixes – ACI Method

## 7.8 SUMMARY

Addition of steel fibers to high performance alkali activated slag concrete mixes has been shown to marginally increase the compressive strengths (at both early 3-days as well as at 28-days). The ultimate flexural strengths of all the candidate mixes, however, were observed to increase for the various mixes tested herein. Increase in the percentage of steel fibers has shown to increase the toughness indices of all the candidate mixes tested herein. HFSASC-3 mix exhibited the best toughness performance as indicated by the larger values of the toughness indices computed by both of Barr and Hasso ( $T_{BH2}$ ) and ACI ( $T_{ACI}$ ) methods.

In general, High performance alkali activated slag concrete mixes reinforced with steel fibers showed an increase in compressive strength toughness characteristics, as compared with OPC-based reference concrete mixes; hence can be used as substitution for steel fiber reinforced high performance – OPC based concrete mixes in actual site conditions.

.....

# **CHAPTER 8**

## **FLEXURAL BEHAVIOUR OF REINFORCED HIGH PERFORMANCE ALKALI ACTIVATED SLAG CONCRETE BEAMS**

### **8.1 GENERAL**

All Portland cement-based matrices are quite weak in tension (as compared to compression), and hence in all structural components, appropriately designed steel reinforcement is required to be provided to resist the tensile stresses. Thus, providing steel reinforcement is very essential in most of structures. The efficiency of any structural component then depends on the realization of a perfect bond between the concrete and the steel rebars. Increased application of AASC in structures would thus require the demonstration of existence of such bond between steel rebars and concrete matrix and hence good structural performances of beams and columns made of AASC mixes. Such an evaluation of the flexural behaviour of reinforced HPAASC beams in comparison to that of a conventional reinforced HSS-OPC-based concrete beam is hence necessary and the same is attempted as detailed in this chapter.

### **8.2 EXPERIMENTAL DETAILS**

In the present phase of experiments, the same five mixes that were considered for detailed durability studies as discussed in (Chapter 5) and study of performance under elevated temperatures (Chapter 6), based on their higher performances in terms of their flow ability properties and strengths (Chapter 4), were again taken, as candidate mixes, for a detailed study on evaluation of the flexural performances of reinforced beams made with them. They are mixes HPAASC-3, HPAASC-5, HPAASC-7, HPAASC-10 and HPAASC-15. Twelve reinforced concrete beams, two with each of the five HPAASC mixes and also with the one OPC-based reference concrete mix, were designed as simply supported, under-reinforced sections with adequate shear reinforcement so as to prevent the failure in shear. The beams were tested under conventional third point loading test. The 28-days strengths obtained were considered as the strength of the concrete mixes, in all theoretical calculations. Two different sizes

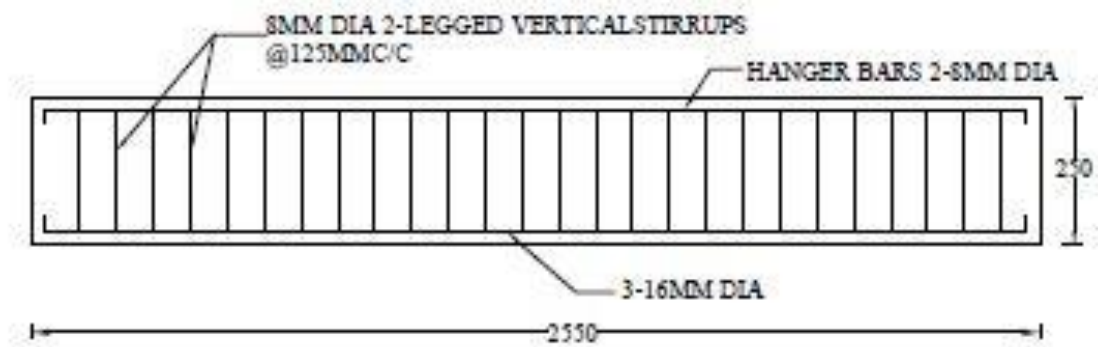
of deformed steel bars were used as the longitudinal and shear reinforcement while casting reinforced concrete beam specimens. Samples of steel bars were tested in the laboratory and the results are shown in Table 8.1. Tensile reinforcement at approximately 1.609% in the form of three 16mm diameter bars, corresponding to under reinforced sections was used in each of the beams tested. In all the beams, shear reinforcement was provided in the form of 2-legged, 8mm stirrups, spaced at a uniform spacing of 125 mm c/c throughout the span. Two hanger bars of 8mm diameter were provided in the compression side to support the stirrups as shown in Fig 8.1.

**Table 8.1 Properties of steel reinforcement bars used**

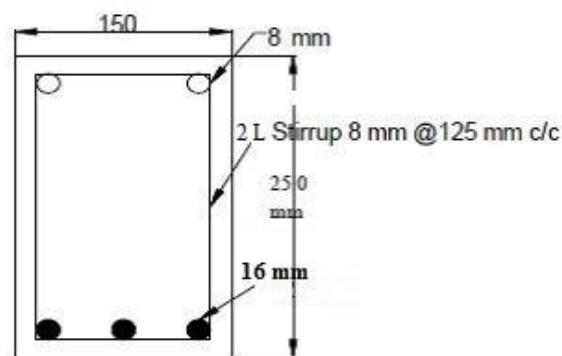
<b>Steel For</b>	<b>Diameter (mm)</b>	<b>Nominal Area (mm<sup>2</sup>)</b>	<b>Yield Strength (MPa)</b>	<b>Ultimate Strength (MPa)</b>
Longitudinal Reinforcement	8	50.26	516	580
Shear Reinforcement	16	201.2	520	595

### 8.2.1 Casting of the Beam Specimens

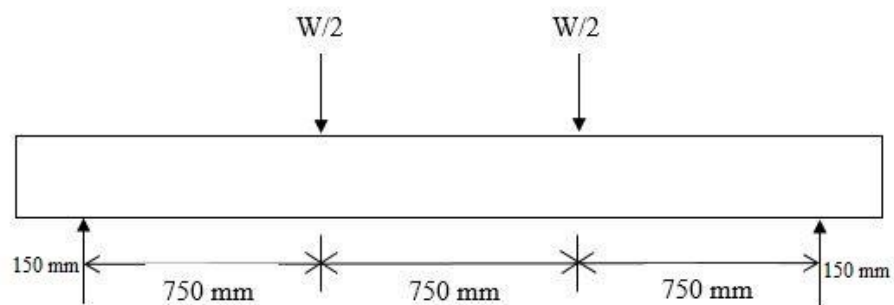
To facilitate easy de-moulding, rigid, strong wooden beam forms of size 150 mm x 250 mm x 2550 mm were fabricated for casting the reinforced AAS/OPC concrete beams. They were coated with lubricating oil on their inner surfaces. A constant clear cover of 25 mm was maintained to the individual reinforcement bars using cover blocks (mortar) at regular intervals. On these cover blocks, the reinforcement cage was placed (Fig 8.2). To maintain uniform holding of the cover blocks along the sides of the reinforcements, cover blocks were tied at regular intervals to the stirrups along the longitudinal direction. The mixing of concrete was done in three batches and poured into the moulds in three layers. Each beam was provided with two hooks at equal distance from the ends, to facilitate in easy lifting and transportation. All the beams were demoulded after 24-hours of casting.



(a)



(b)



(c)

**Fig 8.1 Reinforcement details provided, and the loading arrangements for testing the RC beam**

While the beams of HPAASC mixes were cured under the ambient laboratory condition, the reference OPC-based concrete beams were cured by wrapping them with wet gunny bags and spraying water at regular intervals till the completion of 28- days of curing. Companion cube specimens (100 mm-size) were also simultaneously cast, along with the beams, with each of the High performance alkali activated slag concrete

(HPAASC) and ordinary Portland cement concrete (OPCC) mixes and were cured, as appropriate, for 28-days, for ascertaining the cube compressive strengths of the respective mixes used in the reinforced concrete beams. These cubes were also tested, in a compression testing machine (2000 kN capacity), as per IS 516-1999, just before testing the respective beams on the 28-day of curing.



**Fig 8.2 Formwork and reinforcement cage used for casting the beam specimens**

### **8.2.2 Setup for testing the reinforced AAS beams**

The surfaces of the beams were cleaned and white washed with a thin coat to facilitate easy detection of cracks and the propagation of cracks. The beam specimens were tested on a loading frame of 200 kN capacity (Fig.8.3). The beams were supported on steel rollers with plates on both ends. The span and loading scheme remained the same for all the beams. Loading was applied to the beam through a 500 kN-capacity, hand-operated hydraulic jack.

Two point-loading was applied on the test beam using a load-spreader beam and was measured using a proving ring. The hydraulic jack was placed over the center of spreader beam such that there was no eccentricity of the load. The deflections of the beams were measured on the bottom face, both at mid-span, (using a dial gauge with a magnetic base), and at the loading points of the beam using two linear variable differential transformers (LVDTs) having a least count of 0.01 mm (Fig 8.3 and 8.4). Before application of loading that is at no-load stage initial readings of all the dial gauges (LVDTs) were noted. Using the hand-operated pneumatic jack, the load was gradually applied on the beam in small increments. Deflection measurements were made at these regular load intervals. At each load increment, the appearance of any fresh crack and the propagation of old cracks were closely monitored and clearly marked.



**Fig 8.3 Experimental setup for the testing the beams**



**Fig 8.4 LVDTs along with the data acquisition system**

Similarly, the strains in the central constant bending moment section of the beam were measured using a mechanical strain gauge (Demec gauge) with a gauge length of 200 mm. In order to measure such strains, a reference line was marked, along the depth, exactly at the midspan. Two more lines were marked on either side of the reference line at a distance of 100mm each. The concrete surface was well cleaned all along these lines and Araldite-gelue was applied on this cleaned surface. The Demec buttons were now fixed at distances of 10 mm, 45 mm, 85 mm, 125 mm, 165 mm, 205 mm and 240 mm from the top of the beam, along both the lines. They were allowed to dry for 24 hours before the actual testing was started. During the testing of the beam, strains were measured between pairs of such Demec points at same depth, which were 200 mm apart.

Thus the flexural behaviours of HPAASC and OPC-based reference concrete beams under monotonically increasing load are evaluated in terms of loads at first crack, ultimate load, strain-distributions, load-deflection characteristics and also their ductility values etc., as per the provision of IS 456-2000. Moment-curvature relations are derived for all the beams and the development of cracks in the beams under higher loads also is studied. These measurements were made by taking the average of two beams from each of the respective mixes. The crack widths were measured using a crack measuring microscope (Elcometer). The propagation of the cracks with each load-increment was also marked on the test specimens till the completion of test. After failure,

the crack patterns were sketched using a marker pen with the respective load levels also marked. A photograph of the final crack-patterns in each of the beam was also taken. Further the numbers of cracks obtained in flexural zone as well as shear zone were noted down.

### **8.3 FLEXURAL BEHAVIOUR OF REINFORCED HPAASC BEAMS**

#### **8.3.1 Load at First Crack and Ultimate Loads**

The theoretical loads at first crack and ultimate loads for all the beams were calculated as per IS 456:2000 without using any partial safety factor for the materials of concrete and reinforcing steel (Appendix III). These theoretical loads were computed based on the compressive strength values, obtained for the HPAASC mixes (in the range of 81.3MPa – 87.3 MPa) and a value of 75.3 MPa for the OPCC reference mix, at the time of testing the respective beams. Such computed theoretical loads, both at first- crack stage and at ultimate stage are shown in Table 8.2, along with experimentally obtained values. From Table 8.2, it can be observed that very marginally higher first-crack loads have been recorded in tests in case of all the HPAASC beams, as compared to the beam with control OPCC reference mix, in line with their higher compressive strengths. Further the experimental ultimate loads for all the reinforced concrete beams are higher as compared to their own theoretical loads, as expected, in case of all the RCC beams. The ultimate load carrying capacities of all the HPAASC beams, again, are marginally higher than that of the control OPCC-based reference mix, suggesting a comparable performance of these mixes in structural elements.

#### **8.3.2 Deflection at First Crack and Ultimate Loads**

The structural response of HPAASC beams along with control reference HSS-OPCC beam is evaluated with respect to the load-deflection behaviour under flexure. During the tests, deflections were measured at mid span and at load point at all the increments of loads. The measured mid-span deflections with increasing loads are plotted by taking the average of two beams of each of the HSS-OPCC and HPAASC mixes as shown in Fig 8.5. The theoretical deflections for both first crack as well as ultimate loads are also calculated at the mid span as per the standard equation and are tabulated as shown in

Table 8.3. The experimental deflections for the first crack and ultimate load are about 2.0 – 2.5 times higher than the theoretical deflections values as shown in Table 8.3. The changes in the load-deflection are very clearly representing the different events occurred for any standard reinforced concrete member under flexure. The first crack load occurred at the range of 31kN – 35.5kN for all the reinforced beams tested herein during which the first visible crack were observed, which was measured using crack measuring microscope. Further with the increase in the load, for all the HPAASC beams along with reference OPCC beams, the linearity of response continued even upto a load of 130kN.

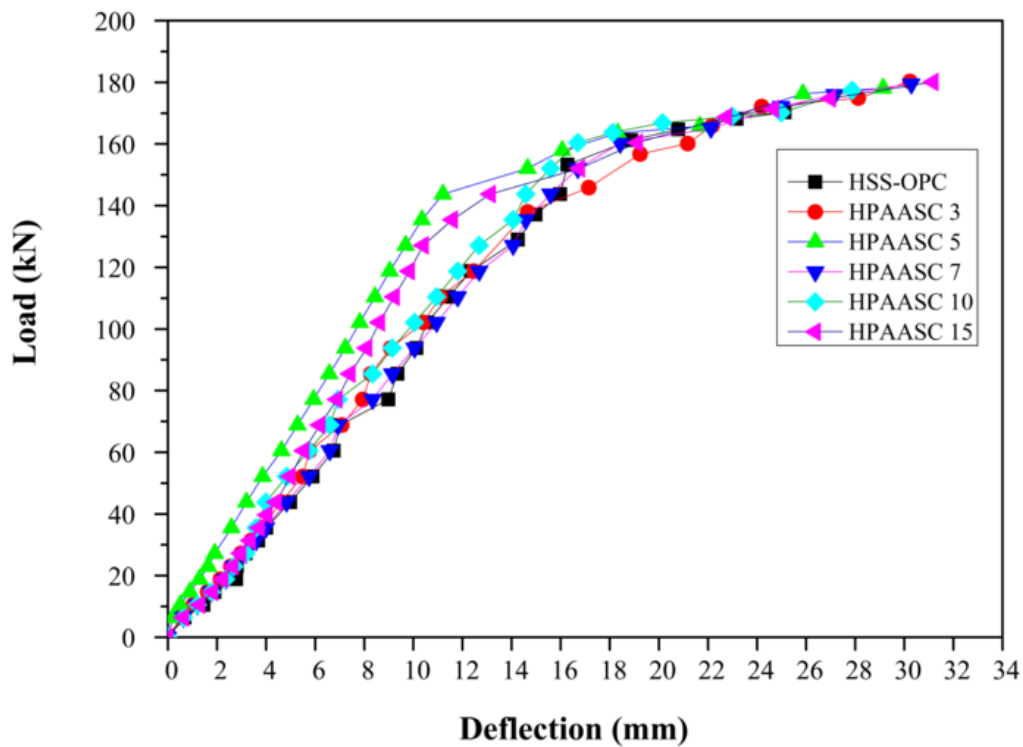


**Fig 8.5 Mid span deflections for reinforced HSS-OPCC and HPAASC beams**

**Table 8.2 Load at first crack and ultimate load for HSS-OPCC and HPAASC**

Beam type	28-day Compressive Strength	Load at first crack		Ultimate load	
	Experimental (MPa)	Theoretical (kN)	Experimental (kN)	Theoretical (kN)	Experimental (kN)
HSS-OPCC	75.3	25.9	27.2	156.6	170.3
HPAASC-3	82.0	28.4	31.4	159.1	180.3
HPAASC-5	83.7	29.0	35.6	159.5	178.2
HPAASC-7	87.3	29.5	31.5	150.3	179.5
HPAASC-10	82.2	27.3	35.4	158.5	177.4
HPAASC-15	81.3	27.8	31.7	158.7	180.1

**Table 8.3 Mid span deflections at first crack and ultimate load**

Beam type	Deflection at first crack		Deflection at ultimate load	
	Theoretical (mm)	Experimental (mm)	Theoretical (mm)	Experimental (mm)
HSS-OPCC	1.39	3.0	14.8	25.2
HPAASC-3	1.36	3.4	13.5	30.3
HPAASC-5	1.37	3.2	13.4	29.1
HPAASC-7	1.29	3.7	12.5	30.3
HPAASC-10	1.33	3.6	13.7	27.9
HPAASC-15	1.34	3.4	13.6	31.2

### 8.3.3 Span Deflection profiles

Deflection profiles along the span are plotted in Fig 8.6 and 8.7 for the entire HSS-OPCC beam and the HPAASC beams, at two representative load levels i.e., load at first-crack and ultimate load. Near failure load, the beams deflected significantly, thus indicating that the tensile steel to have yielded. At the ultimate load of the beams, the concrete in the compression zone started getting slowly cracked, without showing any spalling behaviour. While the experimental mid-span deflection value at first crack load is 2.15 times the theoretical deflection in OPCC beam, such deflections are 2.5, 2.33, 2.87, 2.70 and 2.54 times the theoretical values for reinforced beams of HPAASC mixes -3, -5, -7, -10 and -15 mixes respectively.

Similarly at their ultimate loads, the experimental mid-span deflections are similar at an average 1.7, 2.24, 2.17, 2.4, 2.0 and 2.29 times their theoretical values for the OPCC beam and the five HPAASC beams respectively. Again, at ultimate loads, the magnitude of measured deflections of HPAASC is comparatively in the range of higher at 1.10 – 1.24 times the deflection of the OPCC beam respectively (Table 8.3).

The load that is responsible for causing the change in the elastic response of the load-deflection curve is considered as the yield load. Further the non-linear portion occurred beyond a load ranging between (135.5 – 152.1 kN) and continued upto the ultimate load

for all the reinforced concrete beams. In order to check the ductility characteristics of all the reinforced concrete beams tested herein, ductility values were calculated as the ratio of the deflection value corresponding to the ultimate load ( $\Delta_u$ ) to the deflection value corresponding to the yield load ( $\Delta_y$ ) as shown in Table 8.4.

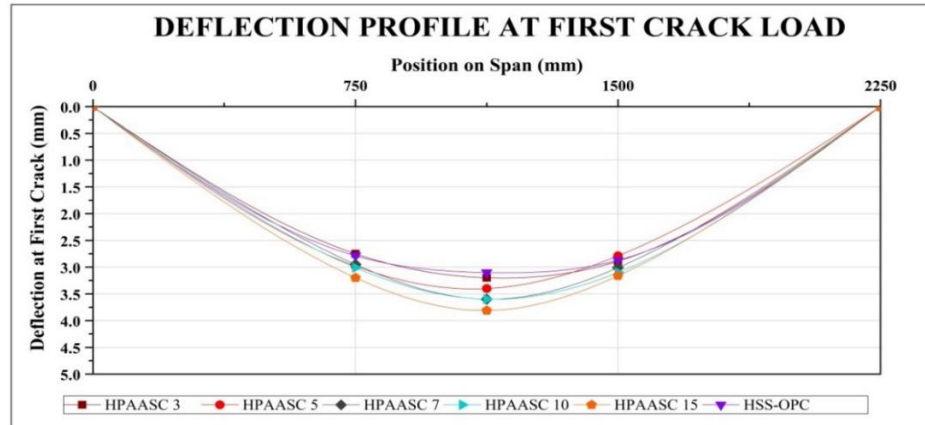


**Fig 8.6 Deflection profile of beams at first crack loads**

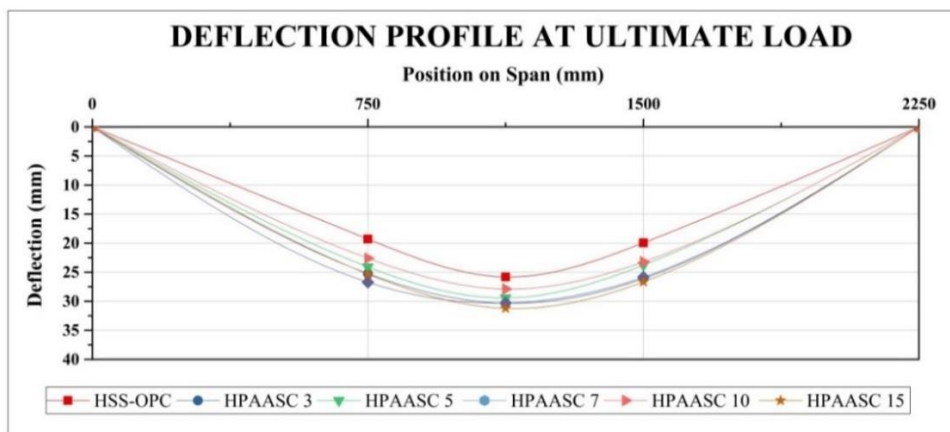


**Fig 8.7 Deflection profile of beams at ultimate loads**

The ductility ratios of all the HPAASC beams shows a higher values in the range of (1.8–2.7) as compared to the control HSS-OPCC beam (ductility value = 1.6). The increased ductility values clearly indicate the higher ability of the member to absorb more energy without causing any increase in the critical failure (Kathirvel and Kaliyaperumal 2016).

**Table 8.4 Ductility values of all the HPAASC beams**

<b>MIX ID</b>	<b>Yield Load (kN)</b>	<b>Deflection at yield (<math>\Delta_y</math>) (mm)</b>	<b>Ultimate Load (kN)</b>	<b>Ultimate Deflection (<math>\Delta_u</math>) (mm)</b>	<b>Ductility Ratio <math>\Delta_u/\Delta_y</math></b>
HSS-OPCC	143.8	16.0	170.3	25.1	1.6
HPAASC-3	138.0	14.7	180.3	30.2	2.0
HPAASC-5	143.7	11.2	178.1	29.2	2.6
HPAASC-7	143.8	16.0	179.5	30.3	1.9
HPAASC-10	152.1	15.6	177.4	27.9	1.8
HPAASC-15	135.5	11.6	180.1	31.2	2.7

Hence, all the HPAASC beams have shown better performance as compared to control HSS-OPCC beams in terms of their ductility behaviour. Further, the deflections (ranging between 27mm – 31mm) for all the HPAASC-beams, at ultimate loads, as compared with the ultimate deflection (25.2 mm) of HSS-OPCC beam also prove better ductility characteristics of all the HPAASC beams. The slightly higher ultimate deflection values obtained for all HPAASC beams also relatively indicates a lower stiffness of all these HPAASC beams as compared to the control HSS-OPCC beam tested herein.

#### **8.4 MOMENT CURVATURE RELATIONS FOR HPAASC MIXES**

A study of moment-curvature relations of RCC beams assists in evaluating the rotation capacities of the beams and helps in assessing the capacity of the structure to redistribute the bending moments after yielding. The ultimate moments and corresponding curvatures of all the reinforced HSS-OPCC beam and HPAASC beams are computed based on the test results and are tabulated in Table 8.5.

Variation of curvatures in the central sections of the test beams, with increasing magnitude of the bending moments, are shown in Fig 8.8. In these moment-curvature plots, during the initial phase of loading, with both the concrete and steel being linearly elastic in the uncracked section, a linear steep slope can be appreciated.

**Table 8.5 Ultimate moment and curvatures for HSS-OPCC and HPAASC beams**

Sl. No	Beam Type	Ultimate moment (kN-m)	Ultimate curvature ( $\times 10^{-6}$ radians/mm)
1	HSS-OPCC	57.7	70.5
2	HPAASC -3	66.4	81.8
3	HPAASC -5	60.1	88.8
4	HPAASC -7	65.2	95.6
5	HPAASC -10	64.1	93.3
6	HPAASC -15	63.9	78.5

As the load increases, concrete cracks in the tension region, (now the section is termed as cracked RC section), the cracking moment being observed in the range of 52.5 – 57.5 kN-m as observed in Fig 8.8 for all the reinforced concrete mixes tested herein. In case of reinforced HSS-OPCC mix, after a moment of 52.5kN-m, yielding of the steel bars has occurred, later showing a constant moment with further increase in curvature measured upto to maximum of  $70.5 \times 10^{-6}$  radians/mm; this region is termed as inelastic region.

However the moment carrying capacities of all the HPAASC mixes further increase, in the range of 55-65 kN-m, with a slightly non- linear behaviour with curvature, in the cracked section wherein both the materials are possibly in semi-linear elastic region. Later, the moment carrying capacity for all the HPAASC mixes remains almost constant over larger increases in curvature, falling under inelastic response behaviour of RCC members, wherein both concrete and steel are in inelastic region. Further the ultimate moment carrying capacities for all the HPAASC mixes were in the range of 60.1 – 66.4 kN-m. It can be observed that, both the ultimate moment carrying capacities and the ultimate curvatures of all the reinforced HPAASC beams were found to be higher as compared to their values for the control reinforced HSS-OPCC beam.

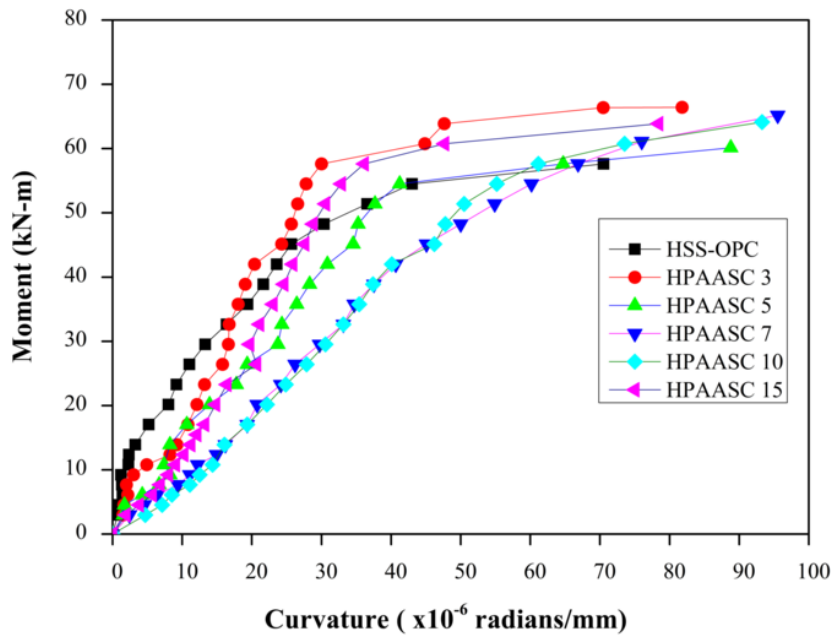


**Fig 8.8 Moment curvature relations for the test beams**

### 8.5 STRAIN VARIATIONS FOR HPAASC MIXES

Testing of RC beams herein also included the measurement of longitudinal strains through the thickness at mid-span section. The variation of the strains, as measured using a Demec gauge, across the midspan section at increasing load levels, for the reinforced concrete beams of HSS-OPCC mix and all the five HPAASC mixes are shown in Fig 8.9(a-f). The basic idea of these strain plots is to observe the patterns of strain-variations across the depth of the beam and the changes in the position of the neutral axis (NA), in the beams of different mixes, with increase in the applied load. In general, for RC members, the neutral axis always tends to moves towards the region which is relatively stiffer within the cross-section. To be more precise, the neutral axis moves towards the concrete region for under-reinforced sections and towards tensile steel for over-reinforced sections. It can be observed that, in general, as the load on the beam was increased (thus accounting for increased bending moment at any section), the neutral axis moved towards the top compression fiber in all the reinforced beams, thus complying with the theoretical understanding of under-reinforced sections. Again, the strain-distributions tended to be slightly non-linear at higher loads nearer to ultimate

loads, in some beams. It can also be appreciated that, in some cases, the maximum surface tensile strains in concrete (measured near the bottom surface) were much larger than the corresponding compressive strains measured near the top edge, essentially due to presence of rebars. Further increased ductility of all the reinforced HPAASC beams is also justified through the increased values of strain at both extreme fibers.

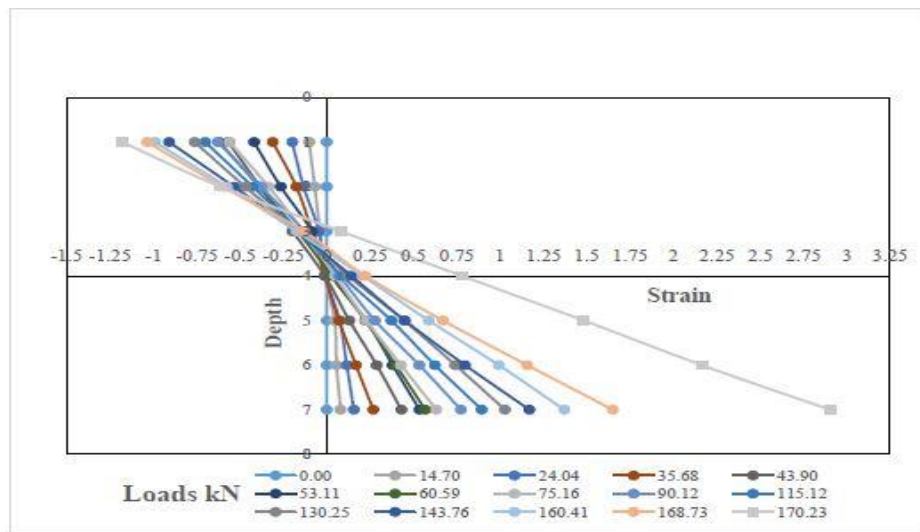


**Fig 8.9(a) Variation of Strains for HSS-OPCC mix**

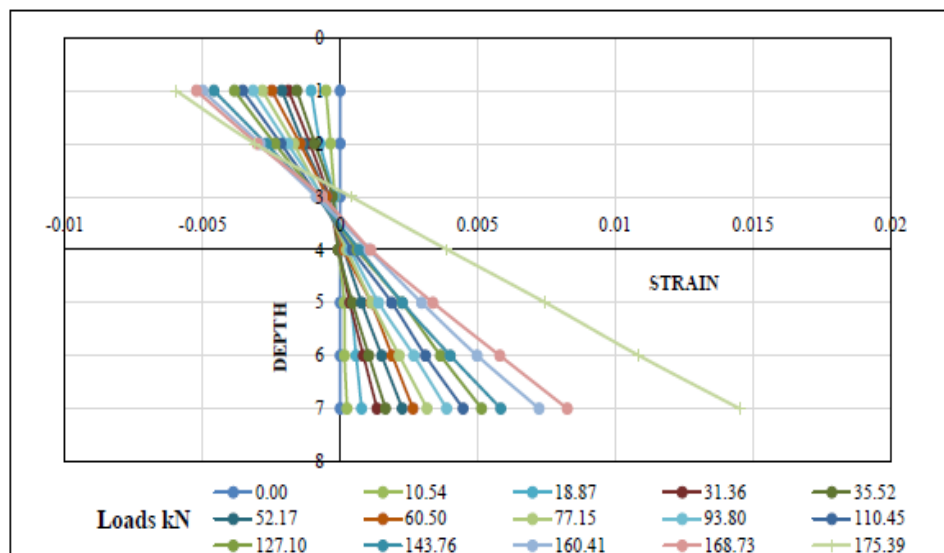


**Fig 8.9(b) Variation of Strains for mix HPAASC-3**

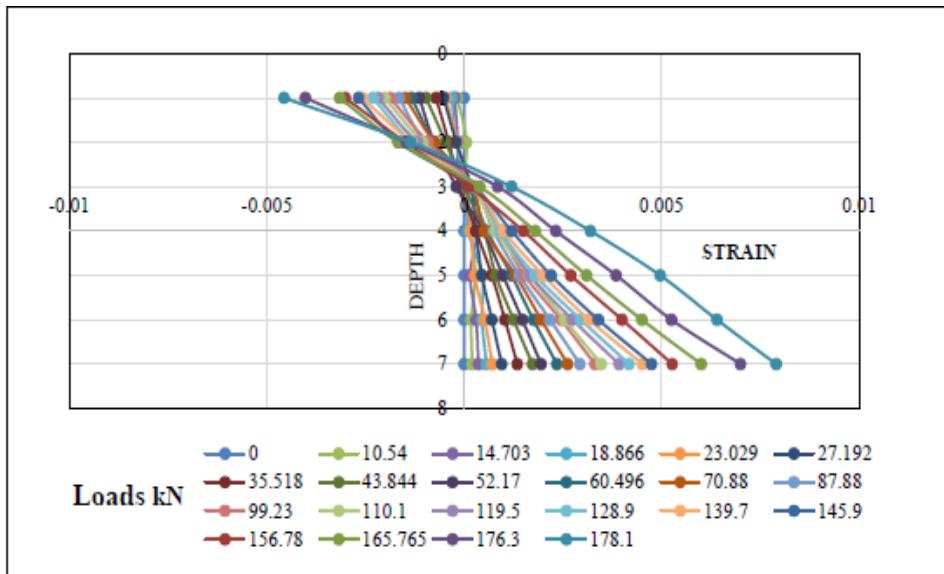


**Fig 8.9(c) Variation of Strains for mix HPAASC-5**

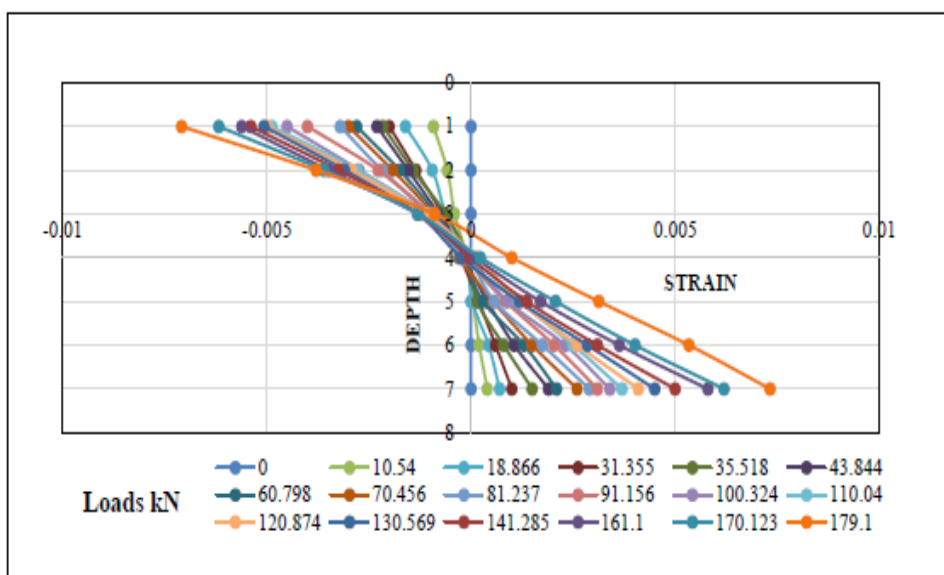


**Fig 8.9(d) Variation of Strains for mix HPAASC-7**

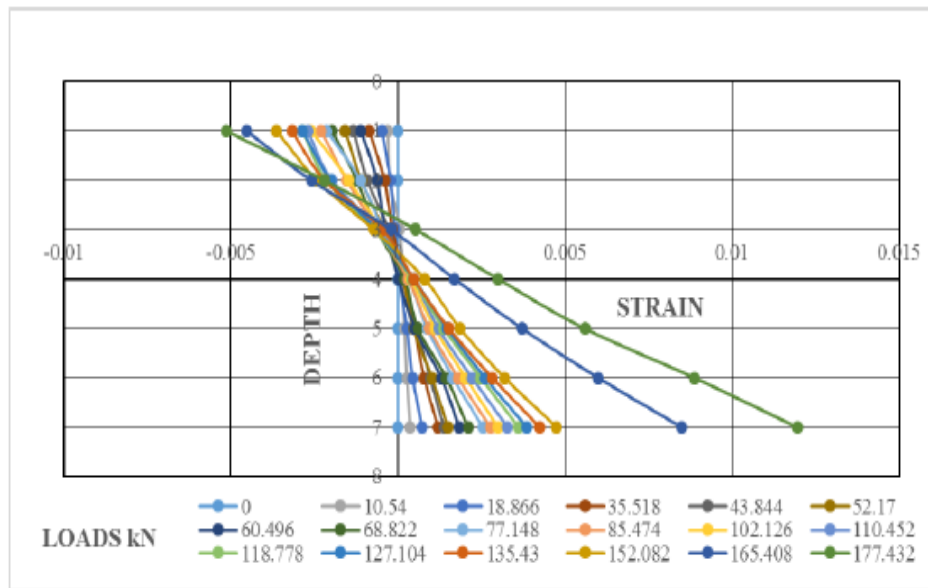


**Fig 8.9(e) Variation of Strains for mix HPAASC-10**

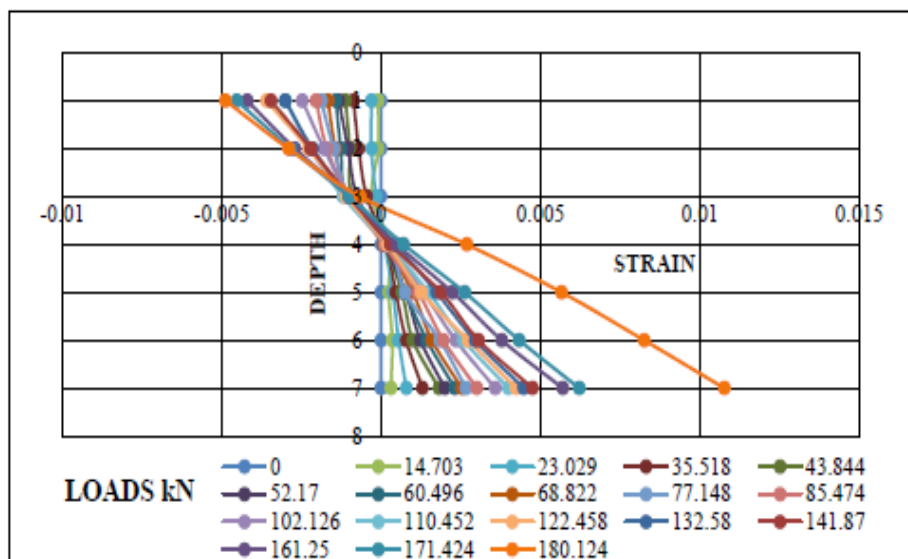


**Fig 8.9(f) Variation of Strains for mix HPAASC-15**

## 8.6 CRACK PATTERNS

As expected flexural cracks got initiated in the pure bending zone for all the HPAASC and HSS-OPCC beams. As the load was increased, existing cracks propagated and new cracks got developed along the span. The flexural cracks developed in different

HPAASC beams and the HSS-OPCC beam in the shear zone turned into inclined cracks due to the effect of shear force. The numbers of cracks in the flexural zone and shear zones, total number of cracks, maximum width of first crack at ultimate load are tabulated as shown in Table 8.6. The number of cracks at ultimate load in the flexural zone and shear zones of HPAASC beams are almost similar to that of the HSS-OPCC beam. The cracks at the mid-span opened widely near failure. The width of the widened first crack at ultimate load is slightly higher for HPAASC beams as compared to the HSS-OPCC beam. From Fig 8.10, it can be seen that the final crack-patterns of all the HPAASC beams are very much similar to control HSS-OPCC beam.

**Table 8.6 Test Results of the crack profiles**

<b>Beam Designation</b>	<b>Total no. of cracks</b>	<b>No. of cracks in flexural zone</b>	<b>No. of cracks in shear zones</b>	<b>Width of first crack (mm)</b>	<b>Width of first crack at ultimate load (mm)</b>
HSS-OPCC	24	9	15	0.02	0.56
HPAASC -3	26	10	16	0.10	0.70
HPAASC -5	25	11	14	0.02	1.01
HPAASC -7	27	11	16	0.04	0.76
HPAASC -10	25	10	15	0.06	1.05
HPAASC -15	26	10	16	0.02	1.02

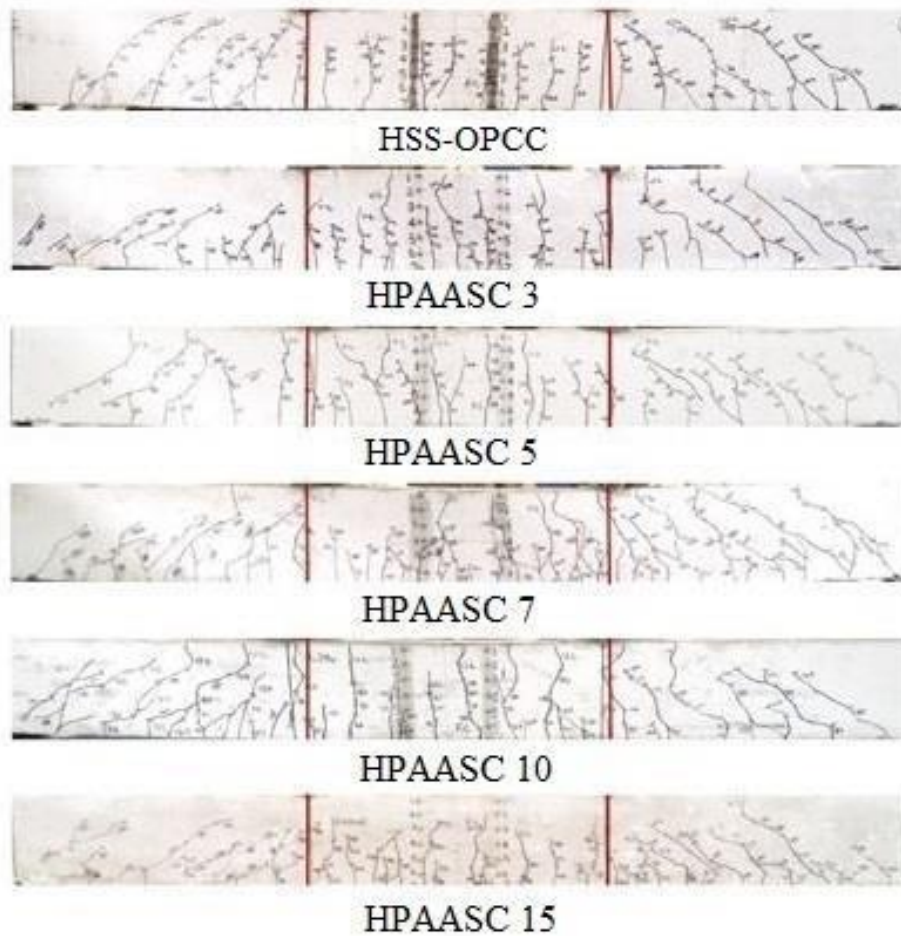


**Fig 8.10 Crack Patterns for all the test beams**

### **8.7 SUMMARY**

Summing up it is possible to obtain to comparable flexural responses in reinforced HPAASC beams produced with the maximum utilization of the industrial by-products both in terms of binders as well as aggregates, as obtained in case of HSS-OPC based concrete beams in terms of load or moment carrying capacity, ductility, stiffness (deflection or curvature), variation of strains at the extreme fibers and the cracking behaviour.

.....

## CHAPTER 9

### ECOLOGICAL ANALYSIS OF CONCRETE MIXES

#### 9.1 GENERAL

Cement is manufactured from a combination of naturally occurring minerals – calcium (60% by weight) mainly from limestone ( $\text{CaCO}_3$ ), silicon (20%), aluminium (10%), iron (10%) and small amounts of other ingredients and heated in a kiln to about  $1500^\circ\text{C}$  to get the clinker. The main sources of emission of  $\text{CO}_2$  herein is in the use of fossil fuels in the burning process and the calcination process where  $\text{CaCO}_3$  is broken down to calcium oxide, other sources being processes such as operation of mining equipment to extract the raw materials and transportation of the raw materials to the cement plant (NRMCA, 2008). Global  $\text{CO}_2$  emissions from cement production (377 million metric tons of carbon in 2007) represent 4.5% of global  $\text{CO}_2$  releases from fossil-fuel burning and cement production (Marland et al. 2007). Concrete uses about 7% to 15% cement by weight, average being around  $250\text{ kg/m}^3$  of concrete; with concrete density of  $2400\text{ kg/m}^3$ , about 100 to 300 kg of  $\text{CO}_2$  is embodied in concrete which amounts to 5% to 13% of the weight of concrete (Marceau et al. 2007). It is also estimated that 33% to 57% of the  $\text{CO}_2$  emitted from calcination will be reabsorbed through carbonation of concrete surfaces over a 100 -year life cycle (Pade et al. 2007). It is reported that building industry contributes 22% of  $\text{CO}_2$  emissions in the world (Reddy 2010).

Sustainable development in the context of the concrete industry may really mean utilising the available, non-renewable natural resources to the minimum possible extent and also using more and more of locally available alternate construction materials, which require lesser amounts of energy for their production. Some of these materials which are economically cheaper in cost, and are having a very low impact on the environmental credentials in terms of their own carbon footprints, are also capable of producing good quality binders both in terms of their mechanical strength properties as well as durability properties. Environmental impact of any of material is generally indicated in terms of the two major parameters namely, the Embodied energy and Embodied  $\text{CO}_2$  emission. The term Embodied energy (EE) is defined as the total energy required and the Embodied  $\text{CO}_2$  ( $\text{ECO}_{2e}$ ) is the total amount of carbon-di-oxide emitted

throughout the life cycle of a material i.e from its cradle to grave. In the present study, the Embodied energy (EE) and Embodied CO<sub>2</sub> (ECO<sub>2e</sub>) of all the concrete mixes are calculated by considering their production process from the point of extraction to the process of manufacturing. Towards these calculations, the values of the Embodied energy (EE) and Embodied CO<sub>2</sub> (ECO<sub>2e</sub>) for all the individual materials (on per kg basis) were selected, as per the sources as indicated in Table 9.1

**Table 9.1 Values for EE and ECO<sub>2e</sub> for all the materials used in concrete mixes**

<b>Ingredients</b>	<b>EE (MJ/kg)</b>	<b>ECO<sub>2e</sub> (kgCO<sub>2e</sub>/kg)</b>	<b>Reference</b>
<b>OPC</b>	<b>4.8</b>	<b>0.93</b>	<b>(Bhardwaj and Kumar, 2019)</b>
<b>GGBFS</b>	<b>0.31</b>	<b>0.052</b>	
<b>NaOH Flakes</b>	<b>8.75</b>	<b>0.76</b>	
<b>Liquid Sodium Silicate</b>	<b>5.37</b>	<b>0.71</b>	
<b>Water</b>	<b>0.2</b>	<b>0.0008</b>	
<b>Natural River Sand</b>	<b>0.081</b>	<b>0.0051</b>	
<b>Natural Granite chips – Jelly – 12.5mm downsize</b>	<b>0.083</b>	<b>0.0048</b>	
<b>HRWR Admixture</b>	<b>11.5</b>	<b>0.6</b>	
<b>Steel Slag Sand</b>	<b>0</b>	<b>0</b>	<b>Mithun and Narasimhan (2016)</b>
<b>Fine Quartz powder</b>	<b>0.920</b>	<b>0.0234</b>	<b>(Sheng et al. 2018)</b>
<b>Quartz Sand</b>	<b>0.850</b>	<b>0.020</b>	<b>(Chen et al. 2017)</b>
<b>EAF Slag</b>	<b>0</b>	<b>0</b>	<b>(Palankar et al. 2016)</b>
<b>Di-Basic Sodium Phosphate</b>	<b>5.80</b>	<b>0.3</b>	<b>(Angus chemical company, 2017)</b>

**Table 9.2 Total Embodied energy and Embodied CO<sub>2</sub> emitted for various concrete mixes**

Ingredients	Embodied Energy (MJ/m <sup>3</sup> )							Embodied CO <sub>2</sub> (kgCO <sub>2e</sub> /m <sup>3</sup> )						
	EE (MJ/kg)	OPCC	ASC3	ASC5	ASC7	ASC10	ASC15	ECO <sub>2e</sub> (kgCO <sub>2e</sub> /kg)	OPCC	ASC3	ASC5	ASC7	ASC10	ASC15
OPC	4.80	2592	-	-	-	-	-	0.9300	502.2	-	-	-	-	-
GGBFS	0.31	-	184.5	197.6	210.8	184.5	210.8	0.0520	-	30.90	33.15	35.40	30.90	35.40
Quartz powder	0.92	55.2	96.6	103.5	110.4	96.6	110.4	0.0234	1.40	2.50	2.60	2.80	2.46	2.80
NaOH Flakes	8.75	-	306.3	323.8	350	306.3	350	0.7600	-	26.60	28.10	30.40	26.60	30.40
Liquid Sodium Silicate	5.37	-	800.1	864.6	918.3	800.1	918.3	0.7100	-	105.80	114.30	121.40	105.80	121.40
Water	0.20	48	45.8	46.0	46.0	43.2	49.2	0.0008	0.19	0.18	0.18	0.18	0.17	0.197
Natural River Sand	0.08	54.9	-	-	-	-	-	0.0051	3.46	-	-	-	-	-
Natural – Jelly - 12.5mm	0.08	56.6	-	-	-	-	-	0.0048	3.28	-	-	-	-	-
Slag Sand	0.00	-	0.0	0.0	0.0	0.0	0.0	0.0000	-	0.00	0.00	0.00	0.00	0.00
Quartz Sand	0.85	192.1	145.35	135.1	125.8	142.8	114.8	0.0200	4.52	3.42	3.18	2.96	3.36	2.70
EAF Slag – 12.5mm	0.00	-	0.0	0.0	0.0	0.0	0.0	0.0000	-	0.00	0.00	0.00	0.00	0.00
HRWR Admixture	11.50	24.84	32.2	34.5	36.8	32.2	36.8	0.6000	1.3	1.68	1.80	1.92	1.68	1.92
Sodium Phosphate	5.80	-	40.6	43.5	46.4	40.6	46.4	0.3000	-	2.10	2.25	2.40	2.10	2.40
<b>TOTAL</b>		<b>3024</b>	<b>1651.5</b>	<b>1748.6</b>	<b>1845</b>	<b>1646.3</b>	<b>1836.7</b>		<b>516.3</b>	<b>173.2</b>	<b>185.6</b>	<b>197.5</b>	<b>173.1</b>	<b>197.3</b>

**NOTE:** ASC 3, ASC 5, ASC 7, ASC 10, ASC 15 refers to HPAASC 3, HPAASC 5, HPAASC 7, HPAASC 10 and HPAASC 15

The EEs of all the six concrete mixes including the five HPAASC mixes calculated in the range of 1646.3 (for HPAASC-10 mix) to 1844.5 MJ/m<sup>3</sup> (for HPAASC-7mix) (Table 9.2) are found to be lower by 39 - 45.6% as compared to that of the OPC - based reference concrete mix (3024 MJ/kg). Again, the embodied carbon dioxide emissions are much lower by 61.7 - 66.5% at 173.1 (for HPAASC-10 mix) to 197.5 kgCO<sub>2</sub>e/m<sup>3</sup> for (HPAASC-7 mix) as compared to 516.3 kgCO<sub>2</sub>e/m<sup>3</sup> for OPC-based control reference concrete mix.

.....

## **CHAPTER 10**

### **CONCLUSIONS**

#### **10.1 GENERAL**

The present thesis presents the detailed investigations carried out on the development of a new class of High Performance Alkali-activated Slag Concrete (HPAASC) mixes using finely ground blast furnace slag as the principal alumino-silicate source material, along fine quartz powder. This new class of mixes again attempted, incorporating slag sand and EAF slag, both by-products from the iron and steel industry, as fine and coarse aggregates respectively. These HPAASC mixes have been shown to exhibit superior flow ability, mechanical strengths and durability properties, with enhanced toughness characteristics. Detailed microstructural characterization of all the mixes developed herein, both in the regular service conditions as well as after getting exposed to severe acid-, and sulphate environments as well as elevated temperatures (upto 800<sup>0</sup>C) has been attempted, which has facilitated a better understanding of the different strength-degradation mechanisms. The representative mixes are also seen to exhibit better flexural performance when applied in structural elements by embedding steel rebars in them. It has been demonstrated that they have lower carbon foot prints as compared to control OPC-based high strength self-compacting concrete mixes. Thus the results from the investigations have confirmed that the HPAASC mixes can be developed more effectively with their possible applications in design of various structural concrete elements.

#### **A. Flow ability and Strength properties of HSAASC Mixes**

- A new class of high strength, self-compacting, alkali-activated slag concrete (HSAASC) mixes were successfully developed herein, incorporating slag sand and EAF slag, both by-products from the iron and steel industry, as fine and coarse aggregates respectively. While finely ground, blast furnace slag was used as the principal alumino-silicate source material in these mixes, fine amorphous quartz powder is also used additionally, for improved pore-filling

and pore-refinement effects. While all the mixes do, generally, satisfy the relevant EFNARC guidelines for self-compacting mixes, relatively higher binder contents cause a slight decrease in the flowability characteristics. This may be due to the increased yield stresses in the mixes due to the increase in the total amount of finer particles. Addition of small amounts of sodium phosphate, as an additive, has led to a construction-friendly increase in the initial setting times of all the HSAASC mixes tested herein from an initial-low of 15 minutes to a healthy 60 minutes or so.

- Use of increased binder contents in the range of 700 – 800 kg/m<sup>3</sup> has proved to be essential to develop the targeted strength levels in these HSAASC mixes as compared to control OPCC reference mix. Significant enhancements in mechanical strengths have been achieved in all the fifteen HSAASC candidate mixes tested herein with the desired levels of flow ability properties as compared to control OPC reference concrete mix.
- HSAASC mixes developed herein have shown higher compressive strengths ranging between 78 MPa – 90 MPa. Formation of more amounts of C-A-S-H gels due to the higher binder contents employed has possibly caused enhanced compressive strengths. It can also be additionally due to the effective pore-filling and pore-refinement effects provided by the reactive silica in the fine amorphous quartz powder used, dissolution with CaO present in GGBFS, leading to more C-A-S-H gels.
- The regression equations developed herein for the various strength parameters, at different ages, based on a statistical analysis of experimental results under Taguchis Design of experiments (DOE) approach, have exhibited very good predictive capabilities.
- HSAASC mixes developed herein have shown relatively higher moduli of elasticity (30.1 to 36.2 GPa), better split-tensile (5.1 to 6.0 MPa), and flexural strengths (6.5 to 7.5MPa) and decreased initial and saturated water absorption values ranging between 2.4% - 3.5%, as compared to the OPC-based reference concrete mix.

- It is clearly evident, from the analyses of SEM micrograms, associated EDX analysis and, in some cases, XRD, that it is possible to design and develop HSAASC mixes, with very dense micro-structures, with much less micro-cracks and pores, leading to better engineering properties.

## **B. Durability studies on HSAASC Mixes**

- Increase in the total binder contents (GGBFS+fine amorphous quartz powder) have shown the possibility of both pore-filling and pore-refinement in all the HSAASC mixes and hence the mixes exhibited reduced chloride permeabilities in the bulk diffusion tests, compared to conventional OPC-based reference concrete mix.
- Test samples of OPC-based control concrete mix had losses in their compressive strengths of the order of 75% by 56-days, 95% by 90-days and 100% (i.e. complete deterioration) by 103 days under sulphuric acid attack. However, such losses for the different HSAASC mixes were much lower, in the range of 36.4 - 39.1%, even by the end of one year. Such smaller strength losses in all the HSAASC mixes, under sulphuric acid attack, were due to the gradual deterioration of the higher amounts of C-A-S-H gels available in them initially. Again, even on such long exposure to acids, no deterioration effects were observed in either of the fine and coarse slag aggregates.
- The HSAASC mixes showed strength deterioration in the range of 15.5 to 20.5% on exposure to an aggressive environment of 10% MgSO<sub>4</sub> solution, for full one year. However, these results were marginally higher as compared up to 15.3% loss in strength exhibited by the control OPC-based concrete mix, under similar sulphate attack.
- Thus the present class of alkali activated slag concrete mixes, all of which are produced using large quantities of industrial by-products (which otherwise present safe disposal problems) and are having the required levels of enhanced flow ability, higher mechanical strengths and comparable durability properties,

can be referred to as **HIGH PERFORMANCE ALKALI ACTIVATED SLAG CONCRETE MIXES.**

### **C. Elevated Temperature Performance of HPAASC mixes**

- All the HPAASC specimens maintained their structural stability even after exposure to an elevated temperature as high as 800°C, without showing any signs of concrete spalling as exhibited by the test specimens of control OPC-based concrete mix even before attaining a temperature of about 600°C. Relatively higher strength retentions (in the range of 21 to 26%), were recorded by all the HPAASC mixes, even after exposure to an elevated temperature of 800°C, with almost 50% of their initial strengths retained upto 600°C, as compared to the OPC- based reference concrete mix.

### **D. Flexural Toughness characteristics of HPAASC Mixes**

- Addition of steel fibers to High performance alkali activated slag concrete mixes has been shown to marginally increase the compressive strengths (at both early 3-days as well as at 28-days) in the range of 10-15% only. The ultimate flexural strengths of all the candidate mixes, however, were observed to increase in a higher range of 20.8 - 44.0 %, for the various mixes tested herein.
- Increase in the percentage of steel fibers has shown to increase the toughness indices of the candidate mixes tested herein. HFSASC 3 mix exhibited the best toughness performance, as indicated by the larger values of the toughness indices computed by both of Barr and Hasso ( $T_{BH2}$ ) and ACI ( $T_{ACI}$ ) methods. Such indices are almost 1.35 – 1.60 times higher than those of the respective OPC-based concrete reference mixes.

### **E. Flexural Behaviour of Reinforced HPAASC Beams**

- The flexural performance of all the reinforced HPAASC beams was found to be, in general, quite similar to that of the HSS-OPCC control beam, with comparable load-carrying capacities at first crack and at ultimate stage.
- The deflection-response of all the reinforced HPAASC beams under flexure, indicating comparatively lower stiffness of these beams which is reflected in terms of the higher deflection values, at same loads, as compared to the control HSS-OPCC beam. Again, the AAS-based reinforced concrete beams could sustain larger deflections as compared to control beams, upto failure thus showing a higher ductility values available in all these HPAASC beams.
- The moment curvature plots for all the reinforced HPAASC beams showed higher ultimate moments in them, as observed along with higher curvatures till failure, as compared to control HSS-OPCC beam.
- None of the Reinforced HPAASC beams did exhibit any appreciable spalling of concrete during their ultimate stage, during testing and failure was similar to that of the control HSS-OPCC reference beam indicating better flexural performances of all these beams as compared to control reinforced OPC-based concrete beams.
- One has to recognize that all the HPAASC mixes developed herein made use of higher quantities of industrial by-products only – GGBFS as the principal binder, Slag sand and EAF slag as the fine and coarse aggregates. The mixes developed are shown to have both higher strengths (28-day compressive strengths of the order of 81 - 87 MPa), and self-compacting properties; Neither heat-curing nor the regular water-curing has been adopted. Hence, they can be accepted as “Greener, sustainable alternatives’ to OPC-based concrete in all structural concrete applications. They can also effectively contribute in building large-scale infrastructural facilities using a sustainable concrete construction technology.

Use of HPAASC mixes with GGBFS as binder, Slag sand as fine aggregate and EAF slag as coarse aggregate have ten major advantages over the use of OPCC, namely

- They consume lesser embodied energy.
- They lead to lower emissions of CO<sub>2</sub>.
- They save a lot of water due to requirement of only ambient curing.
- They utilize large amounts of industrial by-product GGBFS, as the major binder, which in turn saves larger amounts of non-renewable natural resources in terms of limestone, coal etc. which are the primary requirements for the production of cement.
- They lead to maximum utilization of an industrial by-product, Slag sand as fine aggregate.
- They lead to good utilization of another industrial by-product, EAF slag as coarse aggregate.
- They can contribute to large reduction in number of issues related to sand mining and problems related to quarrying of natural aggregates.
- They avoid using large areas of land required as landfills of the waste materials.
- SCC property of AAS concrete being very user-friendly to concrete construction industry.
- Early age strength development of these concrete mixes allows for earlier stripping of the form works, thus facilitating faster constructions with associated cost benefits.

## **10.2 SCOPE FOR FUTURE STUDY**

The present investigation can be extended to:

- Extensive study on the development of these HPAASC mixes with an extended initial setting time as per the requirements for the RMC technology.
- Development of these HPAASC mixes with one part activator solution with a lower cost can be studied.

- Performance evaluation of the structural elements made of HPAASC mixes after being subjected to sustained elevated temperatures.
- Investigation on the long term shrinkage and creep properties of these HPAASC mixes.
- Extensive study on the fracture properties of these HPAASC mixes can be evaluated.
- Effect of Hybrid Fibers on the performance evaluation of these HPAASC mixes can be extensively studied.

-----

## REFERENCES

- Abdollahnejad, Z., Luukkonen, T., Mastali, M., and Kinnunen, P. (2019). "Development of one-part alkali-activated ceramic/slag binders containing recycled ceramic aggregates". *Journal of Materials in Civil Engineering*, 31(2), 1 -13.
- ACI Committee 544. (1988). "Measurement of properties of fiber reinforced concrete". *ACI Material Journal*, 85, 583 -593.
- Adak, D., Sarkar, M., and Mandal, S. (2017). "Structural performance of nano-silica modified fly-ash based geopolymer concrete". *Construction and Building Materials*, 135, 430-439.
- Adam, A.A. (2009). "Strength and durability properties of alkali activated slag and fly ash-based geopolymer concrete". (*Ph.D. Dissertation*), RMIT University, Melbourne.
- Alaa, M.R. (2013). "A comprehensive overview about the influence of different additives on the properties of alkali-activated slag – A guide for Civil Engineer". *Construction and Building Materials*, 47, 29-55.
- Alaa, M.R., and Mervat, H.K. (2013). "A preliminary study of alkali-activated slag blended with silica fume under the effect of thermal loads and thermal shock cycles". *Construction and Building Materials*, 40, 522-532.
- Alaa, M. R., Dina, M. S., and Hassan, A. H. (2016). "An investigation on blast-furnace slag as fine aggregate in alkali activated slag mortars subjected to elevated temperatures". *Journal of Cleaner Production*, 112, 1086-1096.
- Al-Amoudi, O. S. B., Maslehuddin, M., and Saadi, M. M. (1995). "Effect of magnesium sulfate and sodium sulfate on the durability performance of plain and blended cement". *ACI Materials Journal*, 92(1), 15-24.
- Ali, A.A., Abd, E. M., and Mohammed, A.E. (2019). "Factors affecting the mechanical properties of alkali-activated ground granulated blast furnace slag concrete". *Construction and Building Materials*, 197, 339 – 355.

Allahverdi, A., and Škvára, F. (2000). “Acidic corrosion of hydrated cement-based materials”. *Ceramics– Silikáty*, 44(4), 152-160.

Angus chemical company. (2017). “Safety data sheet. Di- Basic Sodium Phosphate”. 1-13.

Aylin, O., and Kemalettin, Y. (2013). “Improvement of the performance of alkali activated blast furnace slag mortars with very finely ground pumice”. *Construction and Building Materials*, 48, 26-34.

Bakharev, T., Sanjayan, J. G., and Cheng, Y. B. (1999). “Alkali activation of australian slag cements”. *Cement and Concrete Research*, 29, 113-120.

Bakharev, T., Sanjayan, J. G., and Cheng, Y. B. (2000). “Effect of admixtures on properties of alkali-activated slag concrete”. *Cement and Concrete Research*, 30(9), 1367-1374.

Bakharev, T., Sanjayan, J.G., and Cheng, Y.B. (2002). “Sulfate attack on alkali-activated slag concrete”. *Cement and Concrete Research*, 32(2), 211–216.

Bakharev, T., Sanjayan, J. G., and Cheng, Y. B. (2003). “Resistance of alkali-activated slag concrete to acid attack”. *Cement and Concrete Research*, 33(10), 1607-1611.

Barr, B., and Hasso, E. B. D. (1985). “A study of toughness indices”. *Magazine of Concrete Research*, 37(132), 162-173.

Basheer, P.A.M. (2001). “Permeation analysis”. in *Handbook of analytical techniques in concrete science and technology- principles, techniques and application*, J.J.Noyes,USA, 658-737.

Bazant, Z. P., and Kaplan, M. F. (1996). “Concrete at high temperatures: material properties and mathematical models”. Harlow Longman.

Behfarnia, K., and Rostami, M. (2017). “Effects of micro and nanoparticles of SiO<sub>2</sub> on the permeability of alkali activated slag concrete”. *Construction and Building Materials*, 131, 205 – 213.

- Behfarnia, K., and Shahbaz, M. (2018). "The effect of elevated temperature on the residual tensile strength and physical properties of the alkali-activated slag concrete". *Journal of Building Engineering*, 20, 442 -454.
- Bellmann, F., and Stark, J. (2009). "Activation of blast furnace slag by a new method". *Cement and Concrete Research*, 39(8), 644–650.
- Bernal, S.A., Ruby, D.G., Silvio, D., and Erich, R. (2010). "Performance of an alkali-activated slag concrete reinforced with steel fibers". *Construction and Building Materials*, 24, 208 -214.
- Bernal, S.A., de Gutiérrez, R.M., Pedraza, A.L., Provis, J.L., Rodriguez, E.D., and Delvasto, S. (2011). "Effect of binder content on the performance of alkali-activated slag concretes". *Cement and Concrete Research*, 41 (1), 1–8.
- Bernal, S.A., de Gutiérrez, R.M., and Provis, J.L. (2012). "Engineering and durability properties of concretes based on alkali-activated granulated blast furnace slag/metakaolin blends". *Construction and Building Materials*, 33, 99–108.
- Bernal, S. A. (2015). "Effect of the activator dose on the compressive strength and accelerated carbonation resistance of alkali silicate-activated slag/metakaolin blended materials". *Construction and Building Materials*, 98, 217-226.
- Bhardwaj, B., and Kumar, P. (2019). "Comparative study of geopolymer and alkali activated slag concrete comprising waste foundry sand". *Construction and Building Materials*, 209, 555 -565.
- Borges, H.R.P., Banthia, N., Alcamand, A.H., Vasconcelos, L. W., and Nunes, H.M.E. (2016). "Performance of blended metakaolin/blast furnace slag alkali-activated mortars". *Cement and Concrete Composites*, 71, 42-52.
- Brough, A.R., and Atkinson, A. (2002). "Sodium silicate-based, alkali-activated slag mortars Part I. Strength, hydration and microstructure". *Cement and Concrete Research*, 32(6), 865–879.

Buchwald, A., Kaps, C., Hohmann, M. (2003). "Alkali-activated binders and pozzolan cement binders – complete binder reaction or two sides of the same story? ". In: *Proceedings of the 11th International Conference on the Chemistry of Cement*, Durban, South Africa, 1238–1246.

Cahit, B., Okan, K., Cengiz, D.A., and Serhan, I. (2013). "Influence of admixtures on the properties of alkali-activated slag mortars subjected to different curing conditions". *Materials and Design*, 44, 540-547.

Cang, S., Ge, X., and Bao, Y. (2017). "Assessment of mechanical properties and damage of high performance concrete subjected to magnesium sulphate environment". *Advances in Materials Science and Engineering*, Article ID 9196187.

Cengiz, D.A., Cahit, B., Ozlem, C., and Okan, K. (2009). "Influence of activator on the strength and drying shrinkage of alkali-activated slag mortar". *Construction and Building materials*, 23, 548 -555.

Chaitanya, S.T., and Gunneswara Rao, T.D. (2018<sup>a</sup>). "Mix design procedure for alkali-activated slag concrete using particle packing theory". *Journal of Materials in Civil Engineering*, 30(6), 1 -11.

Chaitanya, S.T., and Gunneswara Rao, T.D. (2018<sup>b</sup>). "Effect of mix design parameters on mechanical and durability properties of alkali-activated slag concrete". *Construction and Building Materials*, 193(30), 173 – 188.

Chan, S. Y. N., Peng, G. F., and Anson, M. (1999). "Fire behaviour of high-performance concrete made with silica fume at various moisture contents". *Materials Journal*, 96(3), 405-409.

Chang, E.H. (2009). "Shear and bond behaviour of reinforced fly ash-based geopolymer concrete beams". *Doctoral Thesis*, Curtin University of Technology, Australia, 1-409.

Chang, J. J. (2003). "A study on the setting characteristics of sodium silicate-activated slag pastes". *Cement and Concrete Research*, 33(7), 1005-1011.

- Chang, J.J., Yeih, W., and Hung, C.C. (2005). "Effects of gypsum and phosphoric acid on the properties of sodium silicate-based alkali-activated slag pastes". *Cement and Concrete Composites*, 27 (1), 85-91.
- Chaparro, W.A., Ruiz, J.H.B., Gómez, R.d.J.T. (2012). "Corrosion of reinforcing bars embedded in alkali-activated slag concrete subjected to chloride attack". *Materials Research*, 15 (1), 57–62.
- Chen, J., Ng, L.P., Jaskulski, R., and Kubissa, W. (2017). "Use of quartz sand to produce low embodied energy and carbon footprint plaster". *Journal of Sustainable Architecture and Civil Engineering*, 1-8.
- Cheng, T. W., and Chiu, J. P. (2003). "Fire-resistant geopolymer produced by granulated blast furnace slag". *Minerals Engineering*, 16(3), 205-210.
- Chi, M. (2012). "Effects of dosage of alkali-activated solution and curing conditions on the properties and durability of alkali-activated slag concrete". *Construction and Building Materials*, 35, 240 -245.
- Chi, M., and Huang, R. (2013). "Binding mechanism and properties of alkali-activated fly ash/slag mortars". *Construction and Building Materials*, 40, 291-298.
- Chitawadagi, M.V., Narasimhan, M.C., and Kulkarni, S.M. (2010). "Axial capacity of rectangular concrete-filled steel tube columns – DOE approach". *Construction and Building Materials*, 24(4), 585 –595.
- Choi, J., Yeon, L.B., Ranade, R., Li, V.C., and Lee, Y. (2016). "Ultra-high-ductile behaviour of a polyethylene fiber-reinforced alkali activated slag-based composite". *Cement and Concrete Composites*, 70, 153-158.
- Collins, F.G., and Sanjayan, J.G. (1999). "Workability and mechanical properties of alkali activated slag concrete". *Cement and Concrete Research*, 29(3), 455-458.
- Criado, M., Fernandez-Jimenez, A., de la Torre., A.G., Aranda, M.A.G., and Palomo, A. (2007). "An XRD study of the effect of the SiO<sub>2</sub>/Na<sub>2</sub>O ratio on the alkali activation of fly ash". *Cement and Concrete Research*, 37(5), 671-679.

Danial, N., Amir, H.P., and Hossein, G., (2018). “The influence of curing conditions and alkaline activator concentration on elevated temperature behaviour of alkali-activated slag (AAS) mortars”. *Construction and Building Materials*, 190, 108 – 119.

Dattatreya, J.K., Rajamane, N.P., Sabitha, D., Ambily, P.S., and Nataraja, M.C. (2011). “Flexural behaviour of reinforced geopolymer concrete beams”. *International Journal of Civil and Structural Engineering*, 2 (1), 138–159.

Davidovits, J., Comrie, D.C., Paterson, J.H., and Ritcey, D.J. (1990). “Geopolymeric concretes for environmental protection”. *ACI Concrete International*, 12, 30–40.

Davidovits, J. (1991). “Geopolymers – inorganic polymeric new materials”. *Journal of Thermal Analysis and Calorimetry*, 37 (8), 1633–1656.

Davidovits, J. (1994). “Properties of geo-polymer cements”. *First International Conference on Alkaline Cements and Concretes*, Kiev, Ukraine, SRIBM, Kiev State Technical University, 131-149.

Didamony, E. H., Amer, A. A., and Elaziz, H. A. (2012). “Properties and durability of alkali-activated slag pastes immersed in sea water”. *Ceramic International*, 38(5), 3773-3780.

Duxson, P., Provis, J.L., Lukey, G.C., Separovic, F., van Deventer, J.S.J. (2005). “<sup>29</sup> Si NMR study of structural ordering in aluminosilicate geopolymer gels”. *Langmuir* 21 (7), 3028–3036

Duxson, P., Fernández-Jiménez, A., Provis, J.L., Lukey, G.C., Palomo, A., and van Deventer, J.S.J. (2007). “Geopolymer technology: the current state of the art”. *Journal of Material Science*, 42 (9), 2917–2933

Ellis, K., Silvestrin, R., Varela, B., Alharbi, N., and Hailstone, R. (2016). “Modeling setting time and compressive strength in sodium carbonate activated blast furnace slag mortars using statistical mixture design”. *Cement and Concrete Composites*, 74, 1-6.

Fernández-Jiménez, A., Palomo, J. G., and Puertas, F. (1999). “Alkali-activated slag mortars: mechanical strength behaviour”. *Cement and Concrete Research*, 29, 1313-1321.

Fernández-Jiménez, A., and Puertas, F. (2001). “Setting of alkali-activated slag cement- Influence of activator nature”. *Advances in Cement Research*, 13(3), 115-121.

Fernandez-Jimenez, A., and Puertas, F. (2003). “Structure of calcium silicate hydrates formed in alkaline-activated slag: influence of the type of alkaline activator”. *Journal of the American Ceramic Society*, 86 (8), 1389-1394.

Ganesan, N., Abraham, R., and Raj, S.D. (2015). “Durability characteristics of steel fiber reinforced geopolymer concrete”. *Construction and Building Materials*, 93, 471–476.

Gao, X., Yu, Q.L., and Brouwers, H.J.H. (2015). “Properties of alkali activated slag– fly ash blends with limestone addition”. *Cement and Concrete Composites*, 59, 119-128.

Georgali, B., and Tsakiridis, P. E. (2005). “Microstructure of fire-damaged concrete - a case study”. *Cement and Concrete Composites*, 27(2), 255-259.

Glukhovsky, V. D. (1959). “Soil Silicates”. Kiev, Ukraine: Gastroi Publishers.

Glukhovsky, V.D., Rotovskaya, G.S., and Rumyna, G.V. (1980). “High strength slag – alkali cement”. *7<sup>th</sup> International Congress on the Chemistry of Cements*, 3, 164-168.

Glukhovsky, V.D. (1994). “Alkaline cements and concretes”. *First International Conference*, Kiev, Ukraine, 1-8.

Gong, C., and Yang, N. (2000). “Effect of phosphate on the hydration of alkali activated red mud–slag cementitious material”. *Cement and Concrete Research*, 30 (7), 1013-1016.

Gourley, J.T., and Johnson, G.B. (2005). “Developments in geopolymer precast concrete”. In: *Proc of Geopolymer World Congress*, Geopolymer green chemistry and sustainable development solutions, Saint –Quentin, France. 139–143.

Guerrieri, M., and Sanjayan, J. (2009). "Behaviour of combined fly ash/slag based geopolymers when exposed to high temperatures". *Fire and Materials*, 34, 163-175.

Guerrieri, M., Sanjayan, J., and Collins, F. (2009). "Residual compressive behaviour of alkali-activated concrete exposed to elevated temperatures". *Fire and Materials*, 33(1), 51-62.

Guerrieri, M., Sanjayan, J., and Collins, F. (2010). "Residual strength properties of sodium silicate alkali activated slag paste exposed to elevated temperatures". *Materials and Structures*, 43(6), 765-773.

Guo, X., Shi, H., and Dick, W.A.(2010). "Compressive strength and microstructural characteristics of class C fly ash geopolymer". *Cement and Concrete Composites*, 32, 142-147.

Haha, M. B., Saout, G. L., Winnefeld, F., and Lothenbach, B. (2011). "Influence of activator type on hydration kinetics, hydrate assemblage and microstructural development of alkali activated blast-furnace slags". *Cement and Concrete Research*, 41(3), 301-310.

Hammad, A.K., Mohammad, S.H.K., Arnaud, C., and Jerry. S. (2018). "Deterioration of alkali-activated mortars exposed to natural aggressive sewer environment". *Construction and Building Materials*, 186, 577 – 597.

Handoo, S. K., Agarwal, S., and Agarwal, S. K. (2002). "Physico-chemical, mineralogical, and morphological characteristics of concrete exposed to elevated temperatures". *Cement and Concrete Research*, 32(7), 1009-1018.

Hardijito, D., and Rangan, B.V. (2005). "Development and properties of low calcium fly ash based geopolymer concrete". *Research Report GCI*, Faculty of engineering curtin university of technology, Perth, Australia.

Heikal, M., Nassar, M.Y., El-Sayed, G., and Ibrahim, S.M. (2014). "Physico-chemical, mechanical, microstructure and durability characteristics of alkali activated egyptian slag". *Construction and Building Materials*, 69, 60–72.

- Hilal, E.H., Ehab, S., and Abdelrahman, A.S. (2018). "Influence of different curing regimes on the performance and microstructure of alkali-activated slag concrete". *Journal of Materials in Civil Engineering*, 30(1), 1 -14.
- Hosny, H., and Abu, E. (1994). "Fire in concrete building". *Egyptian Universities Publishers*.
- Hughes, D. C. (1985). "Sulphate resistance of OPC, OPC/fly ash and SRPC pastes: pore structure and permeability". *Cement and Concrete Research*, 15(6), 1003-1012.
- Ibrahim, M., Johari, M.A.M., Maslehuddin, M., and Rahman, M.K. (2018). "Influence of nano-SiO<sub>2</sub> on the strength and microstructure of natural pozzolan based alkali-activated concrete". *Construction and Building Materials*, 173, 573-585.
- Ismail, I., Bernal, S.A., Provis, J.L., San Nicolas, R., Brice, D.G., Kilcullen, A.R., Hamdan, S., and van Deventer, J.S.J. (2013). "Influence of fly ash on the water and chloride permeability of alkali-activated slag mortars and concretes". *Construction and Building Materials*, 48, 1187–1201.
- Jang, J.G., Lee, N.K., and Lee, H.K. (2014). "Fresh and hardened properties of alkali-activated fly ash/slag pastes with superplasticiser". *Construction and Building Materials*, 50, 169 -176.
- Jeyasehar, C.A., Saravanan, G., Salahuddin, M., and Thirugnanasambandam, S. (2013). "Development of fly ash based geopolymers precast concrete elements". *Asian Journal of Civil Engineering*, 14 (4), 605–615.
- Jin, F., Gu, K., and Al-Tabbaa, A. (2014). "Strength and drying shrinkage of reactive MgO modified alkali-activated slag paste". *Construction and Building Materials*, 51, 395 - 404.
- Jumppanen, U. M., Diederichs, U., and Hinrichsmeyer, K. (1986). "Material properties of F-concrete at high temperatures". *VTT Technical Research Centre of Finland*, 452, 230.

Kamal, M.M., Safan, M.A., Bashandy, A.A., and Khalil, A.M. (2018). “Experimental investigation on the behaviour of normal strength and high strength self-curing self-compacting concrete”. *Journal of Building Engineering*, 16, 79-93.

Kathirvel, P., and Kaliyaperumal, S.R.M. (2016). “Influence of recycled concrete aggregates on the flexural properties of reinforced alkali activated slag concrete”. *Construction and Building Materials*, 102 (1), 51-58.

Keun, H.Y., Ah, R.C., Jin, K.S., and Sang, H.M. (2012). “Hydration products and strength development of calcium hydroxide-based alkali-activated slag mortars”. *Construction and Building Materials*, 29, 410 – 419.

Khaliq, W., and Khan, H.A. (2015). “High temperature material properties of calcium aluminate cement concrete”. *Construction and Building Materials*, 94, 475-487.

Khan, H.A., Khan, M.S.H., Castel, A., and Sunarho, J. (2018). “Deterioration of alkali-activated mortars exposed to natural aggressive sewer environment”, *Construction and Building Materials*, 186, 577-597.

Khoury, G. A. (1992). “Compressive strength of concrete at high temperatures: a reassessment”. *Magazine of Concrete Research*, 44(161), 291-309.

Koch, G.H., Brongers, M.P.H., Thompson, N.G., Virmani, Y.P., and Payer, J.H. (2002). “Corrosion cost and preventive strategies in the united states”. *National Association of Corrosion Engineers*, Houston, TX, US.

Krivenko, P. D. (1994). “Alkaline cements”. *The First International Conference on Alkaline Cements and Concrete*, October, Kiev, Ukraine, 11-14.

Krizan, D., and Zivanovic, B. (2002). “Effects of dosage and modulus of water glass on early hydration of alkali–slag cements”. *Cement and Concrete Research*, 32(8), 1181-1188.

Kühl, H. (1908). “Slag cement and process making the same”. *US Patent* 900,939.

- Kumaravel, S., and Thirugnanasambandam, S. (2013). "Flexural behaviour of reinforced low- calcium fly ash based geopolymer concrete beams". *Global Journal of Research in Engineering*, 13(8), 1-7.
- Law, D.W., Adam, A.A., Molyneaux, T.K., and Patnaikuni, I. (2012). "Durability assessment of alkali activated slag concrete". *Materials and Structures*, 45 (9), 1425–1437.
- Lecomte, I., Henrist, C., Liegeois, M., Maseri, F., Rulmont, A., and Cloots, R. (2006). "(Micro)-structural comparison between geopolymer, alkali-activated slag cement and Portland cement". *Journal of the European Ceramic Society*, 26, 3789-3797.
- Lee, K.M., Choi, S., Choo, J.F., Choi, Y.C., and Yoo, S.W. (2017). "Flexural and shear behaviour of reinforced alkali-activated slag concrete beams". *Advances in Material Science and Engineering*, Article ID5294290, 1-12.
- Lee, N. K., and Lee. H.K. (2013). "Setting and mechanical properties of alkali-activated fly ash/slag concrete manufactured at room temperature". *Construction and Building Materials*, 47, 1201-1209.
- Li, M., Qian, C., and Sun, W. (2004). "Mechanical properties of high-strength concrete after fire". *Cement and Concrete Research*, 34(6), 1001-1005.
- Malkapur, S.M., Divakara, L., Narasimhan, M.C., Karkera, N.B., Goverdhan, P., Sathian, V., and Prasad, N.K. (2017). "Neutron radiation shielding properties of polymer incorporated self-compacting concrete mixes". *Applied. Radiation and Isotopes*, 125, 86 -93.
- Mangat, P. S., and Khatib, J. M. El. (1992). "Influence of initial curing on sulfate resistance of blended cement concrete". *Cement and Concrete Research*, 22(6), 1089- 1100.
- Manjunath, G.S., Radhakrishna, K., Giridhar, C., and Jadhav, H. (2011). "Compressive strength development in ambient cured geopolymer mortar". *International Journal of Earth Sciences and Engineering*, 4, 830-834.

Manu S. N., and Dinakar, P., (2017). “Permeation properties of high strength self-compacting and vibrated concretes”. *Journal of Building Engineering*, 12, 275-281.

Marceau, M., Nisbet, M. A., and Van Geem, M. G. (2007). “Life cycle inventory of Portland cement concrete”. SN3011, *Portland Cement Association*, Skokie, Illinois, PCA, 121-124.

Marland, G., Boden, T.A., and Andres R. J. (2007). “Global, regional, and national CO<sub>2</sub> emissions in trends: a compendium of data on global change”. *Carbon dioxide Information Analysis Centre*, Oak Ridge National Laboratory, U.S. Department of Energy, Oak Ridge, Tenn., U.S.A, 233-239.

Matos, P.R.D., Foiato, M., and Jr, L.R.P. (2019). “Ecological, fresh state and long-term mechanical properties of high-volume fly ash high-performance self-compacting concrete”. *Construction and Building Materials*, 203, 282-293.

McGannon, H. (1971). “The Making, Shaping and Treating of Steel”. *United States Steel Corporation*, Eighth Edition.

Mejía de Gutierrez, R., Maldonado, J., and Gutiérrez, C. (2004). “Performance of alkaline activated slag at high temperatures”. *Materiales De Construccion*, 54(276), 87-92.

Memon, S.A., Shah, S.F.A., Rao, A. K., and Baloch, W.L. (2019). “Durability of sustainable concrete subjected to elevated temperature – A review”. *Construction and Building Materials*, 199, 435-455,

Mishra, A., Choundhary, D., Jain, N., Kumar, M., Sharda, N., and Dutt, D. (2008). “Effect of concentration of alkaline liquid and curing time on strength and water absorption of geopolymer concrete”. *ARPJ Journal of Engineering and Applied Sciences*, 3, 14-18.

Mithun, B.M, and Narasimhan, M.C. (2016).“Performance of alkali activated slag concrete mixes incorporating copper slag as fine aggregate”. *Journal of Cleaner Production*, 112, 837-844.

- Montgomery, D. (2004). "Design and analysis of experiments". 5th Ed. New York: John Wiley & Sons (Asia) Pvt. Ltd.
- Moruf, O.Y., Megat, A.M.J., Zainal, A.A., and Mohammad, M. (2014). "Evolution of alkaline activated ground blast furnace slag–ultrafine palm oil fuel ash based concrete". *Materials and Design*, 55, 387-393.
- Narasimhan, M. C., Nayak, G., Ajith, B. T., and Rao, M. K. (2011). "Development of alternative binders to portland cement concrete using fly ash and blast furnace slag: some experiences". *Proceedings of the International UKIERI Concrete Congress*, New Delhi, India, 43-60.
- Natali, M. A., Manzia, S., and Bignozchia, M.C. (2011). "Novel fiber-reinforced composite materials based on sustainable geopolymer matrix". *Procedia Engineering*, 21, 1124-1131.
- Natali, M. A., Rickard, W.D.A., Bignozzi, M.C., Van Riessen, A. (2013). "High temperature behaviour of ambient cured alkali-activated materials based on ladle slag". *Cement and Concrete Research*, 43, 51-61.
- Ning, L., Caijun, S., Zuhua, Z., Deju, Z., Hyeon, J.H., Yuhan, Z., and Tengjiao, S. (2018). "A mixture proportioning method for the development of performance-based alkali-activated slag-based concrete". *Cement and Concrete Composites*, 93, 163 – 174.
- Otaibi, S.A. (2008). "Durability of concrete incorporating GGBS activated by water glass". *Construction and Building Materials*, 22 (10), 2059–2067.
- Özge, A. Ç., Oğuzhan, Ç, and Kambiz, R. (2008). "Effect of high temperature on mechanical and microstructural properties of cement mortar". *Proceedings of 11 DBMC International Conference on Durability of Building Materials and Components*, Istanbul, Turkey, 11-14.
- Pacheco-Torgal, F., Gomes, J., and Jalali, S. (2010). "Durability and environmental performance of alkali-activated tungsten mine waste mud mortars". *Journal of Materials in Civil Engineering*, 22, 897–904.

Pacheco-Torgal, F., Abdollahnejad, Z., Camões, A.F., Jamshidi, M., and Ding, Y. (2012). “Durability of alkali-activated binders: A clear advantage over portland cement or an unproven issue?”. *Construction and Building Materials*, 30, 400-405.

Pade, C., Guimaraes, M., Kjellsen, K., and Nilsson, A. (2007). “The CO<sub>2</sub> uptake of concrete in the perspective of life cycle inventory”. *International Symposium on Sustainability in the Cement and Concrete Industry, Lillehammer, Norway*. 121-124.

Palacios, M., Houst, Y.F., Bowen, P., and Puertas, F. (2009). “Adsorption of superplasticizer admixtures on alkali-activated slag pastes”. *Cement and Concrete Research*, 39(8), 670 – 677.

Palankar, N., Shankar, A.U.R., and Mithun, B.M. (2016). “Durability studies on eco-friendly concrete mixes incorporating steel slag as coarse aggregates”. *Journal of Cleaner Production*, 129, 437- 448.

Palankar N, Shankar, A.U.R., and Mithun, B.M. (2017). “Investigations on alkali activated slag/fly-ash concrete with steel slag coarse aggregate for pavement structures”. *International Journal of Pavement Engineering*, 18(6), 500-512.

Pan, Z., Li, D., Yu, J., and Nanru, Y. (2003). “Properties and microstructure of the hardened alkali-activated red mud–slag cementitious material”. *Cement and Concrete Research*, 33(9), 1437–1441.

Park, J.W., Ann, K.Y., and Cho, C.G. (2015). “Resistance of alkali-activated slag concrete to chloride-induced corrosion”. *Advances in Materials Science and Engineering*, 1-7.

Park, S.M., Jang, J.G., Lee, N.K., and Lee, H.K. (2016). “Physicochemical properties of binder gel in alkali-activated fly ash/slag exposed to high temperatures”. *Cement and Concrete Research*, 89, 72-79.

Parthiban, K., and Saravana, R. M. K. (2016). “Influence of recycled concrete aggregates on the flexural properties of reinforced alkali activated slag concrete”. *Construction and Building Materials*, 102, 51-58.

Pedro, D., Brito, J.D., and Evangelista, L. (2018). “Durability performance of high-performance concrete made with recycled aggregates, fly ash and densified silica fume”. *Cement and Concrete Composites*, 93, 63-74,

Pereira, A., Akasaki, L. J., Melges, L.P.J., Tashima, M.M., Soriano, L., Borrachero, M.V., Monzó, J., and Jordi, P. (2015). “Mechanical and durability properties of alkali-activated mortar based on sugarcane bagasse ash and blast furnace slag”. *Ceramic International*, 41(10), 13012-13024.

Petzold, A., Röhrs, M., and Neville A. M. (1971). “Concrete for high temperatures”. Translated from the German by A. B. Phillips and F. M. Turner, Maclaren 1970, 235 pp. £6, *Building Science*, 6(1), 33-34.

Phan, L. T. (1996). “Fire performance of high-strength concrete: A report of the state of the art”. *US Department of Commerce, Technology Administration, National Institute of Standards and Technology, Office of Applied Economics, Building and Fire Research Laboratory*.

Pineaud, A., Pimienta, P., Rémond, S., and Carré, H. (2016). “Mechanical properties of high performance self-compacting concretes at room and high temperature”. *Construction and Building Materials*, 112(1), 747-755.

Poon, C. S., Azhar, S., Anson, M., and Wong, Y. L. (2001). “Comparison of the strength and durability performance of normal-and high-strength pozzolanic concretes at elevated temperatures”. *Cement and Concrete Research*, 31(9), 1291-1300.

Pradeep, J., Sanjay, R., and Ashwath, M. U. (2012). “Experimental study on flexural behaviour of fly-ash and GGBS based geopolymer concrete beams in bending”. *International Journal of Emerging Trends in Engineering and Development*, 6, 419-428.

Provis, J.L., Lukey, G.C., Van Deventer, J.S.J. (2005). “Do geopolymers actually contain nanocrystalline zeolites? A re-examination of existing results”. *Chemistry of Materials*, 17 (12), 3075–3085.

Provis, J.L. (2009). “Activating solution chemistry for geopolymers”. In: Provis, J.L., Van Deventer, J.S.J. (eds.) *Geopolymers: Structure, Processing, Properties and Industrial Applications*, Wood head, Cambridge, 50–71.

Provis, J.L., and Bernal, S.A. (2014). “Geopolymers and related alkali-activated materials”. *Annual Review of Materials Research*, 44, 299–327.

Provis, J.L., and Van Deventer, J.S.J. (2014). “Alkali activated materials: State of the Art Report, RILEM TC 224-AAM”. Springer, New York, London, 13.

Provis, J.L. (2018). “Alkali-activated materials”. *Cement and Concrete Research*, 114, 40-48.

Puertas, F., Ramírez, S. M., Alonso, S., and Vazquez, T. (2000). “Alkali-activated fly ash/slag cements: strength behaviour and hydration products”. *Cement and Concrete Research*, 30(19), 1625-1632.

Puertas, F., Palacios, M., Maroto, A.G., and Vázquez, T. (2009). “Alkali-aggregate behaviour of alkali-activated slag mortars: Effect of aggregate type”. *Cement and Concrete Composites*, 31, 277 -284.

Puertas, F., Palacios, M., Manzano, H., Dolado, J.S., Rico, A., and Rodríguez. J. (2011). “A model for the C-A-S-H gel formed in alkali-activated slag cements”. *Journal of the European Ceramic Society*, 31(12), 2043-2056.

Puertas, F., and Torres, C.M. (2014). “Use of glass waste as an activator in the preparation of alkali-activated slag. Mechanical strength and paste characterization”. *Cement and Concrete Research*, 57, 95 -104.

Puertas, F., Varga, C., and Alonso, M.M. (2014). “Rheology of alkali-activated slag pastes. Effect of the nature and concentration of the activating solution”. *Cement and Concrete Composites*, 53, 279-288.

Puertas, F., González-Fonteboa, B., González-Taboada, I., Alonso, M.M., Torres-Carrasco, M., Rojo, G., and Martínez-Abella, F. (2018). “Alkali-activated slag concrete: Fresh and hardened behavior”. *Cement and Concrete Composites*, 85, 22- 31.

- Purdon, A. (1940). "The action of alkalis on blast furnace slag". *Journal of the Society of Chemical Industry*, 59, 191-202.
- Rahier, H., Simons, W., Mele, B.V., and Biesemans, M. (1997). "Low-temperature synthesized aluminosilicate glasses: Part III Influence of the composition of the silicate solution on production, structure and properties". *Journal of Material Science*, 32 (9), 2237–2247.
- Rajamane, N.P., Nataraja, M.C., Dattatreya, J.K., Lakshmanan, N., and Sabitha, D. (2012<sup>a</sup>). "Sulphuric acid resistant eco-friendly concrete from geopolymerization of blast furnace slag". *Indian Journal of Engineering and Materials Sciences*, 19(5), 357-367.
- Rajamane, N.P., Nataraja, M.C., Dattatreya, J.K., Lakshmanan, N., and Sabitha, D. (2012<sup>b</sup>). Sulphate resistance and eco-friendliness of geopolymer concrete". *Indian Concrete Journal*, 86(1), 13-22.
- Ranani, M.A.A. (2012). "An experimental study on the effect of pozzolan on durability of conventional and fiber reinforced self-compacting concrete in frost exposure". Civil Engineering Department, *Isfahan University of Technology*.
- Rattanasak, U., and Chindaprasirt, P. (2009). "Influence of NaOH solution on the synthesis of fly ash geopolymer". *Mineral Engineering*, 22, 1073-1078.
- Ravikumar, D., Peethamparan, S., and Neithalath, N. (2010). "Structure and strength of NaOH activated concretes containing fly ash or GGBFS as the sole binder". *Cement and Concrete Composites*, 32(6), 399-410.
- Ravikumar, D., and Neithalath, N. (2013). "Electrically induced chloride ion transport in alkali-activated slag concretes and the influence of microstructure". *Cement and Concrete Research*, 47, 31–42.
- Ravikumar, D., and Neithalath, N., (2013). "An electrical impedance investigation into the chloride ion transport resistance of alkali silicate powder activated slag concretes". *Cement and Concrete Composites*, 44, 58-68.

Reddy, B. V. V. (2010). "Embodied energy in buildings". (IISC, Bangalore), [www.ese.iitb.ac.in/events/other/renet\\_files/21/Session%203/Energy%20in%20buildings\\_\(B.V.V.Reddy\).pdf](http://www.ese.iitb.ac.in/events/other/renet_files/21/Session%203/Energy%20in%20buildings_(B.V.V.Reddy).pdf), 47-55.

Rodríguez, E., Bernal, S., Gutiérrez, R.M.D., and Puertas, F. (2008). "Alternative concrete based on alkali-activated slag". *Materiales de Construcción*, 58(291), 53-67.

Rostami, M., and Behfarnia, K. (2017). "The effect of silica fume on durability of alkali activated slag concrete". *Construction and Building Materials*, 134, 262–268.

Rovnanik, P., Bayer, P., and Rovnanikova, P. (2013). "Characterization of alkali activated slag paste after exposure to high temperatures". *Construction and Building Materials*, 47, 1479-1487.

Roy, D. M. (1999). "Alkali-activated cements opportunities and challenges". *Cement and Concrete Research*, 29(2), 249-254.

Ruilin, C., Baoliang, L., Nanqiao, Y., Yamei, Z., and Zuhua, Z. (2018). "Properties of alkali-activated ground granulated blast furnace slag blended with ferronickel slag". *Construction and Building Materials*, 192, 123 – 132.

Sakkas, K., Nomikos, P., Sofianos, A., and Panias, D. (2013). "Inorganic polymeric materials for passive fire protection of underground constructions". *Fire and Materials*, 37(2), 140-150.

Sanjay, R., Ashwath, M.U., and Singh, S. (2012). "An experimental study on flexural behaviour of reinforced concrete beams with recycled aggregates in bending". *International Journal of Emerging Trends in Engineering and Development*, 6, 186-199.

Sarker, P.K. (2015). "Structural behaviour and design of geopolymer concrete members". *Civil Engineering Dimension*, 17(3), 133-139.

Sathia, K., Babu, K.G., and Manu, S. (2008). "Durability study of low calcium fly ash geopolymer concrete". *Proceeding of the third ACF International Conferences*, 1153-1159.

- Se, J.C., Jeong, C., Jin, K.S., and Bang, Y.L. (2015). "Rheological and mechanical properties of fiber-reinforced alkali-activated composite". *Construction and Building Materials*, 96, 112 -118.
- Seleem, H. E. H., Rashad, A. M., and Elsokary, T. (2011). "Effect of elevated temperature on physico-mechanical properties of blended cement concrete". *Construction and building Materials*, 25(2), 1009-1017.
- Semiha, A., and Cuneyt, U. (2014). "Recycling of waste PET granules as aggregate in alkali-activated blast furnace slag/metakaolin blends". *Construction and Building Materials*, 58, 31 -37.
- Serdar, A., and Bulent, B.S. (2013). "The effect of fiber properties on high performance alkali-activated slag/silica fume mortars". *Composites: Part B*, 45, 63-69.
- Sheng, R.L., Wang, X.Y., and Zhang, G.Y. (2018). "Effects of quartz powder on the microstructure and key properties of cement paste". *Sustainability*, 10, 3369, 1-16.
- Shi, C. (1996). "Strength, pore structure and permeability of alkali-activated slag mortars". *Cement and Concrete Research*, 26 (12), 1789–1799.
- Shi, C., and Stegemann, J.A. (2000). "Acid corrosion resistance of different cementing materials". *Cement and Concrete Research*, 30(5), 803-808.
- Shi, C., Roy, D., and Krivenko, P. (2006). "Alkali-activated cements and concretes". *CRS Press*, Taylor and Francis publications, Abingdon, UK.
- Shutong, Y., Jinjin, X., Chaohui, Z., Rui, L., Qiubo, Y., and Shuguang, S. (2019). "Mechanical properties of alkali-activated slag concrete mixed by seawater and sea sand". *Construction and Building Materials*, 196, 395 – 410.
- Stanish, K.D., Hooton, D., and Thomas, M.D.A. (1997). "Testing the chloride penetration resistance of concrete: A literature review". Dept. of Civil Engineering, University of Toronto, Ontario, Canada.

- Sturma, P., Glutha, G.J.G., Jägerb, C., Brouwersc, H.J.H., and Kühnea, H.C. (2018). Sulfuric acid resistance of one-part alkali-activated mortars”. *Cement and Concrete Research*, 109, 54-63.
- Sullivan, P. J. E., and Sharshar, R. (1992). “The performance of concrete at elevated temperatures as measured by the reduction in compressive strength”. *Fire Technology*, 28(3), 240-250.
- Sumajouw, D.M.J., and Rangan, B.V. (2006). “Low calcium based geopolymer concrete: reinforced beams and columns”. *Research report GC3*, Curtin University of Technology, Perth, Australia.
- Sun, Z., Lin, X., Liu, P., Wang, D., Vollpracht, A., and Oeser, M. (2018). “Study of alkali activated slag as alternative pavement binder”. *Construction and Building Materials*, 186, 626-634.
- Tang, L. (1996). “Chloride transport in concrete: Measurement and Prediction Chalmers”. *University of Technology*, Sweden, 200.
- Taylor, H.F.W. (1997). “Cement chemistry”. (2<sup>nd</sup> Ed), London: T. Telford.
- Thomas, R.J., Ariyachandra, E., Lezama, D., and Sulapha, P. (2018). “Comparison of chloride permeability methods for Alkali-Activated concrete”. *Construction and Building Materials*, 165, 104 – 111.
- Türker, H.T., Balçikanli, M., Durmus, I.H., Özbay, E., Erdemir, M. (2016). “Micro-structural alteration of alkali activated slag mortars depend on exposed high temperature level”. *Construction and Building Materials*, 104, 169 -180.
- Un, C.H., Sanjayan, J.G., San Nicolas, R., and Van Deventer, J.S.J. (2016). “Predictions of long-term deflection of geopolymer concrete beams”. *Construction and Building Materials*, 94, 10-19.
- Vilaplana, J.L., Baeza, F.J., Galao, O., Alcocel, E.G., Zornoza, E., and Garcés, P. (2016). “Mechanical properties of alkali activated blast furnace slag pastes reinforced with carbon fibers”. *Construction and Building Materials*, 116, 63-71.

- Wagh, A.S. (2004). Chemically bonded phosphate ceramics. Elsevier, Oxford.
- Wan, H.Y., Dong, W.R., Dong, C.P., Woo, J.K., and Chee, H.S. (2014). “A study of the effect of light-burnt dolomite on the hydration of alkali-activated Portland blast-furnace slag cement”. *Construction and Building Materials*, 57, 24-29.
- Wanchai, Y. (2014). “Application of fly ash-based geopolymer for structural member and repair materials”. *Advances in Science and Technology, Research Journal*, 92, 74–83.
- Wang, H. Y. (2008). “The effects of elevated temperature on cement paste containing GGBFS”. *Cement and Concrete Composites*, 30(10), 992-999.
- Wang, S. D., Scrivener, K. L., and Pratt, P. L. (1994). “Factors affecting the strength of alkali-activated slag”. *Cement and Concrete Research*, 24(6), 1033-1043.
- Wang, S.D., and Scrivener, K.L. (1995). “Hydration products of alkali-activated slag cement”. *Cement and Concrete Research*, 25 (3), 561-571.
- Wang, S.D., and Scrivener, K.L. (2003). “<sup>29</sup>Si and <sup>27</sup>Al NMR study of alkali-activated slag”. *Cement and Concrete Research*, 33 (5), 769-774.
- Wen, T.K., and Tsung, C.H. (2014). “Engineering properties of alkali-activated binders by use of desulfurization slag and GGBFS”. *Construction and Building Materials*, 66, 229-234.
- Xiao, J., Xie, M., and Zhang, C. (2006). “Residual compressive behaviour of pre-heated high-performance concrete with blast furnace slag”. *Fire Safety Journal*, 41(2), 91-98.
- Xu, Y., Wong, Y. L., Poon, C. S., and Anson, M. (2001). “Impact of high temperature on PFA concrete”. *Cement and Concrete Research*, 31(7), 1065-1073.
- Yang, K., Yang, C., Zhang, J., Pan, Q., Yu, L., and Bai, Y. (2018). “First structural use of site-cast, alkali-activated slag concrete in China”. *Structures and Building*, 171(10), 800–809.

Yang, L.Y., Jia, Z.J., Zhang, Y.M., and Dai, J.M. (2015). "Effects of nano-TiO<sub>2</sub> on strength, shrinkage and microstructure of alkali activated slag pastes". *Cement and Concrete Composites*, 57, 1-7.

Yeonung, J., Hyeoneun, P., Yubin, J., Jae, H.J., and Jae, E.O. (2016). "Influence of slag characteristics on strength development and reaction products in a CaO-activated slag system". *Cement and Concrete Composites*, 72, 155-167.

Yost, J.R., Radlinska, A., Ernst, S., Salera, M., and Martignetti, N.J. (2013). "Structural behaviour of alkali activated fly ash concrete. Part 2: structural testing and experimental findings". *Materials and Structures*, 46(3), 449–462.

Zhenzhen, J., Ying, W., Wenzhong, Z., and Wenxuan, H. (2019). "Effect of the activator on the performance of alkali-activated slag mortars with pottery sand as a fine aggregate". *Construction and Building Materials*, 197, 83 – 90.

Zuda, L., Pavlík, Z., Rovnaníková, P., Bayer, P., and Černý, R. (2006). "Properties of alkali activated aluminosilicate material after thermal load". *International Journal of Thermo physics*, 27(4), 1250-1263.

Zuhau, Z., Yingcan, Z., Tao, Y., Liang, F.L., Huajun, Z., and Hao, W. (2017). "Conversion of local industrial wastes into greener cement through geopolymer technology: A case study of high-magnesium nickel slag". *Journal of Cleaner Production*, 141, 463-471.

ASTM C 642-06. "Standard test method for density, absorption and voids in hardened concrete". *ASTM International*, West Conshohocken, PA, USA.

ASTM C 1202-12. "Standard test method for electrical indication of concrete's ability to resist chloride ion penetration". *ASTM International*, West Conshohocken, PA, USA.

ASTM C1556-04. "Standard test method for determining the apparent chloride diffusion co-efficient of cementitious mixtures by bulk diffusion". *ASTM International*, West Conshohocken, PA, USA.

ASTM C1611-14. “Standard Test Method for slump flow of self-consolidating concrete”. *ASTM International*, West Conshohocken, PA, USA.

EFNARC 2002. “Specification and guidelines for self-compacting concrete”. *EFNARC, Association house*, 99 West Street, UK.

IS: 383-1970. “Indian standard specification for coarse and fine aggregates from natural sources for concrete (Second revision)”. *Bureau of Indian Standards*, New Delhi, India.

IS: 456-2000, Reaffirmed 2005. “Plain and Reinforced Concrete - Code of Practice”. *Bureau of Indian Standards*, New Delhi, India.

IS: 516-1959. “Method of test for strength of concrete”. *Bureau of Indian Standards*, New Delhi, India.

IS: 8142-1976. “Method of test for determining setting time of concrete by penetration resistance”. *Bureau of Indian Standards*, New Delhi, India.

IS: 2386-1963. “Methods of test for aggregates for concrete”. *Bureau of Indian Standards*, New Delhi, India.

IS: 5816-1999. “Splitting tensile strength of concrete - method of test”. *Bureau of Indian Standards*, New Delhi, India.

IS: 12269-2013. “Ordinary Portland cement, 53 grade-specification (First revision)”. *Bureau of Indian Standards*, New Delhi, India.

IS: 10262-2009. “Indian standard concrete mix proportioning (First revision)”. *Bureau of Indian Standards*, New Delhi, India.

IS: 12089 - 1987. “Indian standard specification for granulated slag for the manufacture of Portland slag cement”. *Bureau of Indian Standards*, New Delhi, India.

IS -14212-1995. “Sodium and potassium silicates-Methods of test”. *Bureau of Indian Standards*, New Delhi, India.

## APPENDIX - I

### Mix Design for High Strength Self-Compacting OPC Concrete

For the OPC based control concrete mix, OPC 53 grade cement was used as the binder. Natural River Sand and Quartz sand were used as fine aggregate. Locally available crushed granite aggregates of 12.5 mm down size was used as coarse aggregate. The mix design was carried out by using absolute volume method.

#### Input parameters

Grade of cement	=	53
Sp. gravity of Cement	=	3.13
Sp. gravity of Fine Quartz powder	=	2.65
Sp. gravity of River sand	=	2.65
Sp. gravity of Quartz sand	=	2.65
Sp. gravity of coarse aggregate - Jelly	=	2.68
Maximum size of aggregate (MAS) mm	=	12.5

The aggregates are used in saturated surface dry condition.

Total Binder Content =  $600\text{kg/m}^3$  (**Cement: Fine Quartz Powder = 540: 60**)

Water to Binder = 0.40 = 240 lit

Proportioning of Fine aggregates: Coarse aggregates = 60:40

#### Mix Calculations

(a) Volume of concrete =  $1\text{m}^3$

(b) Volume of cement =  $(\text{Mass of cement}/\text{specific gravity of cement}) * 1/1000$   
 $= 540/3130$   
 $= 0.173\text{ m}^3$

(c) Volume of Fine quartz powder =  $(\text{Mass of quartz powder} / \text{specific gravity of quartz powder}) * 1/1000$   
 $= 60/2650$   
 $= 0.023\text{ m}^3$

- (d) Volume of super plasticizer (0.4% by weight of binder content)  
 $= (\text{Mass of chemical admixture} / \text{specific gravity of chemical admixture}) * 1/1000$   
 $= 2.40/1200$   
 $= 0.002 \text{ m}^3$
- (e) Volume of water =  $(\text{Mass of water} / \text{specific gravity of water}) * 1/1000$   
 $= 240/1000 = 0.24 \text{ m}^3$
- (f) Volume of all in aggregate =  $[a - (b + c + d + e)]$   
 $e = 1 - (0.173 + 0.023 + 0.002 + 0.24)$   
 $e = 0.562 \text{ m}^3$
- (g) Mass of coarse aggregate  
 $= e * \text{volume fraction of coarse aggregate} * \text{specific gravity of coarse aggregate} * 1000$   
 $= 0.562 * 0.4 * 2.68 * 1000$   
 $= \mathbf{602.5 \text{ kg/m}^3}$
- (h) Mass of fine aggregate – River Sand  
 $= e * \text{volume of fine aggregate} * \text{specific gravity of fine aggregate} * 1000$   
 $= 0.562 * 0.6 * 2.65 * 0.75 * 1000$   
 $= \mathbf{670.2 \text{ kg/m}^3}$
- (i) Mass of fine aggregate – Quartz Sand  
 $= e * \text{volume of fine aggregate} * \text{specific gravity of fine aggregate} * 1000$   
 $= 0.562 * 0.6 * 2.65 * 0.25 * 1000$   
 $= \mathbf{223.4 \text{ kg/m}^3}$

**Mix proportions - Quantities in kg/m<sup>3</sup> (considering aggregates in SSD condition)**

Binder content		Fine aggregates		Coarse aggregates	Water	w/b
Cement	Fine quartz powder	River Sand	Quartz Sand	Jelly 12.5mm MAS		
540	60	670	224	603	240	0.40

## APPENDEIX – II

### Sample Mix Design for High Performance Alkali Activated Slag Concrete Mixes

#### Input parameters:

Specific gravity of GGBFS = 2.9

Specific gravity of fine quartz = 2.65

Specific gravity of slag sand = 2.65

Specific gravity of quartz sand = 2.65

Specific gravity of EAF slag Coarse aggregates = 3.0

Specific gravity of NaOH = 2.1

Specific gravity of Sodium Silicate liquid = 1.57

Specific gravity of Sodium Phosphate (Retarder: 1% of Binder) = 1.5

Maximum size of coarse aggregates = 12.5 mm

#### Estimation of Ingredients for HPAASC:

Na<sub>2</sub>O dosage required = 5%

Water/binder ratio=0.40

Binder content (GGBFS) =700 kg/m<sup>3</sup>

M<sub>s</sub> (Activation modulus) = (SiO<sub>2</sub>) / (Na<sub>2</sub>O)) required=1.0

#### Calculations for alkali solution

Sodium silicate solution is having 14.7% Na<sub>2</sub>O, 32.8%, SiO<sub>2</sub>, 52.5% of Water (by weights). Hence 1 kg of Sodium silicate contains 0.147 kg of Na<sub>2</sub>O, 0.328 kg of SiO<sub>2</sub>, 0.525 kg of Water.

Na<sub>2</sub>O fraction in NaOH flakes = 0.775

M<sub>s</sub> of sodium silicate solution = (SiO<sub>2</sub>) / (Na<sub>2</sub>O) = 2.23

Dosage of Na<sub>2</sub>O = 5 % of binder content

$$= 0.05 \times 700 = 35 \text{ kg/m}^3$$

SiO<sub>2</sub> dosage = M<sub>s</sub> × Na<sub>2</sub>O = 1 × 35 = 35 kg/m<sup>3</sup>

Quantity of Sodium silicate required for 35 kg of  $\text{SiO}_2 = 35/0.328$

$$= 106.71 \text{ kg/m}^3$$

$\text{Na}_2\text{O}$  present in 106.71 kg of Sodium Silicate

$$= 0.147 \times 106.71 \text{ kg}$$

$$= 15.69 \text{ kg}$$

$\text{Na}_2\text{O}$  required from NaOH

$$= 35.0 - 15.69 = 19.31 \text{ kg}$$

NaOH required for 19.31 kg of  $\text{Na}_2\text{O}$

$$= 19.31/0.775$$

$$= 24.92 \text{ kg/m}^3$$

Water/binder (W/b) = 0.40

$$W = 0.40 \times 700 = 280 \text{ kg}$$

Water present in Sodium Silicate =  $106.71 \times 0.528$

$$= 56.343 \text{ kg}$$

Net quantity of water required externally =  $280 - 56.343$

$$= 223.657 \text{ kg/m}^3$$

### Mix calculations

Volume of concrete =  $1 \text{ m}^3$

Replacing 15 % of GGBS by quartz powder and 25% of slag sand by quartz sand.

Total Binder Content = $700 \text{ kg/m}^3$	
GGBFS (85 %)	Fine Quartz Powder (15 %)
$595 \text{ kg/m}^3$	$105 \text{ kg/m}^3$

$$\text{Volume of Paste} = \frac{595}{2.9 \times 1000} + \frac{105}{2.65 \times 1000} + \frac{106.71}{1.57 \times 1000} + \frac{24.92}{2.1 \times 1000} + \frac{223.657}{1 \times 1000} + \frac{0.01 \times 700}{1.5 \times 1000} + \frac{0.004 \times 700}{1 \times 1000}$$

$$\text{Volume of Paste} = \frac{700}{2.9 \times 1000} + \frac{106.71 + 24.92 + 223.657}{1.25 \times 1000} = \mathbf{0.559 \text{ m}^3}$$

$$\text{Total aggregate volume} = 1 - 0.559 = 0.441 \text{ m}^3$$

The Proportioning of Fine aggregate: Coarse aggregate 60%: 40 %.

$$\text{Weight of fine aggregate for } 1 \text{ m}^3 \text{ concrete} = 0.441 \times 2.65 \times 0.60 \times 1000$$

$$= \mathbf{701.19 \text{ kg/m}^3}$$

<b>Fine Aggregate = 701.19 kg/m<sup>3</sup></b>	
Slag Sand (75 %)	Quartz Sand (25 %)
525.89 kg/m <sup>3</sup>	175.3 kg/m <sup>3</sup>

$$\text{Weight of Coarse aggregate for } 1 \text{ m}^3 \text{ concrete} = 0.441 \times 3.0 \times 0.40 \times 1000$$

$$\text{Coarse Aggregates: Electric Arc furnace Slag} = \mathbf{529.2 \text{ kg/m}^3}$$

## APPENDEX – III

### Sample Theoretical calculations for Beams – OPCC

#### General:

The theoretical calculations are carried out in accordance with IS: 456 – 2000. Theoretical calculations are made for all the beams and the calculation for OPCC beams is only presented here for illustrative purposes.

#### Geometric Properties of Beam:

Breadth of beam,  $b = 150$  mm

Depth of beam,  $d = 250$ mm

Clear cover to rebars = 25mm

Effective cover = 33mm

Effective depth of beam,  $d = 217$ mm

Span of the beam = 2250 mm

#### Material properties:

Compressive strength of concrete cube,  $f_{ck} = 75.3$  N/mm<sup>2</sup>

Yield stress of steel,  $f_y = 540$  N/mm<sup>2</sup>

Elastic modulus of concrete,  $E_c = 2.86 \cdot 10^4$  N/mm<sup>2</sup>

Elastic modulus of steel,  $E_s = 2 \cdot 10^5$  N/mm<sup>2</sup>

#### Tension Reinforcement:

Provided tension reinforcement = 3 no of 16mm diameter bars

$$A_{st} = 603 \text{ mm}^2$$

Check for maximum percentage of reinforcement:

$$\text{Maximum reinforcement} = 0.04 \cdot b \cdot D$$

$$= 0.04 \cdot 150 \cdot 250$$

$$= 1500 \text{ mm}^2 > \text{Provided } 603 \text{ mm}^2$$

Check for minimum percentage of reinforcement:

$$\text{Minimum reinforcement} = 0.85 \text{ bd} / f_y$$

$$= 0.85 \cdot 150 \cdot 217 / 500$$

$$= 55 \text{ mm}^2 < \text{provided } 603 \text{ mm}^2$$

Hence, the required reinforcement is within the maximum and minimum limits.

**Calculation of theoretical moment of resistance:**

$$\frac{x_{u\max}}{d} = 0.438$$

$$= 95.05 \text{ mm}$$

$$x_u = (f_y * A_{st}) / (0.546 * f_{ck} * b)$$

$$= 48.92 \text{ mm}$$

$$\text{Lever Arm} = d - 0.417X_u$$

$$= 196.60 \text{ mm}$$

Ultimate moment, Mu is given by

$$\text{Mu} = \text{Force} * \text{Lever arm}$$

$$= f_y * A_{st} * (d - 0.417 X_u)$$

$$= 59.32 \text{ kN-m}$$

**Load Calculation:**

$$\text{Self-weight of Beam} = 0.15 * 0.25 * 25$$

$$= 0.9375 \text{ kN/m}$$

$$M_u = \frac{W_{\text{applied}} * L}{6} + \frac{W_{\text{self weight}} * L^2}{8}$$

$$59.32 = \frac{W_{\text{applied}} * 2.25}{6} + \frac{0.9375 * 2.25^2}{8}$$

$$W_{\text{applied}} = 156.60 \text{ kN}$$

### Shear reinforcement calculations:

Total ultimate load = 156.60 kN

Ultimate shear force,  $V_u = 156.60/2 = 78.30$  kN

$$\begin{aligned}\text{Nominal shear stress, } \tau_{vu} &= \frac{V_u}{b \cdot d} \\ &= \frac{78.30}{150 \cdot 217} \\ &= 2.41 \text{ N/mm}^2\end{aligned}$$

$$\tau_{c \text{ max}} = 4 \text{ N/mm}^2$$

$\tau_v < \tau_{c \text{ max}}$ , Hence safe.

Check for shear reinforcement

$$\frac{100 \cdot A_{st}}{b \cdot d} = \frac{100 \cdot 603}{150 \cdot 217} = 1.85$$

From table 19, IS 456-2000, for the above value, on interpolation, we get

$$\tau_c = 0.856 \frac{\text{N}}{\text{mm}^2}$$

$\tau_c < \tau_v$ , hence shear reinforcement is required.

Shear force to be resisted by the shear reinforcement is

$$V_{us} = V_u - \tau_c \cdot b \cdot d$$

$$V_{us} = 50.44 \text{ kN}$$

Spacing of vertical stirrups with 8mm bars

$$S_v = \frac{f_y \cdot A_{sv} \cdot d}{V_{us}}$$

$$S_v = 216.16 \text{ mm}$$

Spacing of the stirrups for minimum shear reinforcement as per IS: 456-2000,

$$S_v = \frac{f_y * A_{sv}}{0.4 * b}$$

$$S_v = 837.33 \text{ mm}$$

Maximum spacing of shear reinforcement, as per IS: 456-2000, is the minimum of the following

- (i)  $0.75*d = 0.75 * 217 = 162.75 \text{ mm}$
- (ii)  $300 \text{ mm}$

Considering all the above calculated factors, to be safe in shear, a stirrups spacing of 125mm is adopted.

### **Check for Lateral stability**

As per IS 456 – 2000, Slenderness limit for simply supported beam is minimum of the following. The length of the beam should be less than the value of,

- (i)  $60 * b = 60 * 150 = 9000 \text{ mm}$
- (ii)  $250 * \frac{b^2}{d} = 25921.66 \text{ mm}$

However, the actual span used for the test is 2250 mm, which is less than 9000 mm.

Hence, the beam is laterally stable.

### **Check for bond**

Maximum stress can be expected at mid span. The development length available at the beam-ends with 25mm cover without any hooks is given by,

$$L_d = \frac{2250}{2} - 25 = 1100 \text{ mm}$$

As per IS 456 – 2000 Cl 26.2.1, required development length for the beam with deformed bars is,

$$L_d = \frac{\phi * \sigma_s}{4 * \tau_{bd}}$$

$$L_d = \frac{16 * 500}{4 * 1.9 * 1.6 * 1.25}$$

$$L_d = 526.32 \text{ mm}$$

### Calculation of cracking load

$$\text{Cracking moment, } M_{cr} = \frac{f_{cr} * I_{gr}}{y_t}$$

$$\text{Modulus of rupture, } f_{cr} = 6.61 \text{ N/mm}^2$$

$$I_{gr} = \frac{b * D^3}{12}$$

$$Y_t = D/2 = 125 \text{ mm}$$

$$M_{cr} = \frac{f_{cr} * I_{gr}}{y_t}$$

$$M_{cr} = 10.33 \text{ kN - m}$$

$$\text{First crack load, } W_{cr} = \frac{6}{L} \left[ M_{cr} - \frac{w * l^2}{8} \right]$$

$$W_{cr} = 25.96 \text{ kN}$$

Where, W= Self weight of the beam

$$W_{cr} = 25.96 \text{ kN}$$

### Deflection for short-term loading – Calculation under elastic theory

$$E_{\text{concrete}} = 28600 \text{ N/mm}^2$$

$$E_{\text{steel}} = 200000 \text{ N/mm}^2$$

$$\text{Modular ratio, } m = \frac{E_{\text{steel}}}{E_{\text{concrete}}}$$

$$m = 6.99$$

For actual depth of neutral axis, based on the elastic theory,

$$\frac{b * x^2}{2} = m * A_{\text{st}} * (d - x)$$

$$\text{Solving, } x = 85.88 \text{ mm}$$

$$I_{\text{gr}} = 195312500 \text{ mm}^4$$

For cracked moment of inertia,

$$I_{\text{cr}} = \frac{1}{3}bx^3 + m * A_{\text{st}} * (d - x)^2$$

$$I_{\text{cr}} = 104218235.5 \text{ mm}^4$$

$$I_{\text{cr}} < I_{\text{gross}}$$

Theoretical Ultimate moment

$$M_{\text{Ultimate}} = 59.32 \text{ kN-m}$$

Theoretical Ultimate load,

$$W_{\text{Ultimate}} = 156.60 \text{ kN}$$

$$\frac{x}{d} = 0.40$$

$$Z = d - \frac{x}{3} = 13.56 \text{ mm}$$

$$\frac{Z}{d} = 0.062$$

$$\frac{b_w}{b} = 1$$

Effective moment of inertia for cracked section is

$$I_{\text{effective}} = \frac{I_{\text{cr}}}{1.2 - \frac{M_{\text{cr}}}{M_{\text{ultimate}}} \frac{Z}{d} \left(1 - \frac{x}{d}\right) \frac{b_w}{b}}$$

$$I_{\text{effective}} = 87326757.86 \text{ mm}^4$$

$$I_{\text{gr}} > I_{\text{cr}} > I_{\text{eff}}$$

### **Total elastic deflection**

$$\Delta_{\text{Cr}} = \Delta_{\text{applied load}} + \Delta_{\text{self weight}}$$

$$\Delta_{\text{Cr}} = \frac{23 * W_{\text{cr}} * L^3}{1296 * E * I_{\text{gr}}} + \frac{5 * w * L^4}{384 * E * I_{\text{eff}}}$$

$$\Delta_{\text{Cr}} = 1.00 \text{ mm}$$

## **PUBLICATIONS BASED ON THE PRESENT RESEARCH**

### **INTERNATIONAL / NATIONAL JOURNALS**

1. **Manjunath, R.,** Narasimhan, M.C., Umesh, K.M., Shivam Kumar., and Bala Bharathi,U.K. (2019). “Studies on development of high performance, self-compacting alkali activated slag concrete mixes using industrial wastes”. *Construction and Building Materials, Elsevier, Vol 198, pp 133 – 147.*
2. **Manjunath, R.,** Narasimhan, M.C., and Umesh, K.M. (2019). “Studies on high performance alkali activated slag concrete mixes subjected to aggressive environments and sustained elevated temperatures”. *Construction and Building Materials, Elsevier, Vol 229, pp 1-19.*
3. **Manjunath, R.,** and Narasimhan, M.C. (2018). “An experimental investigation on self-compacting alkali activated slag concrete mixes”. *Journal of Building Engineering, Elsevier, Vol 17, pp 1-12.*
4. **Manjunath, R.,** and Narasimhan, M.C. (2018). “Setting behaviour of alkali activated slag concrete mixes – Effect of chemical admixtures”. *Indian Concrete Journal, Vol 92, Issue 9, pp 45-51.*
5. **Manjunath, R.,** Narasimhan, M.C., and Shivam Kumar. “Effects of fiber on performance of high performance alkali activated slag concrete mixes – An experimental evaluation”. *European Journal of Environmental and Civil Engineering, Taylor and Francis (Accepted).*
6. **Manjunath, R,** Narasimhan, M.C., and Bala Bharathi, U.K. “Flexural behaviour of reinforced high performance self-compacting alkali activated slag concrete beams”. *Indian Concrete Journal (Accepted).*

### **BOOK CHAPTER**

1. **Manjunath, R.,** and Narasimhan, M.C. - A Book chapter on **Alkali Activated Concrete Systems – A State of Art** in the book entitled “NEW MATERIALS IN CIVIL ENGINEERING”. Elsevier. Chief Editors: Pijush Samui, Dookie Kim, Nagesh Iyer and Sandeep Chaudhary (Accepted).

## **INTERNATIONAL CONFERENCES**

1. **Manjunath, R.**, Narasimhan, M.C., and Naveen, U. (2018). “Steel fiber reinforced alkali activated slag concrete mixes – An experimental evaluation”. *2<sup>nd</sup> International Conferences on Advances in Concrete, Structural and Geotechnical Engineering, (ACSGE 2018), Pilani, Feb 24–26.*
2. **Manjunath, R.**, Narasimhan, M.C., and Ashwin, P.V. (2018). “Effect of addition of silica fume on performance of alkali activated slag concrete Mixes”. *3<sup>rd</sup> International Symposium on Advances in Science and Technology of Concrete (ACI and ICACI), Mumbai, Dec 14 – 15.*
3. **Manjunath, R.**, and Narasimhan, M.C. (2019). “Studies on eco-friendly concrete mixes incorporating industrial by-products”. *UKIERI Concrete Congress, Jalandhar, Mar 5–8.*
4. **Manjunath, R.**, and Narasimhan, M.C. (2019). “High strength flowable alkali activated slag concrete mixes produced using industrial wastes”. *First International Conference on Materials Science and Manufacturing Technology, Coimbatore, April 12-13.*
5. **Manjunath, R.**, and Narasimhan, M.C. (2019). “Effect of addition of OPC on the performance characteristics of self–compacting alkali activated slag concrete mixes”. *First International Conference on Materials Science and Manufacturing Technology, Coimbatore, April 12-13*

## RESUME

Name : Mr. Manjunath. R  
Permanent Address : No 2622/10, 11<sup>th</sup> Main Road, E Block  
2<sup>nd</sup> Stage Rajajinagar, Bangalore-560010  
Karnataka, India  
Contact Number : 8197203686, 812389299  
E-mail ID : rmanju301@gmail.com

### ACADEMIC QUALIFICATION:

Degree	Specialization	Institute	Duration
Ph.D.	Civil Engineering	NITK, Surathkal	2016-2019
M.Tech	Construction Technology	BMSCE, Bangalore	2012-2014
B E	Civil Engineering	UVCE, Bangalore	2009-2012

### PUBLICATIONS:

#### International/National – Journals/Conferences:

1. **Manjunath, R.**, Narasimhan, M.C., Umesh, K.M., Shivam Kumar., and Bala Bharathi, U.K. (2019). “Studies on development of high performance, self-compacting alkali activated slag concrete mixes using industrial wastes”. Construction and Building Materials, Elsevier, Vol 198, pp 133 – 147.
2. **Manjunath, R.**, Narasimhan, M.C., and Umesha, K.M. (2019). “Studies on high performance alkali activated slag concrete mixes subjected to aggressive environments and sustained elevated temperatures”. Construction and Building Materials, Elsevier, Vol 229, pp 1-19.

3. **Manjunath, R.,** and Narasimhan, M.C. (2018). “An experimental investigation on self-compacting alkali activated slag concrete mixes”. *Journal of Building Engineering*, Elsevier, Vol 17, pp 1-12.
4. **Manjunath, R.,** and Narasimhan, M.C. (2018). “Setting behaviour of alkali activated slag concrete mixes – Effect of chemical admixtures”. *Indian Concrete Journal*, Vol 92, Issue 9, pp 45-51.
5. **Manjunath, R.,** Narasimhan, M.C., and Naveen, U. (2018). “Steel fiber reinforced alkali activated slag concrete mixes – An experimental evaluation”. 2nd International Conferences on Advances in Concrete, Structural and Geotechnical Engineering, (ACSGE 2018), Pilani, Feb 24–26.
6. **Manjunath, R.,** Narasimhan, M.C., and Ashwin, P.V. (2018). “Effect of addition of silica fume on performance of alkali activated slag concrete mixes”. 3rd International Symposium on Advances in Science and Technology of Concrete (ACI and ICACI), Mumbai, Dec 14 – 15.
7. **Manjunath, R.,** and Narasimhan, M.C. (2019). “Studies on eco-friendly concrete mixes incorporating industrial by-products”. UKIERI Concrete Congress, Jalandhar, Mar 5–8.
8. **Manjunath, R.,** and Narasimhan, M.C. (2019). “High strength flowable alkali activated slag concrete mixes produced using industrial wastes”. First International Conference on Materials Science and Manufacturing Technology, Coimbatore, April 12-13.
9. **Manjunath, R.,** and Narasimhan, M.C. (2019). “Effect of addition of OPC on the performance characteristics of self-compacting alkali activated slag concrete mixes”. First International Conference on Materials Science and Manufacturing Technology, Coimbatore, April 12-13.
10. **Manjunath, R.,** and Ranganath, R.V. (2019). “Performance evaluation of fly-ash based self-compacting geopolymer concrete mixes”. First International Conference on Materials Science and Manufacturing Technology, Coimbatore, April 12-13.

11. **Manjunath, R.**, Narasimhan, M.C., and Rajath, R.L. (2017). “To study the mechanical properties of fly-ash based geopolymer concrete with partial replacement of Bagasse ash and GGBFS”. Global Civil Engineering Challenges in Sustainable Development and Climate Change (ICGCSC), MITE, March 17 - 18.
12. **Manjunath, R.**, and Mule, R. (2018). “Studies on fresh and hardened properties of sugarcane bagasse ash blended self-compacting concrete mixes”. International Conference on Sustainable Construction and Building, NITK, June 18-22, Lecture Notes in Civil Engineering, Springer Nature, Vol 25, pp 265 - 274. [https://doi.org/10.1007/978-981-13-3317-0\\_24](https://doi.org/10.1007/978-981-13-3317-0_24).
13. **Manjunath, R.**, Narasimhan, M.C., and Prakash, U. (2019). “Performance evaluation of deep beams using self-compacting concrete mixes”. International Conference on Civil Engineering Trends and Challenges for Sustainability (CTCS), May 23-24 – Best Paper Award.
14. **Manjunath, R.**, Narasimhan, M.C., and Nambiar, C.B. (2019). “Performance evaluation of deep beams using self-compacting concrete subjected to corrosion”. International Conference on Civil Engineering Trends and Challenges for Sustainability (CTCS), May 23-24.
15. **Manjunath, R.**, Narasimhan, M.C., and Janagam. (2019). “Performance evaluation of steel fiber reinforced deep beams using self-compacting concrete”. International Conference on Civil Engineering Trends and Challenges for Sustainability (CTCS), May 23-24.
16. **Manjunath, R.**, Narasimhan, M.C., Shashanka, M., Vijayanand, S.D., and Vinayaka, J. (2019). “Experimental studies on shear strength characteristics of alkali activated slag concrete mixes”. First International Conference on Recent Advances in Materials and Manufacturing (ICRAMM), Sep 12 – 14.